



The University of
Nottingham

School of Chemistry

SOLVENT BASED SWITCHING OF THE PHOTOPHYSICAL PROPERTIES OF TRANSITION METAL COMPLEXES

Wassim Zuhair Alsindi, M.Sci.

Thesis submitted to the University of Nottingham for
the degree of Doctor of Philosophy

April 2007

**GEORGE GREEN LIBRARY OF
SCIENCE AND ENGINEERING**

Declaration

Except where specific reference is made to other sources or collaborators, the work presented in this Thesis is the original work of the author. It has not been submitted, in whole or in part, for any other Degree.

Signed: 

Wassim Alsindi

Date: 01/06/07

Solvent Based Switching of the Photophysical Properties of Transition Metal Complexes

Abstract

The work presented in this Thesis describes the modular design and spectroscopic study of polynuclear systems based on ruthenium (II) and rhenium (I) complexes. A combination of UV/vis, luminescence and TRIR spectroscopies, electrochemistry, spectroelectrochemistry and conformational analysis have been employed to understand the electronic structure of the ground and excited states of these compounds.

Chapter 1 gives an introductory background to this Thesis. An overview of transition metal photophysics and excited states, and the typical spectroscopic and electrochemical techniques used in their study is presented. Previous studies of the ground and excited state properties of the complexes $[\text{Ru}(\text{bpy})_3]^{2+}$ and $[\text{ReCl}(\text{CO})_3(\text{bpy})]$ which are used as supramolecular building blocks in this Thesis are presented and a number of relevant studies of supramolecular systems are described.

Chapter 2 contains a study extending the known family of $[\text{Ru}(\text{CN})_4(\text{NN})]^{2-}$ complexes and describes their unique advantages over $[\text{Ru}(\text{bpy})_3]^{2+}$. The results obtained are discussed alongside previous studies. This completes the introduction of the molecular building blocks used in Chapters 3 and 4.

Chapter 3 details a study of through-space PEnT in bimetallic systems constructed from the complexes introduced in Chapters 1 and 2, bridged by a saturated alkyl linker between bpy ligands on either metal. This Chapter demonstrates the solvent-switchable nature of the direction and gradient of PEnT, using ps-TRIR spectroscopy to directly probe these processes *in real time*.

Chapter 4 describes a study of bimetallic systems bridged by conjugated the ligand 2,2'-bipyrimidine. Monometallic, homobimetallic and heterobimetallic systems are studied and questions arising from limitations of previous studies are addressed. In particular ps-TRIR spectroscopy gives new insight into the numerous ultrafast processes occurring.

Chapter 5 summarises the achievements of this Thesis and suggests promising directions for extending this work in the future.

Chapter 6 describes the experimental and theoretical techniques used in this Thesis.

Acknowledgements

Firstly I would like to extend sincere thanks and appreciation to my supervisor Professor Mike George for his guidance, support and encouragement over the course of my studies. I have also received a great deal of help from past members of the Nottingham Photochemistry and Spectroscopy group in the early stages of this work, notably Dr. Peter Portius, Dr. Jason Hyde, Dr. Julia Weinstein, Dr. Jixin Yang and Dr. Marina Kuimova. Thanks also go to Dr. Stephen Davies for his help with electrochemistry and Dr. Jon McMaster for his assistance with computational chemistry.

Thanks also goes to current and recent members of the group for their friendship, day-to-day help in the laboratory and interesting discussions, in particular Alex Cowan, Chris Brookes, Dani Lampus and Dr. Xue-Zhong Sun. I would also like to extend a special thanks to the School of Chemistry support staff, without whom much of this work would have been much more difficult or impossible. Mark Guyler, Richard Wilson, Peter Fields, David Litchfield and Grant Howard have all been extremely helpful.

This project had a strong collaborative focus and I have worked in tandem with Tim Easun and Professor Mike Ward at the University of Sheffield who have been excellent co-workers. The Ward group's expertise in synthetic chemistry has complemented our spectroscopic and photophysical skills and this project would not have been possible had it not been for their preparation of all the bespoke complexes in this Thesis. Thanks go to Tim Easun for being such a motivated collaborator and Nina Depperman and Dr. Juan-Manuel Herrera for their role in the preparation of some of the complexes.

This work would have not been possible without access to the PIRATE spectrometer at the Lasers for Science Facility in the Central Laser Facility at the Rutherford Appleton Laboratory. I would like to thank Tony Parker, Pavel Matousek, Emma Belcher and particularly Kate Ronayne and Mike Towrie for the amount of time and effort put into keeping our experiments running late into the night and helping us to unravel the often mysterious spectra that we obtained. Dr. Xue-Zhong Sun and Tim Easun also deserve

praise for their commitment and dedication to getting the most out of our limited experimental time, often working in the laboratory until past bedtime!

I would also like to thank Dr. June McCombie, Dr. Helen Fraser and Professor Ewine van Dishoeck for giving me the opportunity to undertake my Masters research project in the wonderful surroundings of de Sterrewacht (Astronomical Observatory), working in the *Raymond and Beverly Sackler Laboratory for Experimental Astrophysics*, University of Leiden. The semester I spent there in early 2003 was a fantastic prelude to my Ph.D. studies and provided the perfect opportunity to 'cut my teeth' at a world leading institution.

A special thank you goes to Katharine T. Adcock for her support and understanding throughout the writing process and praise also goes to my business partner Darren Gower for his patience over the last six months, as I haven't been pulling my weight with the day-to-day workload of running our company!

Finally I would like to thank my family and in particular my parents, Zuhair and Sahar Alsindi who have made so many sacrifices for their children's future. My thoughts are perpetually with my extended family, who have suffered war, displacement and hardship since I began this work in 2003. The world may have forgotten about you and the millions of Iraqi diaspora but I have not.

Wassim Zuhair Alsindi, Nottingham, 25th March 2007.

List of Abbreviations

ΔE	Energy difference
ΔOD	Change in absorbance
λ	Wavelength
λ_{abs}	Absorption wavelength
λ_{em}	Emission wavelength
λ_{ex}	Excitation wavelength
λ_{max}	Wavelength maximum of peak
μs	Microsecond (10^{-6} s)
ν	Wavenumber
τ	Excited state lifetime
ϕ	Luminescence quantum yield
χ^2	Goodness of fit test
1	Singlet (excited state)
3	Triplet (excited state)
(NN)	α -Diimine
§	Section/Chapter
Å	Angström (10^{-10} m)
A / Abs	Absorbance
A. N.	Gutmann Acceptor Number
BL	Bridging Ligand
CV	Cyclic Voltammetry
DCM	Dichloromethane
DFT	Density Functional Theory
DMF	Dimethyl formamide
DMSO	Dimethyl sulfoxide
D. N.	Gutmann Donor Number
Et	Ethyl
FTIR	Fourier Transform Infrared
H-bonding	Hydrogen-bonding
HAT	Hexaaza-triphenylene
HOMO	Highest Occupied Molecular Orbital
IC	Internal conversion
IL	Intra-ligand
IR	Infrared
IRF	Instrument Response Function/Time
ISC	Intersystem Crossing
IVCT	Inter-Valence Charge Transfer
LC	Ligand-centred
LMCT	Ligand-to-Metal Charge Transfer
LUM	Luminescence
LUMO	Lowest Unoccupied Molecular Orbital

M	Metal centre
MC	Metal-Centred
MCT	Mercury Cadmium Telluride
Me	Methyl
MLCT	Metal-to-Ligand Charge Transfer
NMR	Nuclear Magnetic Resonance
ns	Nanosecond (10^{-9} s)
OTE	Optically Transparent Electrode
OTTLE	Optically Transparent Thin Layer Electrode
PEnT	Photoinduced Energy Transfer
PET	Photoinduced Electron Transfer
ps	Picosecond (10^{-12} s)
PIRATE	Picosecond Infrared Absorption Transient Excitation
PMT	Photo-Multiplier Tube
PPN ⁺	Bis(triphenylphosphine)iminium
r	Förster interchromophoric distance
RAL	Rutherford Appleton Laboratory
SSDA	Second Sphere Donor-Acceptor
T2D-IR	Transient Two-Dimensional Infrared
TCSPC	Time-Correlated Single Photon Counting
TRIR	Time Resolved Infrared
UV	Ultraviolet
UV/vis	Ultraviolet-visible

Table of Contents

Chapter 1: Introduction

1.1	Supramolecular Photoscience.....	1-1
1.1.1	Overview and Excited States.....	1-1
1.1.2	Monometallic Complexes.....	1-3
1.1.3	Bimetallic and Polynuclear Complexes.....	1-4
1.2	Solvatochromism.....	1-6
1.2.1	General Solvent-Solute Effects in UV/visible Absorption Spectra.....	1-7
1.2.2	General Solvent-Solute Effects in Luminescence Spectra.....	1-8
1.2.3	Specific Solvent-Solute Effects.....	1-9
1.2.4	The Influence of Solvent on the Electronic Structure of Cyanide Complexes.....	1-9
1.3	Spectroscopic and Electrochemical Methods Used in this Work.....	1-9
1.4	Previous Studies of Relevant Complexes and Supramolecular Systems.....	1-14
1.4.1	Monometallic Units.....	1-14
1.4.1.1	[Ru(bpy) ₃] ²⁺ and related complexes.....	1-14
1.4.1.2	<i>fac</i> -[ReCl(CO) ₃ (bpy)].....	1-18
1.4.1.3	Other Monometallic Complexes.....	1-20
1.4.2	Photoinduced Processes in Polynuclear Systems.....	1-22
1.4.2.1	Polypyridyl-linked systems.....	1-22
1.4.2.2	CN linked systems.....	1-25
1.5	Closing Points.....	1-25
1.6	References.....	1-28

Chapter 2: Tetracyanoruthenate (II) Polypyridyl Complexes

2.1	Introduction.....	2-1
2.1.1	[Ru(CN) ₄ (bpy)] ²⁻	2-1
2.1.2	[Ru(CN) ₄ (bpm)] ²⁻	2-4
2.1.3	[Ru(CN) ₂ (bpy) ₂] and other Ruthenium Cyanide Complexes.....	2-5
2.1.4	Summary of [Ru(CN) ₄ (NN)] ²⁻ Properties.....	2-6
2.2	Scope, Results and Discussion.....	2-7
2.2.1	UV/vis Absorption and Luminescence Spectroscopy.....	2-8
2.2.2	Electrochemistry.....	2-10
2.2.2	FTIR and Time Resolved Infrared Spectroscopy.....	2-11
2.3	Discussion and Closing Points.....	2-15
2.4	References.....	2-18

Chapter 3: Solvent-Based Switching of the Gradient and Direction of Förster Photoinduced Energy Transfer in Polynuclear Complexes

3.1	Introduction.....	3-1
3.2	RuCNdmb.....	3-7
3.2.1	UV/visible Absorption and Luminescence Spectroscopy.....	3-8
3.2.2	Cyclic Voltammetry.....	3-9
3.2.3	Infrared Spectroelectrochemistry.....	3-10
3.2.4	UV/visible/nIR Spectroelectrochemistry.....	3-11
3.2.5	FTIR and Time-Resolved Infrared Spectroscopy.....	3-11
3.2.6	Closing Points.....	3-12
3.3	Rubpyamide-BL ¹	3-14
3.3.1	UV/Visible Absorption and Luminescence Spectroscopy.....	3-15
3.3.2	Cyclic Voltammetry.....	3-16
3.3.3	Infrared Spectroelectrochemistry.....	3-17
3.3.4	UV/visible/nIR Spectroelectrochemistry.....	3-20
3.3.5	FTIR and Time-Resolved Infrared Spectroscopy.....	3-21
3.3.6	Closing Points.....	3-24

3.4.	Rubpyamide-BL ²	3-25
3.4.1	UV/Visible Absorption and Luminescence Spectroscopy.....	3-26
3.4.2	Cyclic Voltammetry.....	3-27
3.4.3	FTIR and Time-Resolved Infrared Spectroscopy.....	3-28
3.4.4	Closing Points.....	3-30
3.5	RuCN-BL ¹ -Rubpyamide.....	3-32
3.5.1	UV/visible Absorption and Luminescence Spectroscopy.....	3-33
3.5.2	Cyclic Voltammetry.....	3-43
3.5.3	FTIR and Time-Resolved Infrared Spectroscopy.....	3-44
3.5.4	Computational Studies and Conformational Analysis.....	3-61
3.5.5	Discussion and Closing Points.....	3-63
3.6	RuCN-BL ² -Rubpyamide.....	3-68
3.6.1	UV/visible Absorption and Luminescence Spectroscopy.....	3-69
3.6.2	Cyclic Voltammetry.....	3-76
3.6.3	FTIR and Time-Resolved Infrared Spectroscopy.....	3-77
3.6.4	Computational Studies and Conformational Analysis.....	3-93
3.6.5	Closing Points.....	3-96
3.7	ReCO-BL ¹ -Rubpyamide.....	3-99
3.7.1	UV/visible Absorption and Luminescence Spectroscopy.....	3-100
3.7.2	Cyclic Voltammetry.....	3-105
3.7.3	FTIR and Time-Resolved Infrared Spectroscopy.....	3-106
3.7.4	Computational Studies and Conformational Analysis.....	3-117
3.7.5	Closing Points.....	3-119
3.8	Discussion and Closing Points.....	3-121
3.9	Appendix of Spectra and Voltammograms.....	3-127
3.10	References.....	3-134

Chapter 4: Probing the Excited States of Ruthenium (II) and Rhenium (I) Complexes of 2,2'-Bipyrimidine using TRIR Spectroscopy

4.1	Introduction.....	4-1
4.1.1	2,2'-Bipyrimidine As A Bridging Ligand.....	4-1
4.1.2	Relevant Studies of Re and Ru complexes of bpm.....	4-3
4.1.3	Relevant Studies of Other Polynuclear Complexes.....	4-7
4.2	ReBPM.....	4-10
4.2.1	UV/visible Absorption and Luminescence Spectroscopy.....	4-10
4.2.2	Cyclic Voltammetry.....	4-11
4.2.3	FTIR, IR OTTL and Time-Resolved Infrared Spectroscopy.....	4-12
4.2.4	Closing Points.....	4-14
4.3	RuCNBPM.....	4-15
4.3.1	UV/visible Absorption and Luminescence Spectroscopy.....	4-15
4.3.2	Cyclic Voltammetry.....	4-16
4.3.3	FTIR, IR OTTL and Time-Resolved Infrared Spectroscopy.....	4-16
4.3.4	Closing Points.....	4-20
4.4	RubpyamideBPM.....	4-20
4.4.1	UV/visible Absorption and Luminescence Spectroscopy.....	4-21
4.4.2	Cyclic Voltammetry.....	4-22
4.4.3	FTIR, IR OTTL and Time-Resolved Infrared Spectroscopy.....	4-23
4.4.4	Closing Points.....	4-30
4.5	(Re) ₂ BPM.....	4-30
4.5.1	UV/visible Absorption and Luminescence Spectroscopy.....	4-31
4.5.2	Cyclic Voltammetry.....	4-31
4.5.3	FTIR, IR OTTL and Time-Resolved Infrared Spectroscopy.....	4-32
4.5.4	Closing Points.....	4-35
4.6	(RuCN) ₂ BPM.....	4-36
4.6.1	UV/visible Absorption and Luminescence Spectroscopy.....	4-36

4.6.2	Cyclic Voltammetry.....	4-37
4.6.3	FTIR, IR OTTL and Time-Resolved Infrared Spectroscopy.....	4-37
4.6.4	Closing Points.....	4-42
4.7	(Rbpyamide) ₂ BPM.....	4-42
4.7.1	UV/visible Absorption and Luminescence Spectroscopy.....	4-43
4.7.2	Cyclic Voltammetry.....	4-44
4.7.3	FTIR, IR OTTL and Time-Resolved Infrared Spectroscopy.....	4-44
4.7.4	Closing Points.....	4-51
4.8	ReBPMRuCN.....	4-51
4.8.1	UV/visible Absorption and Luminescence Spectroscopy.....	4-52
4.8.2	Cyclic Voltammetry.....	4-52
4.8.3	FTIR, IR OTTL and Time-Resolved Infrared Spectroscopy.....	4-53
4.8.4	Closing Points.....	4-62
4.9	ReBPMRbpyamide.....	4-63
4.9.1	UV/visible Absorption and Luminescence Spectroscopy.....	4-63
4.9.2	Cyclic Voltammetry.....	4-64
4.9.3	FTIR, IR OTTL and Time-Resolved Infrared Spectroscopy.....	4-65
4.9.4	Closing Points.....	4-73
4.10	RuCNBPMRbpyamide.....	4-77
4.10.1	UV/visible Absorption and Luminescence Spectroscopy.....	4-78
4.10.2	Cyclic Voltammetry.....	4-78
4.10.3	FTIR, IR OTTL and Time-Resolved Infrared Spectroscopy.....	4-79
4.10.4	Closing Points.....	4-88
4.11	Chapter Discussion and Closing Points.....	4-88
4.12	Appendix of Spectra and Voltammograms.....	4-94
4.13	References.....	4-100

Chapter 5: Closing Points and Future Work

5.1	Introduction.....	5-1
5.2	Closing Points and Future Work.....	5-3
5.3	References.....	5-12

Chapter 6: Experimental

6.1	Materials, Measurements and Analysis.....	6-1
6.2	References.....	6-10

Chapter 1:

Introduction

Chapter 1: Introduction

1.1 Supramolecular Photoscience

1.1.1 Overview and Excited States

Supramolecular chemistry is ‘chemistry beyond the molecule’.¹ A supramolecular system consists of molecular components, just as molecules consist of atomic components. Supramolecular systems may possess properties that are not directly related or derived from their constituent units due to the intermolecular interactions taking place in the supramolecular structure. This can have significant effects on their photoreactivity as photoinduced processes between the molecular components become possible.

It is important to distinguish between *photophysical* and *photochemical* processes as these words are often erroneously used interchangeably. Photophysics refers to a process involving the absorption, emission or radiationless quantum transition / event in which there is no chemical change taking place: in other words the process involves a change in electronic structure (the formation of an excited state) without a change in chemical formula of the analyte. Conversely photochemical processes involve a change in chemical formula, which may be reversible or irreversible depending on the experimental conditions used. In this case the change in electronic structure induced by absorption, emission or quantum transition of a photon is accompanied by a chemical reaction. This Thesis is solely concerned with the excited state photophysics of the complexes prepared and studied in Chapters 2-4 and it should be emphasised that no (desired) chemical reactions are taking place.

A Jabłoński diagram may be drawn to give an overview of the events in a system from the formation of an excited state to its deactivation and return to the ground state electronic configuration. Figure 1.1.1.1 contains a generalised form of this diagram which is relevant for the majority of isolated metal centres in this Thesis.

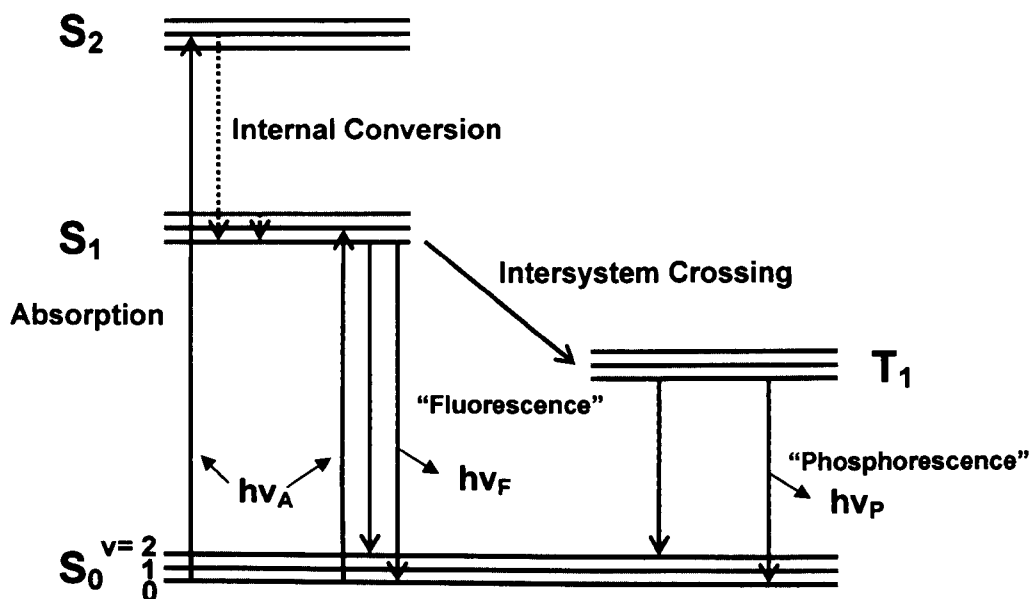


Figure 1.1.1.1: A generalised form of Jablonski diagram relevant to excited states of metal complexes.

With reference to Figure 1.1.1.1, the formation, evolution and subsequent decay of excited state species may be described as follows. Absorption of a photon $h\nu_A$ by a ground state system S_0 leads to formation of a singlet excited state S_1 or S_2 , with excitation into a “hot” excited vibrational energy level ($v > 0$) also being commonplace. Radiationless relaxation of the electronically excited state to the lowest energy singlet species (usually S_1) takes place rapidly. This internal conversion typically occurs on a sub-picosecond timescale.² Following this process the relaxation of vibrationally excited states to the $v = 0$ energy level (vibrational cooling) may then take place, typically on a timescale of a few picoseconds.³ This S_1 excited state may be metastable (particularly in organic systems) and its deactivation may either be radiative (*via* fluorescence or more generally defined as luminescence from a singlet state) or non-radiative.

In systems containing transition metal atoms, the S_1 state may rapidly convert into a T_1 (triplet) excited state (*vide infra*) *via* a process known as intersystem crossing. As with S_1 states, a T_1 excited state may return to the S_0 ground state through radiative (luminescence from a triplet state) or non-radiative deactivation. The words ‘fluorescence’ and ‘phosphorescence’ should be used with care when

referring to transition metal complexes, as mixing of singlet and triplet excited states may occur and the effect of spin-orbit coupling may lead to relaxation of selection rules (§1.1.2). Spin-orbit coupling may have such an effect that pure singlet or triplet emission may not necessarily occur, and the emission is best referred to as luminescence.

1.1.2 Monometallic Complexes

The majority of photophysically interesting coordination compounds in the present day literature contain a metal centre (usually Re^{I} , Ru^{II} , Rh^{I} , Ir^{I} or Pt^{II}) and a N-heterocyclic aromatic ligand, typically a polypyridyl such as 2,2'-bipyridine (bpy). The archetypal complex in this particular paradigm is $[\text{Ru}(\text{bpy})_3]^{2+}$ which is discussed in §1.4.1.1. In photophysical investigations of such complexes, excitation wavelengths are chosen to coincide with the absorption energy of a charge transfer transition, usually metal-to-ligand charge transfer (MLCT). This process involves the transition of the excited electron from the metal based HOMO orbital (normally a $d\pi$ orbital) to the ligand-based LUMO orbital (usually a delocalised $\pi\pi^*$ antibonding orbital) which is typically located on a polypyridyl ligand.

The formation of a $^3\text{MLCT}$ (triplet MLCT) excited state leads to large changes in the charge distribution of electron density in the excited state of the complex. In general $^3\text{MLCT}$ excited states are relatively long lived, with lifetimes in the range of nanoseconds to microseconds, facilitating their study with time-resolved spectroscopic methods on the fast and ultrafast timescales. This is partially due to their triplet nature, *i.e.* the initially formed singlet excited state undergoes a 'spin flip' to generate the energetically favoured triplet species with both unpaired electrons possessing the same spin orientation. This corresponds to the intersystem crossing process in Figure 1.1.1.1. Intersystem crossing is facilitated in photophysically active metal complexes due to efficient spin-orbit coupling mechanisms relaxing spin conservation selection rules owing to the presence of heavy metal atoms (*vide supra*). The lifetime of $^3\text{MLCT}$ excited states is also usually longer than IL (intraligand, transitions within the ligand manifold) or MC

(metal centred) excited states as a result of the ‘spin-forbidden’ transition required to return a triplet excited state to its singlet ground state electronic configuration.

1.1.3 Bimetallic and Polynuclear Complexes

In complexes containing more than one metal centre an intermetallic electronic interaction can occur after one metal centre is initially promoted to an excited state by the absorption of a photon.⁴ These processes are photoinduced interactions in chromophore-quencher systems. The excited state of one component can undergo photoinduced electron-transfer (PET) to or from the adjacent metal centre, resulting in charge-separated states (P^+ and Q^- or P^- and Q^+ in Figure 1.1.3.1); or photoinduced energy-transfer (PEnT) can occur such that the secondary metal fragment ends up in an excited state (Q^*) and the first one returns to its ground state (P , Figure 1.1.3.1).

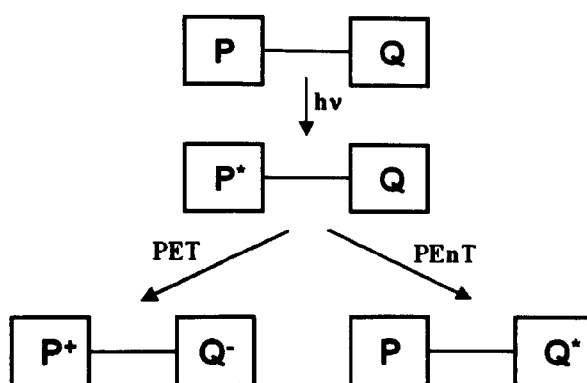


Figure 1.1.3.1: A supermolecule consisting of a photosensitiser (P) and a quencher (Q) may undergo excitation following photon absorption (P^*). PET leads to charge-separation (only one possible product shown) and PEnT leads to the formation of an excited state on the quencher (Q^*) component.

The absorption of a photon leads to the formation of a localised excited state. Photoinduced Electron Transfer (PET) from one metal centre to another can take place *via* a radiationless process, providing that the potential energy surfaces of the excited state system (e.g. P^* - Q in Figure 1.1.3.1) and the charge-separated system

(P⁺-Q⁻) overlap sufficiently and the charge-separated state is thermodynamically more stable than the excited state.⁵

Photoinduced Energy Transfer can occur in two ways: the Förster-type mechanism⁶ and the Dexter-type mechanism.⁷ The Förster mechanism operates at long-ranges and is based on Coulombic interactions. Energy is exchanged through space *via* coupling of donor and acceptor transition dipoles and is efficient when the emission spectrum of the donor is coincident with the absorption spectrum of the donor and there is good orientational alignment of the two transition dipoles. The rate and efficiency of Förster-type PEnT exhibits a sensitive dependence on the distance between the donor and acceptor chromophores:⁸

$$k_T = \frac{(R_0/r)^6}{\tau_D} = A \frac{\kappa^2 k_D}{r^6} J(E)$$

where k_T is the rate of energy transfer, τ_D is the decay time of the donor in the absence of the acceptor, R_0 is the Förster distance (the distance at which PEnT efficiency is 50%), r is the interchromophoric distance, κ^2 is the dipole-dipole orientational factor, k_d is the rate of excited state decay of the donor species in the absence of the acceptor and J is the overlap integral term.

The Dexter mechanism is based on exchange interactions and operates at shorter distances. Direct orbital overlap is necessary for efficient energy transfer *via* the Dexter mechanism. The prevalent mechanism of energy transfer can be influenced by the design of the supramolecular system.⁵

PEnT is of interest in the development of luminescent sensors and systems designed to harvest visible light. Making these interactions switchable, such that an interaction can be switched 'on' or 'off' reversibly and controllably under the influence of some external stimulus, is of great interest to provide mechanisms to control electron and energy transfer.⁹ This Thesis explores the use of solvatochromism and bridging ligand properties such as conjugation, structure and geometry to control photoinduced processes in polynuclear systems.

1.2 Solvatochromism

1.2.1 General Solvent-Solute Effects in UV/vis Absorption Spectra

Solvatochromism is defined as the change in intensity and/or position of a UV/visible absorption profile following a change in the constitution of the solvent medium.¹⁰ It is important to remember that UV/vis absorption spectroscopy probes the Franck-Condon electronic excited states populated instantaneously ($< 10^{-14}$ s) following absorption of a photon. It does not give any information on molecular dynamics and is only influenced by the immediate solvent sphere during the photon absorption event.

Two general trends are observed in solvent effects on absorption transition energies: positive solvatochromism and negative solvatochromism (Figure 1.2.1.1). Positive solvatochromism is a decrease in transition energy (or shift to longer wavelength) as the solvent 'polarity' increases (see §1.2.3). This occurs because the electronic transition accompanying the absorption of a photon causes a redistribution of electron density in the excited state, leading to an increase in the dipole moment. In coordination compounds this is commonly observed for MLCT and (to a lesser extent) intraligand (IL) π - π^* transitions. The greater ability of the surrounding solvent shell to stabilise the increased polarity of the excited state, relative to the ground state, leads to red-shifting of the absorption energy.

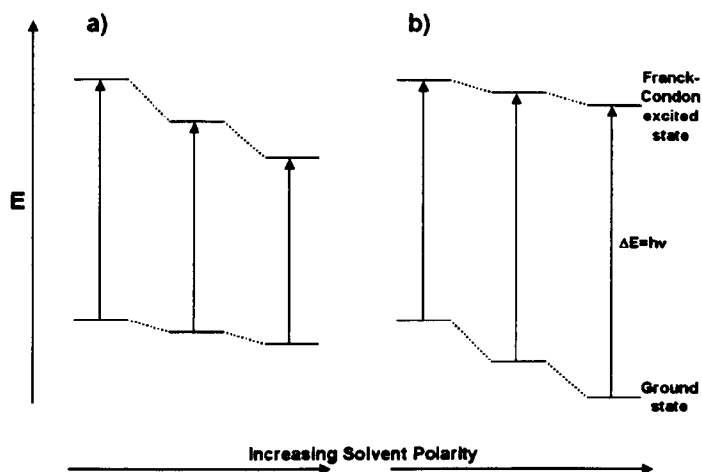


Figure 1.2.1.1: The effects of solvent-solute interactions on transition energies in optical absorption spectroscopy; a) is positive and b) is negative solvatochromism. Adapted from Ref.¹⁰

Negative solvatochromism is an increase in the transition energy (or shift to shorter wavelength) as the solvent ‘polarity’ increases. Here the electronic transition leads to a decrease in the dipole moment of the excited state. This is observed in systems with $n-\pi^*$ transitions.

1.2.2 General Solvent-Solute Effects in Luminescence Spectra

Emission spectroscopy probes much longer timescales than absorption spectroscopy (see §1.3). The solvent molecules align their dipoles with the excited state’s dipole by rotating. This lowers the energy of the excited state before emission of a photon and relaxation to the ground state (Figure 1.2.2.1).¹⁰ The more ‘polar’ the solvent, the greater the excited state stabilisation. Following photon emission the solvent dipoles are still aligned to that of the excited state. Thus the energy of the state formed following photon emission has a higher energy than the initial ground state. These factors lead to emission energies being lower than absorption energies and emission spectra being red-shifted in polar solvents.

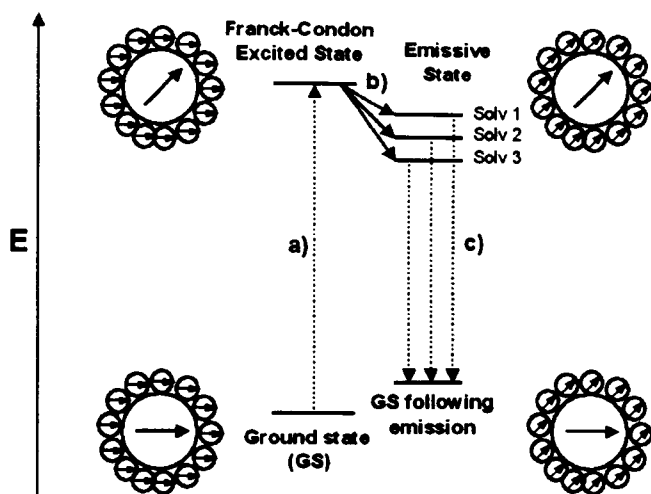


Figure 1.2.2.1: Solvent effects on luminescence spectroscopy. The dipole moments of the molecule (large arrow) and the solvent shell (small arrows) are shown. a) Absorption of a photon, b) solvent relaxation and c) emission. In terms of polarity Solv 3 > 2 > 1. Adapted from Ref.¹⁰

1.2.3 Specific Solvent-Solute Effects

Significant electronic interactions between the solute and the solvent shell can take place in certain situations. For example sites available for H-bonding or coordination may be present on the ligands, allowing Second Sphere Donor-Acceptor (SSDA) interactions to take place between the solvent shell and ligands. These specific effects have been studied in ammine and cyanide complexes,^{11,12} and result in spectroscopic properties which depend on the properties of the solvent.

Several systems have been introduced to quantify the ability of a solvent to participate in donor-acceptor interactions, including the Donor Number (D. N.) and Acceptor Number (A. N.) introduced by Gutmann.¹³ The D. N. is based on the molar reaction enthalpy in 1,2-dichloroethane for the formation of a 1:1 adduct between SbCl_5 and the added solvent as donor. It gives a measure of the ability of solvent molecules to donate an electron pair to SbCl_5 , and is used to describe H-bonding with (Lewis acidic) ammine complexes (Figure 1.2.3.1a).¹⁴

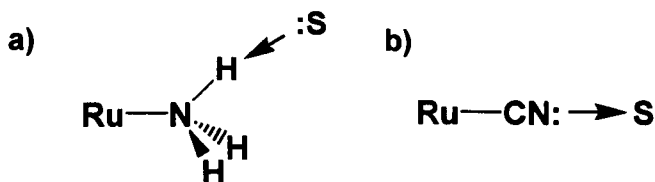


Figure 1.2.3.1: Two examples of specific effects in transition metal complexes. a) Electron-pair and H-bond donation to an ammine complex from the solvent, and b) a solvent molecule accepting electron density from a cyanide complex.

The Acceptor Number is taken as the chemical shift of the ^{31}P resonance of Et_3PO in the solvent relative to two reference measurements. Et_3PO in hexane is assigned A. N. = 0 and the $\text{Et}_3\text{PO}:\text{SbCl}_5$ adduct is taken as A. N. = 100. The Acceptor Number measures the ability of solvent molecules to act as electron-pair acceptors and is used to quantify specific effects with cyanide complexes (Figure 1.2.3.1b).¹⁵ Acceptor Numbers for common solvents are given below in Table 1.2.3.1.

Solvent	Acetone	Pyridine	(CH ₃) ₂ SO	CH ₃ CN	CH ₂ Cl ₂	CH ₃ OH	H ₂ O
Acceptor Number	12.5	14.2	19.3	19.3	20.4	41.3	54.8

Table 1.2.3.1: Gutmann Acceptor Numbers for selected solvents. The higher the Acceptor Number, the greater the solvent's ability to accept electron density from the ligand sphere.¹⁵

1.2.4 The Influence of Solvent on the Electronic Structure of Transition Metal Cyanide Complexes

The donor-acceptor interactions between transition metal cyanide complexes and solvent molecules perturb the electronic structure of the complexes, giving rise to solvent-dependence in the positions and profiles of their UV/visible absorption spectra. As the Acceptor Number of a solution increases, more electron density is donated from $\sigma(\text{CN})$ orbitals which are externally directed towards the solvent sphere into low-lying acceptor orbitals on the solvent (Figure 1.2.3.1b). The cyanide ligands become more able to accept π -electron density from the metal centre into $\pi^*(\text{CN})$ orbitals, stabilising $d\pi(\text{M})$ orbitals by enhancing $d\pi(\text{M})-\pi^*(\text{CN})$ mixing.¹⁵ This negative solvatochromism increases both the oxidation potential of the metal centre and transition energies between metal-centred orbitals and orbitals centred on spectator ligands (e.g. MLCT transition energies).

The effect is less pronounced in the emission spectra of cyanide complexes. In a ³MLCT excited state partial oxidation of the metal centre leads to electron density being shifted from 'CN' to 'M⁺', decreasing the available electron density for donor-acceptor interactions (§1.3). This decreases the extent of $d\pi(\text{M})-\pi^*(\text{CN})$ mixing which leads to the metal centred orbital energies showing less solvent-dependency.¹⁵

1.3 Spectroscopic and Electrochemical Methods Used in this Work

The analytical techniques employed in this Thesis are UV/vis absorption and luminescence spectroscopy, Fourier-transform infrared (FTIR), and time-resolved infrared (TRIR) spectroscopy and electrochemistry. These provide complementary

information on the electronic structure of the ground and excited states of transition metal complexes.

UV/visible absorption spectroscopy is a simple but powerful spectroscopic technique which provides information on the Franck-Condon excited states populated immediately following the absorption of a photon. As the timescale for photon absorption is very short compared to the timescales for molecular motion, the spectra obtained are representative of the average solvent shell surrounding the molecule prior to absorption (§1.2.1). The shape, intensity and solvent sensitivity of these bands provide information on the relative energies of transitions in metal complexes. The absorption profile obtained from UV/vis spectroscopy is crucial for determining the wavelength of ¹MLCT transitions for luminescence and TRIR spectroscopy. Insight into other electronic processes *e.g.* proximity of IL and MC states to MLCT transitions, and presence of IVCT transitions or multiple MLCT bands can also be gained.

Luminescence spectroscopy probes the photons emitted by the complex following excitation. The emissive electronic states are usually the lowest energy excited states in the system and the orbitals involved are usually the HOMO and LUMO. Both the energy and profile of the spectrum, and the lifetime of the emission depend on the electronic structure of the complex and its surrounding environment. The timescale of photon emission is longer than photon absorption (typically nanoseconds or microseconds for metal complexes), and the solvent shell has the opportunity to reorganise itself to solvate the excited state's dipole (§1.2.2, Figure 1.2.2.1). Excited state lifetimes of metal complexes usually follow the 'energy-gap law'.¹⁶ This is a rule-of-thumb which states, for *similar* complexes, as the energy of the emission decreases, the lifetime also decreases due to an increase in the rate of non-radiative deactivation of the emissive excited state.

Time-Correlated Single Photon Counting (TCSPC) is used to determine the lifetime or time-dependency of emission at particular excitation and emission wavelengths. This technique is very useful for probing complex time dynamics and for comparison with TRIR kinetic data. TCSPC data is often collected using a

'line-of-sight' type apparatus which measures the time elapsed between the excitation event (*e.g.* laser or lamp flash) and an emitted photon (of a selected wavelength) hitting the detector PMT.

Fourier-transform infrared spectroscopy (FTIR) is a standard analytical technique which enables spectra across the entire mid-infrared range (*ca.* 50 to 5000 cm^{-1}) to be measured rapidly. It utilises interferometry to generate interference patterns, which may be processed computationally using Fourier analysis to generate FTIR spectra very quickly (typically less than a second per scan). The information on bond vibrations obtained by FTIR spectroscopy is extremely useful for transition metal complexes containing CO and CN ligands. $\nu(\text{CO})$ and $\nu(\text{CN})$ bands have high oscillator strengths and narrow, sharp features in a part of the mid-infrared spectrum which is relatively unoccupied by other chemical groups (2100 – 1850 cm^{-1}).

Time-resolved infrared spectroscopy (TRIR) is a 'pump-probe' technique employing a combination of laser excitation and fast infrared detection. It allows the IR spectrum of metal excited states to be recorded down to the picosecond timescale.¹⁷ TRIR is particularly useful for the determination of transient molecular structure through the changes in vibrational band positions and profiles through the excitation process. The use of IR 'reporter' groups (such as CO and CN) with high oscillator strengths gives intense spectroscopic features, which are sensitive to the electron density of their surroundings. Information about the kinetics of transient formation and decay can also be obtained from TRIR spectroscopy. Further details on the PIRATE apparatus used for ps and ns-TRIR experiments in this Thesis are provided in Chapter 6.

There are some considerable advantages to using TRIR spectroscopy over luminescence spectroscopy for excited state studies of coordination compounds. These advantages are exploited throughout the remainder of this Thesis. TRIR is able to probe 'dark' (non-luminescent) excited states in luminescent complexes, as it is not reliant on the detection of emitted photons. For the same reason it may be used to monitor photophysical processes in real time. These attributes are used in Chapter 3 in particular. The study of excited states with very weak or absent

luminescence may also be performed and TRIR can offer insight into the extent of excited state localisation or delocalisation on the IR timescale (< 1 ps).¹⁸ These features are exploited in Chapter 4.

TRIR spectroscopy has been used to study the common classes of excited states of coordination compounds.^{19,20,21} The general findings are discussed briefly below in reference to IR reporters which are directly ligated to metal centres (*e.g.* CO and CN ligands). IR reporters which are not directly bonded to metal centres (*e.g.* amide-substituted bipyridine ligands) behave somewhat differently and are discussed in §1.4.1.1. Upon excitation the change in electronic structure of the metal centre will directly affect the $\nu(\text{CO})$ or $\nu(\text{CN})$ bands. TRIR spectra show the difference in absorption between the excited state and ground state spectra. Thus excited state bands are recorded as positive signals and depletions of ground state bands are shown as negative features (Figure 1.3.1).

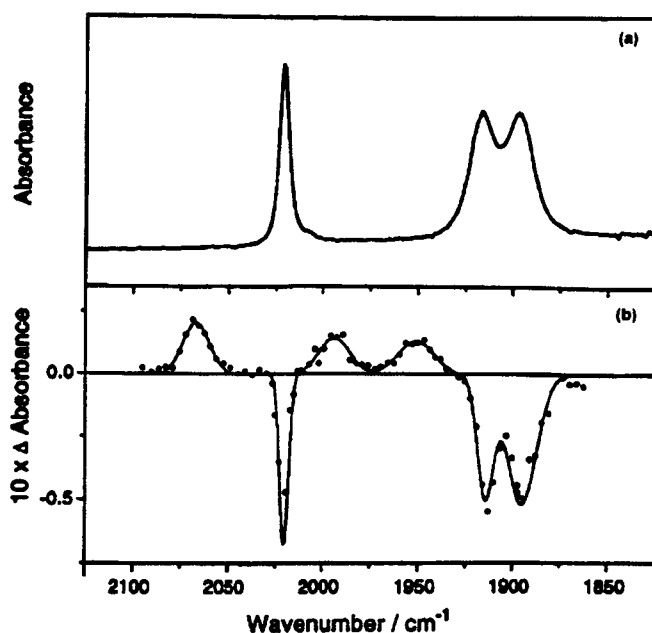


Figure 1.3.1: *a) The FTIR spectrum of $\text{fac-}[\text{ReCl}(\text{CO})_3(\text{bpy})]$ in $n\text{-PrCN}/n\text{-EtCN}$ (5:4 v/v); b) the TRIR spectrum of this solution at 135 K obtained 100 ns after 355 nm excitation. Bands below the axis represent bleaches from the ground state complex and bands above the axis represent new features arising from the excited state species. Adapted from Ref.²⁰*

Following the formation of an excited state which decreases the electron density at the metal centre (e.g. a $^3\text{MLCT}$ excited state) there is a shift of the $\nu(\text{CO})$ or $\nu(\text{CN})$ transient bands to higher energy compared to the ground state bands. Conversely the formation of an excited state which increases the electron density at the metal centre (e.g. a LMCT, ligand to metal charge transfer excited state) will shift $\nu(\text{CO})$ or $\nu(\text{CN})$ bands to lower energy compared to the ground state bands.

The extent of the shifts gives information on the degree of charge transfer in the excited state as well as indications of the energy gap between ground and excited states. This may help to identify the nature and location of the excited state in multichromophoric systems.

In general photoprocesses which do not change the electronic structure of the metal centre (such as the formation of ligand-centred excited states), lead to no change in the TRIR spectrum. However in the case of a π,π^* IL excited state, where the population of the ligand antibonding orbitals is slightly electron donating relative to the ground state, a small shift of the excited state $\nu(\text{CO})$ bands to lower energy is observed. This shift is small because the effect is considered to be of a secondary nature.

Several techniques are commonly used for the probing of electronic structure of electrochemically generated species. Cyclic voltammetry (CV) determines the potentials and thermodynamic reversibility of oxidation and reduction processes in the complex. This provides information on the absolute energies of the orbitals as opposed to the relative ordering and transition energies from absorption and emission spectroscopy. As oxidation removes electrons from the HOMO and reduction adds electrons to the LUMO, photophysics and electrochemistry can be used to probe the same states in different ways (*vide infra*).

Spectroelectrochemistry is the spectroscopic study of electrochemically generated species. The spectra of electrochemically generated compounds can be useful for comparison with spectra of transients produced through photoexcitation. UV/visible absorption and IR spectroelectrochemistry are two methods used by the supramolecular photochemistry community. Insights into the destination of

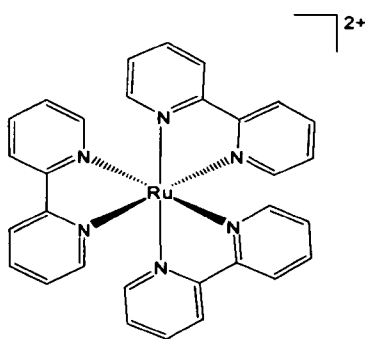
added electrons, and structural changes in complexes as a result of redox processes allow the comparison of the ‘redox’ electronic structure with the ‘spectroscopic’ electronic structure. Koopmans’ theorem treats the atomic or molecular system as a series of independent one-electron orbitals. The 1st ionisation energy is equivalent to the energy of the HOMO, and the results obtained from spectroscopy and electrochemistry may be the same.²² Koopmans’ theorem becomes less valid when there are significant changes in the electronic structure of the system upon adding or removing electrons, and when the difference in the timescale of optical and electrochemical processes (*i.e.* voltammetric vs. Franck-Condon timescales) has a significant impact on the electronic structure and properties of the system.

1.4 Previous Studies of Relevant Complexes and Supramolecular Systems

1.4.1 Monometallic Units

The modular approach to construction of the supramolecular systems in this Thesis is based on the use of the well-known complexes $[\text{Ru}(\text{bpy})_3]^{2+}$, $[\text{Ru}(\text{CN})_4(\text{bpy})]^{2-}$ and $[\text{ReCl}(\text{CO})_3(\text{bpy})]$, where bpy = 2,2’-bipyridine. A brief review of previous research into the spectroscopy, electrochemistry and photophysics of the widely studied $[\text{Ru}(\text{bpy})_3]^{2+}$ and $[\text{ReCl}(\text{CO})_3(\text{bpy})]$ complexes is presented here. $[\text{Ru}(\text{CN})_4(\text{bpy})]^{2-}$ has been less widely studied previously and is discussed at length in Chapter 2.

1.4.1.1 $[\text{Ru}(\text{bpy})_3]^{2+}$ and related complexes



The photophysics, electrochemistry and spectroscopy of $[\text{Ru}(\text{bpy})_3]^{2+}$ and derivatives of it have been widely studied.²³ Its chemical, photochemical and electrochemical stability and its reactive, energetic, emissive and long-lived ³MLCT excited state make it a good photosensitiser. It is easily synthesised and its

electronic structure can be manipulated to a significant extent through modification of the bipyridyl ligands.²³

Most mononuclear complexes incorporating the $[\text{Ru}(\text{bpy})_3]^{2+}$ motif have redox and spectroscopic properties similar to the parent complex. The absorption spectrum of $[\text{Ru}(\text{bpy})_3]^{2+}$ in CH_3CN has intense bands arising from IL $\pi\text{-}\pi^*$ transitions at 185 and 285 nm. Bands at 240 and 450 nm are due to $^1\text{MLCT}$ transitions, and shoulders at 322 and 344 nm are assigned to metal-centred (MC) transitions. The MLCT bands show weak positive solvatochromism, with the absorption wavelengths of the long wavelength band ranging between 450 and 455 nm.²² The addition of electron-withdrawing substituents such as amides and esters at the 4,4' positions on the substituted bipyridyl rings, leads to the MLCT bands being observed at longer wavelengths. These ligands are the ultimate electron-acceptors in MLCT transitions.²⁴ This is due to the stabilisation of the ligand centred π^* orbitals by the substituents.²⁵ Absorption wavelengths for the low energy transitions of complexes relevant to this work are shown in Table 1.4.1.1.1.

Complex	Solvent	$\lambda_{\text{abs}} / \text{nm}$	$\lambda_{\text{abs}} / \text{nm}$	$\lambda_{\text{abs}} / \text{nm}$
$[\text{Ru}(\text{bpy})_3]^{2+}$	CH_3CN	344	415	450
$[\text{Ru}(4,4'-(\text{CO}_2\text{Et})_2\text{bpy})_3]^{2+}$	DMF	362	442	471
$[\text{Ru}(4,4'-(\text{CONEt}_2)_2\text{bpy})_3]^{2+}$	DMF	-	435	459

Table 1.4.1.1.1: Absorption wavelengths for low-energy transitions of $[\text{Ru}(\text{bpy})_3]$ -type complexes relevant to this work. Adapted from Refs.^{20,21}

The emission spectrum of $[\text{Ru}(\text{bpy})_3]^{2+}$ in CH_3CN solution at room temperature has components at 615 nm and 650 nm, with an emission lifetime of *ca.* 850 ns, and a quantum yield of *ca.* 0.07.²³ Emission occurs from a manifold of three close-lying $^3\text{MLCT}$ states (10 and 61 cm^{-1} apart from each other) in thermal equilibrium with each other, which may be effectively treated as a single state. The solvent-dependence of the emission energies, lifetimes and quantum yields of $[\text{Ru}(\text{bpy})_3]^{2+}$ have been investigated at room temperature.¹⁷ Emission wavelengths were found to vary between 605 nm (CH_2Cl_2) and 625 nm (H_2O). The dependence of emission wavelength, emission lifetimes and quantum yields (Table 1.4.1.1.2) were found to

be in accordance with the energy-gap law (§1.3). The emission properties of complexes relevant to this work are shown in Table 1.4.1.1.2.

Complex	Solvent	λ_{em} / nm	Lifetime / ns	Quantum Yield
$[\text{Ru}(\text{bpy})_3]^{2+}$	CH_3CN	615	855	0.07
$[\text{Ru}(\text{bpy})_3]^{2+}$	H_2O	625	630	0.042
$[\text{Ru}(4,4'-(\text{CO}_2\text{Et})_2\text{bpy})_3]^{2+}$	CH_3CN	607	2230	0.3

Table 1.4.1.1.2: Emission properties of complexes relevant to this work. Adapted from Refs.^{17,20,21}

Cyclic voltammetry shows one reversible oxidation for the $\text{Ru}^{\text{II/III}}$ couple and a series of bpy-based reductions. The amount, reduction potential and reversibility of these reductions depends on the ligand identity and experimental conditions (*e.g.* temperature). Several reductions have been observed for complexes with electron-withdrawing substituents (*e.g.* esters and amides) on the bpy ligands.²⁵ These substituents stabilise low formal oxidation states in the complexes. Table 1.4.1.1.3 shows redox potentials for $[\text{Ru}(\text{bpy})_3]^{2+}$ complexes relevant to this work.

Complex	Solvent	$E_{1/2,ox}$ / V	$E_{1/2, red1}$ / V	$E_{1/2, red2}$ / V	$E_{1/2, red3}$ / V
$[\text{Ru}(\text{bpy})_3]^{2+}$	CH_3CN	+0.90	-1.72	-1.93	-2.15
$[\text{Ru}(4,4'-(\text{CO}_2\text{Et})_2\text{bpy})_3]^{2+}$	DMF	+1.01	-1.31	-1.43	-1.61
$[\text{Ru}(4,4'-(\text{CONEt}_2)_2\text{bpy})_3]^{2+}$	DMF	+0.93	-1.54	-1.68	-1.85

Table 1.4.1.1.3: Redox potentials of complexes relevant to this work. All potentials are quoted vs. Fc/Fc^+ . Adapted from Refs.^{23,25}

A number of TRIR studies of Ru(II) polypyridine complexes have been conducted.²⁶ Ester and amide $\nu(\text{CO})$ bands of ligands such as $(4,4'-(\text{CO}_2\text{Et})_2\text{bpy})$ and $(4,4'-(\text{CONEt}_2)_2\text{bpy})$ provide a spectroscopic probe of the electronic structure of the bpy system. The magnitude of the excited state peak shift carries important information on the extent of charge transfer, the HOMO-LUMO energy gap and the degree of localisation of the excited state, as observed on the IR timescale

(§1.3). TRIR spectra are also informative on the identity of the ligand accepting the electron density in an MLCT excited state.²⁷ Information on the energy gap between ground and lowest lying excited state energies has also been extracted from TRIR spectra (§1.4.1.3).

Figure 1.4.1.1.1 shows the excited state spectra obtained for the complexes, $[\text{Ru}(\text{bpy})_2(4,4'-(\text{CO}_2\text{Et})_2\text{bpy})]^{2+}$, $[\text{Ru}(\text{bpy})(4,4'-(\text{CO}_2\text{Et})_2\text{bpy})_2]^{2+}$ and $[\text{Ru}(\text{bpy})_2(4,4'-(\text{CONEt}_2)_2\text{bpy})]^{2+}$ in CH_3CN . In each of these complexes the lowest energy excited state is $(\text{Ru}^{\text{III}})((4,4'-(\text{COX})_2\text{bpy})^*)$.²³ The changes in the spectral profile of the band holds information about the electronic structure of the excited states.

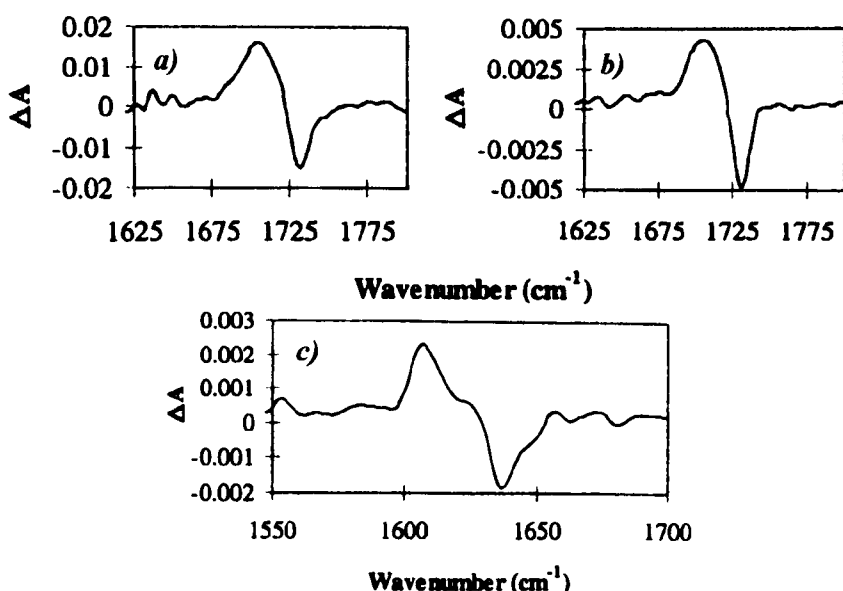


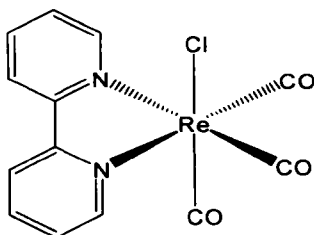
Figure 1.4.1.1.1: Difference TRIR spectra obtained 0 – 100 ns after 355 nm excitation; a) $[\text{Ru}(\text{bpy})_2(4,4'-(\text{CO}_2\text{Et})_2\text{bpy})]^{2+}$, b) $[\text{Ru}(\text{bpy})(4,4'-(\text{CO}_2\text{Et})_2\text{bpy})_2]^{2+}$ and c) $[\text{Ru}(\text{bpy})_2(4,4'-(\text{CONEt}_2)_2\text{bpy})]^{2+}$ in CH_3CN . A negative band indicates a decrease in absorbance and a positive band indicates an increase. Adapted from Ref.²⁴

The excited state shifts of the spectra in Figure 1.4.1.1.1 a) and b) are identical. As a) contains one $(4,4'-(\text{CO}_2\text{Et})_2\text{bpy})$ ligand and b) contains two, this is consistent with the excited electron being localised on one of the $(4,4'-(\text{CO}_2\text{Et})_2\text{bpy})$ ligands.²⁴ If it were delocalised, the excited state shift in b) would only be half as

large as *a*) as the additional electron density would be distributed over both (4,4'-(CO₂Et)₂bpy) ligands. The excited state shift in Figure 1.4.1.1.1 *b*) is approximately twice that of *c*). The two complexes are both of the type [Ru(bpy)₂(4,4'-(COX)₂bpy)]²⁺, with *a*) X=OEt and *b*) X=NEt₂. The smaller excited state shift in the amide-substituted complex indicates that there is a smaller change in electron density in the excited state of *c*) than in *a*). This is consistent with a greater extent of charge transfer in [Ru(bpy)₂(4,4'-(CO₂Et)₂bpy)]²⁺ than [Ru(bpy)₂(4,4'-(CONEt₂)₂bpy)]²⁺ as the amides are less electron-withdrawing than the esters.

1.4.1.2 *fac*-[ReCl(CO)₃(bpy)]

N. B.: In this Thesis all rhenium (I) tricarbonyl complexes referred to will be facial isomers and the “*fac*” notation may not be explicitly stated but is implied in all cases.



The photophysics, electrochemistry and spectroscopy of *fac*-[ReCl(CO)₃(bpy)] and derivatives of it have been studied extensively in the literature, albeit to a lesser extent than polypyridyl complexes of ruthenium (II).²⁸ In a similar way to [Ru(bpy)₃]²⁺, rhenium (I) complexes of bpy also exhibit relative chemical, photochemical and electrochemical stability, although the carbonyl groups are labile under certain conditions. [ReCl(CO)₃(bpy)] has a reactive, energetic, emissive and long-lived ³MLCT excited state making it a good photosensitiser. It is easily synthesised and its electronic structure can be manipulated to a significant extent through modification of the pyridyl ligands. Key differences with ruthenium *tris*-bipyridyls is the option of adding further ancillary ligands through substitution of carbonyl groups and the visibility of CO groups in IR and Raman vibrational spectra. This means that [ReCl(CO)₃(bpy)]-based systems require no further modification to act as spectroscopic reporters. To this end it is a key advantage of this system over other common transition metal complexes that the complex possesses carbonyl ligands which are directly ligated to the metal centre and are

able to act as sensitive reporters of electronic density. This effect is exploited in Chapters 3 and 4 of this Thesis.

The absorption spectrum of $[\text{ReCl}(\text{CO})_3(\text{bpy})]$ in CH_3CN has bands arising from IL $\pi\text{-}\pi^*$ transitions below and around 300 nm. The lowest energy absorption maximum is in the visible region of the spectrum at 370 nm and arises from a $d\pi(\text{Re}) \rightarrow \pi^*(\text{bpy})$ $^1\text{MLCT}$ transition. The $^1\text{MLCT}$ band shows weak positive solvatochromism, with the absorption wavelengths of the long wavelength absorption ranging between 370 and 384 nm in CH_2Cl_2 .²⁹ The ultimate electron-acceptor in MLCT transitions of $[\text{ReCl}(\text{CO})_3(\text{bpy})]$ is the sole polypyridyl ligand and there is no debate over excited state locus and timescale of localisation due to the lack of multiple polypyridyl ligands. This is in contrast to scientific investigations of $[\text{Ru}(\text{bpy})_3]^{2+}$ (*vide supra*).

The emission spectrum of $[\text{ReCl}(\text{CO})_3(\text{bpy})]$ in CH_3CN solution at room temperature has a maximum of 612 nm with an emission lifetime of *ca.* 25 ns and a quantum yield of *ca.* 0.06.^{29,30} The broad, featureless emission profile is indicative of $^3\text{MLCT}$ emission from the energetically lowest-lying $d\pi(\text{Re}) \rightarrow \pi^*(\text{bpy})$ excited state. The solvent-dependence of the emission energies and lifetimes of $[\text{ReCl}(\text{CO})_3(\text{bpy})]$ have been investigated at room temperature, although the sparing solubility of the complex prevents its study in most polar solvents. Emission wavelengths were found to be essentially invariant in CH_2Cl_2 and CH_3CN , although lifetimes were found to be longer in CH_3CN (50 ns) than in CH_2Cl_2 (25 ns).²⁹

Cyclic voltammetry of $[\text{ReCl}(\text{CO})_3(\text{bpy})]$ in CH_3CN shows one irreversible oxidation ($E_p = +1.32$ V *vs* SCE) for the Re^{VII} couple, and one reversible bpy-based reduction ($E_{1/2} = -1.35$ V *vs* SCE).²⁹

A number of investigations have utilised the IR reporting properties of $[\text{ReCl}(\text{CO})_3(\text{bpy})]$ between 1850 and 2100 cm^{-1} and relatively long excited state lifetimes to study its ground state properties using FTIR and its excited state properties using TRIR spectroscopy (see Figure 1.3.1).^{30,31} In CH_3CN , the ground state complex has FTIR bands at 2023, 1917 and 1899 cm^{-1} . The IR band profile

results from the C_s symmetry of the complex, which gives rise to three infrared-active $\nu(\text{CO})$ modes [$A'(1) + A'(2) + A''$]. Upon formation of the $^3\text{MLCT}$ excited state the parent bands are bleached and three new bands are formed at 2069, 1990 and 1957 cm^{-1} .³² These results are closely comparable with those measured in CH_2Cl_2 ,³³ in keeping with the similarity of other spectroscopic and photophysical properties of $[\text{ReCl}(\text{CO})_3(\text{bpy})]$ in low A. N. solvents. Excited state shifts for rhenium (I) tricarbonyl complexes were later shown by both theoretical and experimental approaches (see §1.4.1.3) to be non-trivial, with the ordering of ground and excited state IR bands being significantly different (*vide infra*).

1.4.1.3 Other Monometallic Complexes

An interesting extension to conventional pump-probe spectroscopy of rhenium (I) complexes has recently been demonstrated by Bredenbeck *et al.* in a study of $[\text{ReCl}(\text{CO})_3(4,4'-(\text{CH}_3)_2\text{-bpy})]$.³⁴ Using three laser pulses (one to excite the molecule into an electronically excited state and the other two to label/excite and probe vibrational states), they have performed both labelling and hole-burning 't2D-IR' experiments which have afforded considerable insight into the nature of the bands present in the ground and excited state infrared spectra of rhenium (I) tricarbonyl complexes (Figure 1.4.1.3.1).

Their findings reinforced previous experimental and theoretical work carried out by Dattelbaum *et al.* (*vide infra*) which suggested that the ordering of ground and excited state bands in the infrared spectra were not straightforward. Some bands were shifted to a much greater extent than others, with $\Delta\nu_{\text{CO}(\text{Excited State})} A'(1) > A'(2) > A''$ (*vide infra*).³⁵ The study by Dattelbaum *et al.* relating ground-to-excited state energy gap to $\Delta\nu_{\text{CO}}$ shift in the complexes examined on the complexes *fac*- $[\text{Re}(4,4'\text{-X}_2\text{-bpy})(\text{CO})_3(4\text{-EtPy})]^+$ (where X is H, CH_3 , OCH_3 , or CO_2Et ; 4-EtPy is 4-ethylpyridine). Systematic variations in $\Delta\nu_{\text{CO}}$ were observed with the excited-to-ground state energy gap, derived from a Franck-Condon analysis of emission spectra. The energy gap was tuned using the X_2 substituents on the 4,4'-substituted bpy ligand. It was found that variations in $\nu_{\text{CO}(\text{Ground State})}$ due to differences in backbonding in the complexes are small. A pronounced trend in $\nu_{\text{CO}(\text{Excited State})}$ was observed, as the $\nu_{\text{CO}(\text{Excited State})}$ wavenumber decreased with

increasing energy gap. The mode specific manner of the variations in ground-to-excited state band shifts were also evaluated (*vide supra*), with $\Delta\nu_{\text{CO(ES-GS)}} A'(1) > A'(2) > A''$.³⁵

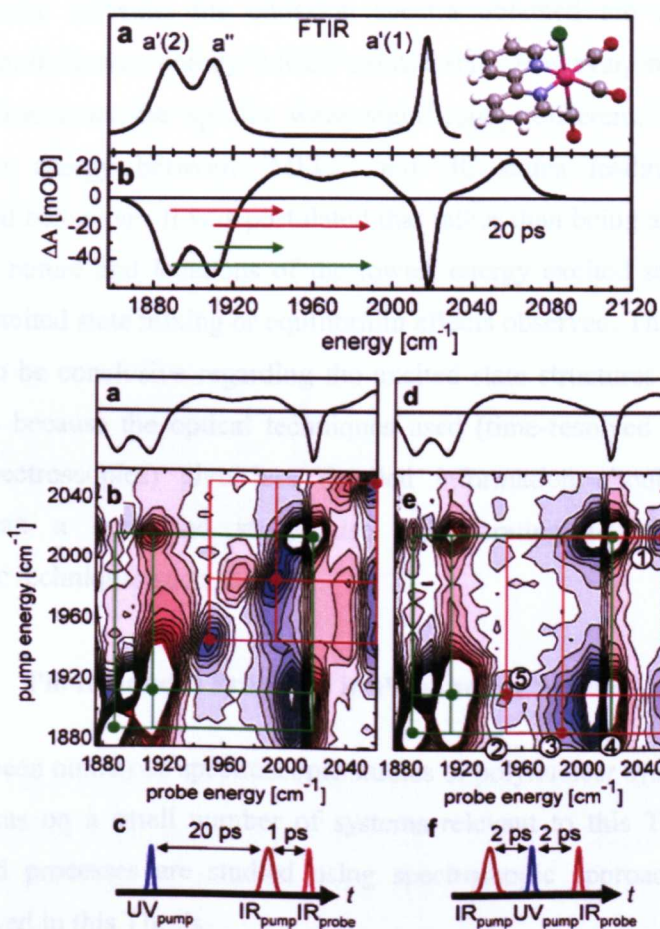


Figure 1.4.1.3.1: Top: a) FTIR and b) 1-D ps-TRIR spectrum (at 20 ps after excitation) of $[\text{ReCl}(\text{CO})_3((\text{CH}_3)_2\text{-bpy})]$ with previous (red) and new (green) excited state assignments. Bottom: 2D-IR spectrum (at 2 ps after excitation) of $[\text{ReCl}(\text{CO})_3((\text{CH}_3)_2\text{-bpy})]$ with cross-correlation peaks identified from the two different pulse sequences employed (left and right). Adapted from Ref.³⁴

A recent example of a photophysical investigation into a complex with a solvent switchable excited state type was demonstrated by Pomestchenko *et al.*³⁶ In this study a multichromophoric platinum (II) complex, $[\text{Pt}(\text{dbbpy})(\text{C}\equiv\text{C-nap})_2]$, where dbbpy = 4,4'-(di-*tert*-butyl)-2,2'-bipyridine and C≡C-nap = 1-ethynyl-naphthalene, was studied in four different solvent environments. As the $d\pi(\text{Pt}) \rightarrow \pi^*(\text{dbbpy})$

MLCT transitions in this complex exhibited negative solvatochromism, increasing solvent polarity raised the energy of the $^3\text{MLCT}$ state.

In low polarity solvents, the emission spectra obtained are consistent with emission from the lowest energy $^3\text{MLCT}$ excited state. However, in higher polarity solvent environments the spectra were significantly different, with the close proximity in energy between $^3\text{MLCT}$ and ^3IL states leading to different photophysical behaviour. It was postulated that rather than being a simple ‘switch over’ of the nature and locations of the lowest energy excited state, there were significant excited state mixing or equilibrium effects observed. The authors found it difficult to be conclusive regarding the excited state structures observed. This was perhaps because the optical techniques used (time-resolved absorption and emission spectroscopies) give less detailed information about excited state structure than a combined study also incorporating transient vibrational spectroscopic techniques such as TRIR.

1.4.2 Photoinduced Processes in Polynuclear Systems

There have been numerous spectroscopic studies of polynuclear systems³⁷ but here we shall focus on a small number of systems relevant to this Thesis in which photoinduced processes are studied using spectroscopic approaches similar to those employed in this Thesis.

1.4.2.1 Polypyridyl-linked systems

An interesting study of PEnT in a bimetallic Ru(II)/Re(I) system bridged by a non-symmetric polypyridyl ligand with two chemically different binding sites was reported by Schoonover and co-workers.³⁸ The isomeric complexes $[(\text{bpy})_2\text{Ru-AB-Re}(\text{CO})_3\text{Cl}]$ (**RuABRe**) and $[(\text{OC})_3\text{ClRe-AB-Ru}(\text{bpy})_2]$ (**ReABRu**, where AB = 2,2':3',2'':6'',2'''-quaterpyridine) were prepared and studied by luminescence and TRIR spectroscopy. The two binding sites, A and B are inequivalent with B being more sterically hindered (Figure 1.4.2.1.1).

From an analysis of emission lifetimes it had been previously demonstrated that at room temperature the emission observed in the **RuABRe** isomer was Ru-based and for **ReABRu** it was Re-based. However this result was not definitive as it relied on emission lifetime measurements which may have been influenced by an excited state equilibrium in the **ReABRu** case, raising the possibility that the Ru-based excited state was lower in both cases. With the emission results proving to be ambiguous, TRIR spectroscopy was employed to probe the excited states involved in PEnT in more detail.

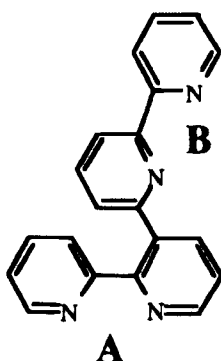


Figure 1.4.2.1.1: The ligand AB.

For the complex **RuABRe**, ps and ns-TRIR spectroscopy gave equivalent spectra, with $\nu(\text{CO})$ excited state bands at 1899, 1921 and 2023 cm^{-1} . These were shifted to lower wavenumber than the FTIR bands recorded for the ground state complex at 1888, 1910 and 2016 cm^{-1} . The shift of the Re-based $\nu(\text{CO})$ bands to lower wavenumber is consistent with the formation of a Ru-based $^3\text{MLCT}$ excited state, as the rhenium centre is reduced by the additional electron density on the bridging ligand. The excited state lifetime was measured to be *ca.* 400 ns.³⁸

The isomer **ReABRu** showed differences in its ps and ns-TRIR spectra. The TRIR spectrum at 100 ps contained ground-state bleaches at 1902, 1922 and 2028 cm^{-1} and excited state bands at 1892, 1912 and 2018 cm^{-1} but also revealed the presence of a broad positive feature near 1965 cm^{-1} (see Figure 1.4.2.1.1). This is consistent with both Re-based and Ru-based $^3\text{MLCT}$ excited states being present at early times - with a statistical mixture of the two transient species present in the ps-TRIR spectrum. Interestingly luminescence spectroscopy only detected the presence of a Re-based $^3\text{MLCT}$ excited state as the emission lifetime (*ca.* 20 ns) is

determined largely by the non-radiative decay rate of the Re-based transient. This highlights the ‘invisibility’ of some photophysical processes and excited states to luminescence spectroscopy.³⁸

This case study illustrates the utility of TRIR in the probing and assigning of excited states and photophysical processes, even with only one of the two metal centres present possessing an IR active reporter group. The polynuclear complexes in this Thesis are designed with reporter groups on both metal centres, leading to a potentially richer data set when interpreting and analysing the photophysical processes occurring.

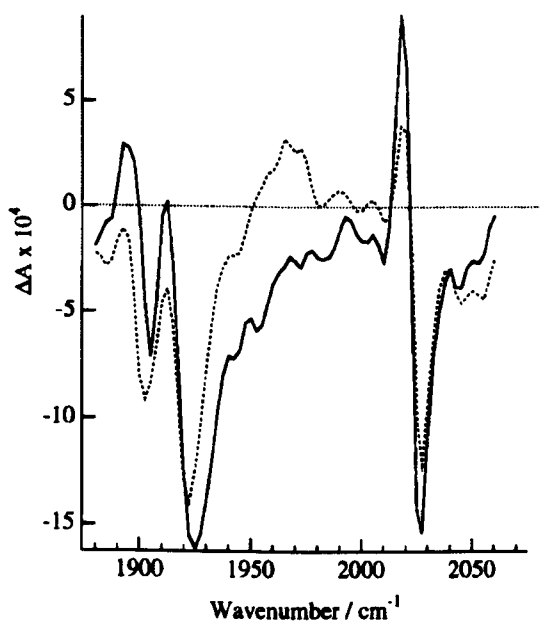


Figure 1.4.2.1.1: TRIR difference spectra of RuABRe (solid line) and ReABRu (dotted line) 100 ps after 405 nm excitation in CH₃CN. Reproduced from Ref.³⁸

Whilst not directly related to the systems described in this Thesis, the reader is directed to an excellent review of the use of ruthenium (II) bipyridine complexes in supramolecular systems by Balzani *et al.*, which highlights the current state of the art in supramolecular machine and device preparation. This perhaps represents the level of intermolecular interaction which can be aimed for in the future with the prospective device components contained in this Thesis.³⁹

1.4.2.2 CN linked systems

An interesting use of emission, transient absorption and TRIR spectroscopies to study energy transfer in bimetallic ruthenium (II) and rhenium (I) complexes was presented by Schoonover *et al.* and Thompson *et al.* over the course of two publications.^{40,41} In their study, ostensibly the first using ps and ns-TRIR to probe intermetallic PEnT, the metal centres were linked using a cyanide bridge. Due to the asymmetry of the cyanide linkage two isomers are possible and the study focussed on comparing the photophysical properties of these two linkage isomers. Previous studies found that energy transfer characteristics in a homobimetallic complex $[(\text{NC})(\text{bpy})_2\text{Ru}(\text{CN})\text{Ru}(\text{bpy})_2(\text{CN})]$ were strongly influenced by the redox asymmetry induced by the bridge.⁴² In both complexes $[(\text{phen})(\text{OC})_3\text{Re}(\text{CN})\text{Ru}(\text{bpy})_2(\text{CN})]^+$ and $[(\text{phen})(\text{OC})_3\text{Re}(\text{NC})\text{Ru}(\text{bpy})_2(\text{CN})]^+$ efficient Re \rightarrow Ru PEnT was found to occur. Multiple excited state species were generated and this was attributed to the unselective excitation of either terminus upon absorption of 355 nm laser light. Unfortunately the study did not include a complete TRIR dataset for both linkage isomers and is not described in detail here.

There have also been a few other noteworthy studies using TRIR to study electron transfer in cyanide-bridged mixed valence bimetallic complexes of d^6 metals such as $[(\text{NC})_5\text{Fe}^{\text{II}}(\text{CN})\text{Ru}^{\text{III}}(\text{NH}_3)_5]^-$ and $[(\text{NC})_5\text{Os}^{\text{II}}(\text{CN})\text{Ru}^{\text{III}}(\text{NH}_3)_5]^-$.^{43,44} In these studies, optical excitation incited forward electron transfer upon population of Franck-Condon excited states, with ultrafast TRIR used to monitor the back electron-transfer process. The focus of these studies by Gilbert and co-workers was to probe the environment-solute coupling through analysis of the spectral dynamics, which is outside of the scope of this work.

1.5 Closing Points

This Chapter has described some of the basic theory supporting the content of later Chapters of this Thesis. The key concepts to take forwards are listed below.

- Supramolecular photophysics may involve the interaction of a potentially unlimited number of components comprised of coordination compounds.

- Transition metal complexes with polypyridyl ligands often exhibit long-lived triplet MLCT excited states which may be utilised as the first step in a supramolecular photoprocess.
- Optical spectroscopic techniques such as UV/vis absorption and luminescence spectroscopy, probe molecular electronic structure and its interaction with the solvent environment on different timescales.
- The prevalent mechanism of photoinduced interaction in a supramolecular system may be influenced by the choice of chromophores and design of the linkage between them.
- Förster-type PEnT is extremely sensitive to the distance between and relative orientation of donor and acceptor chromophores.
- Solvatochromism may have a major effect on the energy levels of transition metal complexes.
- The ability of a solvent to exhibit SSDA interactions may be quantified using the Gutmann Acceptor Number theory.
- Metal-cyanide complexes display remarkably strong negative solvatochromism due to specific solvent-solute interactions.
- Some ligands or chemical groups can act as efficient reporters of electronic structure information in TRIR spectroscopic experiments, potentially enabling the monitoring of PEnT and/or PET *in situ*.
- Having access to multiple spectroscopic techniques and/or reporter groups increases the amount of spectral information available and allows a more complete understanding of the systems under study.
- Luminescence spectroscopy is a powerful tool when the emitted photon carries desired information about the photophysics of the system being studied. However the ‘invisibility’ some photoprocesses to luminescence - ‘dark’, non-radiative or photonless resonance processes – renders the technique less suitable for their study.
- TRIR spectroscopy is a powerful tool for elucidating electronic structure of excited states when ‘vibrational reporter’ chemical groups are present.
- The combined use of luminescence and TRIR spectroscopies may reinforce the findings of each other and reveal subtleties that either technique may have not have raised.

- The complexes $[\text{Ru}(\text{bpy})_3]^{2+}$ and *fac*- $[\text{ReCl}(\text{CO})_3(\text{bpy})]$ have well-studied and characterised excited states which are amenable to incorporation into supramolecular systems.
- Photophysical study of coordination compounds with spectrally similar or multiple chromophores may produce more complicated or convoluted spectral or kinetic information due to unselective excitation producing multiple excited state species.
- Transition metal complexes may be incorporated into larger supramolecular devices.

Chapter 2 will present a study of the $[\text{Ru}(\text{CN})_4(\text{NN})]^{2-}$ (where (NN) = bidentate α -diimine) family of metal complexes. Chapter 3 will present a study of weakly interacting bimetallic supramolecular systems designed to undergo through-space (Förster) PEnT. Chapter 4 will present a study of strongly interacting bimetallic complexes designed to undergo through-bond energy / electron transfer. Chapter 5 will provide an overall summary, discussion and closing points and presents some interesting future directions for research in this area. Chapter 6 will describe the experimental and theoretical approaches used in this Thesis.

1.6 References

- ¹ J. M. Lehn, *Science*, 1985, **227**, 849.
- ² J. K. McCusker, *Acc. Chem. Res.*, 2003, **36**, 876.
- ³ D. J. Liard, M. Busby, P. Matousek, M. Towrie and A. Vlcek, *J. Phys. Chem. A*, 2004, **108**, 2363.
- ⁴ V. Balzani and F. Scandola, *Supramolecular Photochemistry*, Ellis Horwood, 1991.
- ⁵ J.-P. Sauvage, J.-P. Collin, J.-C. Chambron, S. Guillerez, C. Coudret, V. Balzani, F. Barigelletti, L. De Cola and L. Flamigni, *Chem. Rev.*, 1994, **94**, 993.
- ⁶ T. Förster, *Disc. Faraday Soc.*, 1959, **27**, 7.
- ⁷ D. L. Dexter, *J. Chem. Phys.*, 1953, **21**, 836.
- ⁸ J. R. Lakowicz, *Principles of Fluorescence Spectroscopy*, Kluwer Academic/Plenum Publishers, 2nd edn., 1999.
- ⁹ M. D. Ward, *Chem. Ind.*, 1997, 640.
- ¹⁰ S. Nigam and S. Butan, *App. Spec.*, 2001, **55**, 362A.
- ¹¹ B. F. Shraydeh and J. Burgess, *Chem. Month.*, 1993, **124**, 1434.
- ¹² J. C. Curtis, Sullivan B. P. and Meyer, T.J., *Inorg. Chem.*, 1983, 224.
- ¹³ V. Gutmann, *The Donor-Acceptor Approach to Molecular Interactions*, Plenum Press, 1978.
- ¹⁴ P. Y. Chen and T. J. Meyer, *Chem. Rev.*, 1998, **98**, 1439.
- ¹⁵ C. J. Timpson, C. A. Bigozzi, B. P. Sullivan, E. M. Kober and T. J. Meyer, *J. Phys. Chem.*, 1996, **100**, 2915.
- ¹⁶ J. V. Caspar and T. J. Meyer, *J. Am. Chem. Soc.*, 1983, 105.
- ¹⁷ D. C. Grills and M. W. George, in *Handbook of Vibrational Spectroscopy*, ed. J. M. Chalmers and P. R. Griffiths, John Wiley & Sons Ltd., Chichester, 2002, vol. 1, p. 677.
- ¹⁸ K. D. Demadis, C. M. Hartshorn and T. J. Meyer, *Chem. Rev.*, 2001, **101**, 2655.
- ¹⁹ M. K. Kuimova, W. Z. Alsindi, J. Dyer, D. C. Grills, O. S. Jina, P. Matousek, A. W. Parker, P. Portius, X. Z. Sun, M. Towrie, C. Wilson, J. Yang and M. W. George, *J. Chem. Soc. Dalton Trans.*, 2003, 3996.
- ²⁰ M. W. George and J. J. Turner, *Coord. Chem. Rev.*, 1998, **177**, 201.
- ²¹ J. R. Schoonover, C. A. Bigozzi and T. J. Meyer, *Coord. Chem. Rev.*, 1997, **165**, 239.
- ²² A. Vlcek, *Coord. Chem. Rev.*, 1982, **43**, 39.
- ²³ A. Juris, V. Balzani, F. Barigelletti, S. Campagna, P. Belser and A. von Zelewsky, *Coord. Chem. Rev.*, 1988, **84**, 85.
- ²⁴ K. M. Omberg, G. D. Smith, D. A. Kavaliunas, P. Y. Chen, J. A. Treadway, J. R. Schoonover, R. A. Palmer and T. J. Meyer, *Inorg. Chem.*, 1999, **38**, 951.
- ²⁵ C. M. Elliot and E. J. Hershenhart, *J. Am. Chem. Soc.*, 1982, **104**, 7519.
- ²⁶ See for example: P. Y. Chen, R. A. Palmer and T. J. Meyer, *J. Phys. Chem. A*, 1998, **102**, 3042; J. R. Schoonover, *Laser Chem.*, 1999, **19**, 263; P. Y. Chen, K. M. Omberg, D. A. Kavaliunas, J. A. Treadway, R. A. Palmer and T. J. Meyer, *Inorg. Chem.*, 1997, **36**, 954; I. P. Clark, M. W. George and J. J. Turner, *J. Phys. Chem. A*, 1997, **101**, 8367; A. E. Curtright and J. K. McCusker, *J. Phys.*

-
- Chem. A*, 1999, **103**, 7032; D. M. Dattelbaum, K. M. Omberg, J. R. Schoonover, R. L. Martin and T. J. Meyer, *Inorg. Chem.*, 2002, **41**, 6071; D. M. Dattelbaum and T. J. Meyer, *J. Phys. Chem. A*, 2002, **106**, 4519; K. M. Omberg, J. R. Schoonover, J. A. Treadway, R. M. Leasure, R. B. Dyer and T. J. Meyer, *J. Am. Chem. Soc.*, 1997, **119**, 7013; K. M. Omberg, J. R. Schoonover, S. Bernhard, J. A. Moss, J. A. Treadway, E. M. Kober, R. B. Dyer and T. J. Meyer, *Inorg. Chem.*, 1998, **37**, 3505; J. A. Weinstein, J. van Slageren, D. J. Stufkens, S. Zalis and M. W. George, *J. Chem. Soc. Dalton Trans.*, 2001, 2587.
- ²⁷ M. K. Kuimova, K. C. Gordon, S. L. Howell, P. Matousek, A. W. Parker, X.-Z. Sun, M. Towrie and M. W. George, *Photochem. Photobiol. Sci.*, 2006, **5**, 82.
- ²⁸ See for example L. A. Worl, R. Duesing, P. Y. Chen, L. Dellaciana and T. J. Meyer, *J. Chem. Soc. Dalton Trans.*, 1991, 849; K. S. Schanze, D. B. Macqueen, T. A. Perkins and L. A. Cabana, *Coord. Chem. Rev.*, 1993, **122**, 63; D. J. Stufkens and A. Vlcek, *Coord. Chem. Rev.*, 1998, **177**, 127; K. Kalyanasundaram, *Coord. Chem. Rev.*, 1982, **46**, 159; M. Wrighton and D. L. Morse, *J. Am. Chem. Soc.*, 1974, **96**, 998; J. V. Caspar and T. J. Meyer, *J. Phys. Chem.*, 1983, **87**, 952.
- ²⁹ K. Kalyanasundaram, *J. Chem. Soc. Faraday Trans. 2*, 1986, **82**, 2401.
- ³⁰ L. Wallace and D. P. Rillema, *Inorg. Chem.*, 1993, **32**, 3836.
- ³¹ P. Glyn, M. W. George, P. M. Hodges and J. J. Turner, *J. Chem. Soc. Chem. Commun.*, 1989, 1655; J. R. Schoonover, G. F. Strouse, R. B. Dyer, W. D. Bates, P. Y. Chen and T. J. Meyer, *Inorg. Chem.*, 1996, **35**, 273; J. R. Schoonover, G. F. Strouse, K. M. Omberg and R. B. Dyer, *Comments Inorg. Chem.*, 1996, **18**, 165.
- ³² M. W. George, F. P. A. Johnson, P. M. Hodges, J. R. Westwell and J. J. Turner, *J. Chem. Soc. Dalton Trans.*, 1993, 2977.
- ³³ I. P. Clark, Ph.D. Thesis, University of Nottingham, 1997.
- ³⁴ J. Bredenbeck, J. Helbing and P. Hamm, *J. Am. Chem. Soc.*, 2004, **126**, 990.
- ³⁵ D. M. Dattelbaum, K. M. Omberg, J. R. Schoonover, R. L. Martin and T. J. Meyer, *Inorg. Chem.*, 2002, **41**, 6071.
- ³⁶ I. E. Pomstchenko and F. N. Castellano, *J. Phys. Chem. A*, 2004, **108**, 3485.
- ³⁷ D. Gust, T. A. Moore and A. L. Moore, *Chem. Commun.*, 2006, 1169; G. D. Scholes, *Ann. Rev. Phys. Chem.*, 2003, **54**, 57; M. D. Ward and F. Barigelletti, *Coord. Chem. Rev.*, 2001, **216**, 127; L. De Cola and P. Belsler, *Coord. Chem. Rev.*, 1998, **177**, 301; M. D. Ward, *Chem. Soc. Rev.*, 1997, **26**, 365.
- ³⁸ J. R. Schoonover, A. P. Shreve, R. B. Dyer, R. L. Cleary, M. D. Ward and C. A. Bignozzi, *Inorg. Chem.*, 1998, 2598.
- ³⁹ V. Balzani, G. Bergamini, F. Marchioni and P. Ceroni, *Coord. Chem. Rev.*, 2006, **250**, 1254.
- ⁴⁰ J. R. Schoonover, K. C. Gordon, R. Argazzi, W. H. Woodruff, K. A. Peterson, C. A. Bignozzi, R. B. Dyer and T. J. Meyer, *J. Am. Chem. Soc.*, 1993, **115**, 10996.
- ⁴¹ D. W. Thompson, J. R. Schoonover, T. J. Meyer, R. Argazzi and C. A. Bignozzi, *J. Chem. Soc. Dalton Trans.*, 1999, 3729.

⁴² C. A. Bignozzi, R. Argazzi, J. R. Schoonover, K. C. Gordon, R. B. Dyer and F. Scandola, *Inorg. Chem.*, 1992, **31**, 5260.

⁴³ C. W. Wang, B. K. Mohny, B. B. Akhremitchev and G. C. Walker, *J. Phys. Chem. A*, 2000, **104**, 4314.

⁴⁴ A. V. Tivanski, C. Wang and G. C. Walker, *J. Phys. Chem. A*, 2003, **107**, 9051.

Chapter 2:

**Tetracyanoruthenate (II)
Complexes With α -Diimine
Ligands**

Chapter 2: Tetracyanoruthenate (II) Complexes With α -Diimine Ligands

2.1. Introduction

In this Chapter a series of tetracyanoruthenate (II) complexes with bidentate α -diimine ligands are presented along with the results of electronic and vibrational spectroscopic and electrochemical measurements. The findings are discussed with reference to previously published studies.

2.1.1. $[\text{Ru}(\text{CN})_4(\text{bpy})]^{2-}$

$[\text{Ru}(\text{CN})_4(\text{bpy})]^{2-}$ was first reported by Bignozzi *et al.* as a mono-bipyridyl analogue of $[\text{Ru}(\text{bpy})_3]^{2+}$.¹ The extent and timescale of delocalisation of the lowest energy ³MLCT excited state of $[\text{Ru}(\text{bpy})_3]^{2+}$ was (and still is) the subject of considerable debate. $[\text{Ru}(\text{bpy})_3]^{2+}$ has been compared with $[\text{Ru}(\text{CN})_4(\text{bpy})]^{2-}$ where two bpy ligands have been replaced by strong field CN ligands. These studies addressed some of the unanswered questions regarding excited state delocalisation in ruthenium (II) polypyridyl complexes.^{2,3} $[\text{Ru}(\text{CN})_4(\text{bpy})]^{2-}$ possesses a localised ³MLCT excited state and the strong field cyanide ligands increase the energy difference between metal centred (MC) states thus raising the lowest ³MC excited state energy and reducing the occurrence of radiationless deactivation following thermal promotion to these states.

Several studies have focused on $[\text{Ru}(\text{CN})_4(\text{bpy})]^{2-}$ and its behaviour in varying solvent environments.^{4,5,6} Its spectroscopic, electrochemical and photophysical properties exhibit strong negative solvatochromism due to donor-acceptor (SSDA) interactions between the cyanide ligands and solvent molecules (§1.2.3). Table 2.1.1.1 shows the absorption and emission wavelengths and oxidation potentials for $[\text{Ru}(\text{CN})_4(\text{bpy})]^{2-}$ in a number of solvents. λ_{abs}^1 is assigned to an intraligand π - π^* transition and λ_{abs}^2 and λ_{abs}^3 are assigned to ¹MLCT transitions. The solvent-dependence of the IL transitions is due to mixing between the $d\pi(\text{Ru})$ and $\pi(\text{bpy})$ orbitals, which introduces some MLCT character into the IL transitions.

Solvent	A. N.	λ_{abs}^1 / nm	λ_{abs}^2 / nm	λ_{abs}^3 / nm	λ_{em} / nm	$E_{1/2, \text{ox}}$ / V
H ₂ O	54.8	285	300	404	621	+0.77
CH ₃ OH	41.3	291	329	450	684	+0.27
CH ₃ CH ₂ OH	37.1	293	342	471	712	+0.11
CH ₂ Cl ₂	20.4	297	370	528	776	-
CH ₃ CN	19.3	295	374	535	805	-0.18

Table 2.1.1.1: Absorption and emission wavelengths and oxidation potentials for $[\text{Ru}(\text{CN})_4(\text{bpy})]^{2-}$ in a selection of solvents. Adapted from Ref.⁴

Linear correlations between the absorption and emission energies in ruthenium (II) cyanide complexes and the Acceptor Number of the solvent were found by Timpson *et al.* and can be explained using the theory of SSDA interactions in cyanide complexes (§1.2.4).⁴

The factors affecting the lifetime and quantum yield of $[\text{Ru}(\text{CN})_4(\text{bpy})]^{2-}$ and similar complexes in normal and deuterated solvents have been studied by Kovács and Horváth.^{7,8} Lifetimes were found to be around 3 times longer in D₂O (355 ns) and CD₃OD (162 ns) as compared with H₂O (113 ns) and CH₃OH (62 ns) and quantum yields were similarly enhanced approximately threefold. The enhancement of the emission lifetime in deuterated solvents has been attributed to a decrease in the rate of non-radiative deactivation through a fourth ³MLCT state which lies *ca.* 1000 -1400 cm⁻¹ above the ground state manifold of three ³MLCT states in thermal equilibrium (Figure 2.1.1.1).

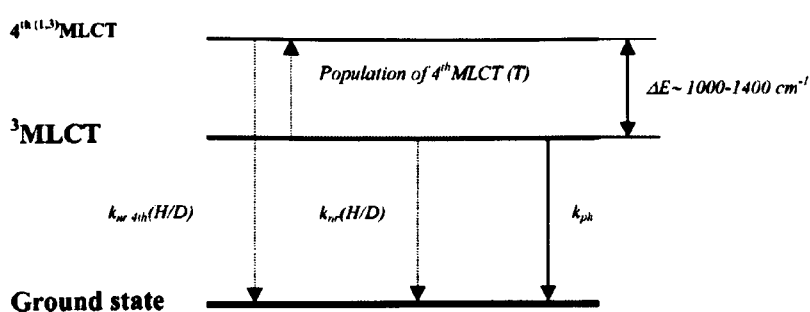


Figure 2.1.1.1: A schematic of the decay pathways in the $[\text{Ru}(\text{CN})_4(\text{bpy})]^{2-}$ system. Thermal population of the 4^{th} MLCT state provides another non-radiative decay pathway for the excited complex. Reproduced from Ref.⁷

The strong influence of solvent deuteration on the excited state decay rates shows the importance of hydrogen bonding in the relaxation mechanism. This study also included a brief discussion of similar results obtained with the related complexes $[\text{Ru}(\text{CN})_4((5,5\text{-CH}_3)_2\text{bpy})]^{2-}$, $[\text{Ru}(\text{CN})_4(\text{phen})]^{2-}$ and $[\text{Ru}(\text{CN})_4((\text{C}_6\text{H}_5)_2\text{-bpy})]^{2-}$ and a subsequent article presented a temperature-dependence study of the luminescence of $[\text{Ru}(\text{CN})_4(\text{bpy})]^{2-}$ (outside the scope of this work) and a visual interpretation of the SSDA interactions taking place (Figure 2.1.1.2).⁸

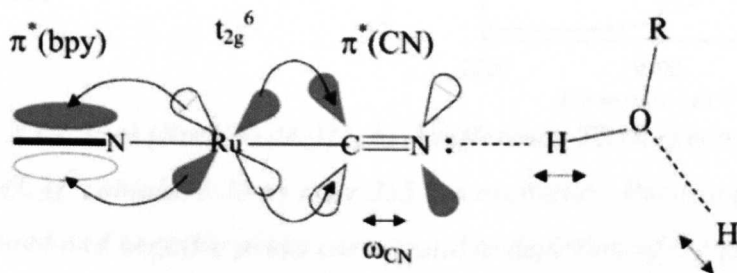


Figure 2.1.1.2: Schematic of the SSDA interactions between $[\text{Ru}(\text{CN})_4(\text{bpy})]^{2-}$ and aqueous/alcoholic solvents. Reproduced from Ref.⁸

A TRIR study of a complex related to $[\text{Ru}(\text{CN})_4(\text{bpy})]^{2-}$ has been carried out (Figure 2.1.1.3 a).⁹ Although the polypyridyl ligand is somewhat different from bpy, similar behaviour upon excitation would be expected, with a $(\text{Ru}^{\text{III}})(\text{L}_2^{\cdot-})^3\text{MLCT}$ excited state being formed. The difference TRIR spectrum (Figure 2.1.1.3b) in the $\nu(\text{CN})$ region shows a transient (positive peak) at *ca.* 50 cm^{-1} higher than the peak in the ground state spectrum (Figure 2.1.1.3c). The shift to higher wavenumber in the excited state is consistent with the formation of a $^3\text{MLCT}$ excited state. Partial oxidation of Ru^{II} to Ru^{III} increases the amount of Ru-C backbonding (Figure 2.1.1.2) which strengthens the C-N bond. This increases the energy of the $\nu(\text{CN})$ stretch, leading to the band's increase in wavenumber. The study also demonstrated considerable pH-dependence on the emission properties of $[\text{Ru}(\text{CN})_4(\text{L}_2)]^{2-}$ which is outside the scope of this work.

Much of the above has recently been discussed in a timely review article.¹⁰

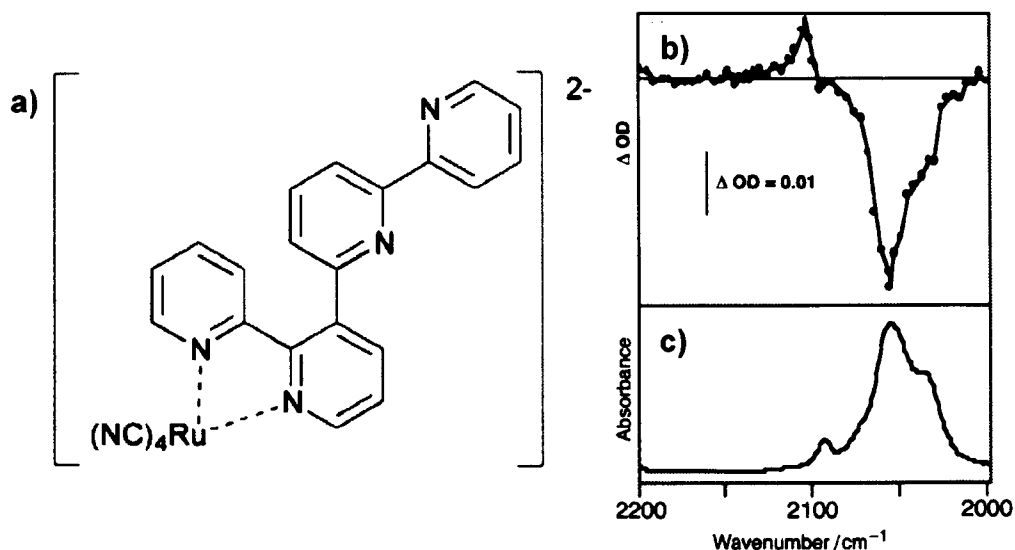


Figure 2.1.1.3: a) $[\text{Ru}(\text{CN})_4(\text{L}_2)]^{2-}$, b) A difference TRIR spectrum for $[\text{Ru}(\text{CN})_4(\text{L}_2)]^{2-}$, obtained 30 ns after 355 nm excitation. Positive peaks are transients formed and negative peaks correspond to depletion of the parent species. c) The FTIR spectrum of the ground state of $[\text{Ru}(\text{CN})_4(\text{L}_2)]^{2-}$. Adapted from Ref.⁹

2.1.2. $[\text{Ru}(\text{CN})_4(\text{bpm})]^{2-}$

An important property of the 2,2'-bipyrimidine ligand is its ability to chelate two metal centres within 550 pm of each other across a planar, conjugated network thus facilitating electronic coupling between the two units.¹¹ This effect forms the basis of Chapter 4. $[\text{Ru}(\text{CN})_4(\text{bpm})]^{2-}$ has been less widely studied than $[\text{Ru}(\text{CN})_4(\text{bpy})]^{2-}$ and only one published study has investigated the solvatochromism of this complex.

Samuels and DeArmond have conducted a brief study of the spectroscopy, photophysics and electrochemistry of $[\text{Ru}(\text{CN})_4(\text{bpm})]^{2-}$.¹² The absorption bands corresponding to ¹MLCT transitions show considerable negative solvatochromism in $\text{CH}_3\text{CH}_2\text{OH}$ and DMF (Figure 2.1.2.1a). This trend is consistent with the effects of specific solvent-cyanide interactions (§1.2.3), with $\lambda_{\text{max}} = 375$ and 490 nm in ethanol and $\lambda_{\text{max}} = 425$ and 590 nm in DMF. The low-temperature emission spectrum in $\text{CH}_3\text{CH}_2\text{OH}$ shows $\lambda_{\text{max}} = 550$ nm, with shoulders at 580 and 620 nm (Figure 2.1.2.1b). This ³MLCT emission wavelength is significantly shorter than in

$[\text{Ru}(\text{CN})_4(\text{bpy})]^{2-}$, which has $\lambda_{\text{max}} = 712 \text{ nm}$ in ethanol.⁴ No emission was detected at 298 K. Thus the energies of $^3\text{MLCT}$ emission of $[\text{Ru}(\text{CN})_4(\text{bpy})]^{2-}$ and $[\text{Ru}(\text{CN})_4(\text{bpm})]^{2-}$ have been shown to be considerably different (*vide supra*, §2.2.1).

Cyclic voltammetry of $[\text{Ru}(\text{CN})_4(\text{bpm})]^{2-}$ showed one reversible reduction at $E_{1/2} = -2.09 \text{ V}$ (vs. Fc/Fc^+) in DMF at a less negative potential than the corresponding couple in $[\text{Ru}(\text{CN})_4(\text{bpy})]^{2-}$, $E_{1/2} = -2.46 \text{ V}$.^{4,12} Oxidation potentials for the $\text{Ru}^{\text{II/III}}$ couple were not reported. Thus $[\text{Ru}(\text{CN})_4(\text{bpm})]^{2-}$ has lower-lying unoccupied ligand-based orbitals (from electrochemistry) and lower energy MLCT transitions (from spectroscopy) than $[\text{Ru}(\text{CN})_4(\text{bpy})]^{2-}$.

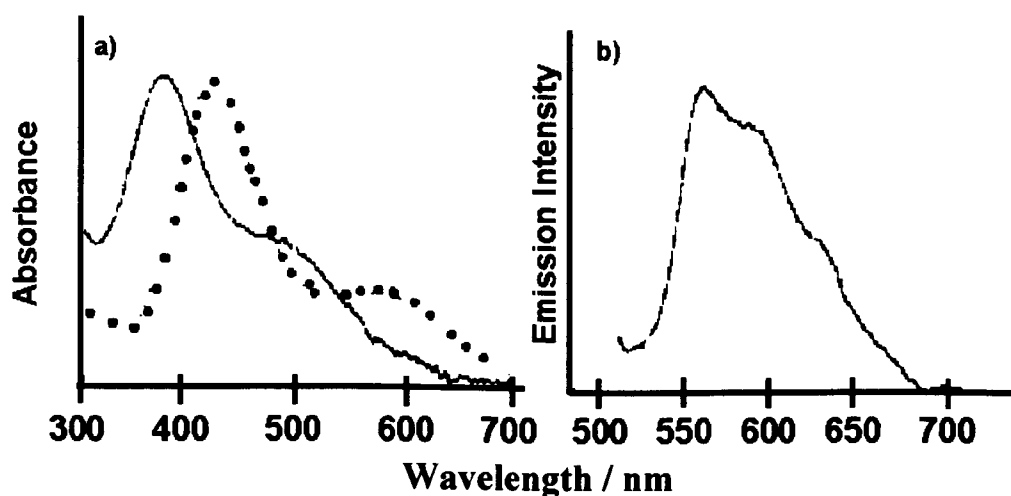


Figure 2.1.2.1: a) Absorption and b) low-temperature emission spectra for $[\text{Ru}(\text{CN})_4(\text{bpm})]^{2-}$ in ethanol (solid line) and DMF (dotted line). Adapted from Ref.¹²

2.1.3. $[\text{Ru}(\text{CN})_2(\text{bpy})_2]$ and Other Ruthenium Cyanide Complexes

The related complex $[\text{Ru}(\text{CN})_2(\text{bpy})_2]$ was first prepared and characterised in the late 1960s by Crosby and co-workers,^{13,14} who noted and discussed the differences in absorption spectra obtained in CH_3OH and DMF solutions. Later studies compared ruthenium (II) polypyridyl complexes with 1-4 CN groups, showing that the degree of solvatochromism observed was linearly related to the number of CN groups ligated to

the metal centre.⁴ The pH and temperature dependence of the luminescence¹⁵ and TRIR spectrum¹⁶ of $[\text{Ru}(\text{CN})_2(\text{bpy})_2]$ in solution have also been reported.

2.1.4. Summary of $[\text{Ru}(\text{CN})_4(\text{NN})]^{2-}$ Properties

The salient points to be taken from the literature reviewed above may be summarised in terms of three significant properties of the $[\text{Ru}(\text{CN})_4(\text{NN})]^{2-}$ unit. Firstly, its strong negative solvatochromism which arises from (SSDA) interactions between the externally-directed electron lone pairs on the cyanide ligands and solvent molecules. This means that its ³MLCT energy and its ground and excited state redox potentials are highly solvent dependent, for example the ³MLCT luminescence maximum varies from 640 nm in H₂O to 818 nm in (CH₃)₂NCHO, and the Ru^{II/III} redox potential varies from +0.77 V to -0.28 V (vs. Fc/Fc⁺) between the same solvents.¹⁷ This also applies in the solid state as demonstrated by Evju *et al.* using a crystalline salt of $[\text{Ru}(\text{CN})_4(\text{bpy})]^{2-}$ as a humidity sensor on the basis of its reversible colour change from purple to yellow in the presence of humidity. This effect arises because atmospheric H₂O molecules form hydrogen bonds to the externally directed lone pairs of the cyanide ligands, modulating the MLCT transition energy and as a result the colour of the complex.¹⁸

Secondly, the IR-active cyanide ligands of $[\text{Ru}(\text{CN})_4(\text{NN})]^{2-}$ allow the transfer of excitation energy and electrons in transition metal complexes to be monitored by time-resolved infrared (TRIR) spectroscopy, since the $\nu(\text{CN})$ vibrations are sensitive to redistribution of electron density in the complex. One relevant example of the application of TRIR to a ruthenium (II) cyanide complex (§2.1.1) has provided some background and insight into the spectroscopic behaviour of tetracyanoruthenate (II) polypyridyl complexes.⁹

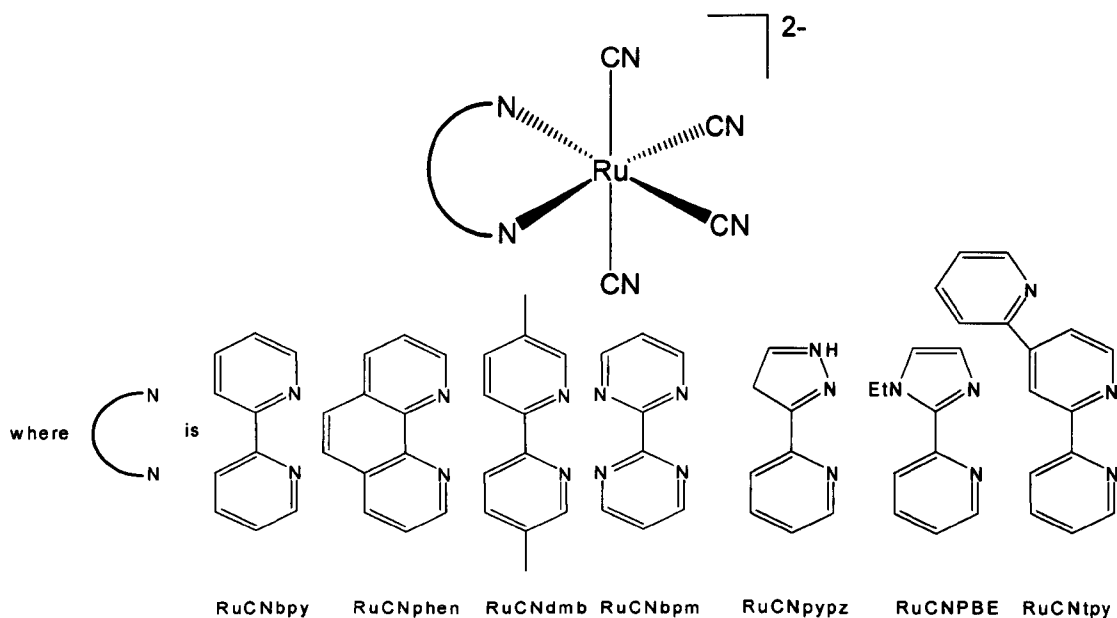
Finally, the externally directed lone pairs on the nitrogen atoms of the cyanide ligands of $[\text{Ru}(\text{CN})_4(\text{NN})]^{2-}$ are capable of acting as hydrogen bond acceptors, allowing the complex to act as a component of hydrogen bonded assemblies; and the lone pairs can

also coordinate to additional metal cations, allowing formation of polynuclear complexes *via* Ru–CN–M linkages (for examples see §1.4.2.2) or the binding of bare metal ions (metallochromism, §3.5.3).^{19,20}

These properties have not been fully exploited previously but form a major part of the work described in this Thesis. We have designed systems to exploit these advantages which present new applications for transition metal polypyridyl complexes in supramolecular photochemistry. Furthermore analogues and derivatives of $[\text{Ru}(\text{CN})_4(\text{bpy})]^{2-}$ have been scarcely studied, beyond addition of methyl substituents or simple replacement of bipyridine by phenanthroline.⁷

2.2. Scope, Results and Discussion

A range of $[\text{Ru}(\text{CN})_4(\text{NN})]^{2-}$ complexes (shown below) were studied using UV/vis absorption, luminescence, FTIR and TRIR spectroscopy and cyclic voltammetry in D_2O and CH_3CN where not limited by solubility or solvent windows.



2.2.1. UV/vis Absorption and Luminescence Spectroscopy

In aqueous solution all of the complexes display an absorption band arising from a Ru \rightarrow diimine $^1\text{MLCT}$ transition at $\lambda_{\text{abs}} \sim 400$ nm (Table 2.2.1.1, spectra not shown).ⁱ **RuCNBPM** is unique in this series and exhibits two clearly-resolved transitions in water at 342 and 438 nm. Upon cation exchange (replacing K^+ with PPN^+) some of the complexes were also soluble in CH_3CN ; in these cases comparison with the spectra recorded in D_2O shows the extent of negative solvatochromism exhibited in complexes of this type.⁴ In CH_3CN the $^1\text{MLCT}$ absorption profile is resolved into two components, one of which is at much lower energy than in D_2O . For example in **RuCNdmb** the MLCT absorption in water occurs at 393 nm, whereas in CH_3CN there are two bands at 372 and 514 nm. For **RuCNBPM** the two transitions apparent in D_2O (342, 437 nm) are red-shifted to 415 and 575 nm respectively in CH_3CN .

Complex	Solvent	$\lambda_{\text{abs,max}} / \text{nm}$	$\lambda_{\text{em}} / \text{nm}$	τ / ns	Φ	$E_{\text{RuII/III}} / \text{V}$
RuCNbpy	D_2O	285, 300, 404	620	360	0.028	+0.89
RuCNphen	D_2O	263, 387	624	–	0.011	+0.88
RuCNdmb *	D_2O	261, 291, 393	621	370	0.030	+0.85
	CH_3CN	372, 514	758	36	0.002	
RuCNBPM *	D_2O	342, 437	–	–	–	+1.05
	CH_3CN	415, 575	–	–	–	
RuCNtpy	D_2O	296, 411	655	106	0.025	+0.70 [#]
RuCNpypz	D_2O	229, 272, 353	556	17	0.001	+0.83
RuCNPBE	D_2O	242, 313, 404	665	471	0.007	+0.79

Table 2.2.1.1: UV/visible and luminescence data for tetracyanoruthenate (II) complexes. *UV/vis and luminescence spectra of **RuCNdmb** and **RuCNBPM** are shown and discussed in detail in later Chapters (§3.2.1 and §4.3.1). CV in H_2O with 0.1 M KCl electrolyte. [#]Irreversible Processes.

ⁱ The spectra for **RuCNdmb** and **RuCNBPM** are presented and discussed in detail in Chapters 3 and 4 respectively.

In every case in D₂O solution, excitation into the ¹MLCT absorption transition results in broad, structureless luminescence in the range 550-670 nm which arises from the ³MLCT excited state, consistent with the extensive literature studies of ruthenium (II) polypyridyl complexes.²¹ Kovács and Horváth recently showed that using D₂O as the solvent affords considerably longer-lived luminescence from complexes of this type than in H₂O due to attenuation of non-radiative decay pathways (§2.1.1).⁸ As discussed above the complexes **RuCNdmb** and **RuCNphen** have been reported previously and will not be discussed in detail, although reinvestigating them gave satisfactory agreement between the results here and previously published studies.¹⁷

In **RuCNtpy** the ¹MLCT absorption and ³MLCT luminescence are red-shifted by 35 nm compared to **RuCNbpy**, despite the donor set being nominally identical. In the solid state, this may be ascribed to the long bond Ru(1)–N(8) (2.19 Å),²² involving the central ring of the terpyridyl ligand, which is lengthened by virtue of having the sterically bulky pyridyl residue at its C² position, *ortho* to the site of coordination. Lengthening this bond will weaken the ligand field of the coordinated bipyridyl fragment compared to normal un-encumbered bpy (Ru–N separation *ca.* 2.10 Å), which will slightly raise the d(π) orbital set and hence reduce the MLCT absorption and emission energies. This has been observed previously in derivatives of [Ru(bpy)₃]²⁺ in which the bpy ligands have a bulky substituent at the C²/C⁶ position.²³

Variation of the nature of the α-diimine ligand results in significant changes to the ¹MLCT absorption and ³MLCT luminescence energies for electronic reasons. The highest-energy absorption and luminescence in the series come from **RuCNpypz**, implying that the pypz ligand has a higher-energy LUMO than the other diimines. This is corroborated by the short luminescence lifetime (17 ns) which is a consequence of the high-lying ³MLCT excited state being close in energy to the metal-centred d-d state, which provides a facile thermally-activated route for radiationless deactivation. Despite the relatively short luminescence lifetime, the high ³MLCT energy of **RuCNpypz** will make it of particular value as an energy-donor in polynuclear assemblies (*e.g.* for use as a charge-injector into nanocrystalline TiO₂).²⁴

The luminescence of **RuCNBPM** at room temperature is too weak to allow the excited state lifetime to be measured by our apparatus. Replacement of bipyridine by bipyrimidine has been shown in other complexes to result in much weaker, shorter-lived emission (see Chapter 4 for a full discussion of this effect). For those complexes studied in CH₃CN, the ³MLCT emission maxima (like the ¹MLCT absorption maxima) are substantially red-shifted ($\lambda_{\text{max}} > 700$ nm) compared to the situation in water, with very weak (often barely detectable) and short lived emission. The luminescence quantum yields in CH₃CN are at least 10 times smaller than in water, with short lifetimes (usually $\tau < 5$ ns) that were difficult to measure by luminescence methods because of the weakness of the signal.

2.2.2. Electrochemistry

Cyclic voltammetric studies of the potassium salts of the tetracyanoruthenate (II) complexes in water showed that all but one of the complexes possess a reversible, one-electron oxidation process. By analogy with the known behaviour of [Ru(CN)₄(bpy)]²⁻,¹² this couple may be assigned as a metal-centred Ru^{II/III} couple. The redox potentials measured are listed in Table 2.2.1.1. In most cases this process is reversible (peak-peak separation 60-80 mV, equal cathodic and anodic peak currents, peak current proportional to square root of scan rate) on the voltammetric timescale. For **RuCNtpy** however the process is completely irreversible with no return wave. A possible explanation for this is that following oxidation the pendant pyridyl group displaces a cyanide ligand and becomes coordinated to the metal centre. There is no other apparent reason why this alone of all the complexes should show irreversible behaviour on oxidation. The strong π -accepting effects of 2,2'-bipyrimidine are apparent, with the Ru^{II/III} redox potential being at a more positive potential (+1.05 V vs. Ag/AgCl) than all the others (+0.70 to +0.89 V) because the metal centre is more electron-deficient. The expected ligand-centred reductions were not accessible within the limits of the potential window in H₂O.

2.2.3. FTIR and Time-Resolved Infrared Spectroscopy

A recent vibrational spectroscopic study by Kettle and co-workers of homoleptic tetra and hexacyanometallate complexes boldly attempts to present a framework for the comparison of transition metal carbonyl and cyanide ligands, on the basis of the isoelectronic nature of CO and CN⁻.²⁵ Relevant aspects of the study are discussed below. Kettle *et al.* highlight the significant electrostatic differences between the two ligands (CO is neutral whilst CN is anionic) and how this may facilitate cation binding, discussed in terms of “non-innocence” of the counter-ion. This can have significant effects on the electronic and vibrational spectra obtained; this effect is termed metalochromism and is investigated in §3.5.3.^{19,20} More subtle effects such as decreased dipole moment and increased quadrupole moment in metal cyanide complexes are investigated. These are postulated to give rise to unexpected band frequency ordering and intensity effects as first-order “ball-and-spring” models are proposed to be inaccurate for such complexes when quadrupolar interactions become significant (Figure 2.2.3.1).²⁵

A section of the paper is devoted to a DFT study exploring the dependence of vibrational band frequency on the formal charge of the metal centre in both metal carbonyl and cyanide complexes, an effect which is central to the sensitivity and utility of TRIR spectroscopy. The results suggest that the calculated vibrational band frequency varies non-linearly with the nuclear charge of the metal centre in both types of complex (Figure 2.2.3.2).²⁵ As mentioned in Chapter 1 there is a plethora of TRIR data for metal carbonyl complexes which rely on this effect,²⁶ but prior to this Thesis there have been very few TRIR studies of mononuclear transition metal cyanide complexes and a theoretical verification of the underlying concept of this Thesis is most timely and welcome!

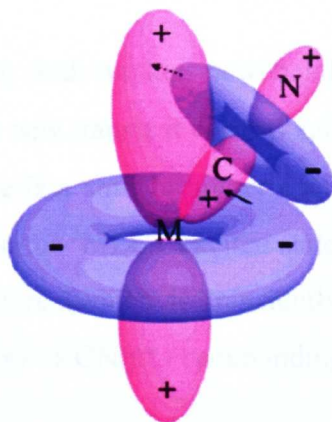


Figure 2.2.3.1: Diagram of a possible metal-CN derived quadrupole coupling in a $M(\text{CN})_3$ unit with C_{3v} symmetry. Charge displacements are shown; violet corresponds to a charge decrease and blue corresponds to a charge increase.

Reproduced from Ref.²⁵

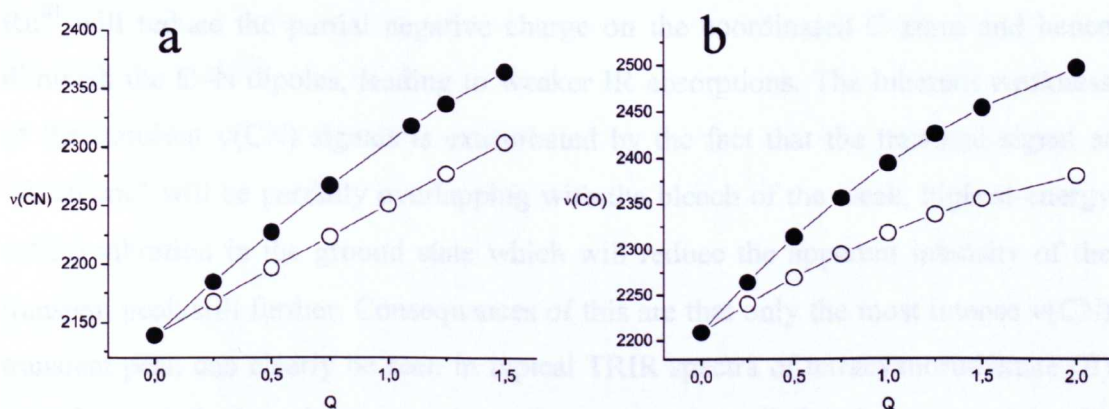


Figure 2.2.3.2: Calculated effect (DFT) of a variable positive charge placed 1.5 Å (black circles) or 2.0 Å (white circles) from the C atom on the stretching frequency of a) CN and b) CO in cm^{-1} . Reproduced from Ref.²⁵

$[\text{Ru}(\text{CN})_4(\text{NN})]^{2-}$ complexes have C_{2v} symmetry and therefore these complexes should have four IR-active CN vibrations. In the solid state these are apparent as three closely spaced strong peaks between about 2030 and 2060 cm^{-1} , with a less intense peak at around 2090 cm^{-1} . In aqueous solution these are not all resolved; the three closely spaced bands merge to give a strong peak at 2050 – 2060 cm^{-1} , and a weaker one appearing as a shoulder about 20 – 30 cm^{-1} higher (Table 2.2.3.1). Figures 2.2.3.1 and 4.3.3.1 show the ps-TRIR spectra of **RuCNbpy** and **RuCNBPM** in D_2O following 400 nm excitation respectively. In the spectrum of **RuCNBPM**, the parent

$\nu(\text{CN})$ vibrations are bleached, and weaker new bands appear at higher energy. Assuming that the most intense new transient corresponds to the most intense peak in the ground-state spectrum, there is a shift to higher energy of 52 cm^{-1} of this $\nu(\text{CN})$ vibration when the complex is in the $^3\text{MLCT}$ excited state, as a consequence of loss of electron density on the Ru centre (which is transiently oxidised to Ru^{III}) and the corresponding decrease in $\text{Ru}(\text{d}\pi) \rightarrow \text{CN}(\pi^*)$ backbonding.

The low signal intensity of the transient $\nu(\text{CN})$ vibration compared to the ground state vibration is consistent with previous observations⁹ and suggests that the dipole of the C–N bonds is reduced in the $^3\text{MLCT}$ excited state. This is reasonable as cyanide ligands formally have the negative charge on the C atom: transient oxidation of Ru^{II} to Ru^{III} will reduce the partial negative charge on the coordinated C atom and hence diminish the C–N dipoles, leading to weaker IR absorptions. The inherent weakness of the transient $\nu(\text{CN})$ signals is exacerbated by the fact that the transient signal at $\sim 2100 \text{ cm}^{-1}$ will be partially overlapping with the bleach of the weak, highest-energy $\nu(\text{CN})$ vibration in the ground state which will reduce the apparent intensity of the transient peak still further. Consequences of this are that only the most intense $\nu(\text{CN})$ transient peak can clearly be seen in typical TRIR spectra of tetracyanoruthenate (II) complexes and that these complexes can not be studied using two-colour IR ‘vibration-labelling’ experiments (§1.4.1.3).

Similar spectroscopic behaviour is shown by all of the complexes in D_2O , with a shift to higher energy of the most intense $\nu(\text{CN})$ vibration of between 46 and 52 cm^{-1} in the $^3\text{MLCT}$ excited state, as evinced by a bleach of the ground-state vibrations and a less intense transient peak at higher energy. These values are the same within the limits of accuracy of the experiment, notwithstanding the $8\text{-}9 \text{ cm}^{-1}$ resolution for the spectra and the low intensity of the transients. The fast timescale of this technique allowed us to determine accurately the lifetime of **RuCNBPM**, which could not be determined by luminescence methods as the emission was too weak and short-lived. §4.3.3 contains the TRIR difference spectrum for this complex, the kinetics of transient decays and

parent recovery and a detailed analysis of the results obtained. The rates derived from this data match closely and give $\tau = 3.4 (\pm 0.3)$ ns for the $^3\text{MLCT}$ excited state in D_2O .

Two of the complexes were studied in CH_3CN to probe the effect of changing solvent on their transient IR behaviour. TRIR spectra of **RuCNdmb** and **RuCNBPM** measured in CH_3CN are similar to those recorded in D_2O , with the exception that the shift to higher energy of the main $\nu(\text{CN})$ vibration was smaller - being 36 cm^{-1} for **RuCNdmb** (*cf.* 46 cm^{-1} in D_2O) and 30 cm^{-1} for **RuCNBPM** (*cf.* 48 cm^{-1} in D_2O). This is probably a consequence of the fact that the most intense $\nu(\text{CN})$ vibration in the ground state is at higher energy in CH_3CN than in water (for **RuCNdmb**, $2068 \text{ vs. } 2049 \text{ cm}^{-1}$; for **RuCNBPM**, $2068 \text{ vs. } 2057 \text{ cm}^{-1}$), an effect which is ascribable to differences in hydrogen bonding with the solvent. The lifetime of the $^3\text{MLCT}$ excited state of **RuCNBPM** in CH_3CN was found to be $250 (\pm 50)$ ps, an order of magnitude shorter than the value observed in water, in keeping with the general trend expected for complexes of this series and the 'energy-gap law' (§1.3).

In order to simulate a higher-definition TRIR spectrum of the $[\text{Ru}(\text{CN})_4(\text{NN})]^{2-}$ unit, two spectra of **RuCNbpy** were taken in D_2O solution at $\Delta t = 100$ ps with data points approx $4\text{-}5 \text{ cm}^{-1}$ from each other and interpolated so as to simulate a spectrum with *ca.* 4 cm^{-1} resolution, as shown in Figure 2.2.3.3. Even with an increased effective resolution only moderate insights may be taken from the spectrum, mainly in the clearer resolution of multiple features contributing to the transient peak profile between 2090 and 2130 cm^{-1} . This feature is best fitted to 2 components, centred at *ca.* 2099 and 2110 cm^{-1} (fits not shown). Some spectra in later chapters (despite their lower resolution) clearly indicate the presence of two bands in similar positions. A particularly interesting example of this is the ps-TRIR spectrum of **RuCN-BL¹-Rubpyamide** in D_2O (Figure 4.5.3.1), which ostensibly shows the interconversion of 2 transient bands in this region.

Complex	Solid State ν_{CN} (ground state)/ $\text{cm}^{-1,*}$	Solvent	TRIR Bleach centre/ cm^{-1}	TRIR Transient centre/ cm^{-1}	Δ/cm^{-1}
RuCNbpy	2032, 2047, 2056, 2089	D ₂ O	2051	2103	52
RuCNdmb [#]	2034, 2040, 2054, 2090	D ₂ O	2049	2095	46
		CH ₃ CN	2068	2104	36
RuCNphen	2032, 2038, 2047, 2088	D ₂ O	2051	2098	47
RuCNtpy	2041, 2047, 2091	D ₂ O	2051	2100	49
RuCNBPM [#]	2046, 2057, 2065, 2102	D ₂ O	2057	2105	48
		CH ₃ CN	2068	2098	30
RuCNPBE	2028, 2044, 2085	D ₂ O	2048	2095	47
RuCNpypz	2028, 2045, 2052, 2092	D ₂ O	2050	2098	48

Table 2.2.3.1: TRIR data for the tetracyanoruthenate (II) complexes. *Solid-state spectra measured on powdered sample using diamond-ATR cell. #Solution FTIR and TRIR spectra of RuCNdmb and RuCNBPM are shown and discussed in detail in later Chapters (§3.2.3 and §4.3.3).

2.3. Discussion and Closing Points

This Chapter has presented highlights of the research literature on $[\text{Ru}(\text{CN})_4(\text{bpy})]^{2-}$ and related complexes in the context of photophysics, optical and vibrational spectroscopy and solvatochromism. The three principal advantages of $[\text{Ru}(\text{CN})_4(\text{NN})]^{2-}$ over $[\text{Ru}(\text{NN})_3]^{2+}$ complexes have been discussed; the solvent-tunability of excited state energy, CN sites providing additional binding sites for metal ions and

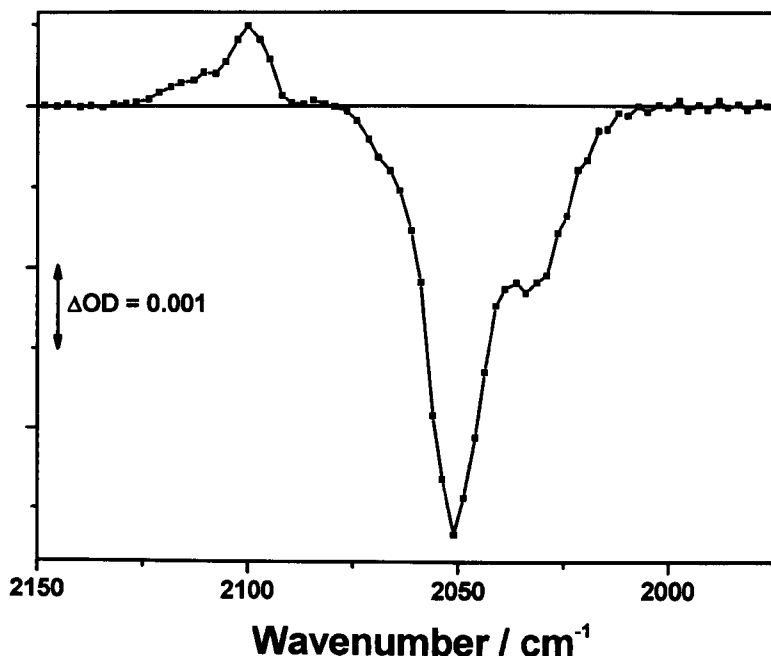


Figure 2.2.3.3: Interpolated “high resolution” ps-TRIR spectrum of $[Ru(CN)_4(bpy)]^{2-}$ in D_2O at $\Delta t = 100$ ps.

the sensitivity of $\nu(CN)$ bands as spectroscopic reporters in the IR region of the electromagnetic spectrum.

We have extended the family of known tetracyanoruthenate (II) complexes with polypyridyl ligands and have documented their photophysical and electrochemical properties. All of the complexes reported in this Chapter have similar absorption and emission properties arising from the 1MLCT and 3MLCT transitions respectively, although synthetic manipulation of the complexes has altered their photophysical properties. Where studied the negative solvatochromism of the complexes is evident from the difference in absorption peak profile and emission energy, lifetime and quantum yield and confirms that solvatochromism is a potential external stimulus which may be used to modulate the excited state properties. TRIR spectroscopy has been successfully used to characterise the excited state properties of $[Ru(CN)_4(NN)]^{2-}$ complexes. These findings will be exploited and studied in more detail in Chapters 3 and 4 where $[Ru(CN)_4(NN)]^{2-}$ is used as a component of supramolecular assemblies designed to undergo intermetallic PEnT and PET between metal centres respectively

and TRIR spectroscopy is used to directly monitor the photophysical processes *in real time*.

2.4. References

- ¹ C. A. Bignozzi, C. Chiorboli, M. T. Indelli, M. A. R. Scandola, G. Varani and F. Scandola, *J. Am. Chem. Soc.*, 1986, **108**, 7872.
- ² J. V. Caspar and T. J. Meyer, *J. Am. Chem. Soc.*, **105**, 1983, 105.
- ³ M. Kato, S. Yamauchi and N. Hirota, *J. Phys. Chem.*, 1989, **93**, 3422.
- ⁴ C. J. Timpson, C. A. Bignozzi, B. P. Sullivan, E. M. Kober and T. J. Meyer *J. Phys. Chem.*, 1996, **100**, 2915.
- ⁵ P. Belser, *Gazz. Chim. Ital.*, 1985, **115**, 723.
- ⁶ T. Meyges, G. Schubert, M. Kovács, T. Radnai, T. Grosz, I. Bako, I. Papai and A. Horváth, *J. Phys. Chem. A*, 2003, **107**, 9903.
- ⁷ M. Kovács and A. Horváth, *Inorg. Chim. Acta*, 2002, **335**, 69.
- ⁸ M. Kovács and A. Horváth, *J. Photochem. Photobiol. A*, 2004, **163**, 13.
- ⁹ S. Encinas, A. F. Morales, F. Barigelletti, A. M. Barthram, C. M. White, S. M. Couchman, J. C. Jeffery, M. D. Ward, D. C. Grills, and M. W. George, *J. Chem. Soc. Dalton Trans.*, 2001, 3312.
- ¹⁰ M. D Ward, *Coord. Chem. Rev.*, 2006, **250**, 3128.
- ¹¹ W. Matheis and W. Kaim, *Inorg. Chim. Acta*, 1991, **181**, 15.
- ¹² A. C. Samuels and M. K. DeArmond, *Inorg. Chem.*, 1995, **34**, 5548.
- ¹³ D. M. Klassen and G. A. Crosby, *J. Chem. Phys.*, 1968, **48**, 1853.
- ¹⁴ J. N. Demas, T. F. Turner and G. A. Crosby, *Inorg. Chem.*, 1969, **8**, 674.
- ¹⁵ F. Barigelletti, A. Juris, P. Belser and A. von Zelewsky, *J. Phys. Chem.*, 1987, **91**, 1095.
- ¹⁶ M. K. Kuimova, M. Y. Mel'nikov, J. A. Weinstein and M. W. George, *Dalton Trans.*, 2002, 2857.
- ¹⁷ N. R. M. Simpson, M. D. Ward, A. F. Morales and F. Barigelletti, *J. Chem. Soc. Dalton Trans.*, 2002, 2449.
- ¹⁸ J. K. Evju and K. R. Mann, *Chem. Mater.*, 1999, **11**, 1425.
- ¹⁹ Y. P. Kovtun, Y. O. Prostota and A. I. Tolmachev, *Dyes and Pigments*, 2003, **58**, 83.
- ²⁰ Y. J. Kubo, *J. Chem. Soc. Perkin Trans. 1*, 1994, 1787.
- ²¹ See for example: A. Juris, V. Balzani, F. Barigelletti, S. Campagna, P. Belser and A. von Zelewsky, *Coord. Chem. Rev.*, 1988, **84**, 85; V. Balzani, A. Juris, M. Venturi, S. Campagna and S. Serroni, *Chem. Rev.*, 1996, **96**, 759; C. A. Bignozzi, J. N. Schoonover and F. Scandola, *Prog. Inorg. Chem.*, 1997, **44**, 1; M. D. Ward, *Chem. Soc. Rev.*, 1997, **26**, 365.
- ²² H. Adams, W. Z. Alsindi, G. M. Davies, M. B. Duriska, T. L. Easun, H. E. Fenton, J.-M. Herrera, M. W. George, K. L. Ronayne, X.-Z. Sun, M. Towrie and M. D. Ward, *Dalton Trans.*, 2006, 39.
- ²³ See for example: R. H. Fabian, D. M. Klassen and R. W. Sonntag, *Inorg. Chem.*, 1980, **19**, 1977; J. M. Kelly, C. Long, C. M. O'Connell, J. G. Vos and A. H. A. Tinnemans, *Inorg. Chem.*, 1983, **22**, 2818; E. C. Constable, M. J. Hannon, A. M. W. Cargill Thompson, D. A. Tocher and J. V. Walker, *Supramol.*

Chem., 1993, **2**, 243; A. M. Barthram, M. D. Ward, A. Gessi, N. Armaroli, L. Flamigni and F. Barigelletti, *New J. Chem.*, 1998, **22**, 913; D. A. Bardwell, F. Barigelletti, R. L. Cleary, L. Flamigni, M. Guardigli, J. C. Jeffery and M. D. Ward, *Inorg. Chem.*, 1995, **33**, 2438.

²⁴ T. J. Meyer, *Pure Appl. Chem.*, 1986, **58**, 1193; K. Kalyanasundaram, *Coord. Chem. Rev.*, 1982, **46**, 159.

²⁵ S. F. A. Kettle, G. L. Aschero, E. Diana, R. Rosetti and P. L. Stanghellini, *Inorg. Chem.*, 2006, **45**, 4928.

²⁶ J. M. Butler, M. W. George, J. R. Schoonover, D. M. Dattelbaum and T. J. Meyer, *Coord. Chem. Rev.*, 2007, **251**, 492 and references therein.

Chapter 3:

Solvent Based Switching of the Gradient and Direction of Förster Photoinduced Energy Transfer in Polynuclear Complexes

Chapter 3: Solvent Based Switching of the Gradient and Direction of Förster Photoinduced Energy Transfer in Polynuclear Complexes

3.1. Introduction

In this Chapter a series of bimetallic complexes and their monometallic precursors are presented. They have been optimised for through-space (Förster) photoinduced energy transfer (PEnT) by the use of saturated organic bridging ligands, more precisely linkers between 2,2'-bipyridine molecules ligated to different metal centres. Here we develop supramolecular systems in which the direction and thermodynamic gradient of PEnT can be reversibly manipulated through changes in the solvent environment. The control of such processes by external stimuli is of considerable interest to the photophysical community and has applications in sensor devices¹ and the development of molecular wires and photonics technologies.²

Two relevant examples of bichromophoric solvent-switchable PEnT systems incorporating the $[\text{Ru}(\text{CN})_4]^{2-}$ moiety are discussed in the literature. Ward and co-workers studied the system $\{(\text{NC})_4\text{Ru}(\mu\text{-BL})\text{Ru}(\text{bpy})_2\}$ (hereafter **RuCN-BL-Rubpy**) shown in Figure 3.1.1, consisting of a $[\text{Ru}(\text{CN})_4(\text{bpy})]^{2-}$ unit covalently attached to a $[\text{Ru}(\text{bpy})_3]^{2+}$ unit through a flexible, 6-atom length polyoxoethylene chain.³ The lowest energy excited state of both chromophores may be formalised as $\text{Ru} \rightarrow \text{bpy}_{\text{BL}} {}^3\text{MLCT}$ (where bpy_{BL} is a 2,2'-bipyridine forming part of the bridging ligand BL). The $[\text{Ru}(\text{CN})_4(\text{bpy})]^{2-}$ unit (hereafter **RuCN**) exhibits negative solvatochromism (§1.2.4, Chapter 2) whereas the photophysics and spectroscopy of $[\text{Ru}(\text{bpy})_3]^{2+}$ (hereafter **Rubpy**) are virtually solvent-independent.

The absorption spectra obtained for **RuCN-BL-Rubpy** in H_2O and $(\text{CH}_3)_2\text{SO}$, dimethylsulfoxide (hereafter DMSO) are shown in Figure 3.1.2. The main difference in the spectral profile in the two solvents is the prominence of a feature at $\lambda_{\text{max}} = 550$ nm in DMSO. This coincides with the lowest energy absorption of $[\text{Ru}(\text{CN})_4(\text{bpy})]^{2-}$, also at $\lambda_{\text{max}} = 550$ nm (§2.2.1). In water the absorption of the **RuCN** terminus is at

$\lambda_{\text{max}} = 452 \text{ nm}$ and is obscured by the absorption from the **Rubpy** terminus, which shows little variation in the two solvents.

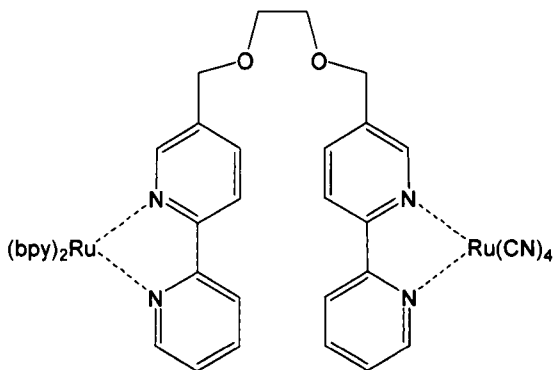


Figure 3.1.1: The bimetallic complex RuCN-BL-Rubpy.³

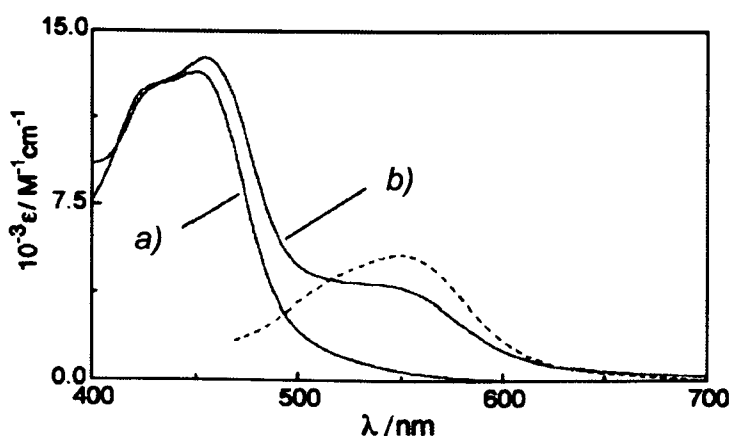


Figure 3.1.2: The absorption spectra of RuCN-BL-Rubpy (full lines) in (a) H₂O and (b) DMSO. For comparison part of the spectrum of [Ru(CN)₄(bpy)]²⁻ in DMSO is displayed (dotted line). Reproduced from Ref.³

The luminescence spectra of **RuCN-BL-Rubpy** measured in a series of DMSO:H₂O mixtures are shown in Figure 3.1.3. The emission maximum (following excitation of the **Rubpy** terminus) is invariant in the spectra with values in the range $\lambda_{\text{max}} = 615$ to 620 nm, indicating that emission from the Ru → bpy ³MLCT excited state of the solvent-independent **Rubpy** terminus dominates the spectrum. The intensity and lifetime of the emission progressively decreases from H₂O to DMSO as the luminescence from the **Rubpy** unit becomes quenched more effectively by the **RuCN** terminus. As the solvent A. N. decreases the [Ru(CN)₄(bpy)]²⁻ unit becomes both a

better energy acceptor (due to its lower energy $^3\text{MLCT}$ state) and a better electron donor (due to its less positive oxidation potential, §1.4.1.2). The mechanism of quenching was proposed to be through-space PEnT and a pictorial representation of the photophysical model is shown in Figure 3.1.4. Emission from the $[\text{Ru}(\text{CN})_4(\text{bpy})]^{2-}$ unit was found to be weak and undetected in either solvent. The authors suggested that this was obscured by the much more intense luminescence of the $[\text{Ru}(\text{bpy})_3]^{2+}$ unit or efficient non-radiative decay pathways.

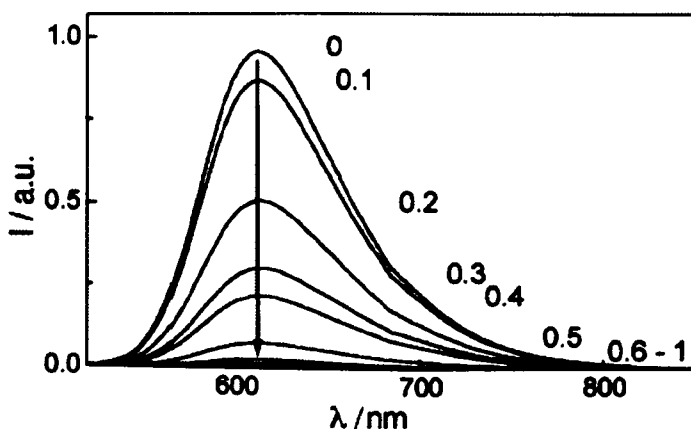


Figure 3.1.3: The luminescence spectra of RuCN-BL-Rubpy in a series of DMSO:H₂O fractions (labelled). Reproduced from Ref.³

The authors proposed a photophysical model to rationalise the results observed. In H₂O the $^3\text{MLCT}$ energies of the two termini are similar ($\Delta E = 230 \text{ cm}^{-1}$ from luminescence spectroscopy of the monometallic model complexes) and the monoexponential emission lifetime of 360 ns is consistent with the lowest $^3\text{MLCT}$ excited states on either terminus being in thermal equilibrium. In DMSO the negative solvatochromism of the **RuCN** unit is expected to result in a much lower $^3\text{MLCT}$ energy than the **Rubpy** terminus ($\Delta E = 3600 \text{ cm}^{-1}$ from luminescence spectroscopy of the monometallic model complexes). Emission is quenched fiftyfold in DMSO ($\phi_{\text{H}_2\text{O}} = 0.026$ whereas $\phi_{\text{DMSO}} = 0.0005$) and luminescence from the unquenched **Rubpy** termini is detected with a lifetime of 4 ns. The authors estimated the intermetallic distance from luminescence studies as 8 Å, representing a considerable degree of folding in the bridging ligand (the maximum distance possible being *ca.* 14 Å).³

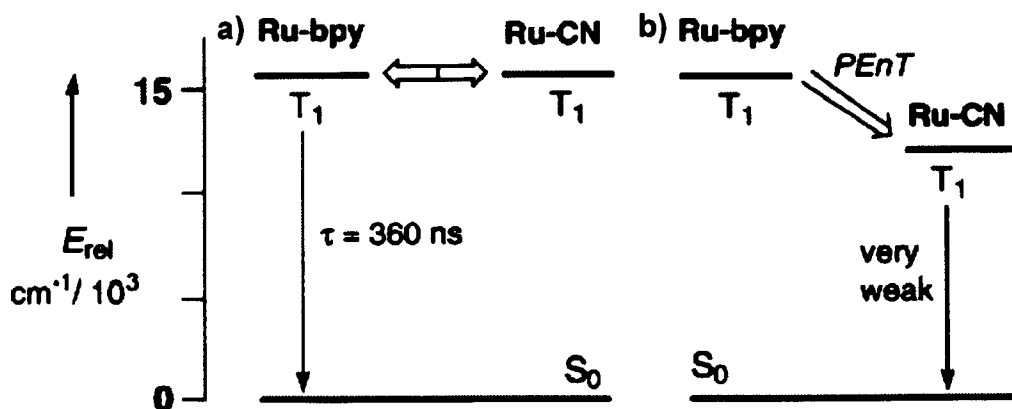


Figure 3.1.4: A schematic of the photophysics of RuCN-BL-Rubpy in a) H_2O and b) DMSO. Reproduced from Ref.³

Indelli *et al.* linked the $[Ru(CN)_4(bpy)]^{2-}$ unit with either one or two pyrene molecules via an ethane spacer through the bipyridyl ring at the 4,4' positions.⁴ The molecules RuCNpyr and RuCN(pyr)₂ are shown in Figure 3.1.5. In contrast to the work of Simpson *et al.*, the lowest energy excited states of the two chromophores in 5 and 6 are Ru \rightarrow bpy ³MLCT and pyrene ³ π - π^* transitions. The MLCT transition energies of the $[Ru(CN)_4(bpy)]^{2-}$ unit show the expected strong negative solvatochromism (§1.2.4) whereas the energies of the pyrene π - π^* transitions are virtually solvent-independent.

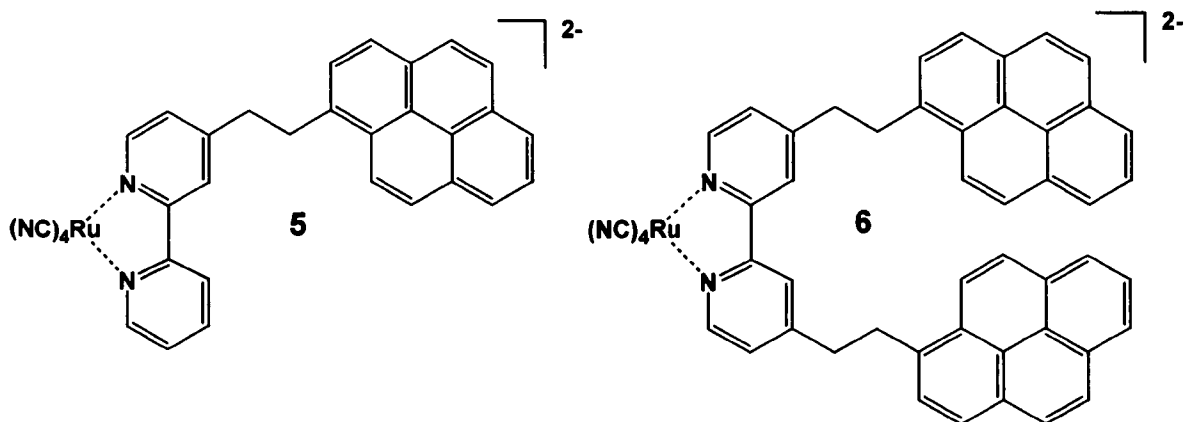


Figure 3.1.5: The complexes RuCNpyr and RuCN(pyr)₂.

The absorption spectra of 5 in CH_3CN , CH_3OH and H_2O are shown in Figure 3.1.6. The ¹MLCT absorption maximum varies from 392 nm in H_2O to 530 nm in CH_3CN ,

exhibiting the expected negative solvatochromism of the **RuCN** unit (§1.2.1.4). Pyrene $^1\pi-\pi^*$ transitions occur below 350 nm and are not shown in the Figure below.

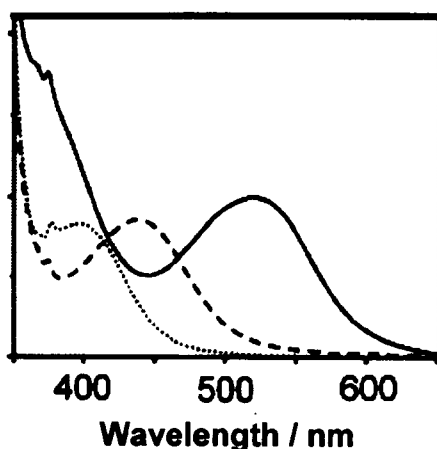


Figure 3.1.6: Absorption spectra of RuCNpyr in H₂O (grey dotted line), CH₃OH (dashed line) and CH₃CN (solid line). Reproduced from Ref.⁴

The emission spectra of **RuCNpyr** and **RuCN(pyr)₂** were found to be strongly solvent-dependent. In H₂O their luminescence is extremely weak ($\lambda_{\text{max}} = 600$ nm), whereas in CH₃CN the emission ($\lambda_{\text{max}} = 780$ nm) is much stronger and is consistent with luminescence from a $^3\text{MLCT}$ excited state. In CH₃OH the emission energy lies between the two extremes ($\lambda_{\text{max}} = 640$ nm) and the emission was found to decay with biexponential kinetics, with a major short-lived component and a minor longer-lived minor component. This is consistent with two states (one $^3\text{MLCT}$ and one $^3\pi-\pi^*$) of similar energy both emitting.

In H₂O the $^3\text{MLCT}$ excited state of the **RuCN** terminus lies higher in energy than the $^3\pi-\pi^*$ transition of the pyrene, and is completely quenched. Efficient energy transfer from the **RuCN** terminus to the pyrene group takes place. In CH₃CN the $^3\text{MLCT}$ excited state energy of $[\text{Ru}(\text{CN})_4(\text{bpy})]^{2-}$ is lower in energy due to the negative solvatochromism of transition metal cyanide complexes (§1.2.4) and lies lower in energy than the pyrene-based $^3\pi-\pi^*$ transitions. Emission is observed from the **RuCN** terminus.

In CH₃OH the ³MLCT excited state of the RuCN terminus and the ³π-π* excited state of the pyrene are of similar energy. The initially populated ³MLCT excited state undergoes energy transfer to the pyrene-based ³π-π* state but the process is reversible as the states are in equilibrium. The photophysics of the system is summarised in Figure 3.1.7, where the reversal of the ordering of the energies of the ³MLCT and ³π-π* excited states is illustrated.

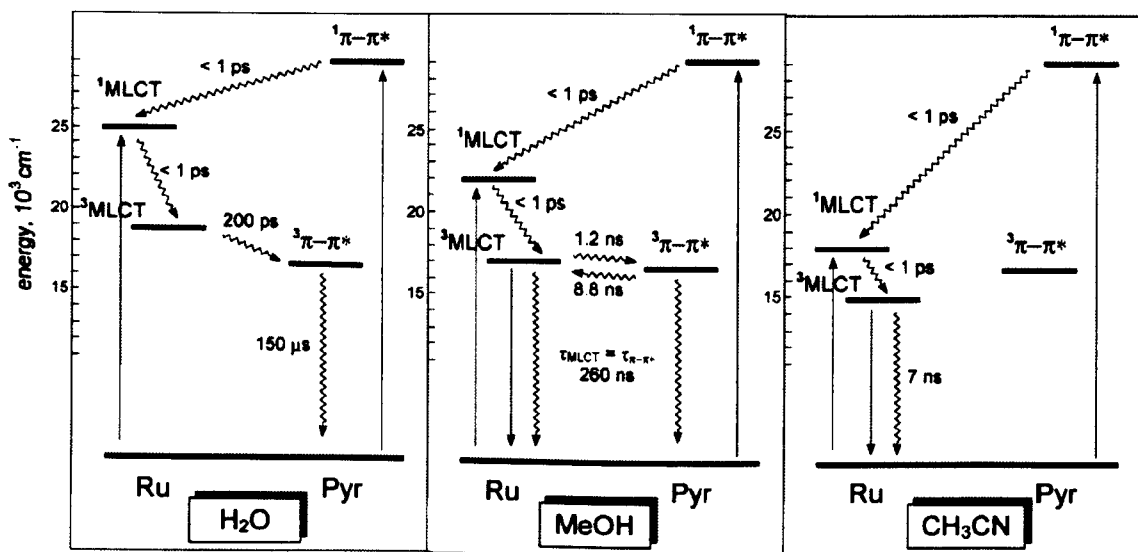


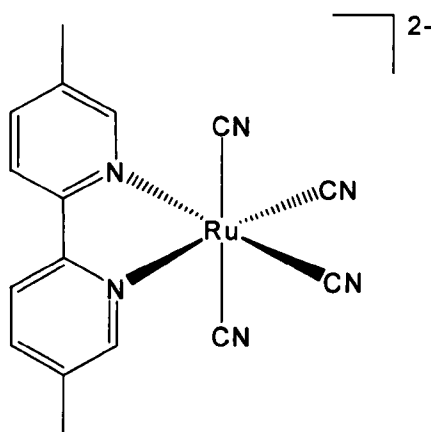
Figure 3.1.7: The photophysics of RuCNpyr in H₂O (left), CH₃OH (centre) and CH₃CN (right). Reproduced from Ref.⁴

These two studies illustrate the utility of the [Ru(CN)₄(bpy)]²⁻ unit in systems where solvent composition can be used to tune the excited state ordering in either bimetallic or organic-inorganic systems. However there are limitations in the amount of useful information one can derive from luminescence spectra in these cases – especially in the case of RuCN-BL-Rubpy – as the broad, featureless nature of ³MLCT emission peaks and the low quantum yield and short lifetime of the [Ru(CN)₄(bpy)]²⁻ unit, particularly in low A. N. solvents (§2.1.1) prevent conclusive understanding of the nature and mechanism of the PenT process. This is compounded by the fact that luminescence only provides information on the energy transfer process through the sensitised luminescence of the energy-accepting chromophore. Emission from this

process can be difficult to disentangle from other luminescence processes, such as direct excitation of the acceptor chromophore, which for a strongly luminescent chromophore such as $[\text{Ru}(\text{bpy})_3]^{2+}$ may dominate the spectrum.

For these reasons, in addition to luminescence we have employed ultrafast TRIR spectroscopy to monitor the vibrational spectra of both termini of our bimetallic complexes (based on the design of **RuCN-BL-Rubpy**) with the aim of directly monitoring the Förster PEnT process in real time. §3.2, 3.3 and 3.4 detail the photophysics and electrochemistry of the novel model complexes which the bimetallics in §3.5, 3.6 and 3.7 are based upon. The results and implications of the studies above are compared with those from this Thesis and analysed in more detail in the Chapter Discussion (§3.8).

3.2. $[\text{Ru}(\text{CN})_4((5,5'\text{-CH}_3)_2\text{bpy})]\text{X}_2$ ($\text{X}=\text{K}^+$ or PPN^+), **RuCNdmb**



RuCNdmb is a member of the $[\text{Ru}(\text{CN})_4(\text{NN})]^{2-}$ family which have been studied with electrochemistry and absorption, luminescence and TRIR spectroscopy in Chapter 2. Methyl groups have been introduced at the 5,5' positions on the bpy ligand in order to more closely simulate the electronic environment of the metal centre in the dinuclear complexes **RuCN-BL¹-Rubpyamide** (§3.5) and **RuCN-BL²-Rubpyamide** (§3.6), which are linked by an ethyl spacer. Spectroscopic studies have demonstrated that the remote shielding of the cyanide ligand induces a downfield shift in the NMR spectrum of the hydrogens in the 6,6' positions located above and below the ligand in

RuCNdmb. This is in contrast to the general aromatic ring current effect, which leads to an upfield shift in the ^1H NMR signals for the other aromatic protons.⁵

The similar ground and excited state properties of **RuCNdmb** and $[\text{Ru}(\text{CN})_4(\text{bpy})]^{2-}$ were compared in Chapter 2, and as expected **RuCNdmb** displays strong negative solvatochromism.

3.2.1. UV/visible Absorption and Luminescence Spectroscopy

The UV/visible absorption spectra of **RuCNdmb** have been measured in D_2O , H_2O , CH_3OH and CH_3CN (see Appendix §3.9 for spectra). The results are presented in Table 3.2.1.1. The observed negative solvatochromism of these complexes is due to SSDA interactions between the externally directed cyanide ligands and solvent molecules (§1.2.4). This phenomenon is responsible for a difference in the energy of the lowest energy $^1\text{MLCT}$ excited state of *ca.* 4600 cm^{-1} between H_2O and CH_3CN .

Solvent	$\lambda^{\text{max}} / \text{nm}$		
	D_2O	293	320
H_2O	293	320	396
CH_3OH	293	347	431
CH_3CN	297	361	483
$\lambda^{\text{max}} (\text{CH}_3\text{CN}-\text{H}_2\text{O})$	4	41	88
Assignment	IL $\pi-\pi^*$	$^1\text{MLCT}$	$^1\text{MLCT}$

Table 3.2.1.1: Table of peak positions and assignments for UV/visible absorption spectra of RuCNdmb in D_2O , H_2O , CH_3OH and CH_3CN solutions.

The emission spectra of **RuCNdmb** were measured in D_2O , H_2O , CH_3OH and CH_3CN and the results are presented in Table 3.2.1.2. The broad, structureless emission observed is consistent with emission from $^3\text{MLCT}$ excited states, as observed in the family of $[\text{Ru}(\text{CN})_4(\text{NN})]^{2-}$ complexes in Chapter 2. The observed variation in $^3\text{MLCT}$ excited state energy ($\Delta E_{\text{H}_2\text{O}-\text{CH}_3\text{CN}} = 1800\text{ cm}^{-1}$) is significantly

smaller than the energy separation derived from the absorption spectrum ($\Delta E_{\text{H}_2\text{O}-\text{CH}_3\text{CN}} = 4600 \text{ cm}^{-1}$). In $\text{Ru} \rightarrow (\text{NN})^3\text{MLCT}$ excited states partial oxidation of the metal centre leads to electron density being redistributed from CN^- to Ru^{III} , decreasing the available electron density for donor-acceptor interactions (§1.2.4, also see §3.1.2).⁶

	A. N.	$\lambda^{\text{max}} / \text{nm}$	$\lambda^{\text{max}} \text{ Energy} / \text{cm}^{-1}$	τ / ns	ϕ
D_2O	54.8	614	16300	1020*	0.030
H_2O	54.8	614	16300	375 (± 42)	0.012
CH_3OH	41.3	649	15400	210 (± 15)	0.007
CH_3CN	19.3	729	14500	49 (± 12)	0.002

Table 3.2.1.2: Table of peak positions, lifetimes and quantum yields from luminescence spectroscopy of RuCNdmb in D_2O , H_2O , CH_3OH and CH_3CN solutions. *The statistical error from curve fitting is $\pm 1 \text{ ns}$, however this is smaller than a reasonable instrumental error.

The longer lifetime of RuCNdmb in D_2O relative to H_2O is attributed to a decrease in the non-radiative decay rate in deuterated solvents, as in the related complex $[\text{Ru}(\text{CN})_4(\text{bpy})]^{2-}$ (§2.1.2).⁷ The fluorescence lifetimes decrease as the Acceptor Numbers (A. N.) decrease and the emission energies decrease. This is in accordance with the ‘energy-gap law’, which states that the rate of non-radiative decay for a MLCT transition increases exponentially as the emission energy decreases (§1.3).⁸ The trend in quantum yield for the $^3\text{MLCT}$ emission also follows this pattern, with $\phi_{\text{em}}(\text{D}_2\text{O}) > \phi_{\text{em}}(\text{H}_2\text{O}) > \phi_{\text{em}}(\text{CH}_3\text{OH}) \approx \phi_{\text{em}}(\text{CH}_3\text{CN})$, in a similar manner to other $[\text{Ru}(\text{CN})_4(\text{NN})]^{2-}$ complexes (§2.1.2).

3.2.2. Cyclic Voltammetry

Cyclic voltammetry of RuCNdmb in CH_3CN was measured (see Appendix §3.9 for voltammograms) and the results are presented in Table 3.2.2.1 below. Features corresponding to one reduction and one oxidation couple are observed. Neither couple is easily discerned from the voltammogram. In particular the reduction was detected

as a discontinuity at a potential outside the solvent window (*ca.* -2 to +2 V vs. Ag/AgCl), so its reversibility was not determined. Upon application of potentials outside the solvent window the voltammogram shows features consistent with the products of solvent decomposition.

$E_{1/2}/V$ (vs. Fc/Fc ⁺)	Reversibility	Assignment
-0.03	Quasi-reversible	Ru ^{II/III}
-2.57	Undetermined (<i>vide supra</i>)	(5,5'-CH ₃) ₂ bpy) ^{0/+•-}

Table 3.2.2.1: Table of potentials for redox couples and assignments for the cyclic voltammogram of RuCNdmb in CH₃CN solution.

The oxidation potential is comparable to that of [Ru(bpy)(CN)₄]²⁻ in CH₃CN ($E_{1/2, \text{ox}} = -0.14$ V (vs. Fc/Fc⁺)).⁹ The reduction potential is similar to that of [Ru(bpy)(CN)₄]²⁻ in (CH₃)₂NCHO $E_{1/2, \text{red}} = -2.46$ V (vs. Fc/Fc⁺).¹⁰ It appears that the electron-donating effect of the methyl groups in the 5,5' positions makes the ligand reduction more difficult due to an increase in the energy of the ligand-based π^* LUMO.

Attempts to study **RuCNdmb** in H₂O are hampered by the potential range permitted by the solvent (*ca.* -1 to +1 V vs. the Ag/AgCl). The bpy-based reduction is expected to have a similar potential in H₂O (*ca.* -2.5 V) and hence be outside the measurement range, whilst the oxidation would be expected to occur at a similar potential to that of [Ru(bpy)(CN)₄]²⁻. With $E_{1/2, \text{ox}} = +0.77$ V (vs. Fc/Fc⁺),⁹ the required potential vs. an Ag/AgCl reference electrode would be around +1.3 V.

3.2.3. Infrared Spectroelectrochemistry

Attempts to monitor the 1st reduction using FTIR spectroscopy on **RuCNdmb** in CH₃CN solution were unsuccessful as the process is chemically irreversible on the IR-OTTLE experimental timescale.

3.2.4. UV/visible/nIR Spectroelectrochemistry

Attempts to monitor the 1st reduction using UV/vis spectroscopy on **RuCNdmb** in CH₃CN solution were unsuccessful as the process is chemically irreversible on the UVVis-OE experimental timescale.

3.2.5. FTIR and Time-Resolved Infrared Spectroscopy

The $\nu(\text{CN})$ region of the FTIR spectrum of **RuCNdmb** has been measured in CH₃CN and D₂O (see Appendix §3.9 for spectra). The complex has C_{2v} symmetry and should possess 4 IR active bands. It is clear from the spectral profile that several overlapping bands are present; visual inspection and least-squares fitting give at least 3 peak maxima in both CH₃CN and D₂O. These are at 2085, 2069, 2057 and 2044 cm⁻¹ in CH₃CN and at 2091, 2050 and 2030 cm⁻¹ in D₂O. These band positions are comparable with other [Ru(CN)₄(NN)]²⁻ complexes (Chapter 2). The difference in peak maxima is due to the hydrogen-bonding interaction of the cyanide ligands with solvent molecules and is further evidence for solvent-derived perturbation of vibronic energy levels in the complex.

Nanosecond and picosecond-TRIR spectra of **RuCNdmb** were measured in CH₃CN and D₂O solution. Figure 3.2.5.1 shows the ps-TRIR spectra obtained. Immediately after excitation the ground state bands are bleached and a transient feature appears at higher wavenumber. This feature has a maximum at 2108 cm⁻¹ in CH₃CN and 2096 cm⁻¹ in D₂O respectively. No evidence for vibrational cooling can be inferred from the ps-TRIR spectra. The bands formed do not decay over the picosecond timescale. The shifts of the $\nu(\text{CN})$ band to higher wavenumber are consistent with the formation of a Ru → (5,5'-(CH₃)₂bpy) ³MLCT excited state.

As is observed in other members of the [Ru(CN)₄(NN)]²⁻ family (§2.2.3), the intensities of $\nu(\text{CN})$ bands in the IR region are much lower than comparable $\nu(\text{CO})$ bands and this can present spectral detection and signal-to-noise problems,

particularly with dilute or sparingly-soluble samples.¹¹ Furthermore there is significant spectral overlap of the transient bands formed upon excitation with the high energy components of the ground-state $[\text{Ru}(\text{CN})_4(\text{NN})]^{2-}$ spectrum. These issues compound the difficulty in resolving single vibrational bands in both the ground and excited state spectral profiles and in some cases may limit the amount of information which can be extracted from the spectra owing to peaks not being clearly resolved (the PIRATE spectrometer has an instrumental resolution of *ca.* 8-9 cm^{-1} , see Chapter 6 for more details).

The same spectral profile observed in the ps-TRIR spectra is reproduced on the nanosecond scale in both solvents. This profile decays with a time constant of 107 (± 11) ns in CH_3CN . In D_2O the spectra decay with a biexponential time dependence, with time constants 38 (± 9) and 430 (± 130) ns (Figure 3.2.5.2). Lifetimes are calculated by averaging the values obtained from fitting both bleach and transient kinetic data. The TRIR results are summarised in Table 3.2.5.1.

	Ground State/ cm^{-1}			Excited State/ cm^{-1}	τ / ns	
D_2O	2091		2050	2030	2096	430 (± 130)
CH_3CN	2089	2065	2057	2044	2108	107 (± 11)

Table 3.2.5.1: Table of peak positions and lifetimes from TRIR spectra of RuCNdmb in D_2O and CH_3CN solutions.

3.2.6. RuCNdmb: Closing Points

The results from luminescence and TRIR spectroscopy confirm that the lowest-lying excited state of **RuCNdmb** is $\text{Ru} \rightarrow ((5,5'-(\text{CH}_3)_2\text{bpy})^3\text{MLCT}$, with the excited state electron density located on the bipyridyl ring system. There is a strong negative solvatochromic effect on the absorption and emission energies of the MLCT transitions, and the “energy-gap law” may be invoked to rationalise the decrease in excited state lifetime and quantum yields as solvent A. N. decreases (§1.3).⁸ The range of $^3\text{MLCT}$ energies exhibited by **RuCNdmb** varies between 14500 cm^{-1}

(CH₃CN) and 16300 cm⁻¹ (D₂O) and this effect can be exploited to provide a means for modulating the excited state energy of the complex in polynuclear assemblies (*vide supra*). The emission quantum yield decreases by approximately an order of magnitude from H₂O to CH₃CN and hence the sensitising abilities of the complex are strongly solvent-dependent.

Our success in using $\nu(\text{CN})$ features in the infrared spectrum of [Ru(CN)₄(NN)]²⁻ (§2.2.3 and §3.2.5) to probe excited state electronic structure unlocks the possibility of studying the excited state dynamics of **RuCNdmb** (and supramolecular systems incorporating it) using TRIR on the picosecond and nanosecond timescales.

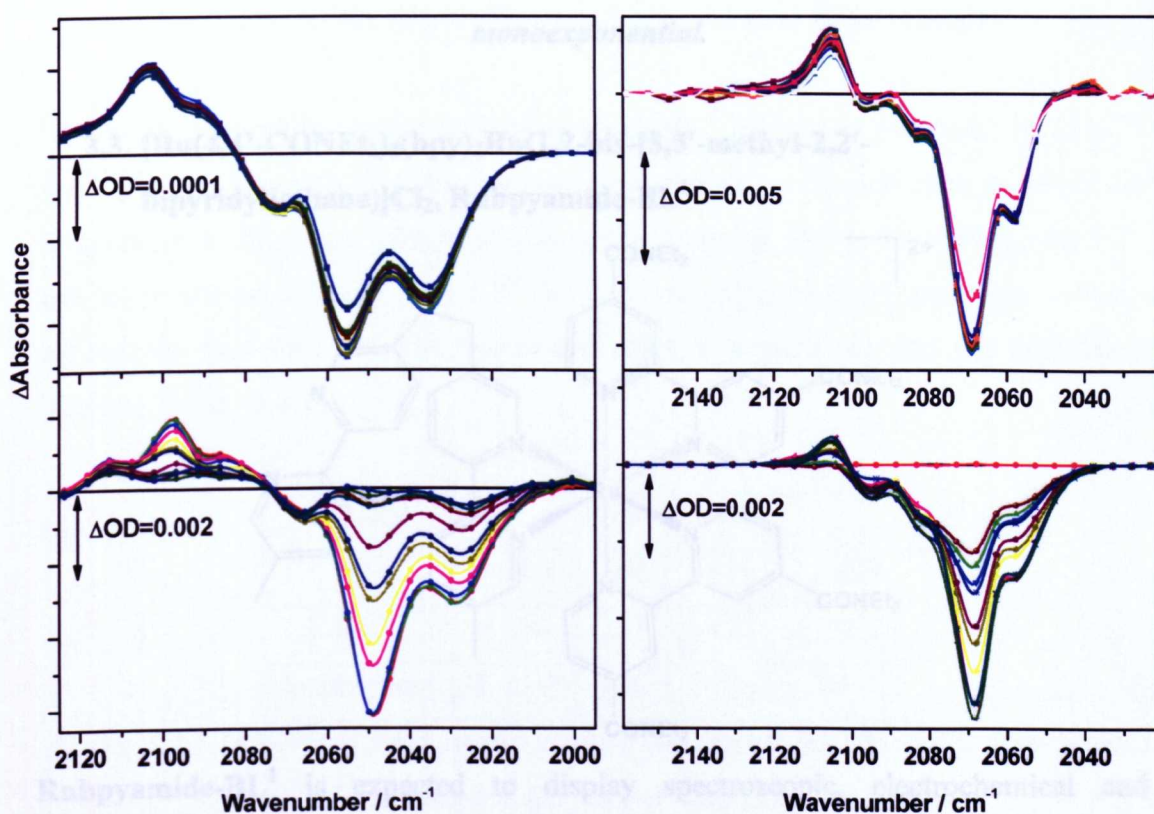


Figure 3.2.5.1: TRIR spectra of RuCNdmb in D₂O (left) and CH₃CN (right).
Top: Spectra recorded between 2 and 1000 ps after 400 nm laser excitation.
Bottom: Spectra recorded between 1 and 1000 ns after 355 nm laser excitation.

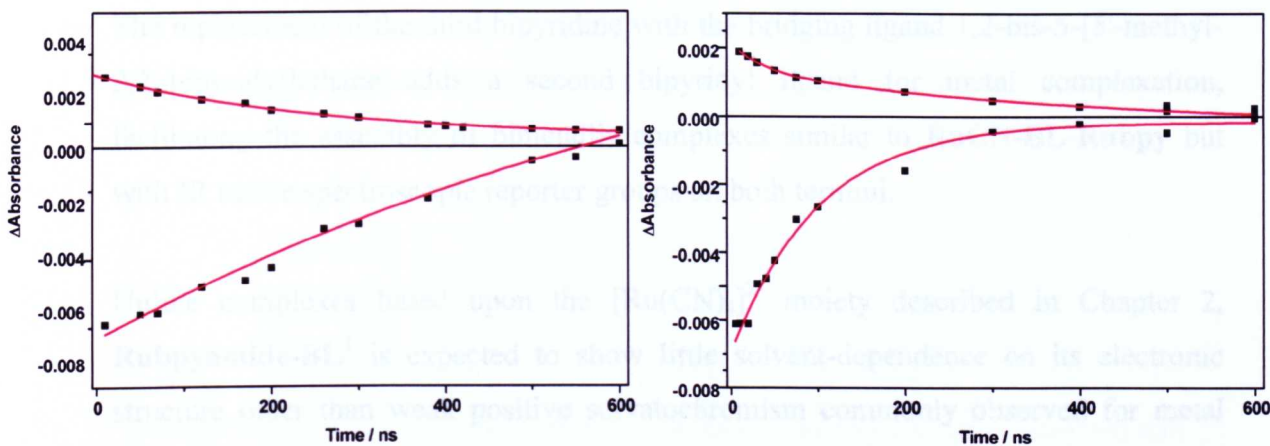
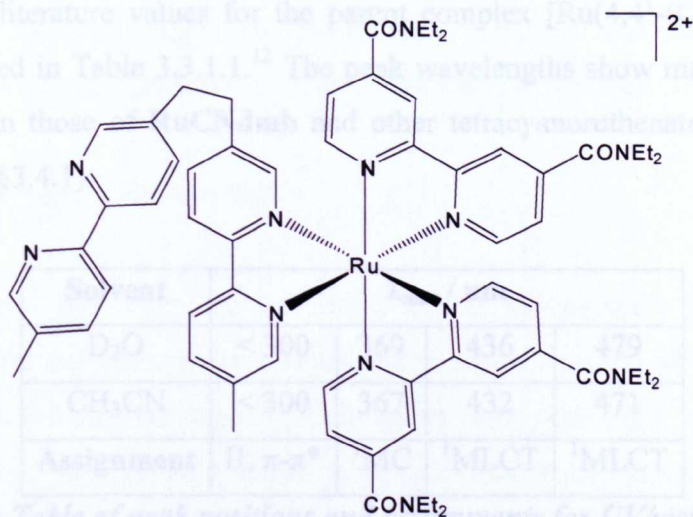


Figure 3.2.5.2: Kinetic traces from ns-TRIR spectra of RuCNdmb in D_2O (transient at 2097 cm^{-1} , top left and bleach at 2051 cm^{-1} , bottom left) and CH_3CN (transient at 2097 cm^{-1} , top right and bleach at 2104 cm^{-1} , bottom right). Fits shown in red are monoexponential.

3.3. $[Ru(4,4'-CONEt_2)_2(bpy)_2Ru(1,2\text{-bis-}[5,5'\text{-methyl-2,2'-bipyridyl]ethane)]Cl_2$, Rubpyamide-BL¹



Rubpyamide-BL¹ is expected to display spectroscopic, electrochemical and photophysical characteristics similar to the parent complex $[Ru(bpy)_3]^{2+}$ and its amide-derivatised analogue $[Ru(4,4'\text{-CO}(\text{NEt}_2)_2bpy)_2(bpy)]^{2+}$ (§1.4.1.1). The $\nu(\text{CO})$ bands of the amide groups provide a spectroscopic handle in the infrared region of the spectrum, probing the electron density on the bipyridyl rings in an analogous manner to studies performed by Meyer and co-workers (see §1.4.1.1 and references therein).

The replacement of the third bipyridine with the bridging ligand 1,2-bis-5-[5'-methyl-2,2'-bipyridyl]ethane adds a second bipyridyl ligand for metal complexation, facilitating the assembly of bimetallic complexes similar to **RuCN-BL-Rubpy** but with IR active spectroscopic reporter groups on both termini.

Unlike complexes based upon the $[\text{Ru}(\text{CN})_4]^{2-}$ moiety described in Chapter 2, **Rubpyamide-BL¹** is expected to show little solvent-dependence on its electronic structure other than weak positive solvatochromism commonly observed for metal complexes (§1.2.2). As a result the emission energies of the complex are expected to be almost solvent-independent.

3.3.1. UV/visible Absorption and Luminescence Spectroscopy

UV/visible absorption spectra of **Rubpyamide-BL¹** have been measured in CH_3CN and D_2O (see Appendix §3.9 for spectra). The spectral profile and peak positions are comparable to literature values for the parent complex $[\text{Ru}(4,4'-(\text{CONEt}_2)_2\text{bpy})_3]^{2+}$ and are presented in Table 3.3.1.1.¹² The peak wavelengths show much less solvent-dependence than those of **RuCNdmb** and other tetracyanoruthenate (II) complexes (Chapter 2 and §3.4.1).

Solvent	$\lambda_{\text{max}} / \text{nm}$			
	D_2O	< 300	369	436
CH_3CN	< 300	367	432	471
Assignment	IL π - π^*	¹ MC	¹ MLCT	¹ MLCT

Table 3.3.1.1: Table of peak positions and assignments for UV/visible absorption spectra of Rubpyamide-BL¹ in D₂O and CH₃CN solutions.

The emission profile of **Rubpyamide-BL¹** has been measured in CH_3CN and D_2O (see Appendix §3.9 for spectra) and the results are presented in Table 3.3.1.2. The broad, structureless spectra are characteristic of emission from ³MLCT excited states and the spectra, lifetimes and quantum yields are comparable with those of $[\text{Ru}(4,4'$

(CONEt)₂bpy)₃]²⁺ (§1.4.1.1).¹² The slightly lower emission energy for **Rubpyamide-BL¹** in D₂O compared to CH₃CN (*ca.* 260 cm⁻¹) is due to increased stabilisation of the excited state by more polar solvent molecules.¹³

Solvent	λ_{\max} / nm	λ^{\max} Energy / cm ⁻¹	τ / ns	ϕ
D ₂ O	652	15340	367 (±41)	0.069
CH ₃ CN	641	15600	341 (±10)	0.061

Table 3.3.1.2: Table of peak positions, ³MLCT emission energies, lifetimes and quantum yields for luminescence spectra of Rubpyamide-BL¹ in D₂O and CH₃CN solutions.

The ³MLCT excited state energy of **Rubpyamide-BL¹** (*ca.* 15500 cm⁻¹) lies within the range of ³MLCT excited state energies determined for **RuCNdmb** (16300 - 14500 cm⁻¹, §3.2.1). It follows that the location of the lowest energy excited state in a dinuclear complex containing the **RuCNdmb** and **Rubpyamide-BL¹** moieties should be tuneable by changing the solvent composition, provided that combination of the two fragments does not significantly perturb their electronic structure.

3.3.2. Cyclic Voltammetry

Rubpyamide-BL¹ has been studied using cyclic voltammetry in CH₃CN (see Appendix §3.9 for the voltammogram) and the results are presented in Table 3.3.2.1. There is one reversible oxidation which arises from the Ru^{II/III} couple, a large irreversible feature at positive potential (due to oxidation of the amide groups) and three reversible reduction couples arising from the bpy-based ligands. The potentials for the oxidation and the 1st and 2nd reductions are similar to those reported for [Ru(4,4'-(CONEt)₂bpy)₃]²⁺: E_{1/2, ox} = +0.93 V, E_{1/2, red1} = -1.54 V and E_{1/2, red2} = -1.68 V (all vs. Fc/Fc⁺, §1.4.1.1).¹⁴

$E_{1/2}/V$ (vs. Fc/Fc^+)	Reversibility	Assignment
+0.95	Reversible	$Ru^{II/III}$
$(E_p) +0.78$	Irreversible	$(4,4'-(CONEt_2)_2bpy)^{0/+}$
-1.57	Reversible	$(4,4'-(CONEt_2)_2bpy)^{0/+}$
-1.76	Reversible	$(4,4'-(CONEt_2)_2bpy)^{0/+}$
-2.15	Reversible	$(BL^1)^{0/+}$

Table 3.3.2.1: Table of potentials for redox couples and assignments for the cyclic voltammogram of Rubpyamide-BL¹ in CH₃CN solution.

The 1st and 2nd reductions occur closely together ($\Delta E_{red2-red1} = -0.19$ V), indicating that they take place on the amide-substituted bpy ligands, which are expected to have lower-energy π^* orbitals than BL¹ due to the electron-withdrawing nature of the amide groups. As there are two identical (4,4'-(CONEt₂)₂bpy) ligands in the complex, the difference between the 1st and 2nd reduction potentials corresponds to the increased repulsion from adding another electron to an already reduced complex.¹⁴ The 3rd reduction takes place at a much more negative potential ($\Delta E_{red3-red2} = -0.39$ V) and is centred on the ligated bipyridyl of BL¹. A 4th reduction centred on the bridging bipyridyl would be expected at more negative potentials, but was not observed in the potential window of CH₃CN (*ca.* +2 to -2 V).

3.3.3. Infrared Spectroelectrochemistry

IR spectroelectrochemistry was used to monitor the change in spectral profile of the amide $\nu(CO)$ bands of Rubpyamide-BL¹ in CH₃CN as each of the redox couples in Table 3.3.2.1 was stepped across.

Ru^{II/III} Oxidation

The change in spectral profile (not shown) is irreversible and the only spectroscopic change observed is a decrease in the absorbance of the parent band. This is attributed

to the decomposition of the amide groups at less positive potentials than that required to oxidise the metal centre.

(4,4'-(CONEt₂)₂bpy)^{0/+} Reduction Couples

Figure 3.3.3.1 shows the spectra obtained as the first and second reductions occur. Between -0.7 and -1.2 V (vs. Ag) the parent feature at 1639 cm⁻¹ decreases in absorbance, its profile broadens and its centre shifts to lower wavenumber. Considerable overlap with a solvent band makes it difficult to extract further information from the raw spectra. This is consistent with an increase in electron density on the (4,4'-(CONEt₂)₂bpy) ligands and confirms that the first two reductions are taking place there, as predicted from the cyclic voltammogram (*vide supra*). The spectra in Figure 3.3.3.1 are broad and structureless, however the subtraction spectra presented in Figure 3.3.3.2 allow the changes in spectral profile to be visually inspected as the reductions take place. Two peaks appear in the spectra at *ca.* 1622 and 1582 cm⁻¹. The 1622 cm⁻¹ band grows in only during the 1st reduction (Figure 3.3.3.2, top) and the 1582 cm⁻¹ band grows in only during the 2nd reduction (Figure 3.3.3.2, bottom).

This suggests that each reduction is *localised* on the IR timescale (§1.3) and takes place on a particular ligand, so that features arising from neutral and reduced (4,4'-(CONEt₂)₂bpy) are present throughout the experiment. If the electron were *delocalised* over both (4,4'-(CONEt₂)₂bpy) ligands then only one peak would appear as the reduction occurred. Previous photophysical and electrochemical studies on *bis*-heteroleptic Ru(II) polypyridine complexes have observed electron localisation on single bipyridyl ligands.^{14,15}

These data are consistent with the findings from the CV measurements that the individual reductions themselves are not isolated processes and there may be singly and doubly reduced species present in the spectra ascribed to the 'first reduction'. Coulometric studies on [Ru((4,4'-(CONEt₂)₂bpy)₃)]²⁺ show that the first reduction involves the addition of 0.8 electrons to the complex and the second adds 1.4.¹⁶

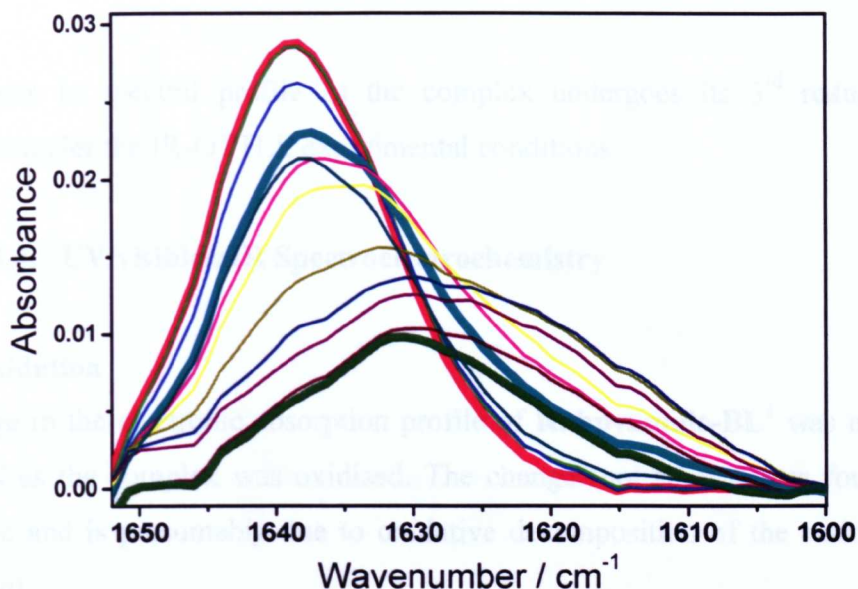


Figure 3.3.3.1: FTIR spectra of the 1st and 2nd reductions of Rubpyamide-BL¹ in CH₃CN. The initial spectrum (A, red), the spectrum obtained after the 1st reduction (B, cyan) and the final spectrum (C, green) are highlighted. Changes in spectral profile are reversible.

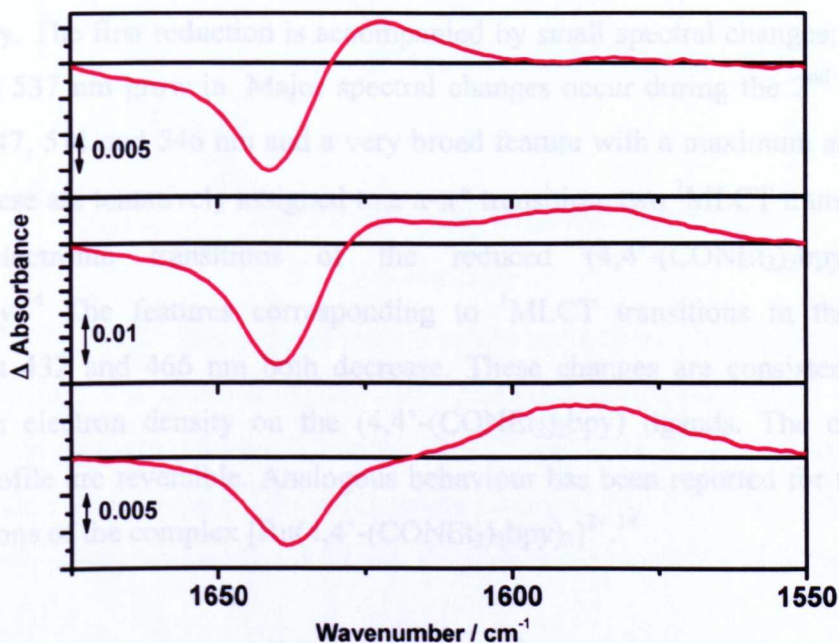


Figure 3.3.3.2: Difference IR spectra of the 1st and 2nd reductions of Rubpyamide-BL¹ in CH₃CN. Top: Difference spectrum obtained from Figure 3.3.3.1 by subtracting the spectrum B from spectrum A. Middle: spectrum C – spectrum A. Bottom: spectrum C – spectrum B.

The changes in spectral profile as the complex undergoes its 3rd reduction are irreversible under the IR-OTTLE experimental conditions.

3.3.4. UV/visible/nIR Spectroelectrochemistry

Ru^{II/III} Oxidation

The change in the electronic absorption profile of **Rubpyamide-BL¹** was monitored in CH₃CN as the complex was oxidised. The change (not shown) was found to be irreversible and is presumably due to oxidative decomposition of the amide groups (*vide supra*).

(4,4'-(CONEt₂)₂bpy)^{0/+} Reduction Couples

Figure 3.3.4.1 shows UV/vis/nIR spectra for **Rubpyamide-BL¹** in CH₃CN as the complex undergoes its first and second reductions at -1.00 and -1.25 V vs. Ag/AgCl respectively. The first reduction is accompanied by small spectral changes; shoulders at 368 and 537 nm grow in. Major spectral changes occur during the 2nd reduction. Peaks at 347, 511 and 546 nm and a very broad feature with a maximum at 1308 nm appear. These are tentatively assigned to a π - π^* transition, two ¹MLCT transitions and various electronic transitions of the reduced (4,4'-(CONEt₂)₂bpy) ligand respectively.¹⁴ The features corresponding to ¹MLCT transitions in the original complex at 432 and 466 nm both decrease. These changes are consistent with an increase in electron density on the (4,4'-(CONEt₂)₂bpy) ligands. The changes in spectral profile are reversible. Analogous behaviour has been reported for the 1st and 2nd reductions of the complex [Ru(4,4'-(CONEt₂)₂bpy)₃]²⁺.¹⁴

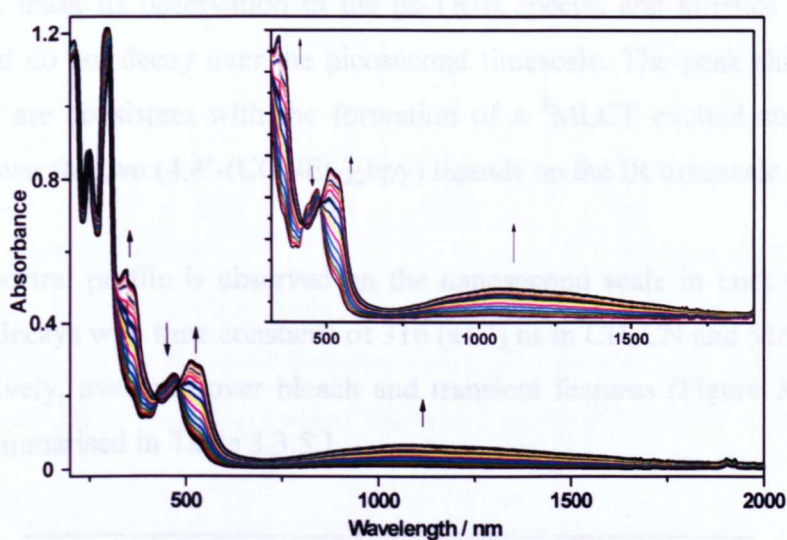
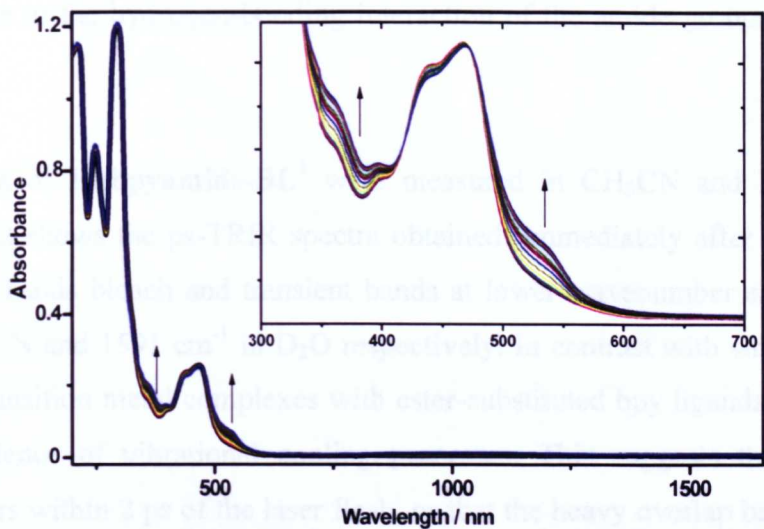


Figure 3.3.4.1: The UV/visible/nIR spectra of the reduction of Rubpyamide-BL¹ in CH₃CN. Top: The 1st reduction at -1.00 V; inset: magnification of the region containing major changes. Bottom: The 2nd reduction at -1.25 V; inset: magnification of the region containing major changes. The initial spectrum (thick black) is emphasised in each case. Potentials are quoted vs. Ag/AgCl.

3.3.5. FTIR and Time-Resolved Infrared Spectroscopy

The amide $\nu(\text{CO})$ region of the FTIR spectrum of Rubpyamide-BL¹ has been measured in CH₃CN and D₂O (see Appendix §3.9 for spectra). There is a single peak present at 1638 cm⁻¹ in CH₃CN and at 1612 cm⁻¹ in D₂O. The difference in the peak

centres is due to the hydrogen-bonding interaction of the amide groups with solvent molecules.

TRIR spectra of **Rubpyamide-BL¹** were measured in CH₃CN and D₂O solution. Figure 3.3.5.2 shows the ps-TRIR spectra obtained. Immediately after excitation the ground state bands bleach and transient bands at lower wavenumber appear at 1621 cm⁻¹ in CH₃CN and 1591 cm⁻¹ in D₂O respectively. In contrast with similar ps-TRIR studies on transition metal complexes with ester-substituted bpy ligands,¹⁷ there is no spectral evidence of vibrational cooling processes. This suggests that vibrational cooling occurs within 2 ps of the laser flash, or that the heavy overlap between bleach and transient mask its observation in the ps-TRIR spectra and kinetics shown. The bands formed do not decay over the picosecond timescale. The peak shifts to lower wavenumber are consistent with the formation of a ³MLCT excited state which is delocalised over the two (4,4'-(CONEt₂)₂bpy) ligands on the IR timescale (§1.3).¹⁸

The same spectral profile is observed on the nanosecond scale in both CH₃CN and D₂O, which decays with time constants of 316 (±17) ns in CH₃CN and 515 (±42) ns in D₂O respectively, averaged over bleach and transient features (Figure 3.3.5.3). The results are summarised in Table 3.3.5.1.

Solvent	Bleach / cm ⁻¹	Transient/ cm ⁻¹	τ / ns
D ₂ O	1612	1591	515 (±42)
CH ₃ CN	1638	1621	316 (±17)

Table 3.3.5.1: Table of peak positions and lifetimes for ns-TRIR spectra of Rubpyamide-BL¹ in D₂O and CH₃CN solutions.

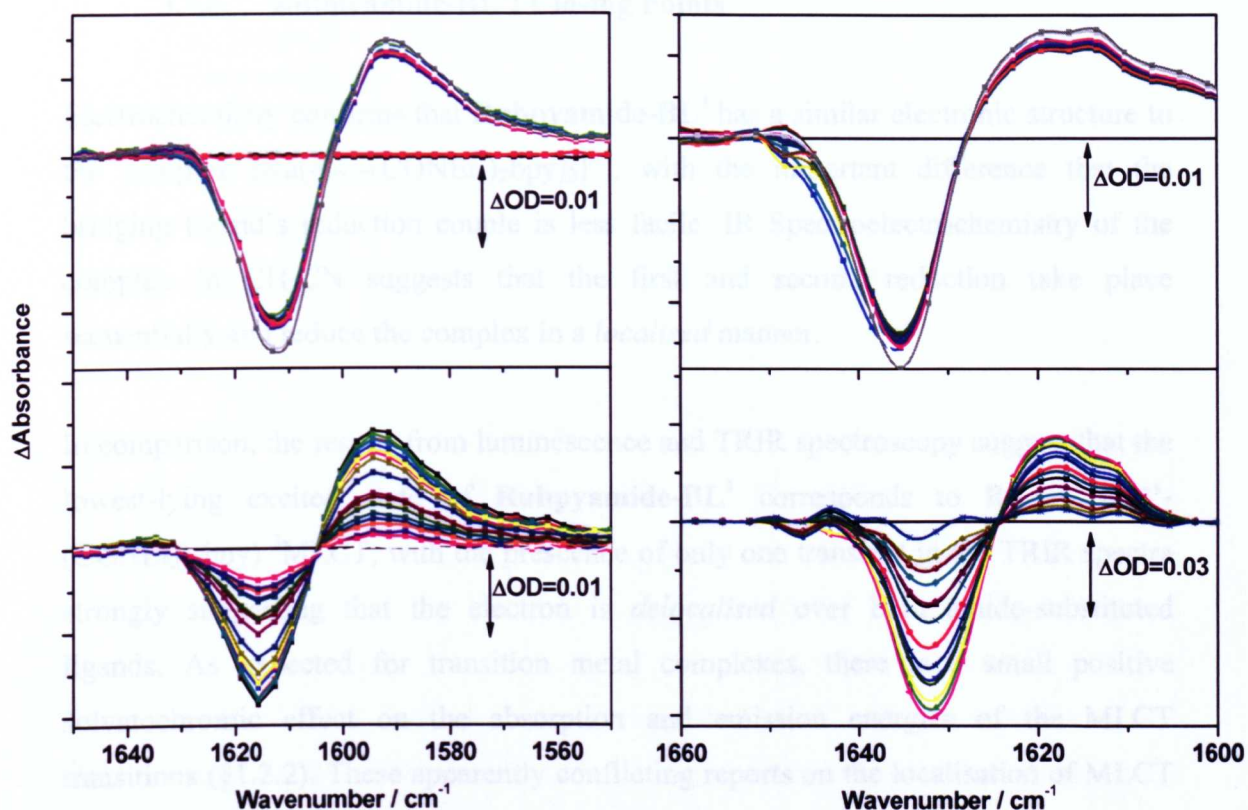


Figure 3.3.5.3: TRIR spectra of Rubpyamide-BL¹ in D₂O (left) and CH₃CN (right).
 Top: ps-TRIR spectra recorded between 2 and 1000 ps after 400 nm excitation.
 Bottom: ns-TRIR spectra recorded between 1 and 1000 ns after excitation.

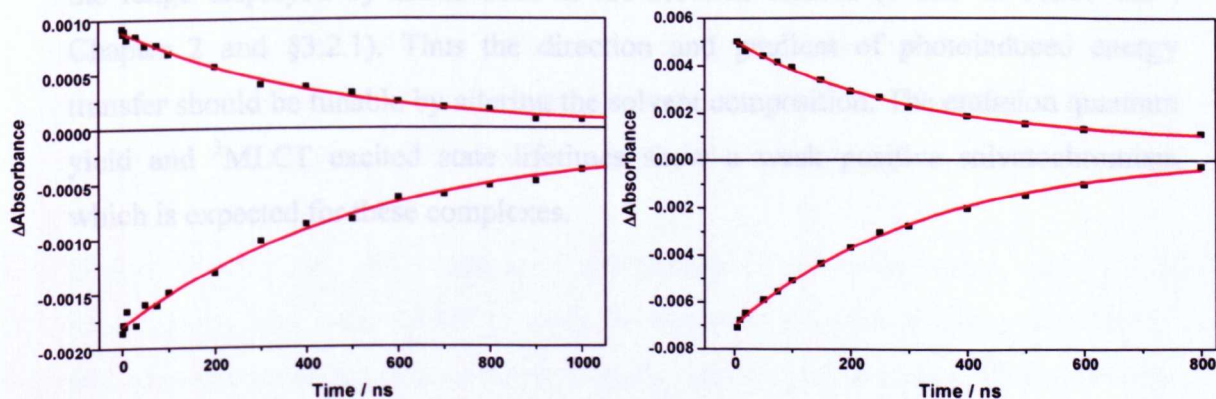


Figure 3.3.5.4: Kinetic traces from TRIR spectra of Rubpyamide-BL¹ in D₂O (transient at 1593 cm⁻¹, top left and bleach at 1617 cm⁻¹, bottom left) and CH₃CN (transient at 1616 cm⁻¹, top right and bleach at 1636 cm⁻¹, bottom right). The fits shown are single exponentials.

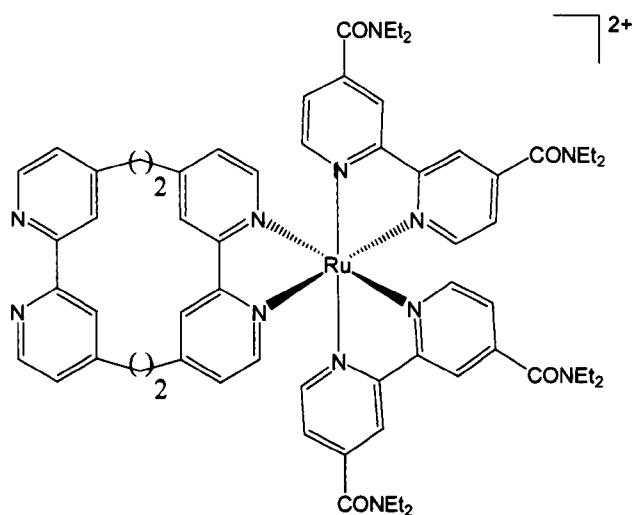
3.3.6. Rubpyamide-BL¹: Closing Points

Electrochemistry confirms that **Rubpyamide-BL¹** has a similar electronic structure to the complex $[\text{Ru}(4,4'-(\text{CONEt}_2)_2\text{bpy})_3]^{2+}$, with the important difference that the bridging ligand's reduction couple is less facile. IR Spectroelectrochemistry of the complex in CH_3CN suggests that the first and second reduction take place sequentially and reduce the complex in a *localised* manner.

In comparison, the results from luminescence and TRIR spectroscopy suggest that the lowest-lying excited state of **Rubpyamide-BL¹** corresponds to $\text{Ru} \rightarrow (4,4'-(\text{CONEt}_2)_2\text{bpy})^3\text{MLCT}$, with the presence of only one transient in the TRIR spectra strongly suggesting that the electron is *delocalised* over both amide-substituted ligands. As expected for transition metal complexes, there is a small positive solvatochromic effect on the absorption and emission energies of the MLCT transitions (§1.2.2). These apparently conflicting reports on the localisation of MLCT excited states are ostensibly due to the *timescale* of the exchange of excited state charge density distributions being faster or slower than the IR timescale (§1.3).

Rubpyamide-BL¹ has excited state energies (15300 to 15600 cm^{-1}) which fall within the range displayed by **RuCNdmb** in the solvents studied (14500 to 16300 cm^{-1} , Chapter 2 and §3.2.1). Thus the direction and gradient of photoinduced energy transfer should be tunable by altering the solvent composition. The emission quantum yield and ³MLCT excited state lifetimes show a weak positive solvatochromism which is expected for these complexes.

3.4. $[\text{Ru}(4,4'\text{-CONEt}_2)_2(\text{bpy}-(4,4'\text{-CH}_2\text{CH}_2)_2\text{-bpy})]\text{Cl}_2$, **Rubpyamide-BL²**



Rubpyamide-BL² is derived from **Rubpyamide-BL¹** with a few important differences. The link between the polypyridyls of the bridging ligand has been modified from a conformationally flexible ethyl chain to a closed ring resembling a macrocycle, and the bpy rings are substituted in the 4,4' positions (as opposed to the 5,5' substitution in **Rubpyamide-BL¹**).¹⁹ This places further restrictions on the ability of the ligand to adopt different spatial geometries and subsequently constricts the free movement of **Rubpyamide-BL²**. The change in substitution pattern on BL² is not expected to make a significant difference to the photophysics or electrochemistry of the complex, as the (4,4'-(CONEt₂)₂bpy) ligands possess lower energy MLCT excited states and less negative reduction potentials than the bridging ligand.

Uv/vis absorption and emission spectroscopy, electrochemistry and TRIR spectroscopy have been utilised to study the electronic structure of **Rubpyamide-BL²** and to compare it with its conformationally unrestricted analogue (**Rubpyamide-BL¹**). As with **Rubpyamide-BL¹**, little or no solvent-dependence on its electronic structure is expected.

3.4.1. UV/visible Absorption and Luminescence Spectroscopy

UV/visible absorption spectra of **Rubpyamide-BL²** have been measured in CH₃CN and D₂O (see Appendix §3.9 for spectra). The spectral profile and peak positions are similar to **Rubpyamide-BL¹** (§3.3.1) and literature values for the complex [Ru(4,4'-(CONEt₂)₂bpy)₃]²⁺ (§1.4.1.1) and are presented in Table 3.4.1.1.¹²

Solvent	λ^{\max} / nm			
	D ₂ O	< 300	360	437
CH ₃ CN	< 300	357	437	468
Assignment	IL π - π^*	¹ MC	¹ MLCT	¹ MLCT

Table 3.4.1.1: Table of peak positions and assignments for UV/visible absorption spectra of Rubpyamide-BL² in D₂O and CH₃CN solutions.

Emission spectra of **Rubpyamide-BL²** have been measured in CH₃CN and D₂O (see Appendix §3.9 for spectra). A broad, featureless spectrum characteristic of ³MLCT emission is obtained, with lifetimes and quantum yields similar to **Rubpyamide-BL¹** (§3.3.1) and [Ru(4,4'-(CO₂Et)₂bpy)₃]²⁺ (§1.4.1.1).¹² The results are presented in Table 3.4.1.2. **Rubpyamide-BL²** also displays the expected slight positive solvatochromism in D₂O compared to CH₃CN.¹³

Solvent	λ^{\max} / nm	λ^{\max} Energy / cm ⁻¹	τ / ns	ϕ
D ₂ O	654	15290	457 (±14)	0.054
CH ₃ CN	647	15460	462 (±8)	0.054

Table 3.4.1.2: Table of peak positions, ³MLCT emission energies, lifetimes and quantum yields for luminescence spectra of Rubpyamide-BL² in D₂O and CH₃CN solutions.

3.4.2. Cyclic Voltammetry

Rubpyamide-BL² has been studied using cyclic voltammetry in CH₃CN (see Appendix §3.9 for the voltammogram) and the results are presented in Table 3.3.2.1. As with **Rubpyamide-BL¹**, there is one reversible oxidation, a large irreversible feature at positive potential (due to oxidation of the amide groups) and three reversible reduction couples arising from the bpy-based ligands. The potentials for the oxidation and the 1st and 2nd reductions are similar to those reported for **Rubpyamide-BL¹** (§3.3.2) and [Ru(4,4'-(CONEt₂)₂bpy)₃]²⁺ (§1.4.1.1).¹⁴

E_{1/2}/V (vs. Fc/Fc⁺)	Reversibility	Assignment
+0.95	Reversible	Ru ^{II/III}
(E _p) +0.78	Irreversible	(4,4'-(CONEt ₂) ₂ bpy) ^{0/+}
-1.57	Reversible	(4,4'-(CONEt ₂) ₂ bpy) ^{0/•-}
-1.76	Reversible	(4,4'-(CONEt ₂) ₂ bpy) ^{0/•-}
<-2.00	Reversible	(BL ¹) ^{0/•-}

Table 3.4.2.1: Table of potentials for redox couples and assignments for the cyclic voltammogram of Rubpyamide-BL² in CH₃CN solution.

The 1st and 2nd reductions occur closely to each other ($\Delta E_{\text{red2-red1}} = -0.19$ V), indicating that they take place on the amide-substituted bpy ligands, which are expected to have lower-energy π^* orbitals than BL¹ due to the electron-withdrawing nature of the amide groups. As there are two identical (4,4'-(CONEt₂)₂bpy) ligands in the complex, the difference between the 1st and 2nd reduction potentials corresponds to the increased repulsion from adding another electron to an already reduced complex.¹⁴ As with **Rubpyamide-BL¹**, the 3rd reduction takes place at a much more negative potential and is centred on the ligated bipyridyl of BL².

3.4.3. FTIR and Time-Resolved Infrared Spectroscopy

The FTIR spectrum of **Rubpyamide-BL²** has been measured in CH₃CN and D₂O in the amide $\nu(\text{CO})$ region (see Appendix §3.9 for spectra). As for **Rubpyamide-BL¹**, there is a single peak present at 1636 cm⁻¹ in CH₃CN and at 1614 cm⁻¹ in D₂O. The difference in the peak centre positions is due to the hydrogen-bonding interaction of the amide groups with solvent molecules.

Nanosecond and picosecond TRIR spectroscopy were performed on **Rubpyamide-BL²** in CH₃CN and D₂O solutions. Figure 3.4.3.1 shows the ps-TRIR spectra obtained. The spectra collected exhibit significant noise levels due to instability of the probe laser during the experimental time allocation at RAL during which the data were collected. Upon excitation the ground state bands bleach and transient bands to lower wavenumber appear at 1617 cm⁻¹ in CH₃CN and 1596 cm⁻¹ in D₂O respectively. No spectral evidence for vibrational cooling following laser excitation is observed in the spectra. The bands formed do not appear to decay over the picosecond timescale. As with **Rubpyamide-BL¹**, the shifts of the $\nu(\text{CO})$ band to lower wavenumber are consistent with charge transfer from the ruthenium atom to the two (4,4'-(CONEt₂)₂bpy) ligands, forming a delocalised ³MLCT excited state (as probed on the IR timescale, §1.3).

A similar spectral profile is observed on the nanosecond scale for each solvent. The peaks decay with biexponential profiles, with time constants (averaged between bleach and transient data) of 7.8 (±1.4) and 500 (±48) ns in CH₃CN. In D₂O a biexponential decay is also observed with time constants 7.5 (±1.1) and 470 (±51) ns (Figure 3.4.3.2). The results obtained are summarised in Table 3.4.3.1.

Solvent	Bleach / cm^{-1}	Transient/ cm^{-1}	τ / ns
D ₂ O	1614	1596	7.5 (± 1.1), 470 (± 51)
CH ₃ CN	1636	1617	7.8 (± 1.4), 500 (± 48)

Table 3.4.3.1: Table of peak positions and lifetimes for TRIR spectra of Rubpyamide-BL² in D₂O and CH₃CN solutions.

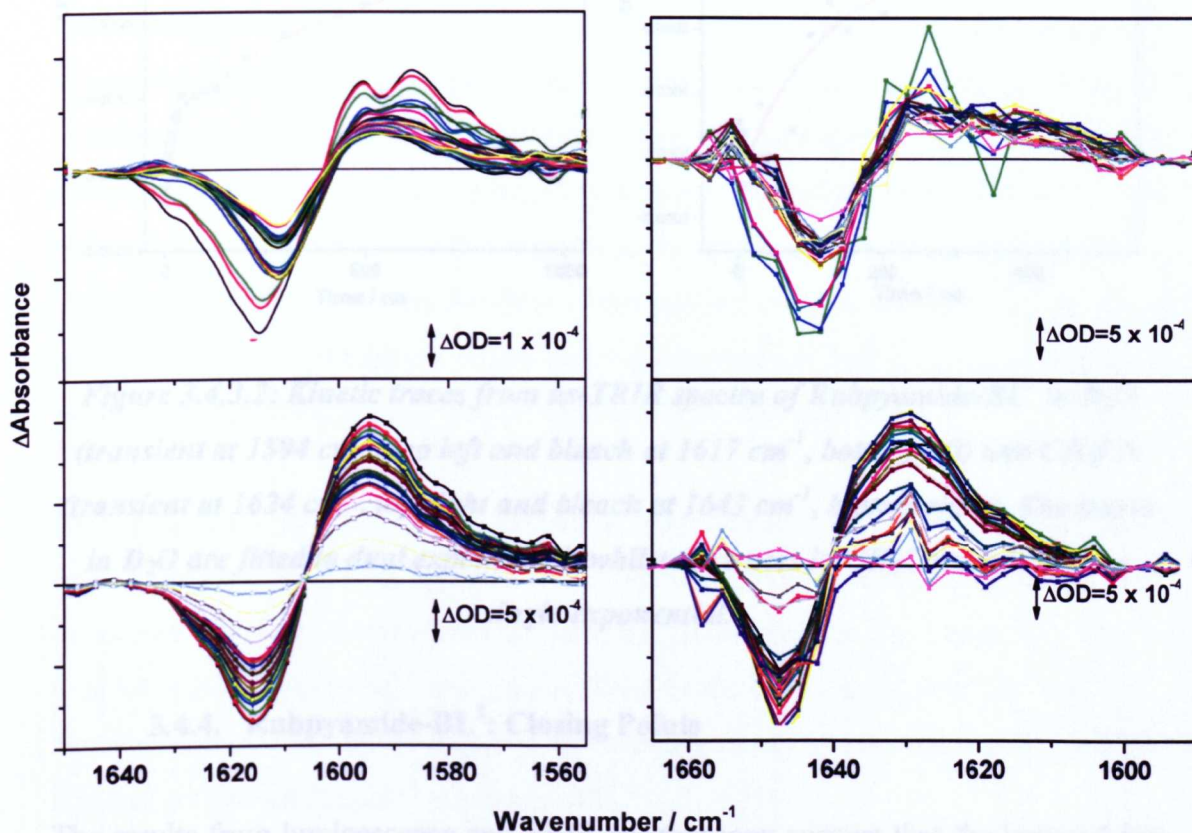


Figure 3.4.3.1: TRIR spectra of Rubpyamide-BL² in D₂O (left) and CH₃CN (right).

Top: ps-TRIR spectra recorded between 2 and 1000 ps after 400 nm excitation.

Bottom: ns-TRIR spectra recorded between 1 and 300 ns after 355 nm excitation.

The spectra recorded were of poor quality due to instability of the PIRATE apparatus' probe laser during the experimental period in which the data were collected.

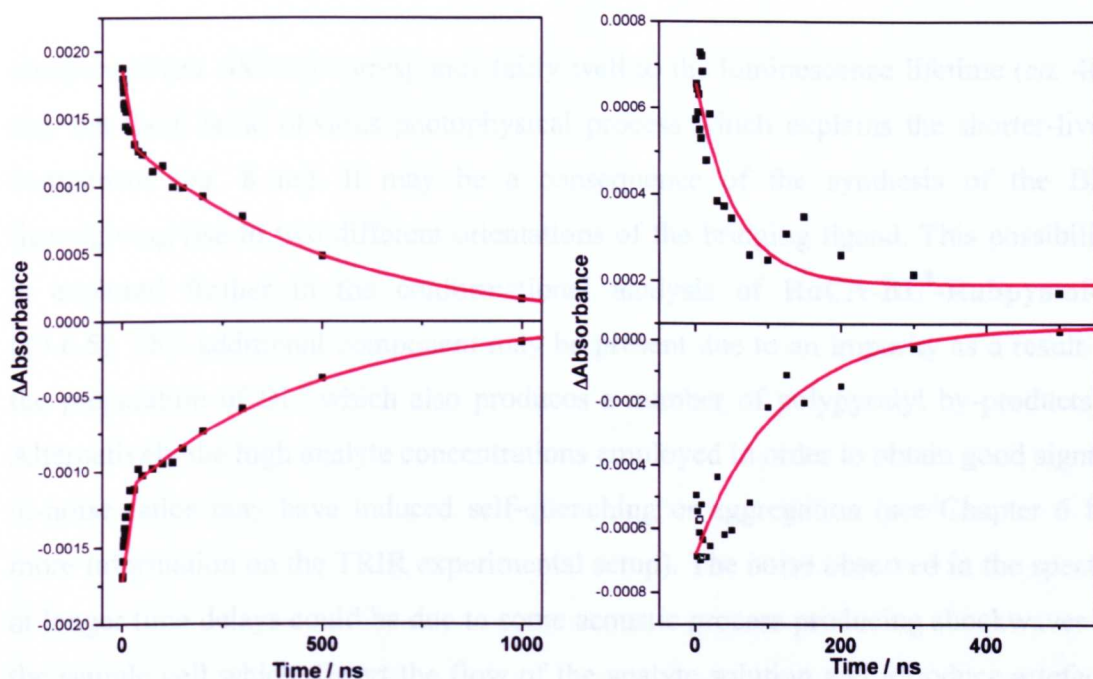


Figure 3.4.3.2: Kinetic traces from ns-TRIR spectra of Rubpyamide-BL² in D₂O (transient at 1594 cm⁻¹, top left and bleach at 1617 cm⁻¹, bottom left) and CH₃CN (transient at 1624 cm⁻¹, top right and bleach at 1643 cm⁻¹, bottom right). The traces in D₂O are fitted to dual exponentials whilst the traces in CH₃CN are fitted to a single exponential.

3.4.4. Rubpyamide-BL²: Closing Points

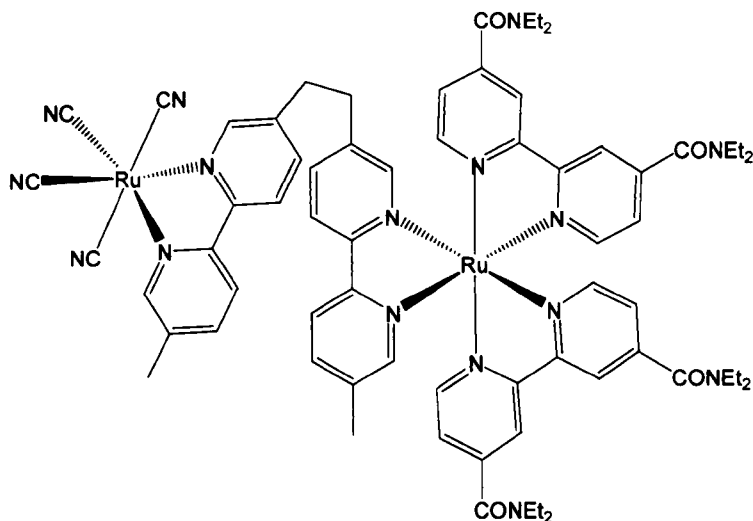
The results from luminescence and TRIR spectroscopy suggest that the lowest-lying excited state of Rubpyamide-BL² is similar to Rubpyamide-BL¹ and corresponds to Ru → (4,4'-(CONEt₂)₂bpy) ³MLCT. Rubpyamide-BL² has excited state energies between 15300 and 15500 cm⁻¹, which fall within the range displayed by RuCNdmb in the solvents studied (14500 to 16300 cm⁻¹, Chapter 2 and §3.2.1). Thus the direction and gradient of photoinduced energy transfer in dyads containing these two chromophores should be controllable through alteration of the solvent environment.

An interesting contrast between the two Rubpyamide-BL^x compounds is the biexponential decay of the ns-TRIR spectra in Rubpyamide-BL². The longer-lived

component (*ca.* 480 ns) corresponds fairly well to the luminescence lifetime (*ca.* 460 ns), but there is no obvious photophysical process which explains the shorter-lived component (*ca.* 8 ns). It may be a consequence of the synthesis of the BL² ligand giving rise to two different orientations of the bridging ligand. This possibility is explored further in the conformational analysis of **RuCN-BL²-Rubpyamide** (§3.6.5). This additional component may be present due to an impurity as a result of the preparation of BL² which also produces a number of polypyridyl by-products.¹⁹ Alternatively the high analyte concentrations employed in order to obtain good signal-to-noise ratios may have induced self-quenching or aggregation (see Chapter 6 for more information on the TRIR experimental setup). The noise observed in the spectra at longer time delays could be due to some acoustic process producing shockwaves in the sample cell which distort the flow of the analyte solution and introduce artefacts into the spectrum. Attempts to collect better quality spectra during other allocations of experimental time using the PIRATE apparatus were unsuccessful.

Having studied the photophysical and electrochemical properties of the model complexes **RuCNdmb**, **Rubpyamide-BL¹** and **Rubpyamide-BL²** this study will now examine the bimetallic complexes prepared by complexing the fragments [Ru(CN)₄]²⁻, [Ru(4,4'-(CONEt₂)₂bpy)₂]²⁺ and [ReCl(CO)₃] to the bridging ligands BL¹ and BL². These complexes should be regarded as second-generation analogues of the **RuCN-BL-Rubpy** system described earlier (§3.1).

3.5. $[\{(4,4'\text{-CON}(\text{CH}_2\text{CH}_3)_2\text{-bpy})_2\text{Ru}(\text{bpy-4,4-CH}_2\text{O}(\text{CH}_2)_2\text{OCH}_2\text{-bpy})\text{Ru}(\text{CN})_4\}$, **RuCN-BL¹-Rubpyamide**



RuCN-BL¹-Rubpyamide may be considered a fusion of the two mononuclear complexes **RuCNdmb** (§3.2) and **Rubpyamide-BL¹** (§3.3) and has been designed to exploit properties of these two building blocks. Both exhibit lowest-lying ³MLCT excited states as characterised by absorption, luminescence and TRIR spectroscopy. SSDA interactions modulate the ³MLCT energy of **RuCNdmb** so that it is *ca.* 700 cm^{-1} higher than the ³MLCT energy of **Rubpyamide** in high A. N. solvents such as D_2O , but *ca.* 190 cm^{-1} lower in solvents such as CH_3CN (*vide supra*). As a result the direction and gradient for PEnT in this system should be reversibly controllable through the tuning of solvent A. N.

There are some key differences between this system and the previously studied **RuCN-BL-Rubpy** (§4.1). The modifications to append amide groups to the 4,4' positions of the bipyridyl ligands of **RuCN-BL¹-Rubpyamide** lowers the energy of $\text{Ru} \rightarrow (4,4'\text{-(CONEt}_2)_2\text{bpy})$ ³MLCT transitions so that they are the lowest-lying excited states in this system. By contrast the lowest energy transition resides on the bridging ligand for both chromophores **RuCN-BL-Rubpy** prepared by Simpson *et al.*³ Secondly the change of bridging ligand length (shortened from 6 in **RuCN-BL-Rubpy** to 4 atoms here) and composition (from a POE chain to an ethyl linker) may affect the interchromophoric distance and conformational distribution sampled during

these solution experiments. These factors may have an effect on the rate and efficiency of through-space PEnT in this system.

The BL¹ bridging ligand 1,2-bis-5-[5'-methyl-2,2'-bipyridyl]ethane allows the intermetallic distance to be modulated. Efficient PEnT *via* the Förster mechanism requires that the centres are spatially proximal and that there is good orientational alignment between the dipoles of the two chromophores.²⁰ The Dexter mechanism is unlikely to operate in this system because the saturated CH₂CH₂ linker prevents direct electronic communication between the two metal centres.

The $\nu(\text{CO})$ bands of the amide groups and the $\nu(\text{CN})$ bands of the cyanide ligands provide complementary vibrational handles in different regions of the IR spectrum, enabling real time direct monitoring of the evolution of the excited state structure on both metal centres. The insights into excited state electronic structure obtained in studies of similar complexes using TRIR have been powerful and informative (§1.4.1 and §2.3).

3.5.1. UV/visible Absorption and Luminescence Spectroscopy

UV/vis Absorption Spectroscopy

UV/visible absorption spectra of **RuCN-BL¹-Rubpyamide** have been measured in CH₃CN and D₂O (see Figure 3.5.1.1). The spectral profile and peak positions correspond to an approximate superposition of the absorption spectra of the model complexes **RuCNdmb** and **Rubpyamide-BL¹**, which supports the notion there is no electronic communication between the two metal centres in their electronic ground states. The peak positions and assignments (by comparison with model complexes in §1.4.1.1 and §2.3.1) are summarised in Table 3.5.1.1.

It is apparent from visual inspection of the spectra that two of the longer wavelength features in the spectrum are relatively solvent-invariant (<10 nm difference between CH₃CN and D₂O) and these can be assigned to Ru → (4,4'-CO(NEt₂)₂bpy) ¹MLCT

transitions. The weaker remaining feature varies over a range of *ca.* 85 nm and exhibits negative solvatochromism as is expected for ruthenium (II) cyanide complexes and is assigned to a Ru → (5,5'-(CH₃)₂)bpy ¹MLCT transition.

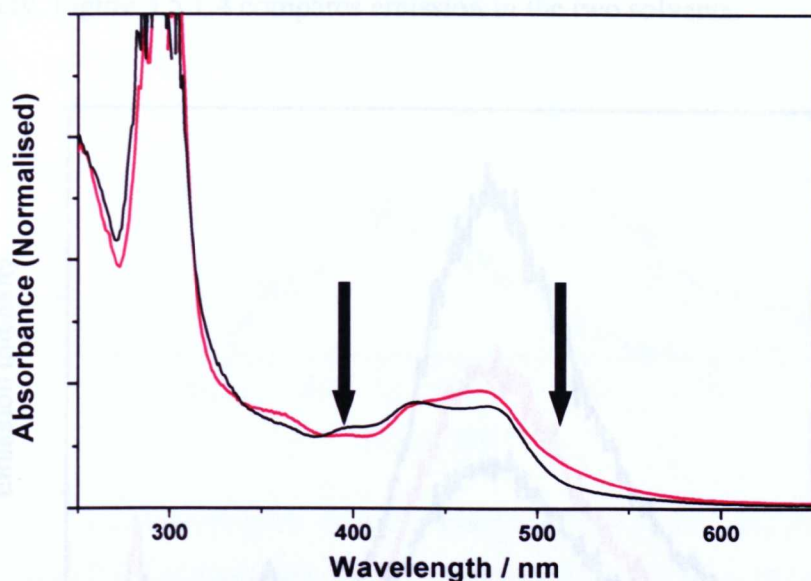


Figure 3.5.1.1: The UV/visible absorption spectra of RuCN-BL¹-Rubpyamide in D₂O (black) and CH₃CN (red). The absorbances are normalised to the 300 nm feature. Arrows denote the position of the strongly solvatochromic peak in the two solvents.

Solvent	$\lambda^{\max} / \text{nm}$					
	D ₂ O	< 300	369	403	439	478
CH ₃ CN	< 300	367		432	468	505
Assignment	IL	¹ MC	¹ MLCT	¹ MLCT		¹ MLCT
Terminus	π - π^*		RuCN	Rubpyamide	RuCN	

Table 3.5.1.1: Table of peak positions and assignments for UV/visible absorption spectra of RuCN-BL¹-Rubpyamide in D₂O and CH₃CN solutions.

Luminescence Spectroscopy

Luminescence spectroscopy was used to study **RuCN-BL¹-Rubpyamide** in D₂O and CH₃CN and are the spectra measured are shown in Figure 3.5.1.2 and 3.5.1.3 respectively. Figure 3.5.1.4 compares emission in the two solvents.

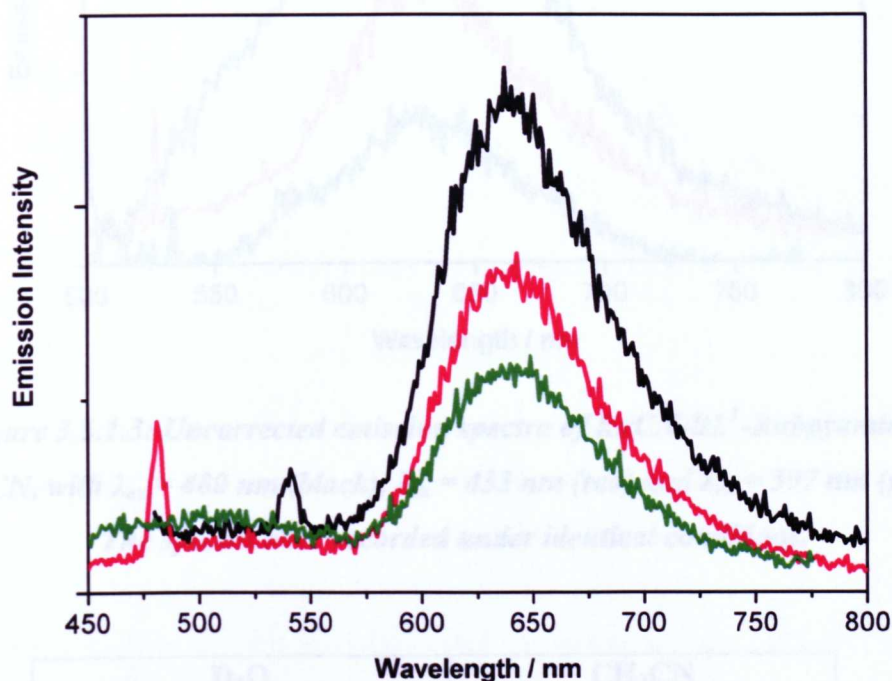


Figure 3.5.1.2: Uncorrected emission spectra of RuCN-BL¹-Rubpyamide in D₂O, with $\lambda_{ex} = 476$ nm (black), $\lambda_{ex} = 429$ nm (red) and $\lambda_{ex} = 394$ nm (green). The spectra were recorded under identical conditions.

The complex is luminescent giving a broad, featureless spectrum with λ_{max} (H₂O) = 656 nm and λ_{max} (CH₃CN) = 646 nm. There is a substantial difference in the emission intensity measured in the two solvents; the luminescence is much weaker in CH₃CN than in D₂O. The emission wavelengths and quantum yields measured are presented in Table 3.5.1.2.

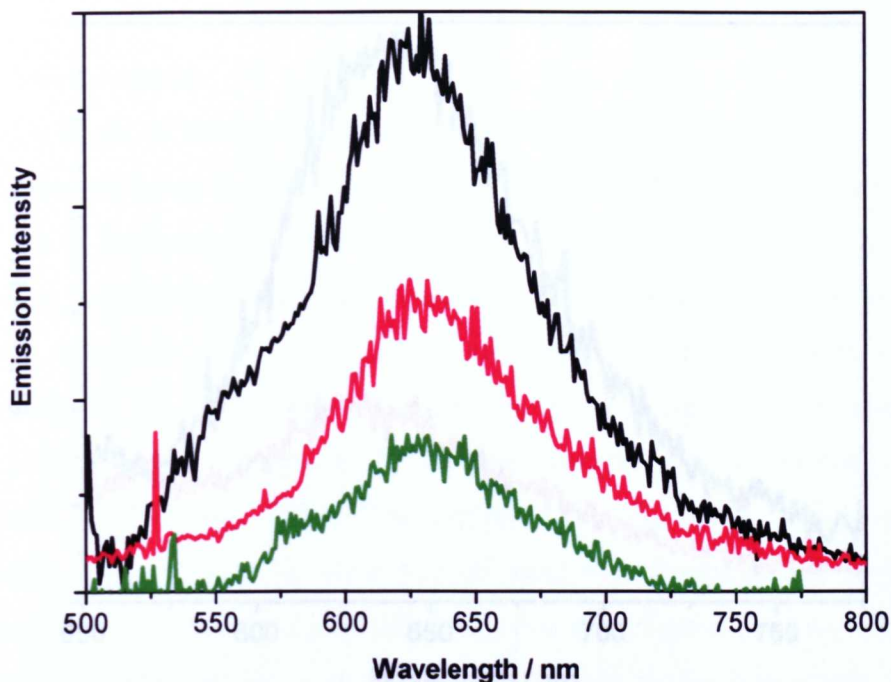


Figure 3.5.1.3: Uncorrected emission spectra of RuCN-BL¹-Rubpyamide in CH₃CN, with $\lambda_{ex} = 480$ nm (black), $\lambda_{ex} = 433$ nm (red) and $\lambda_{ex} = 397$ nm (green).

The spectra were recorded under identical conditions.

D ₂ O			CH ₃ CN		
λ_{ex} / nm	λ_{em} / nm	Φ	λ_{ex} / nm	λ_{em} / nm	ϕ
476	656	0.003(5)	480	646	0.0010
429	656	0.002(3)	433	646	0.0006
394	656	0.002(7)	397	647	0.0003

Table 3.5.1.2: Table of peak positions and quantum yields from luminescence spectroscopy of RuCN-BL¹-Rubpyamide in D₂O and CH₃CN solution.

This is consistent with the emissive states being ³MLCT in nature, with the vast majority of the detected luminescence being derived from the **Rubpyamide** terminus (**Rubpyamide-BL¹** emits at ca. 650 nm).

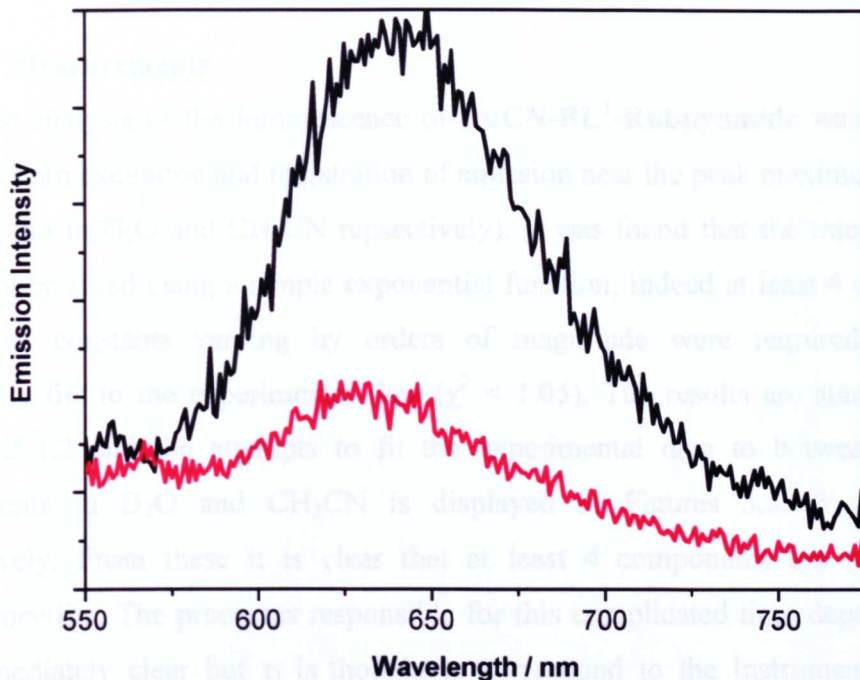


Figure 3.5.1.4: Uncorrected emission spectra of RuCN-BL¹-Rubpyamide in D₂O (black) and CH₃CN (red), with $\lambda_{ex}(D_2O) = 394\text{ nm}$ and $\lambda_{ex}(CH_3CN) = 397\text{ nm}$. The spectra were recorded under identical conditions.

These results confirm that the photoprocesses occurring vary significantly in different solvents. We can rationalise these results in the framework of our photophysical model for these complexes, based on the work of Simpson *et al.* (§3.1).³ In CH₃CN the ³MLCT excited state of the **Rubpyamide** terminus is the higher in energy of the two and thus luminescence is partially quenched by energy transfer to the **RuCNdmb** terminus, which only emits weakly. There is a *ca.* 90% reduction in quantum yield from that of **Rubpyamide-BL²** in CH₃CN. This partial quenching offers us further insight into the efficiency of the PenT process in this system. In D₂O the ³MLCT excited state of the **Rubpyamide** terminus is the lower in energy and thus its luminescence remains unquenched at an intensity comparable to that of **Rubpyamide-BL²**; there is less than 10% difference between the values obtained for the two complexes. The luminescence from the **RuCNdmb** terminus is particularly difficult to detect in this case as it occurs at a wavelength coincident with the intense luminescence from the **Rubpyamide** terminus.

TCSPC Measurements

A kinetic analysis of the luminescence of **RuCN-BL¹-Rubpyamide** was performed using 405 nm excitation and registration of emission near the peak maximum (640 nm and 629 nm in D₂O and CH₃CN respectively). It was found that the traces obtained could not be fitted using a simple exponential function; indeed at least 4 components with time constants varying by orders of magnitude were required to obtain acceptable fits to the experimental data ($\chi^2 < 1.05$). The results are summarised in Table 3.5.1.2 and the attempts to fit the experimental data to between 1 and 4 components in D₂O and CH₃CN is displayed in Figures 3.5.1.5 and 3.5.1.6 respectively. From these it is clear that at least 4 components are required for satisfactory fits. The processes responsible for this complicated time dependence are not immediately clear but τ_1 is thought to correspond to the Instrument Response Function (IRF).

Component	Time constant / ns	% Contribution	Time constant / ns	% Contribution
	D ₂ O ($\chi^2 = 0.980$)		CH ₃ CN ($\chi^2 = 1.024$)	
τ_1	5.42 (± 0.190)	8.07	1.93 (± 0.163)	1.95
τ_2	16.8 (± 2.82)	39.2	7.57 (± 0.241)	8.77
τ_3	60.4 (± 4.3)	5.81	81.6 (± 7.64)	5.39
τ_4	487.1 (± 3.15)	47.0	309.61 (± 19.3)	83.89

Table 3.5.1.2: Table of exponential fit components of luminescence spectra of RuCN-BL¹-Rubpyamide in D₂O and CH₃CN solutions.

The kinetic data obtained is clearly polyexponential in form, although it is important to note that τ_1 in both solvents may arise from the IRF. These results suggest that there are a number of photophysical processes occurring in solution on the nanosecond timescale. We have used TRIR spectroscopy to study these processes in more detail (§3.5.3).

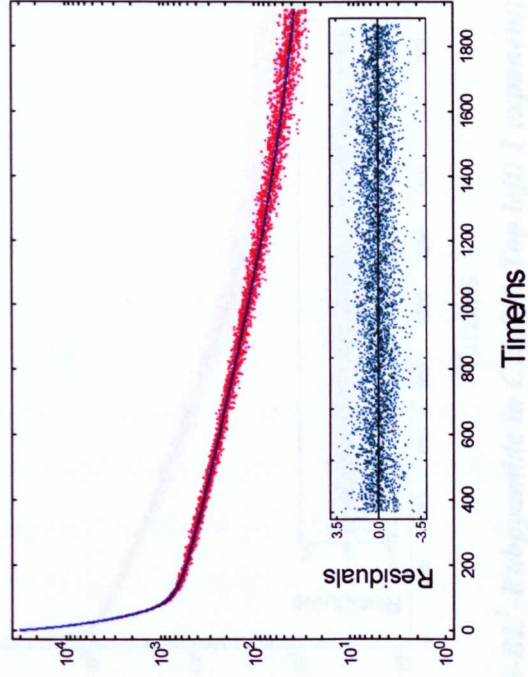
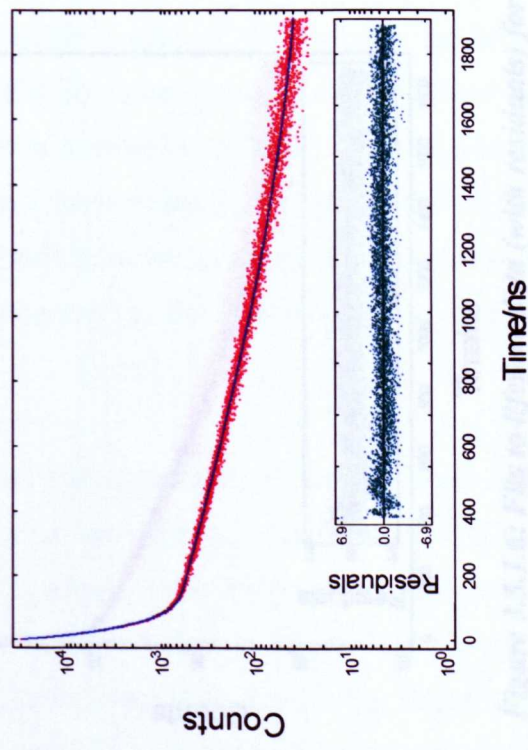
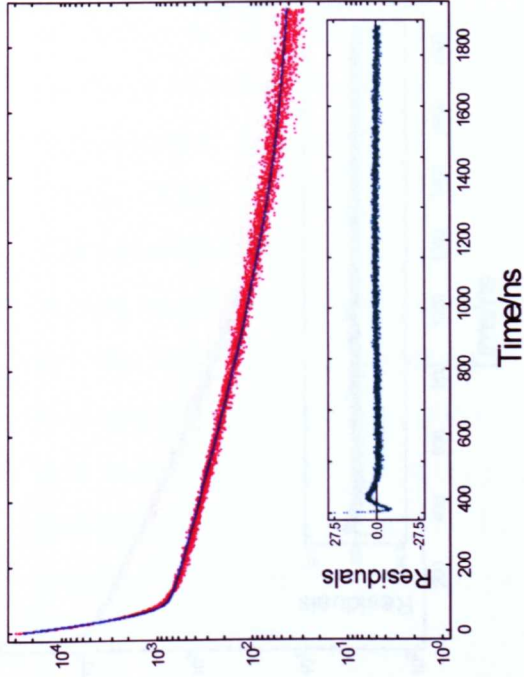
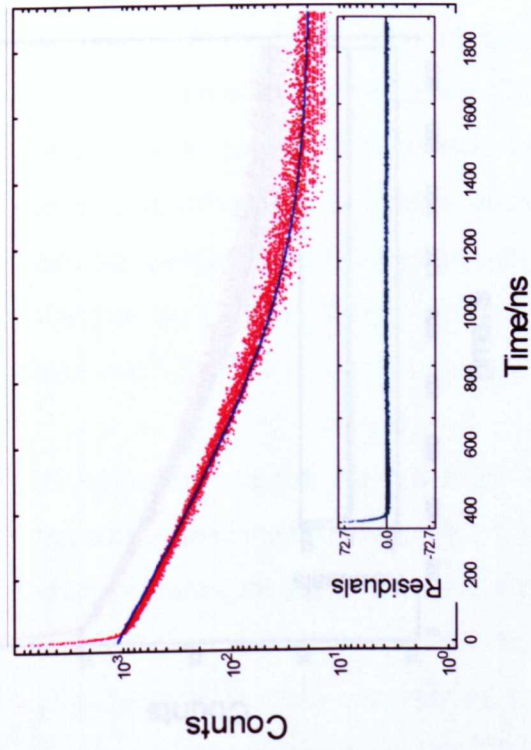


Figure 3.5.1.5: Fits to lifetime data (with residuals) for RuCN-BL'-Rubryamide in D₂O. Top left: 1 exponent; top right: 2 exponents; bottom left: 3 exponents, bottom right: 4 exponents.

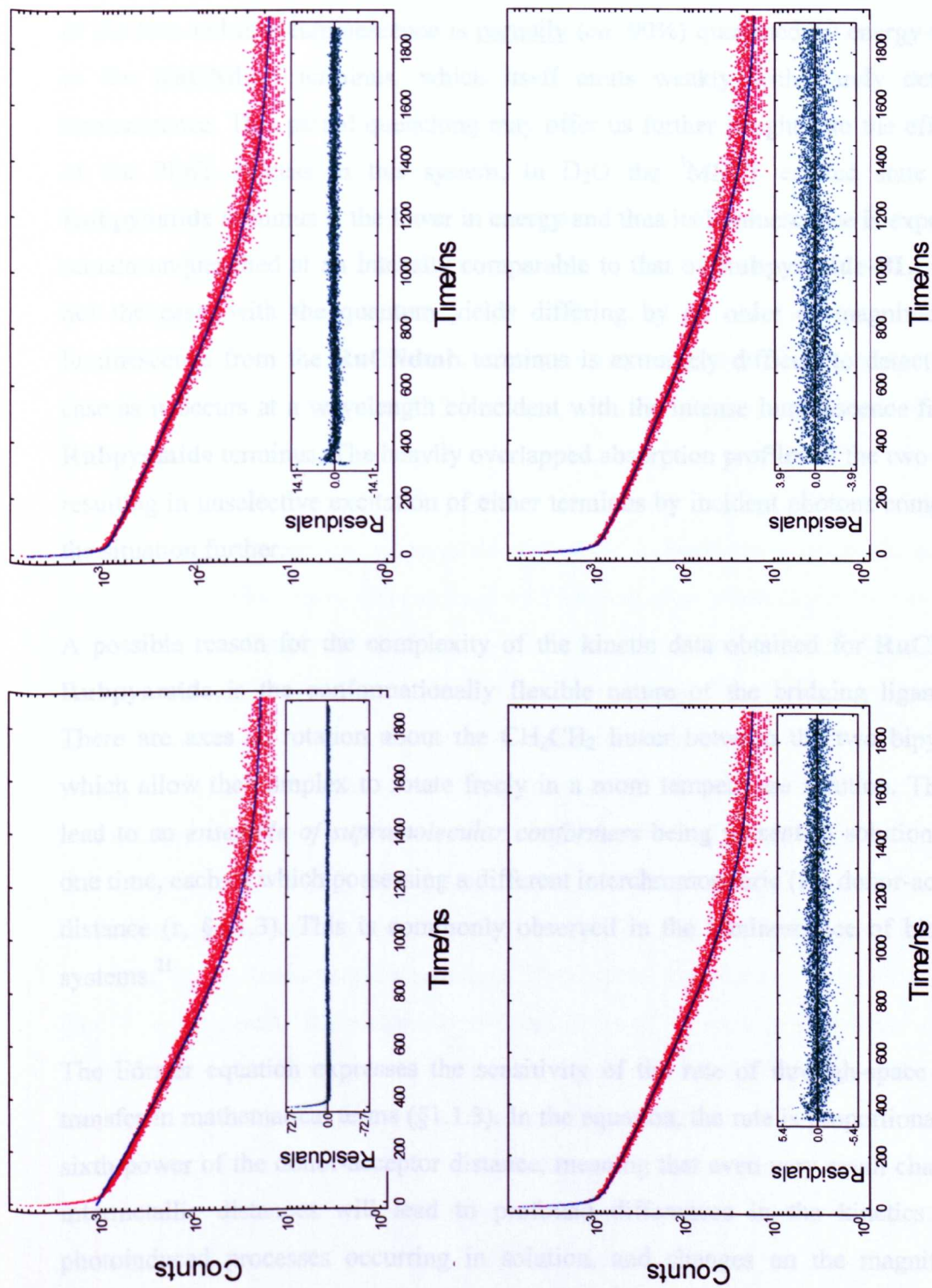


Figure 3.5.1.6: Fits to lifetime data (with residuals) for RuCN-BL¹-Rubryamide in CH₃CN. Top left: 1 exponent; top right: 2 exponents; bottom left: 3 exponents, bottom right: 4 exponents.

We can rationalise these results in the framework of our model for the complex. In CH₃CN the ³MLCT excited state of the **Rubpyamide** terminus is the higher in energy of the two and thus luminescence is partially (*ca.* 90%) quenched by energy transfer to the **RuCNdmb** terminus, which itself emits weakly with barely detectable luminescence. This partial quenching may offer us further insight into the efficiency of the PEnT process in this system. In D₂O the ³MLCT excited state of the **Rubpyamide** terminus is the lower in energy and thus its luminescence is expected to remain unquenched at an intensity comparable to that of **Rubpyamide-BL**¹. This is not the case, with the quantum yields differing by an order of magnitude. The luminescence from the **RuCNdmb** terminus is extremely difficult to detect in this case as it occurs at a wavelength coincident with the intense luminescence from the **Rubpyamide** terminus. The heavily overlapped absorption profiles of the two termini resulting in unselective excitation of either terminus by incident photons complicates the situation further.

A possible reason for the complexity of the kinetic data obtained for **RuCN-BL**¹-**Rubpyamide** is the conformationally flexible nature of the bridging ligand BL¹. There are axes of rotation about the CH₂CH₂ linker between the two bipyridines which allow the complex to rotate freely in a room temperature solution. This may lead to an *ensemble of supramolecular conformers* being present in solution at any one time, each of which possessing a different interchromophoric (*i.e.* donor-acceptor) distance (*r*, §1.1.3). This is commonly observed in the luminescence of biological systems.²¹

The Förster equation expresses the sensitivity of the rate of through-space energy transfer in mathematical terms (§1.1.3). In the equation, the rate is proportional to the sixth power of the donor-acceptor distance, meaning that even very small changes in intermetallic distances will lead to profound differences in the kinetics of the photoinduced processes occurring in solution, and changes on the magnitude of molecular rotation about the CH₂CH₂ axis of BL¹ will lead to a wide range of PEnT rates. This conformational flexibility may also help to explain why the quenching of

luminescence in CH₃CN is only partial – Förster PEnT requires good spatial overlap for efficient energy transfer and if the supramolecular system spends a great deal of its time in geometries which are not favourable for PEnT then energy transfer may have to compete with other radiative and non-radiative excited state decay processes.

Studies of Cyanide-Metal Ion Interactions

The effect of metal ion binding to the cyanide ligands of **RuCN-BL¹-Rubpyamide** was also studied using luminescence spectroscopy. The variation of emission wavelength and intensity was studied as a function of Ba²⁺ concentration in CH₃CN solution. As [Ba²⁺] was increased the luminescence intensity increased substantially (from $\phi_{\text{init}} = 0.001$ to $\phi_{\text{max}} = 0.022$). The spectra recorded are presented in Figure 3.5.1.6.

The physical mechanism responsible for such a dramatic change in emission properties is analogous to that reported by Simpson *et al.* when exploring the solvent dependence of **RuCN-BL-Rubpy** in DMSO:H₂O solvent mixtures (§3.1, Figure 3.1.1.4).³ In that study, as the A. N. of the solvent mixture increased through titration of H₂O into the solution, the intensity of measured emission increased as the ³MLCT energy of the **RuCN** terminus of the bimetallic complex was raised through SSDA interactions. However in this case the modulation of **RuCN** ³MLCT energy occurs through control of [Ba²⁺]. The process of Ba²⁺ binding to **RuCN-BL¹-Rubpyamide** leads to the reversal of the location of the lowest energy excited state from the **RuCN** terminus to the **Rubpyamide** terminus. The crucial consequence of this is that as [Ba²⁺] is increased, **Rubpyamide** → **RuCN** PEnT (which is ostensibly a major luminescence quenching process) becomes thermodynamically unfavourable and the luminescence intensity increases substantially. Addition of a macrocyclic Ba²⁺ sequestration agent (dibenzo-18-crown-6) demonstrates the near total reversibility of this process as the luminescence returns to a level similar to that measured in the absence of Ba²⁺.

This study demonstrates that the excited state energy of the **RuCN** terminus is amenable to reversible modulation by other external factors such as metal ion binding in addition to solvent composition. The experiments discussed above form part of a study presented in a forthcoming publication which explores this effect in more detail.²²

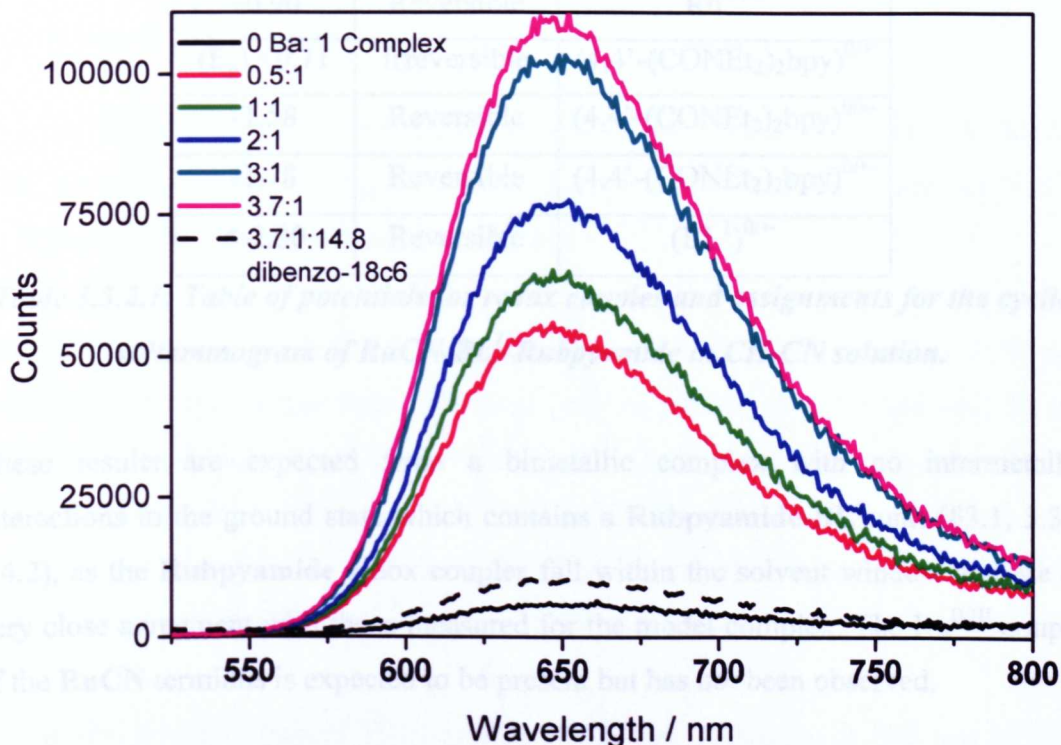


Figure 3.5.1.6: Changes in luminescence spectra of RuCN-BL¹-Rubpyamide in CH₃CN solution upon addition of Ba²⁺ ions (solid lines) and dibenzo-18-crown-6 (dashed line). Relative concentrations corresponding to the line colours are denoted in the legend.

3.5.2. Cyclic Voltammetry

RuCN-BL¹-Rubpyamide has been studied using cyclic voltammetry in CH₃CN (see Appendix §3.9 for the voltammogram) and the results are presented in Table 3.5.2.1. Within the potential window of CH₃CN (ca. +2 V to -2 V) there is one reversible oxidation, a large irreversible feature at positive potential (due to oxidation of the amide groups) and three reversible reduction couples arising from the bpy-based

ligands. The potentials for the oxidation and the 1st and 2nd reductions are very similar to those reported for **Rubpyamide-BL¹** and **Rubpyamide-BL²** (§3.3.2, 3.4.2).

$E_{1/2}/V$ (vs. Fc/Fc ⁺)	Reversibility	Assignment
+0.90	Reversible	Ru ^{II/III}
(E _p) +0.71	Irreversible	(4,4'-(CONEt ₂) ₂ bpy) ^{0/+}
-1.58	Reversible	(4,4'-(CONEt ₂) ₂ bpy) ^{0/e-}
-1.78	Reversible	(4,4'-(CONEt ₂) ₂ bpy) ^{0/e-}
<-2.00	Reversible	(BL ¹) ^{0/e-}

Table 3.5.2.1: Table of potentials for redox couples and assignments for the cyclic voltammogram of RuCN-BL¹-Rubpyamide in CH₃CN solution.

These results are expected from a bimetallic complex with no intermetallic interactions in the ground state which contains a **Rubpyamide-BL^x** unit (§3.1, 3.3.2 3.4.2), as the **Rubpyamide** redox couples fall within the solvent window and are in very close agreement with those measured for the model complex. The Ru^{II/III} couple of the **RuCN** terminus is expected to be present but has not been observed.

3.5.3. FTIR and Time-Resolved Infrared Spectroscopy

Luminescence spectroscopy has provided some indirect evidence for PEnT between the two termini of **RuCN-BL¹-Rubpyamide** (*vide supra*), through the quenching of emission from the **Rubpyamide** terminus in low A. N. solvent environments. TRIR spectroscopy has been used to monitor this process in order to obtain direct evidence for its occurrence. The system has two sets of IR active ‘reporters’, one on each terminus. Both can provide important and complementary information and it is crucial to consider them together when analysing the data.

It is important to remember that due to the very similar nature of the MLCT chromophores appended to the two metal centres and the broadness of ¹MLCT

absorption peaks, there is often a case of unselective excitation, *i.e.* either metal centre may be excited by the incident laser light. This adds another degree of complexity to the study, as there may be more than one excited state species present in solution and as a result *bona fide* PEnT processes must be disentangled from the other primary photophysical processes occurring in order to fully understand the spectra recorded.

Deuterium Oxide Solution

In D₂O, SSDA interactions elevate the energy of the lowest energy **RuCN** ³MLCT state above the corresponding state in the **Rubpyamide** terminus. Therefore **RuCN** → **Rubpyamide** PEnT is expected to take place.

The FTIR spectrum of **RuCN-BL¹-Rubpyamide** in D₂O solution in the ν(CN) and amide ν(CO) regions has been measured (see Appendix §3.9 for spectra). In the cyanide region there is a peak profile characteristic of the tetracyanoruthenate (II) unit with 3 resolved peak maxima at 2091, 2050 and 2030 cm⁻¹. In the amide region there is a single peak present at 1612 cm⁻¹. These results are closely comparable with the model complexes **RuCNdmb** and **Rubpyamide-BL¹** in D₂O solution (§3.2.5, §3.3.5).

Picosecond and nanosecond TRIR spectra (with laser excitation at 400 and 355 nm respectively) of **RuCN-BL¹-Rubpyamide** were recorded in D₂O solution, monitoring both regions in the IR where reporter groups are present.

ps-TRIR Spectroscopy

Figure 3.5.3.1 shows the ps-TRIR spectra obtained for the **RuCN** and **Rubpyamide** termini in D₂O.

RuCN (“Donor”) terminus

The spectral profile obtained following 400 nm excitation resembles that of **RuCNdmb** in D₂O (§3.2.5), with several overlapped bleaches centred between 2030 and 2100 cm⁻¹ and at least two transient bands detected at higher wavenumber between 2090 and 2125 cm⁻¹. There appear to be changes in the profile on the

picosecond timescale, particularly in the region where the high energy bleach is overlapping with the transient. Additional fine structure is observed in the spectrum in comparison with the corresponding spectra in CH₃CN. A possible reason for these additional features is vibrational cooling; however the kinetic data does not definitively exhibit characteristic narrowing and blue-shifting of transient bands on the appropriate timescale ($\tau \sim 10$ ps, *vide infra*) and the solvent-dependent nature of this phenomenon suggests that it is related to the solvatochromic effect (§1.2.3). An alternative hypothesis of a multi-step photoinduced process (ostensibly PEnT) involving the formation and subsequent interconversion of two discrete transient species (plausible in D₂O only) is posited and discussed in detail in the Discussion section below (§3.5.5).

Over the time range of the experiment ($\Delta t = 1$ -1000 ps), the majority of the $\nu(\text{CN})$ bleach and transient signals recover, indicating that there are photophysical processes occurring which facilitate the quenching of the **RuCNdmb** ³MLCT excited state. At $\Delta t = 1$ ns only a weak residual signal remains, indicating that the majority of **RuCNdmb** excited states formed in solution have been quenched.

Rubpyamide (“Acceptor”) terminus

The spectra obtained for the **Rubpyamide** terminus in D₂O resemble the profile observed for the precursor complex **Rubpyamide-BL**¹ (§3.5.5), with an amide $\nu(\text{CO})$ bleach centred at 1615 cm⁻¹ and a transient to lower wavenumber centred at 1591 cm⁻¹. This is consistent with the anticipated ³MLCT lowest excited state for this terminus. The spectra show much less development over the timescale of the experiment than for the **RuCN** terminus, indicating that ultrafast processes are not contributing to excited state quenching to the same extent as in the “donor” terminus. Indeed at $\Delta t = 1$ ns there is still a strong signal remaining, indicating that excited state decay is taking place on longer timescales.

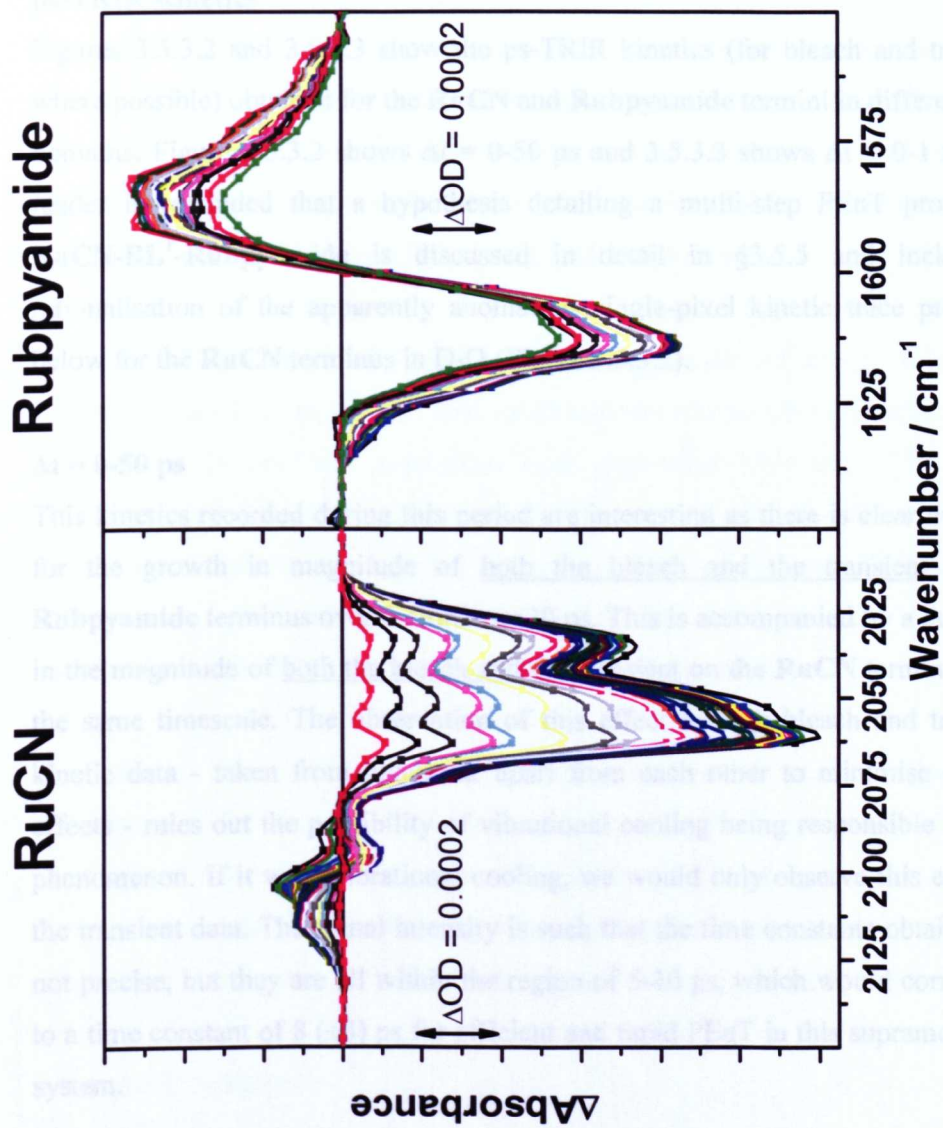


Figure 3.5.3.1: ps-TRIR spectra of RuCN-BL¹-Rubpyamide in D₂O solution in the $\nu(\text{CN})$ and amide $\nu(\text{CO})$ region. The fine structure observed in these spectra is discussed in more detail in §3.5.5.

This initial result is consistent with our model, which predicts that the **RuCN** donor terminus will be quenched by efficient PEnT and have a short-lived excited state, whilst the **Rubpyamide** acceptor terminus will possess a long-lived excited state owing to it being the ultimate excited state being formed.

ps-TRIR Kinetics

Figures 3.5.3.2 and 3.5.3.3 show the ps-TRIR kinetics (for bleach and transient where possible) obtained for the **RuCN** and **Rubpyamide** termini in different time domains. Figure 3.5.3.2 shows $\Delta t = 0-50$ ps and 3.5.3.3 shows $\Delta t = 0-1$ ns. The reader is reminded that a hypothesis detailing a multi-step PEnT process in **RuCN-BL¹-Rubpyamide** is discussed in detail in §3.5.5 and includes a rationalisation of the apparently anomalous single-pixel kinetic trace presented below for the **RuCN** terminus in D₂O (Figure 3.5.3.2).

$\Delta t = 0-50$ ps

This kinetics recorded during this period are interesting as there is clear evidence for the growth in magnitude of both the bleach and the transient on the **Rubpyamide** terminus over the first *ca.* 30 ps. This is accompanied by a depletion in the magnitude of both the bleach and the transient on the **RuCN** terminus over the same timescale. The observation of this effect in both bleach and transient kinetic data - taken from pixels far apart from each other to minimise overlap effects - rules out the possibility of vibrational cooling being responsible for this phenomenon. If it were vibrational cooling, we would only observe this effect in the transient data. The signal intensity is such that the time constants obtained are not precise, but they are all within the region of 5-10 ps, which would correspond to a time constant of 8 (± 3) ps for efficient and rapid PEnT in this supramolecular system.

$\Delta t = 0-1$ ns

In this timescale the processes described above are observed in the early part of the trace, and are followed by signal decay on both termini, indicating that excited state decay by routes other than PEnT has become the major process occurring. As was observed in the luminescence spectroscopy of these complexes, these processes appear to be multi-exponent. This may be due to the offsetting of

excited state decay processes with PEnT-related grow-in of signal - or the opposite situation where there are multiple competing decay processes occurring at varying rates. The time constant for the major decay component in each case is in the region of 300-600 ps.

ns-TRIR Spectroscopy and Kinetics

As observed by luminescence spectroscopy, the **Rubpyamide** terminus has a long-lived excited state in D₂O which can be monitored on the nanosecond timescale. Figures 3.5.3.4 and 3.5.3.5 show the spectroscopy and kinetics measured at $\Delta t = 1$ -500 ns. Attempts to obtain ns-TRIR spectra of the **RuCNdmb** terminus were not successful, conceivably due to its short excited state lifetime.

The ns-TRIR spectral profile measured for **Rubpyamide** following excitation at 355 nm is analogous to the ps-TRIR spectra shown above, with the parent bleach centred at 1616 cm⁻¹ and a transient band centred at 1591 cm⁻¹. The signals detected were weak, implying that much of the excited state had decayed on the picosecond timescale, although the signal intensities over the two timescales are unfortunately not directly comparable due to different laser excitation wavelengths, data collection times and sample concentrations.

Analysis of the kinetics at the bleach and transient peak maxima give multiexponent fits (the data were fitted to at least 3), with components having time constants of 5.5 (± 3), 25 (± 9) and 550 (± 200) ns. This is consistent with the luminescence data presented in §3.5.3.1 and confirms that there are multiple photophysical processes occurring in this system over the timescales investigated.

Acetonitrile Solution

In CH₃CN SEDA interactions stabilise the energy of the **RuCN**³MLCT state so that it is lower than the corresponding state in the **Rubpyamide** terminus. Therefore **Rubpyamide** → **RuCN** PEnT is expected to take place.

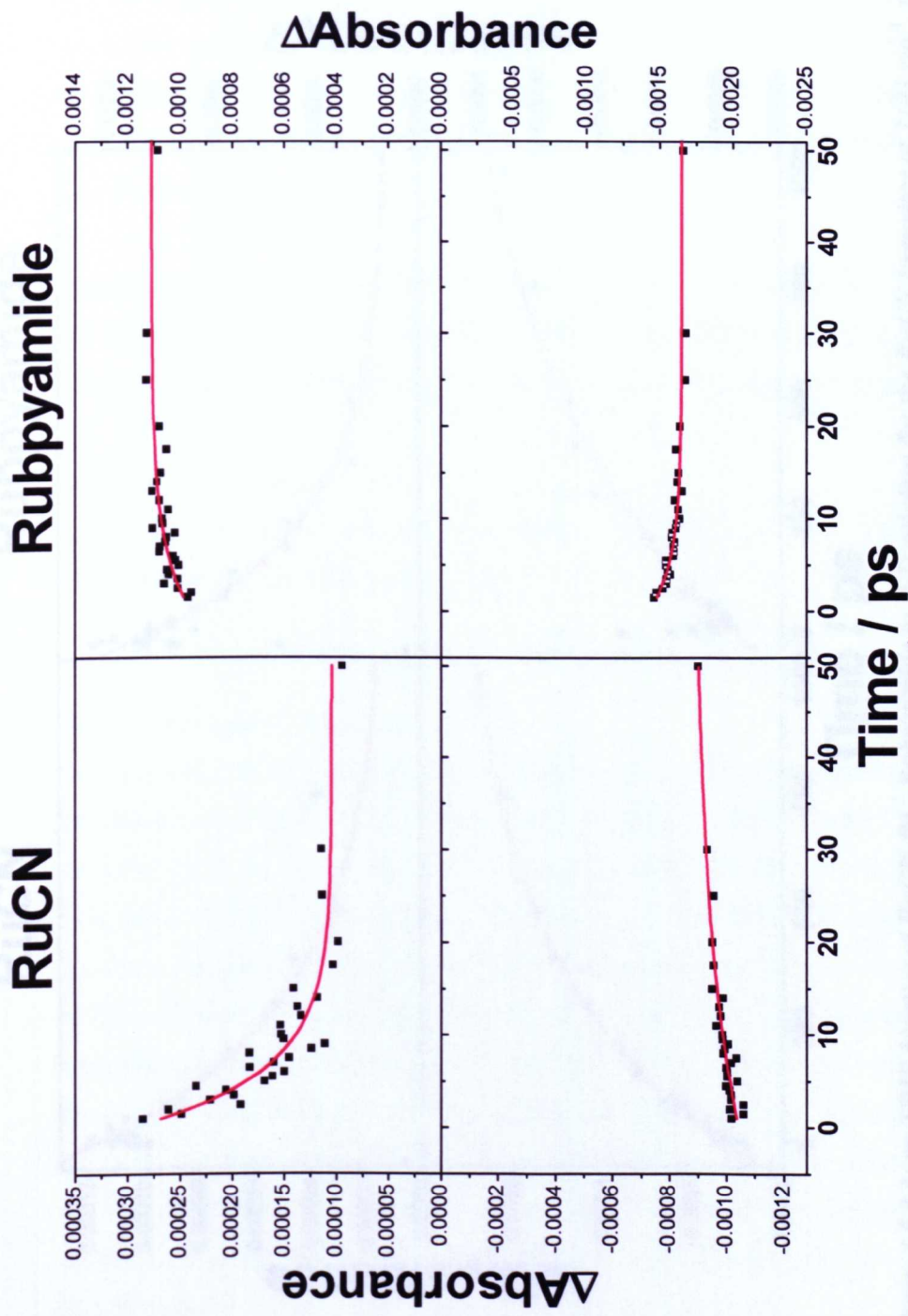


Figure 3.5.3.2: Single pixel ps-TRIR kinetics of RuCN-BL¹-Rubpyamide in D₂O solution for the RuCN (transient at 2101 cm⁻¹, top left and bleach at 2062 cm⁻¹, bottom left) and Rubpyamide (transient at 1584 cm⁻¹, top right and bleach at 1613 cm⁻¹, bottom right) termini for $\Delta t = 0$ -50 ps. The anomalous trace obtained for the RuCN transient is discussed in detail in §3.5.5.

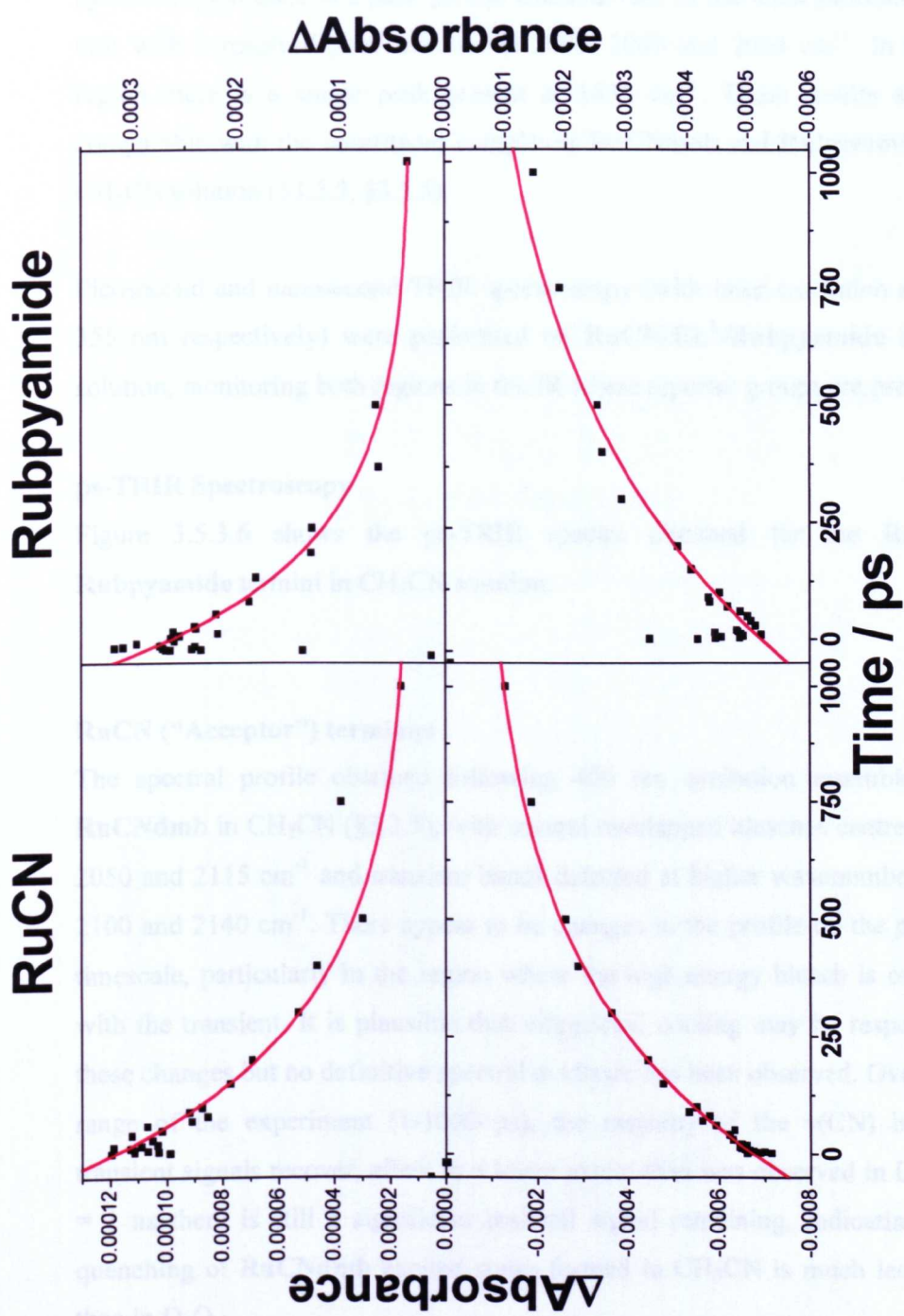


Figure 3.5.3.3: ps-TRIR kinetics of RuCN-BL¹-Rubpyamide in D₂O solution for the RuCN (transient at 2101 cm⁻¹, top left and bleach at 2062 cm⁻¹, bottom left) and Rubpyamide (transient at 1584 cm⁻¹, top right and bleach at 1613 cm⁻¹, bottom right) termini for Δt = 0-1 ns.

The FTIR spectrum of **RuCN-BL¹-Rubpyamide** in CH₃CN solution in the $\nu(\text{CN})$ and amide $\nu(\text{CO})$ region has been measured (see Appendix §3.9 for spectra). In the cyanide region there is a peak profile characteristic of the tetracyanoruthenate (II) unit with 3 resolved peak maxima at 2093, 2069 and 2044 cm⁻¹. In the amide region there is a single peak present at 1638 cm⁻¹. These results are closely comparable with the constituent complexes **RuCNdmb** and **Rubpyamide-BL¹** in CH₃CN solution (§3.2.5, §3.3.5).

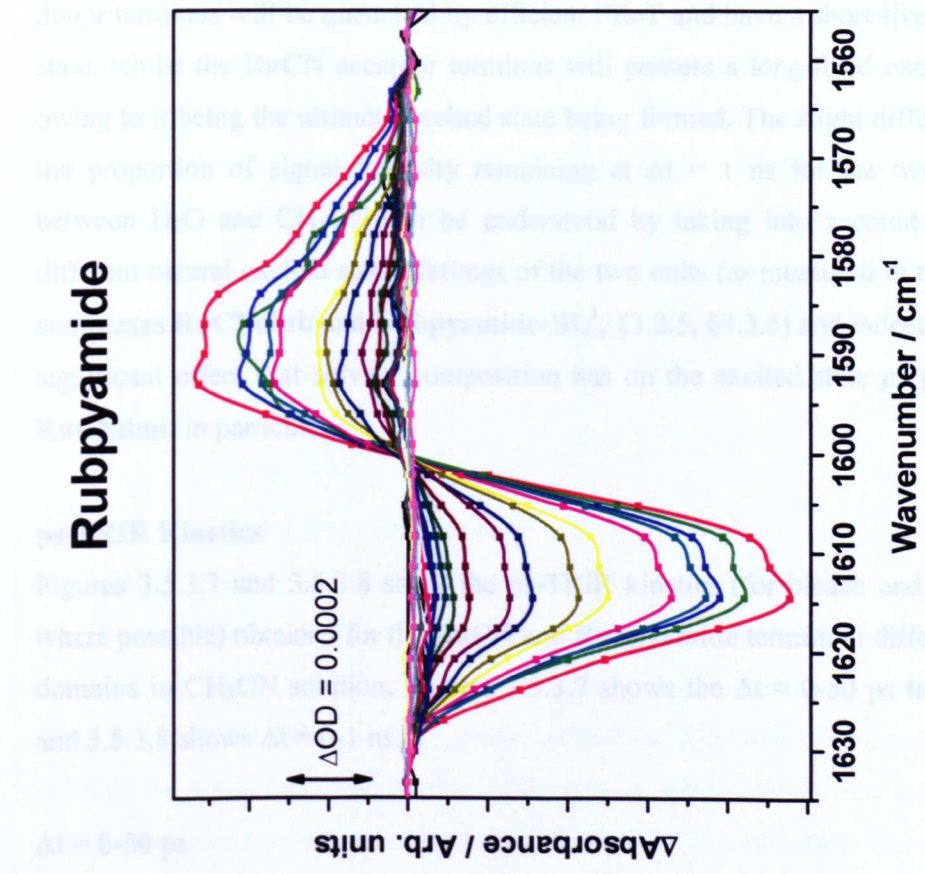
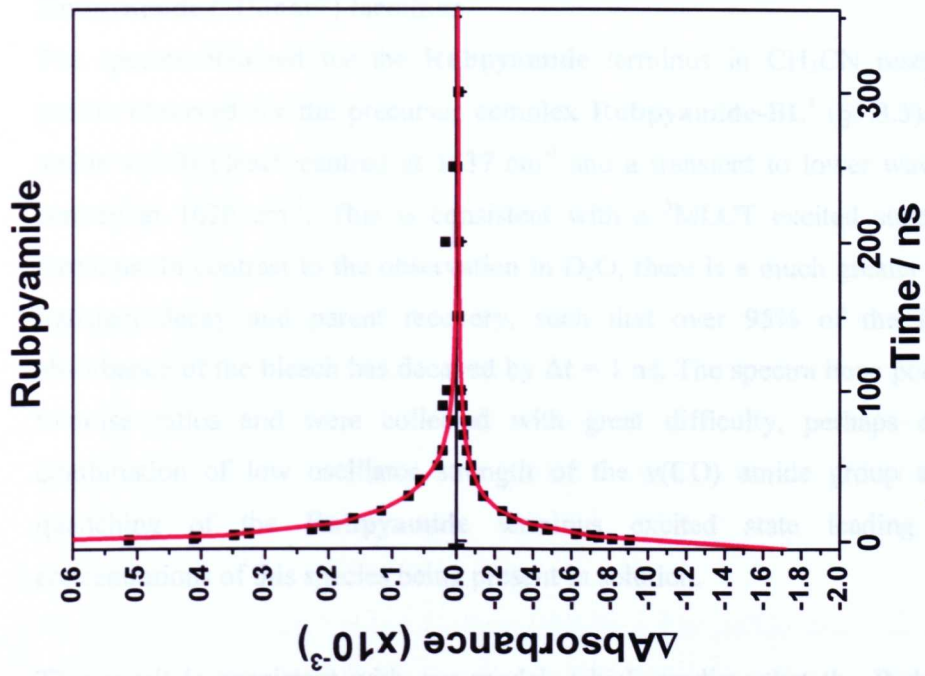
Picosecond and nanosecond-TRIR spectroscopy (with laser excitation at 400 and 355 nm respectively) were performed on **RuCN-BL¹-Rubpyamide** in CH₃CN solution, monitoring both regions in the IR where reporter groups are present.

ps-TRIR Spectroscopy

Figure 3.5.3.6 shows the ps-TRIR spectra obtained for the **RuCN** and **Rubpyamide** termini in CH₃CN solution.

RuCN (“Acceptor”) terminus

The spectral profile obtained following 400 nm excitation resembles that of **RuCNdmb** in CH₃CN (§3.2.5), with several overlapped bleaches centred between 2050 and 2115 cm⁻¹ and transient bands detected at higher wavenumber between 2100 and 2140 cm⁻¹. There appear to be changes in the profile on the picosecond timescale, particularly in the region where the high energy bleach is overlapping with the transient. It is plausible that vibrational cooling may be responsible for these changes but no definitive spectral evidence has been observed. Over the time range of the experiment (1-1000 ps), the majority of the $\nu(\text{CN})$ bleach and transient signals recover, albeit to a lesser extent than was observed in D₂O. At $\Delta t = 1$ ns there is still a significant residual signal remaining, indicating that the quenching of **RuCNdmb** excited states formed in CH₃CN is much less efficient than in D₂O.



Figures 3.5.3.4 and 3.5.3.5: ns-TRIR spectra (left) and kinetics (transient at 1589 cm^{-1} , top right and bleach at 1611 cm^{-1} , bottom right) of RuCN-BL¹-Rubpyamide in D₂O solution for the Rubpyamide terminus for $\Delta t = 0$ -300 ns.

Rubpyamide (“Donor”) terminus

The spectra obtained for the **Rubpyamide** terminus in CH₃CN resemble the profile observed for the precursor complex **Rubpyamide-BL**¹ (§3.3.5), with an amide $\nu(\text{CO})$ bleach centred at 1637 cm⁻¹ and a transient to lower wavenumber centred at 1620 cm⁻¹. This is consistent with a ³MLCT excited state for this terminus. In contrast to the observation in D₂O, there is a much greater extent of transient decay and parent recovery, such that over 95% of the integrated absorbance of the bleach has decayed by $\Delta t = 1$ ns. The spectra have poor signal-to-noise ratios and were collected with great difficulty, perhaps due to a combination of low oscillator strength of the $\nu(\text{CO})$ amide group and rapid quenching of the **Rubpyamide** terminus excited state leading to low concentrations of this species being present in solution.

This result is consistent with our model, which predicts that the **Rubpyamide** donor terminus will be quenched by efficient PEnT and have a short-lived excited state, whilst the **RuCN** acceptor terminus will possess a long-lived excited state owing to it being the ultimate excited state being formed. The slight differences in the proportion of signal intensity remaining at $\Delta t = 1$ ns for the two termini between D₂O and CH₃CN can be understood by taking into account the very different natural excited state lifetimes of the two units (as measured in the model complexes **RuCNdmb** and **Rubpyamide-BL**¹, §3.2.5, §3.3.5) and indeed the very significant effect that solvent composition has on the excited state properties of **RuCNdmb** in particular.

ps-TRIR Kinetics

Figures 3.5.3.7 and 3.5.3.8 show the ps-TRIR kinetics (for bleach and transient where possible) obtained for the **RuCN** and **Rubpyamide** termini in different time domains in CH₃CN solution. Figures 3.5.3.7 shows the $\Delta t = 0$ -50 ps time range and 3.5.3.8 shows $\Delta t = 0$ -1 ns.

$\Delta t = 0$ -50 ps

This kinetics recorded during this period are less definitive than those presented for D₂O, as there is clear evidence for the growth in magnitude of both the bleach and the transient on the **RuCN** terminus over the first *ca.* 30 ps, but unfortunately

no data of comparable clarity for the **Rubpyamide** terminus. For the **RuCN** terminus, which as the acceptor provides the tell-tale grow-in of absorbance on both bleach and transient bands, the signal intensity is such that precise time constants could not be meaningfully obtained. However it is of note that all four of the termini within the region of 9-15 ps. This would correspond to an approximate time constant of 12 (± 3) ps for efficient and rapid PEnT in this supramolecular system. Analysis of the donor terminus data provides few conclusions as no clear processes (grow-in or decay) are observed over the $\Delta t = 0-50$ ps timescale. A possible reason for this is the offsetting of decay processes in the **Rubpyamide** terminus by peak sharpening due to vibrational cooling of the $\nu(\text{CO})$ bands.

$\Delta t = 0-1$ ns

As was observed in D_2O solution, during this time domain the processes described above are observed at early times following excitation, and these are followed by signal decay on both termini, indicating that the excited state decay by mechanisms other than PEnT becomes the major process occurring. These processes appear to be multi-exponent, with fits utilising 1 or 2 components most closely representing the data. This may be due to the offsetting of excited state decay processes with PEnT-related grow-in of signal – or the converse situation where there are multiple competing decay processes occurring at varying rates. There appears to be little consistency in the time constants determined for the fits to the experimental data, with time constants varying between 20 and 500 ps for the major decay component.

ns-TRIR Spectroscopy and Kinetics

In CH_3CN our photophysical model predicts that the **RuCN** terminus will have a long-lived $^3\text{MLCT}$ excited state which can be monitored on the nanosecond timescale. Figures 3.5.3.9 and 3.5.3.10 show the spectroscopy and kinetics measured at $\Delta t = 1-500$ ns. TRIR spectra of the **Rubpyamide** terminus in CH_3CN solution on the nanosecond timescale showed no transient features, conceivably due to the short excited state lifetime of the $^3\text{MLCT}$ excited state located on the **Rubpyamide** terminus.

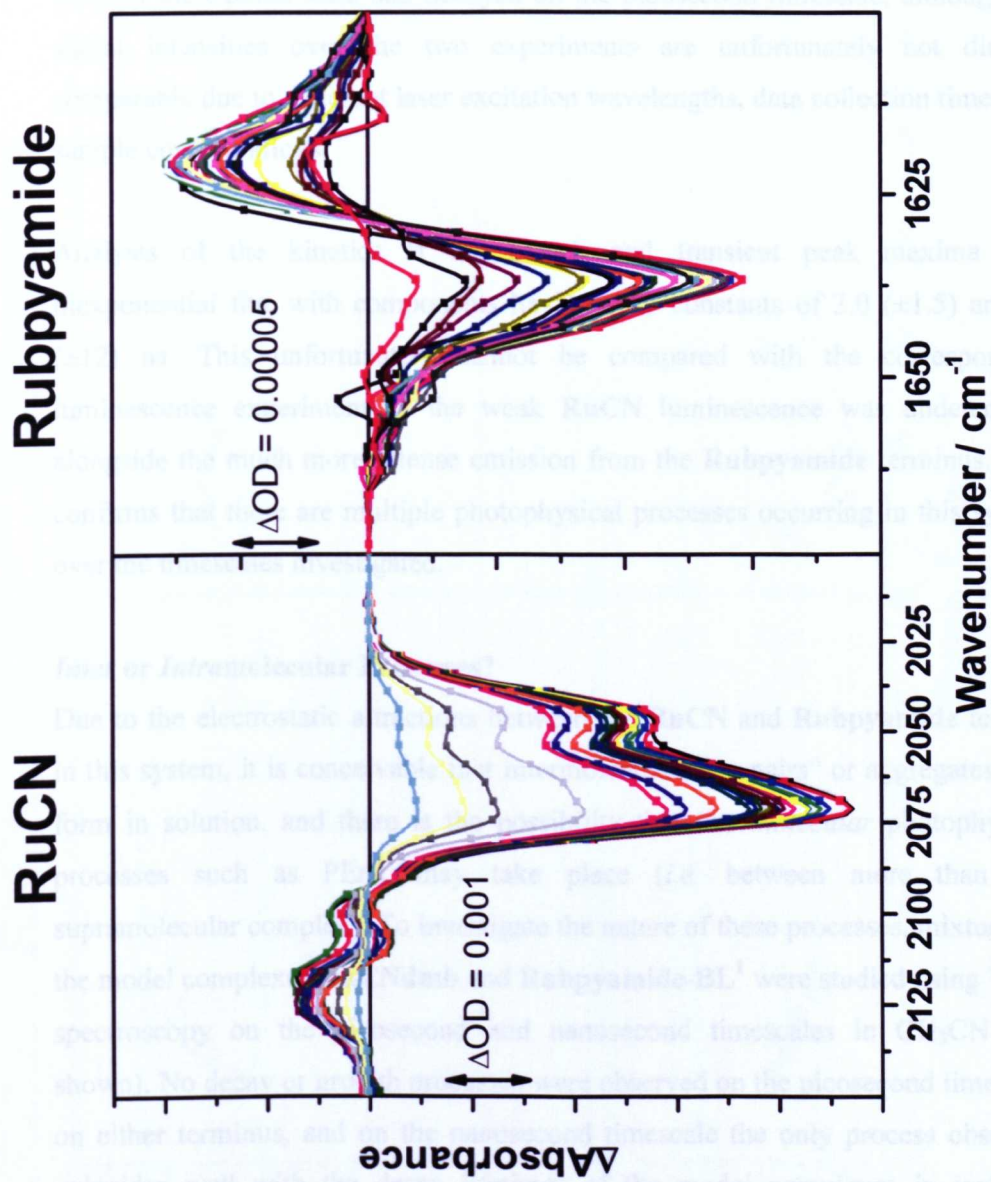


Figure 3.5.3.6: ps-TRIR spectra of RuCN-BL¹-Rubpyamide in CH₃CN solution in the $\nu(\text{CN})$ and amide $\nu(\text{CO})$ region.

The ns-TRIR spectroscopy of the **RuCN** terminus following excitation at 355 nm is analogous to the ps-TRIR spectroscopy shown above, with several overlapped bleaches centred between 2050 and 2085 cm^{-1} and a transient band at higher wavenumber centred at 2095 cm^{-1} . The signals detected were weak, implying that most of the excited state had decayed on the picosecond timescale, although the signal intensities over the two experiments are unfortunately not directly comparable due to different laser excitation wavelengths, data collection times and sample concentrations.

Analysis of the kinetics at the bleach and transient peak maxima give biexponential fits, with components having time constants of 3.0 (± 1.5) and 65 (± 12) ns. This unfortunately cannot be compared with the corresponding luminescence experiment as the weak **RuCN** luminescence was undetectable alongside the much more intense emission from the **Rubpyamide** terminus. This confirms that there are multiple photophysical processes occurring in this system over the timescales investigated.

Inter or Intramolecular Processes?

Due to the electrostatic attractions between the **RuCN** and **Rubpyamide** termini in this system, it is conceivable that intermolecular “ion pairs” or aggregates may form in solution, and there is the possibility that *intermolecular* photophysical processes such as PEnT may take place (*i.e.* between more than one supramolecular complex). To investigate the nature of these processes, mixtures of the model complexes **RuCNdmb** and **Rubpyamide-BL¹** were studied using TRIR spectroscopy on the picosecond and nanosecond timescales in CH_3CN (not shown). No decay or growth processes were observed on the picosecond timescale on either terminus, and on the nanosecond timescale the only process observed coincides well with the decay lifetimes of the model complexes in isolation (§3.2.5, 3.3.5). This provides evidence that intermolecular processes (including PEnT) are not a major consideration in these complexes and the photophysical processes observed in **RuCN-BL¹-Rubpyamide** are *intramolecular* in nature.

RuCN Rubpyamide

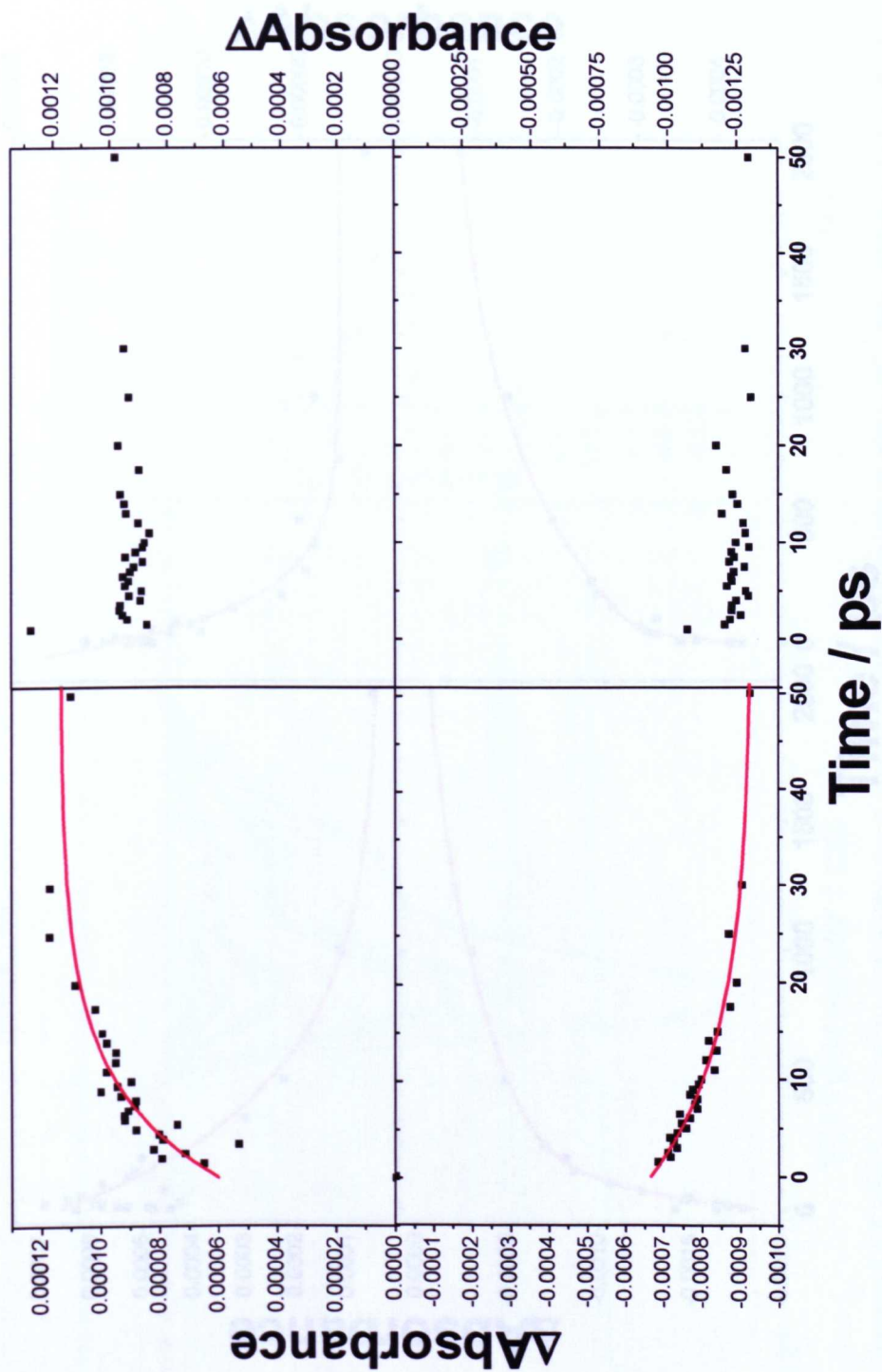


Figure 3.5.3.7: ps-TRIR kinetics of RuCN-BL¹-Rubpyamide in CH₃CN solution for the RuCN (transient at 2114 cm⁻¹, top left and bleach at 2068 cm⁻¹, bottom left) and Rubpyamide (transient at 1616 cm⁻¹, top right and bleach at 1637 cm⁻¹, bottom right) termini for Δt = 0-50 ps.

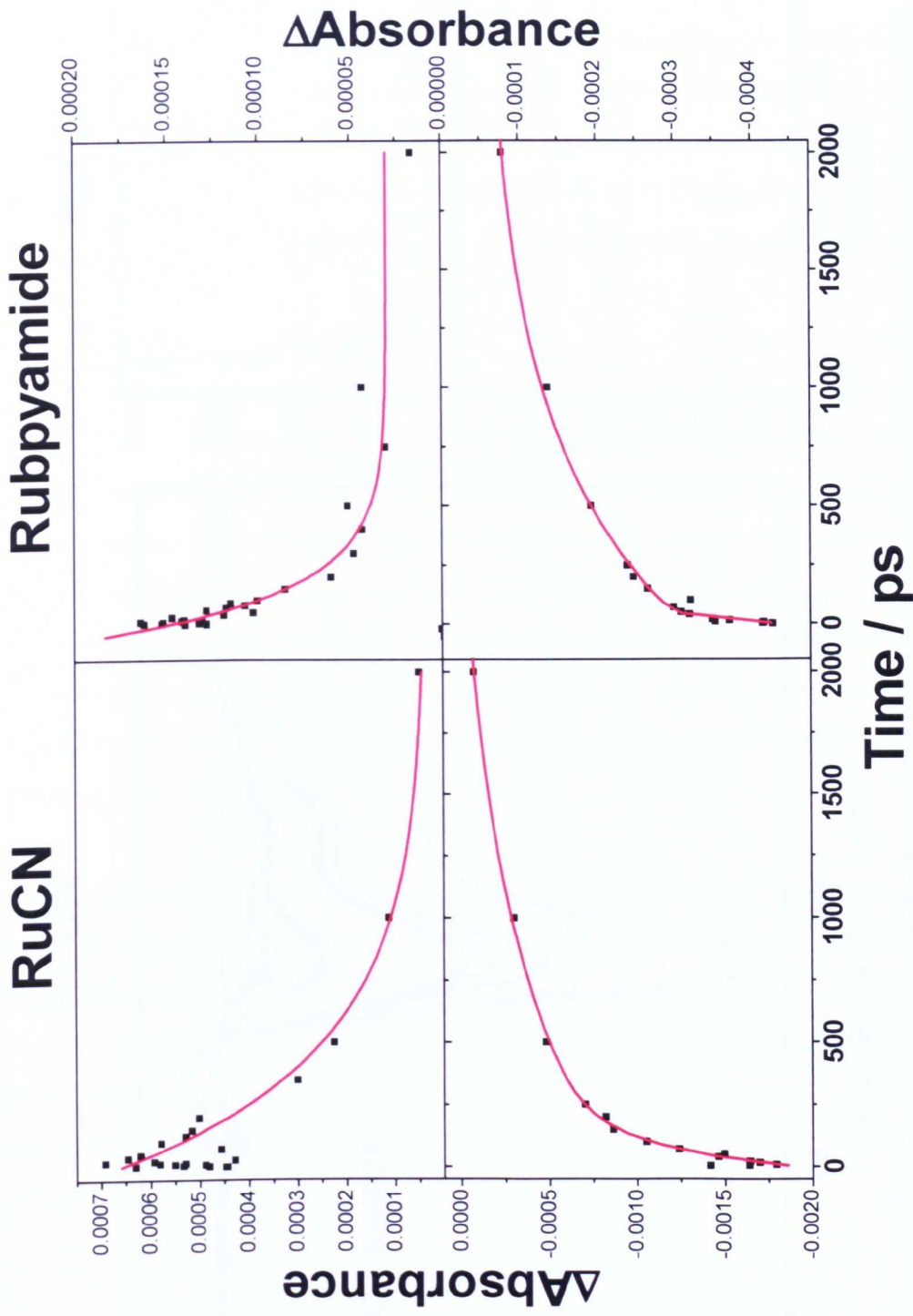
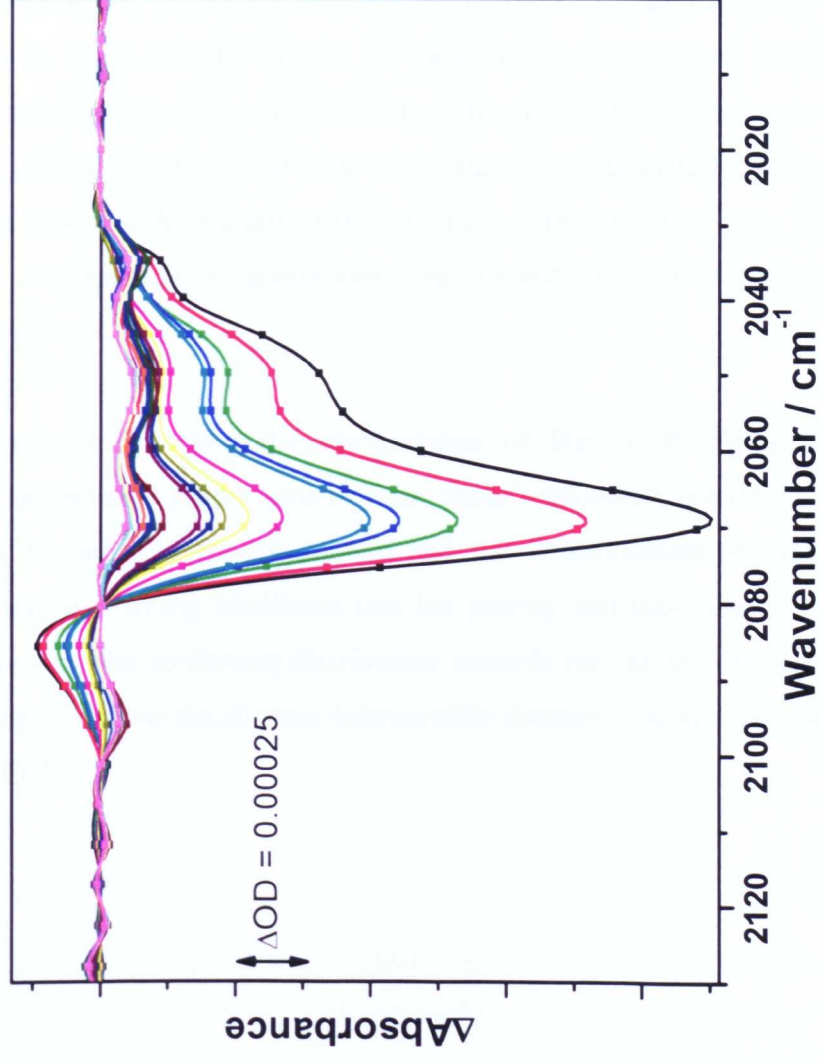
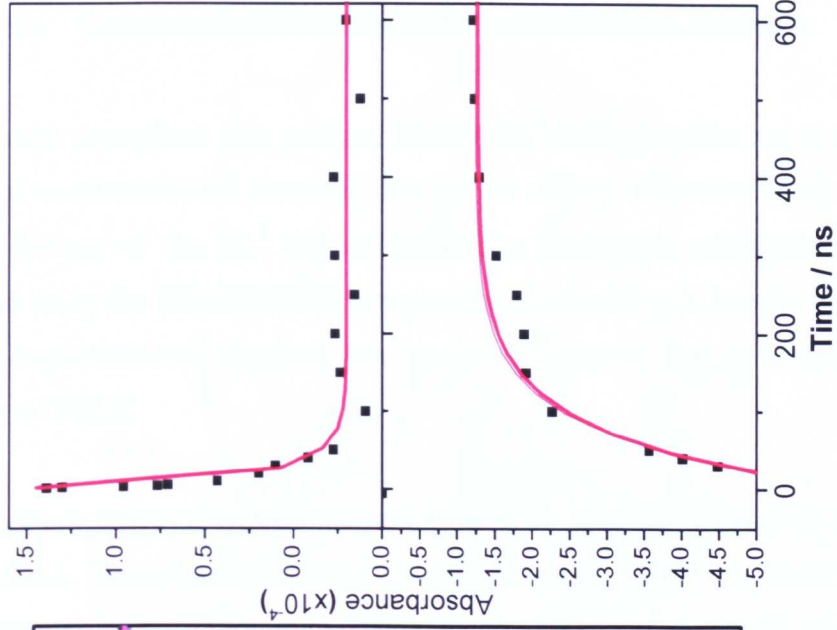


Figure 3.5.3.8: ps-TRIR kinetics of RuCN-BL¹-Rubpyamide in CH₃CN solution for the RuCN (transient at 2114 cm⁻¹, top left and bleach at 1637 cm⁻¹, bottom left) and Rubpyamide (transient at 1616 cm⁻¹, top right and bleach at 1637 cm⁻¹, bottom right) termini for Δt = 0-1 ns.

RuCN



RuCN



Figures 3.5.3.9 and 3.5.3.10: ns-TRIR spectra (left) and kinetics (transient at 2085 cm⁻¹, top right and bleach at 2070 cm⁻¹, bottom right) of RuCN-BL¹-Rubpyamide in CH₃CN solution for $\Delta t = 0$ -600 ns.

3.5.4. Computational Studies and Conformational Analysis

As discussed throughout this section, **RuCN-BL¹-Rubpyamide** has a considerable amount of conformational freedom due to the ability to rotate freely around the CH₂CH₂ linkage of the BL¹ ligand. Molecular mechanics calculations have been performed using the SPARTAN02 computational suite to gain insight into the effect that this conformational freedom has on the parameters that govern the rate and efficiency of PEnT.

Four important cases of conformational behaviour have been isolated, as shown in Figure 3.5.4.1. These consist of two ‘closed’ structures where the two metal centres are in close proximity (although their ligands prevent closer approach) and two ‘open’ conformers in which the BL¹ ligand has unfolded to form a near linear chain. The relative positions of the metal centres in these two pairs of conformers can be thought of as *syn* (*i* and *iii*) or *anti* (*ii* and *iv*) to each other. The intermetallic distances in these cases range from 5.4 Å in conformer (*i*) to 12.7 Å in conformer (*iv*). Therefore it is likely that an ensemble of conformers are present in solution with intermetallic distance $5.41 < r < 12.7$ Å.

It is important to consider the electrostatics of **RuCN-BL¹-Rubpyamide** when estimating the relative proportions of these three conformers present in solution. As the **RuCN** terminus is doubly anionic and the **Rubpyamide** terminus is doubly cationic, there is a strong likelihood that ion pairing will take place to some extent, perhaps skewing the conformer distribution towards the ‘closed’ structure of (*i*). As this conformer exhibits the shortest intermetallic distance it would also be optimal for efficient PEnT.

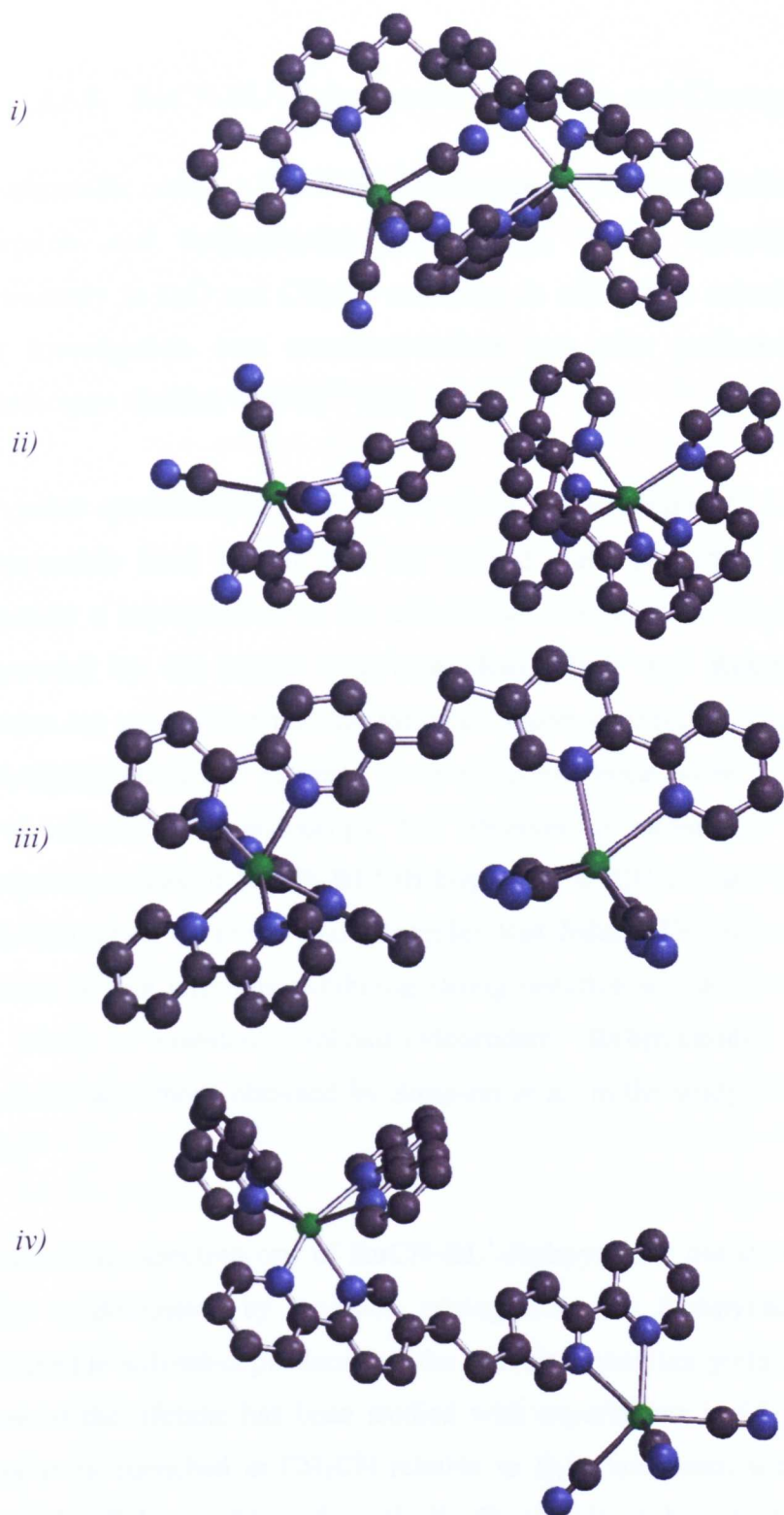


Figure 3.5.4.1: Four important conformers of RuCN-BL¹-Rubpyamide calculated in the gas phase using SPARTAN's molecular mechanics suite: i) and ii) are syn and anti folded conformers of closed structures; iii) and iv) are syn and anti conformers of open structures. Amide groups and H atoms omitted for clarity.

3.5.5. RuCN-BL¹-Rubpyamide: Discussion and Closing Points

The bimetallic complex **RuCN-BL¹-Rubpyamide** has been studied using UV/visible absorption and luminescence spectroscopy, cyclic voltammetry and TRIR spectroscopy in D₂O and CH₃CN solutions. In addition to solvatochromic studies a brief investigation into metalochromism was also performed by way of a luminescence titration with Ba²⁺ ions.

UV/visible spectroscopy (§3.5.1) and cyclic voltammetry (§3.5.2) of **RuCN-BL¹-Rubpyamide** have shown that the ground state properties of the system are essentially a superposition of the constituent monometallic fragments most closely represented by the model complexes **RuCNdmb** and **Rubpyamide-BL¹**. This supports our supposition that the saturated spacer connecting the two bpy ligands in the bridging ligand BL¹ prevents electronic communication between the two termini. UV/vis absorption spectroscopy has observed a measurable difference in the absorption profiles of **RuCN-BL¹-Rubpyamide** in CH₃CN and D₂O which is more subtle than observed in the model complex **RuCNdmb**. This is presumably due to the presence of one terminus exhibiting strong negative solvatochromism (**RuCN**) and one which is essentially solvent-independent (**Rubpyamide**). These results are consistent with those obtained by Simpson *et al.* in the study of **RuCN-BL-Rubpy** (§3.1).³

Luminescence spectroscopy of **RuCN-BL¹-Rubpyamide** has shown that the spectral profile is dominated by emission arising from the **Rubpyamide** terminus. The considerable solvent-dependence of the emission quantum yield and multi-exponent nature of the lifetime has been studied with experiments in CH₃CN and D₂O. The emission is quenched in CH₃CN relative to D₂O, consistent with **Rubpyamide** → **RuCN** PEnT being thermodynamically favourable in low A. N. solvents such as CH₃CN. The presence of multiexponential kinetics may be related to the conformational freedom possessed by the system (§3.5.4, *vide infra*). As with **RuCN-BL-Rubpy** (§3.1), the emission is considerably more intense in high A. N. solvents

($\phi_{D_2O} > \phi_{CH_3CN}$) which may be rationalised using an analogous model (§3.5.1, Figure 3.1.1.4). Also in keeping with literature results for **RuCN-BL-Rubpy** (§3.1) emission from the **RuCN** terminus was not detected, presumably owing to its low quantum yield and/or being obscured by emission from the much more intense **Rubpyamide** terminus.

The metallochromic properties of **RuCN-BL¹-Rubpyamide** have been demonstrated using luminescence spectroscopy²³ and provide an interesting avenue for future work in the areas of metal ion sensing and designing photophysical switches which can respond to multiple independent external stimuli (solvent A. N. and $[M^+]$); this may be a requirement in the design and preparation of future photochemical device components.²⁴

TRIR spectroscopy has been used to directly monitor the processes occurring following photoexcitation of **RuCN-BL¹-Rubpyamide** on the picosecond and nanosecond timescales. In agreement with the model presented in §3.5.3, the results presented in the same section provide very strong evidence for **RuCN** → **Rubpyamide** PEnT in D₂O on the basis of the clear grow-ins of absorbance of bleach and transient signals of the **Rubpyamide** terminus in TRIR kinetic traces in D₂O in the $\Delta t = 0-50$ ps time range following laser excitation (Figure 3.5.3.2). When this is considered in conjunction with the approximately synchronous decays measured for the **RuCN** terminus over the same time period this argument becomes more persuasive.

Evidence for **Rubpyamide** → **RuCN** PEnT in CH₃CN has also been presented (Figure 3.5.3.7) primarily on the basis of the grow-in of absorbance of the **RuCN** bleach and transient signals over the same $\Delta t = 0-50$ ps timescale. The time constants for PEnT were not precisely determined due to the low instrumental spectral resolution of the PIRATE spectrometer (*ca.* 8-9 cm⁻¹) and the limited number of spectra collected in the crucial $\Delta t = 0-20$ ps time range, but approximate values of $\tau_{PEnT,D_2O} \sim 5-10$ ps and $\tau_{PEnT,CH_3CN} \sim 9-15$ ps were obtained, indicating that through-

space PEnT occurs rapidly between the two termini and provides evidence of the reversible control of the direction of PEnT in this bimetallic system through manipulation of the solvent composition.

2-Step PEnT Model

The presence of additional fine structure (particularly in the transient region) in the ps-TRIR spectral profile of the **RuCN** terminus in D₂O (Figure 3.5.3.1) and consequent anomalous appearance of the single-pixel kinetic trace may be rationalised by invoking a photophysical model involving a two-step PEnT process. In D₂O the **RuCN** terminus possesses the highest ³MLCT energy excited state ($\text{Ru}_B\text{CN} \rightarrow \text{bpy}$) of all 3 chromophore types in **Ru_BCN-BL¹-Ru_Abpyamide**, with the two lower energy chromophore types ($\text{Ru}_A \rightarrow \text{BL}^1$ and $\text{Ru}_A \rightarrow \text{bpyamide}$) residing on the **Rubpyamide** terminus (Figure 3.5.5.1). Thus upon photoexcitation PEnT may feasibly take place from the Ru_BCN chromophore (coloured blue in the schematic) to the Ru_ABL^1 chromophore (coloured green in the schematic) which is intermediate in energy of the three. A further PEnT process is thermodynamically favourable in D₂O from the Ru_ABL^1 chromophore to the $\text{Ru}_A\text{bpyamide}$ chromophore. The reader's attention is directed to Figure 3.5.5.1 as the schematic depicts this process in a more elegant and colourful manner! The Figure also illustrates why this process would not be feasible in CH₃CN; namely that the ³MLCT energy of the Ru_ABL^1 chromophore is not intermediate in energy between the ³MLCT excited states of the two termini in this case and is unable to act as a conduit for the PEnT process.

Reinvestigating the spectroscopy and kinetics of the **RuCN** terminus of **RuCN-BL¹-Rubpyamide** in D₂O (first presented in Figures 3.5.3.1 and 3.5.3.2, below as Figure 3.5.5.2) and in particular examining the kinetic behaviour of the **RuCN** transient bands it is quite clear that there is a considerable shift of the transient band to higher wavenumber as Δt increases (Figure 3.5.3.2 inset). By monitoring the single-pixel kinetics at the maxima before and after the band shift (located at 2104 and 2114 cm⁻¹ respectively) it is reasonable to suggest that the two species are interconverting. The 2104 cm⁻¹ feature decays biexponentially with time constants $\tau_1 = 14 (\pm 2)$ ps and $\tau_2 =$

292 (± 108) ps and the 2114 cm^{-1} feature exhibits a grow-in over the time range $\Delta t = 0\text{-}30$ ps followed by a decay with time constant $\tau_1 = 366$ (± 60) ps.

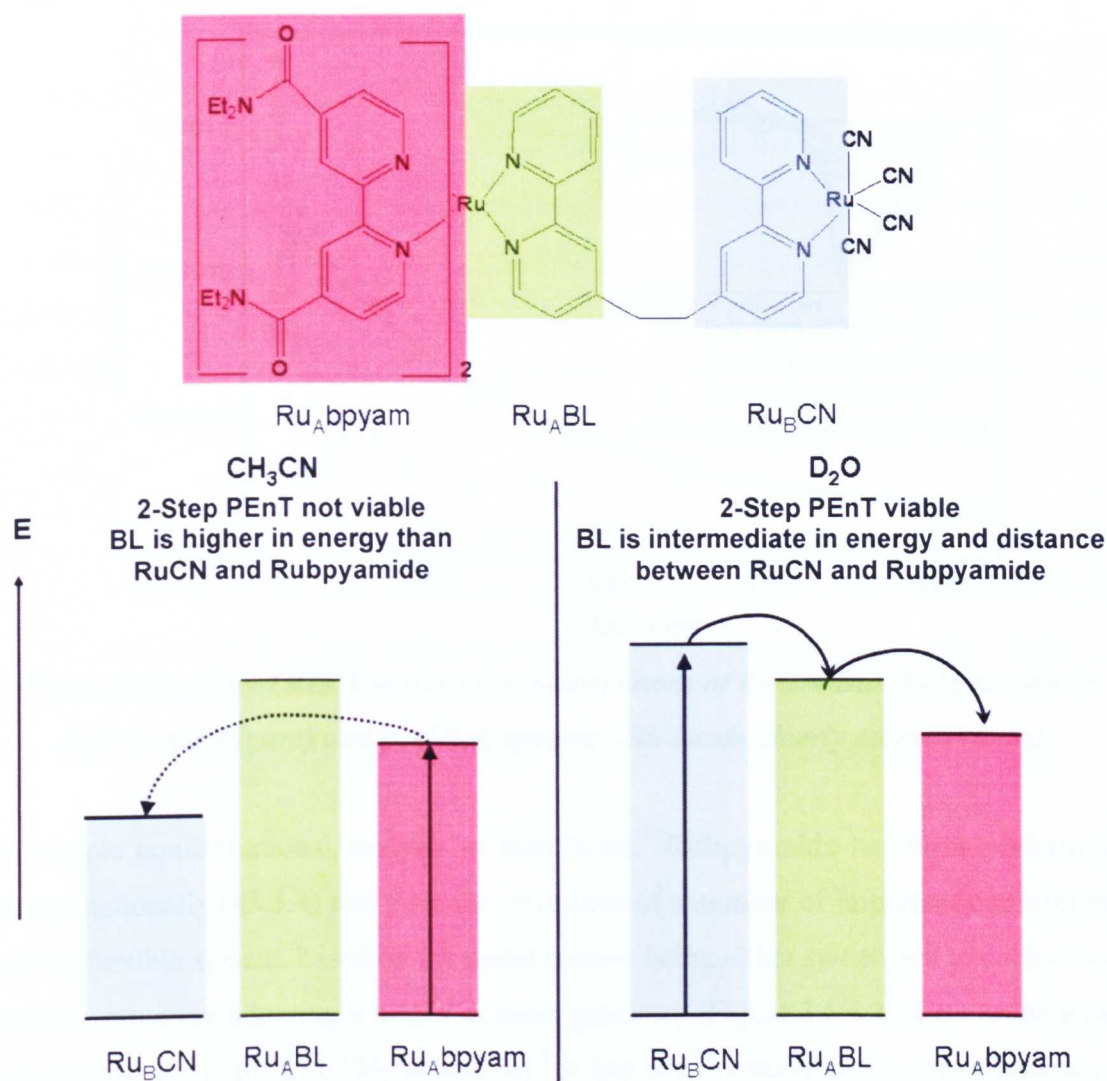


Figure 3.5.5.1: Schematic of the chromophores (top) and energy level ordering (bottom) in $\text{RuCN-BL}^1\text{-Rubpyamide}$ that provides the framework for the 2-step *PENt* model.

A shift of 10 cm^{-1} to higher wavenumber is consistent with excited state electron density being redistributed further away from the RuCN terminus metal centre, as would be expected for a change in the excited chromophore from $\text{Ru}_A \text{BL}$ to $\text{Ru}_A \text{bpyam}$ (Figure 3.5.5.1). The time constants obtained for these features are in satisfactory agreement with each other. The only obvious alternative explanation for

features on this timescale is vibrational cooling, however the lack of observation of any vibrational cooling of $\nu(\text{CN})$ features throughout this Thesis renders this suggestion improbable.

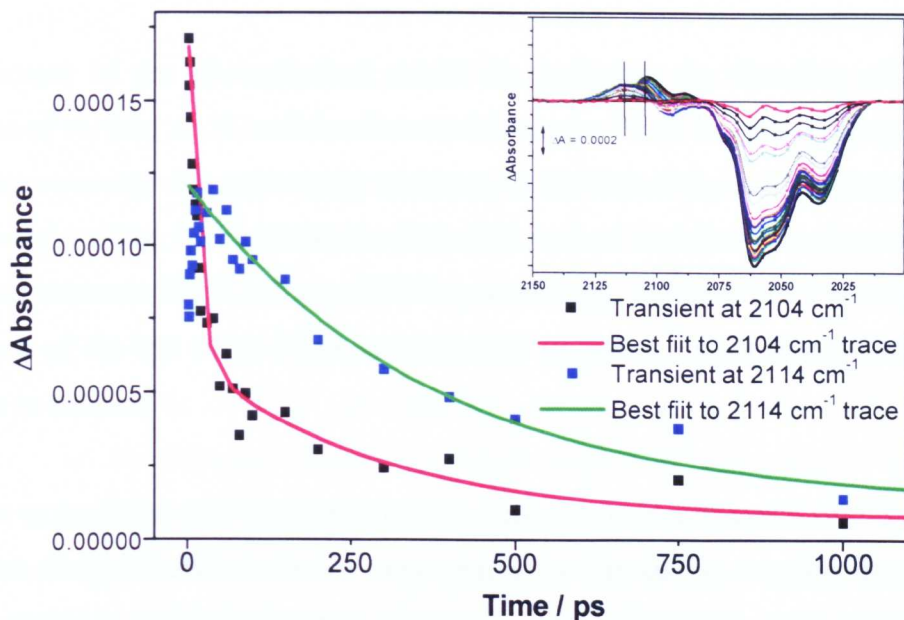


Figure 3.5.5.2: *ps-TRIR kinetics of transient bands of RuCN-BL¹-Rubpyamide in D₂O (main Figure) and ps-TRIR spectra with bands clearly marked (inset).*

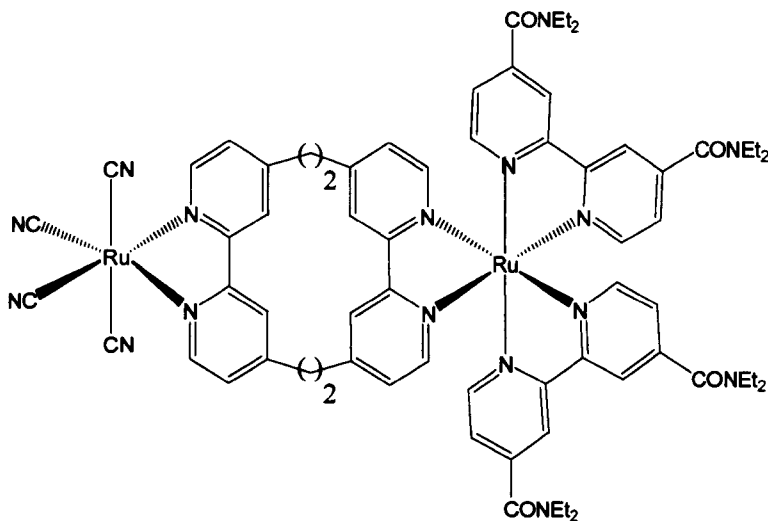
A simple conformational analysis of **RuCN-BL¹-Rubpyamide** has been performed computationally (§3.5.4) and gave the structures of a number of important conformers of the flexible system, based on the metal centres being either *syn* or *anti* to each other and the structure adopting a *folded* or *open* geometry (Figure 3.5.4.1). Due to the ease of rotation about the CH_2CH_2 axis of BL^1 it has been postulated that these structures are likely to be members of an ensemble of conformers present in solution, leading to a range of intermetallic distances between $5.41 < r < 12.7 \text{ \AA}$. This provides a plausible explanation for the multiexponential kinetics obtained by luminescence and TRIR spectroscopy as interchromophoric distance and Förster PEnT rates are sensitively interdependent; $k_{\text{PEnT}} \propto r^6$ (§1.1.3). The electrostatic properties of the system are also important to consider; there may be a strong tendency for the complex to ion-pair as the termini are doubly charged with opposite polarity. This may lead to either *intra* or *intermolecular* ion pairing, affecting the population of conformers present in solution

and hence possibly favouring more closed conformers. A study of FTIR lineshapes of **RuCN-BL¹-Rubpyamide** with varying concentration in H₂O (not shown) was carried out but found no evidence for intermolecular ion-pairing in this system.

The success of the photophysical model in predicting the direction of PEnT in solvents of varying A. N. and the direct evidence for PEnT in both solvents from ps-TRIR spectroscopy is a noteworthy result as, to the best of the author's knowledge at the time of writing, it constitutes the first such case of *real time* direct monitoring of interchromophoric PEnT using ps-TRIR spectroscopy. Furthermore it is certainly the first case of the use of ps-TRIR spectroscopy to probe a solvent-switchable PEnT process in solution.

In order to probe the role that conformation plays in the photophysics of this molecule we have designed and studied a next generation bimetallic complex **RuCN-BL²-Rubpyamide** in which the freedom of rotation in the bridging ligand is constrained.

3.6. $[[((4,4'-\text{CON}(\text{CH}_2\text{CH}_3)_2)_2\text{-bpy})_2\text{Ru}(\text{bpy}-(4,4-\text{CH}_2\text{CH}_2)_2\text{-bpy})\text{Ru}(\text{CN})_4], \text{RuCN-BL}^2\text{-Rubpyamide}$



RuCN-BL²-Rubpyamide may be considered a fusion of the two mononuclear complexes **RuCNdmb** (§3.2) and **Rubpyamide-BL²** (§3.4) and has been designed to exploit properties of these two moieties. As with **RuCN-BL¹-Rubpyamide**, both

termini exhibit lowest-lying $^3\text{MLCT}$ excited states as characterised by absorption, luminescence and TRIR spectroscopy.

The principal difference between this system and **RuCN-BL¹-Rubpyamide** discussed in the previous section is the change in the nature of the bridging ligand, from an open, conformationally flexible structure (BL¹) to a closed-cycle system, in which molecular movements are fairly restricted (BL²). This is postulated to lead to a decrease in the range of interchromophoric distances that can be accessed by **RuCN-BL²-Rubpyamide**, and hence a reduction in the complexity of the kinetic profile of the system, as observed on the nanosecond timescale by luminescence and on the picosecond timescale by TRIR spectroscopy. As the system is also constrained in geometries which allow good spatial overlap between donor and acceptor orbitals, an increase in the efficiency of PenT is also expected. The Dexter mechanism is unlikely to operate in this molecule as the saturated CH₂CH₂ linkers attaching the bridging ligand's bipyridyls together prevent any direct electronic communication between the two metal centres.

3.6.1. UV/visible Absorption and Luminescence Spectroscopy

UV/visible absorption spectra of **RuCN-BL²-Rubpyamide** have been measured in CH₃CN and D₂O (see Appendix §3.9 for spectra) and the peak positions and assignments are presented in Table 3.6.1.1.

Solvent	$\lambda^{\text{max}} / \text{nm}$					
	D ₂ O	< 300	359	412	435	470
CH ₃ CN	< 300	355		434	468	507
Assignment	IL	^1MC	$^1\text{MLCT}$	$^1\text{MLCT}$		$^1\text{MLCT}$
Terminus	$\pi\text{-}\pi^*$		RuCN	Rubpyamide	RuCN	

Table 3.6.1.1: Table of peak positions and assignments for UV/visible absorption spectra of RuCN-BL²-Rubpyamide in D₂O and CH₃CN solutions.

The profiles resemble those obtained for **RuCN-BL¹-Rubpyamide** (§3.5.1) and correspond well to a superposition of the spectra of the model complexes **RuCNdmb** and **Rubpyamide-BL²**, which is consistent with the two containing identical chromophores and little or no electronic communication between the two metal centres in their ground states. As with **RuCN-BL¹-Rubpyamide**, the two relatively solvent-invariant features (<10 nm difference between CH₃CN and D₂O) can be assigned to Ru → (4,4'-(CONEt₂)₂bpy) ¹MLCT transitions. The less intense longer wavelength feature varies over a range of *ca.* 85 nm, exhibiting negative solvatochromism as is expected for ruthenium (II) cyanide transitions and is thus assigned to a Ru → ((5,5'-(CH₃)₂)bpy) ¹MLCT transition.

Emission spectra of **RuCN-BL²-Rubpyamide** in D₂O and CH₃CN are shown in Figure 3.6.1.1 and 3.6.1.2 respectively. Figure 3.6.1.3 compares emission in the two solvents.

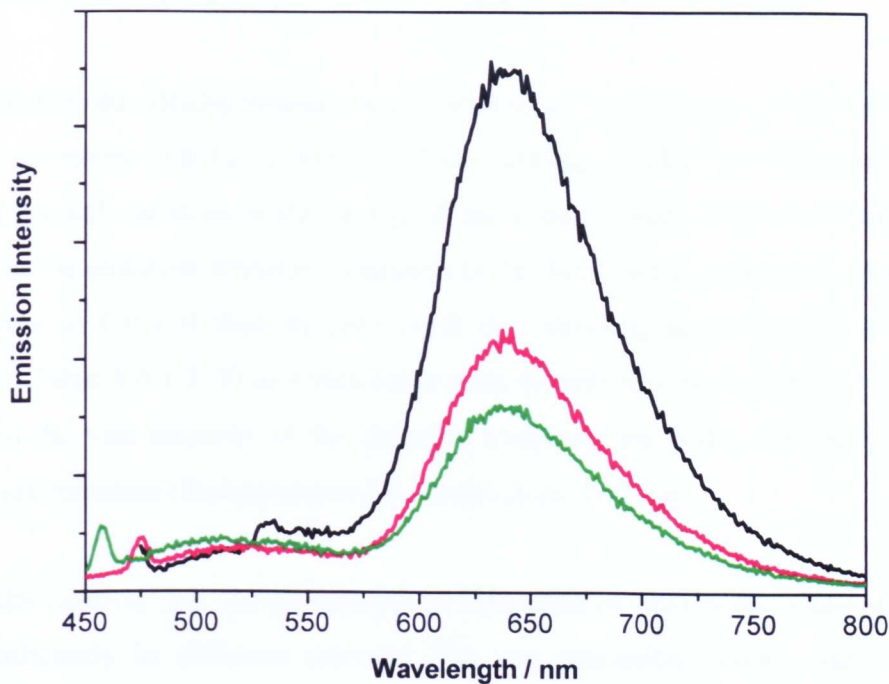


Figure 3.6.1.1: Uncorrected emission spectra of RuCN-BL²-Rubpyamide in D₂O, with $\lambda_{ex} = 469$ nm (black), $\lambda_{ex} = 424$ nm (red) and $\lambda_{ex} = 410$ nm (green). The spectra were recorded under identical conditions.

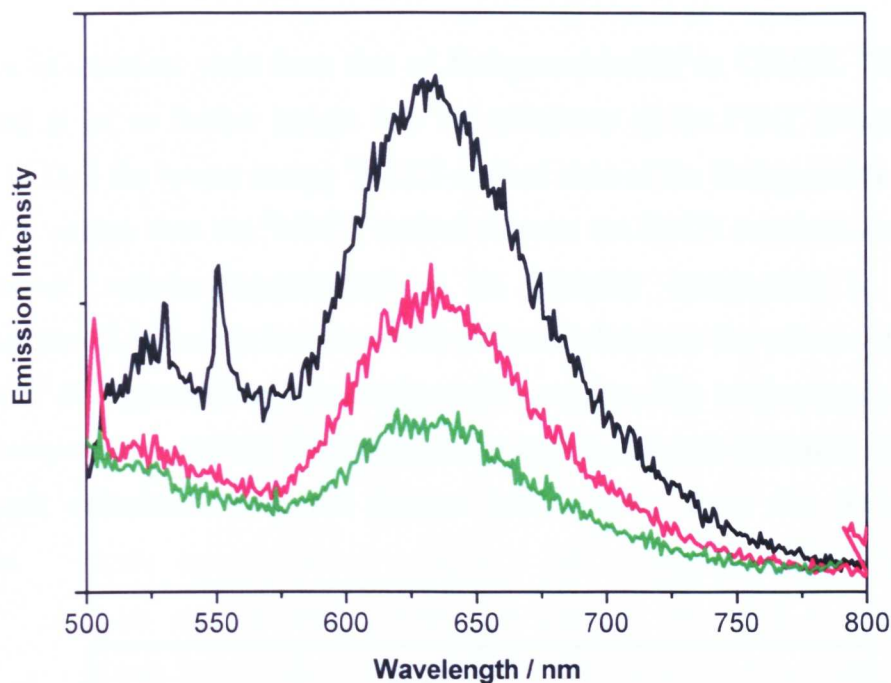


Figure 3.6.1.2: Uncorrected emission spectra of RuCN-BL²-Rubpyamide in CH₃CN, with $\lambda_{ex} = 473$ nm (black), $\lambda_{ex} = 437$ nm (red) and $\lambda_{ex} = 400$ nm (green). The spectra were recorded under identical conditions.

As with **RuCN-BL¹-Rubpyamide**, the complex is luminescent giving a broad, featureless spectrum with λ_{max} (D₂O) = 657 nm and λ_{max} (CH₃CN) = 651 nm. Whilst there is only small variation in the energy of the emissive state, there is a substantial difference in the emission intensity measured in the two solvents; the luminescence is much weaker in CH₃CN than in D₂O, with the wavelengths and quantum yields presented in Table 3.6.1.2. This is consistent with the emissive states being ³MLCT in nature, with the vast majority of the detected luminescence being derived from the **Rubpyamide** terminus (**Rubpyamide-BL²** emits at *ca.* 650 nm).

These results confirm that the photophysical behaviour of **RuCN-BL²-Rubpyamide** varies significantly in different solvents. We can rationalise these results in the framework of our model (§3.1) for these complexes. In CH₃CN the ³MLCT excited state of the **Rubpyamide** terminus is the higher in energy of the two and thus luminescence is partially quenched by energy transfer to the **RuCNdmb** terminus, which only emits weakly with barely detectable luminescence. There is a *ca.* 90%

reduction in quantum yield from that of **Rubpyamide-BL²** in CH₃CN. This partial quenching gives us further insight into the efficiency of the PEnT process in this system. In D₂O the lowest energy ³MLCT excited state of the **Rubpyamide** terminus is lower in energy than the ³MLCT excited state on the **RuCN** terminus and thus its luminescence remains unquenched at an intensity comparable to that of **Rubpyamide-BL²**; there is less than 10% difference between the values obtained for **RuCN-BL²-Rubpyamide** and its amide model complex. The luminescence from the **RuCN** terminus is extremely difficult to detect in this case as it ostensibly occurs at a wavelength coincident with the intense luminescence from the **Rubpyamide** terminus.

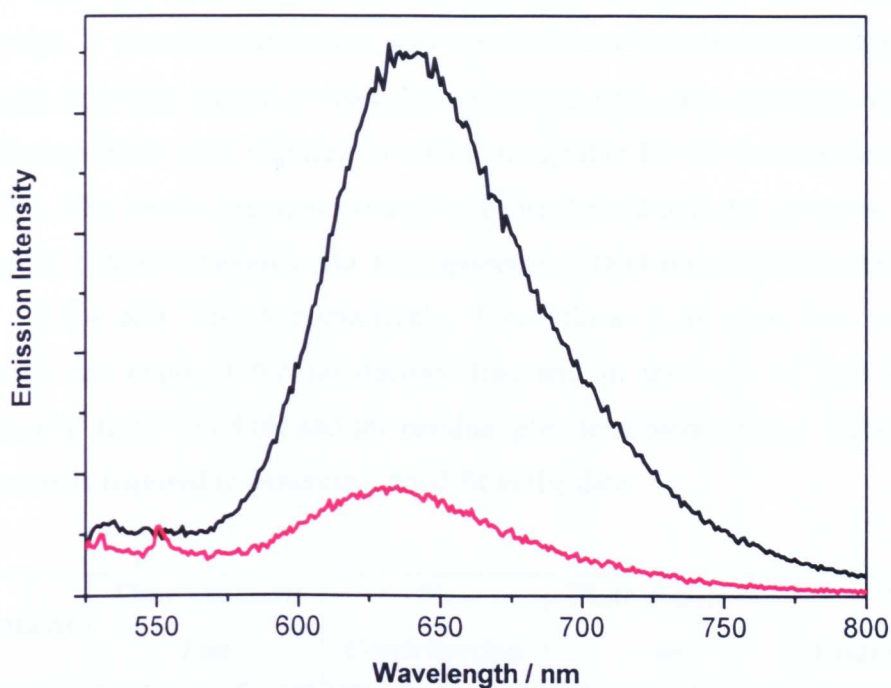


Figure 3.6.1.3: Uncorrected emission spectra of RuCN-BL²-Rubpyamide in D₂O (black) and CH₃CN (red), with λ_{ex} (D₂O) = 410 nm and λ_{ex} (CH₃CN) = 400 nm. The spectra were recorded under identical conditions.

D ₂ O			CH ₃ CN		
$\lambda_{\text{ex}} / \text{nm}$	$\lambda_{\text{em}} / \text{nm}$	Φ	$\lambda_{\text{ex}} / \text{nm}$	$\lambda_{\text{em}} / \text{nm}$	ϕ
469	657	0.005(4)	473	651	0.0007
424	657	0.003(1)	437	650	0.0006
410	656	0.003(0)	400	651	0.0004

Table 3.6.1.2: Table of peak positions and quantum yields from luminescence spectroscopy of RuCN-BL²-Rubpyamide in D₂O and CH₃CN solution.

A kinetic analysis was performed using 405 nm excitation and registration of emission near the peak maximum (644 nm and 631 nm in D₂O and CH₃CN respectively). It was found that the traces obtained could not be fitted using a simple exponential function; indeed at least 4 components with time constants varying by orders of magnitude were required to obtain acceptable fits to the experimental data ($\chi^2 < 1.05$). The results are summarised in Table 3.6.1.2 and the attempts to fit the experimental data to between 1 and 4 components in D₂O and CH₃CN is displayed in Figures 3.6.1.4 and 3.6.1.5 respectively. From these it is clear that at least 4 components are required for satisfactory fits, and in the case of D₂O the large deviation of χ^2 from 1 (1.416) and the residual plot demonstrate that a higher number of exponents is required to generate a good fit to the data.

Component	Time constant / ns	% Contribution	Time constant / ns	% Contribution
	D ₂ O ($\chi^2 = 1.416$)		CH ₃ CN ($\chi^2 = 1.044$)	
τ_1	5.6 ± 0.6	2.37	3.9 ± 0.21	3.97
τ_2	50.4 ± 4.1	34.7	12.0 ± 3.2	5.66
τ_3	100.0 ± 9.3	34.0	100.9 ± 3.2	8.85
τ_4	483.1 ± 27.9	28.9	742.6 ± 34.9	81.54

Table 3.6.1.2: Table of exponential fit components of luminescence spectra of RuCN-BL²-Rubpyamide in D₂O and CH₃CN solutions.

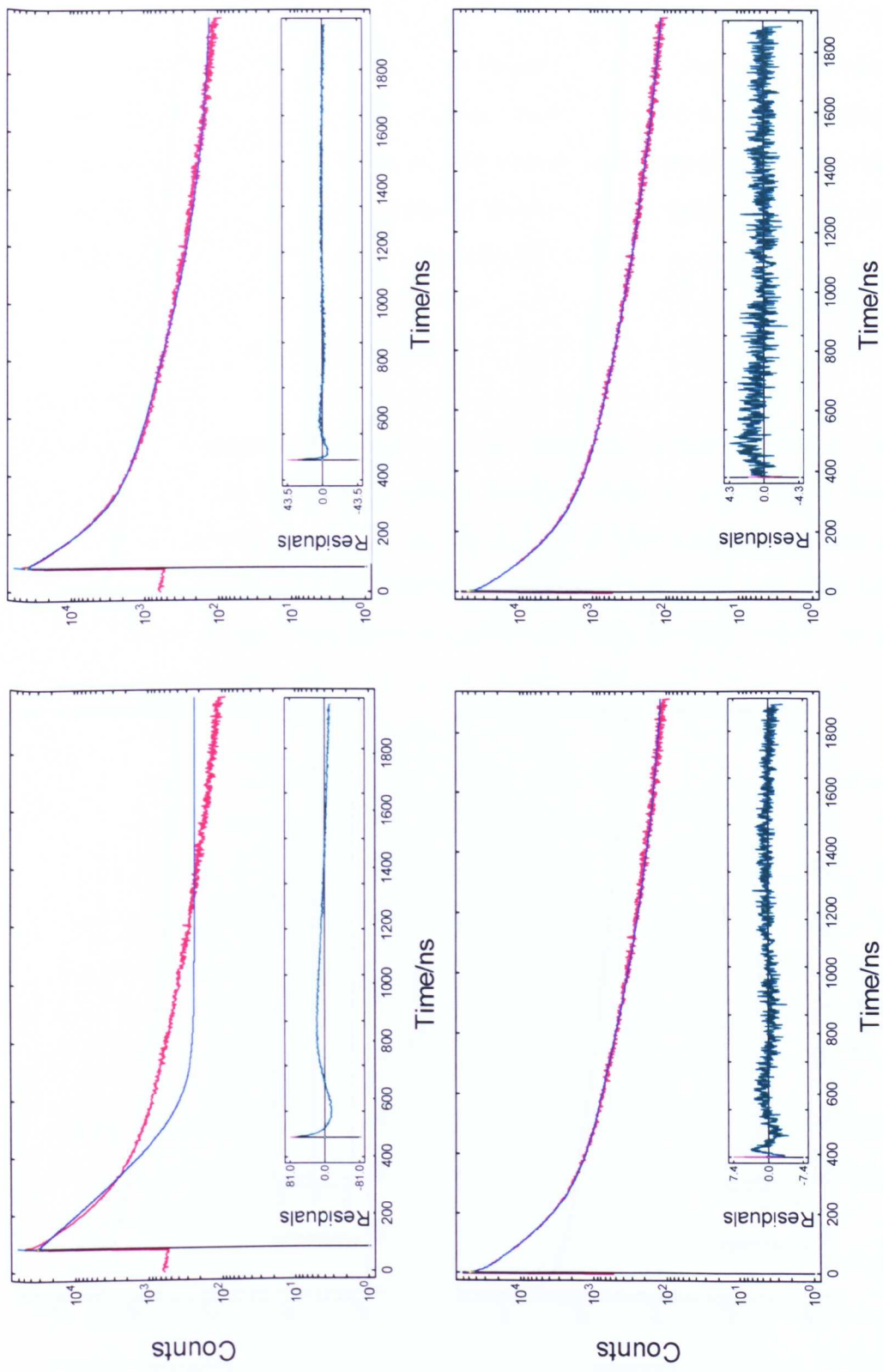


Figure 3.6.1.4: Fits to lifetime data (with residuals) for RuCN-BL²-Rubryamide in D₂O. Top left: 1 exponent; top right: 2 exponents; bottom left: 3 exponents, bottom right: 4 exponents.

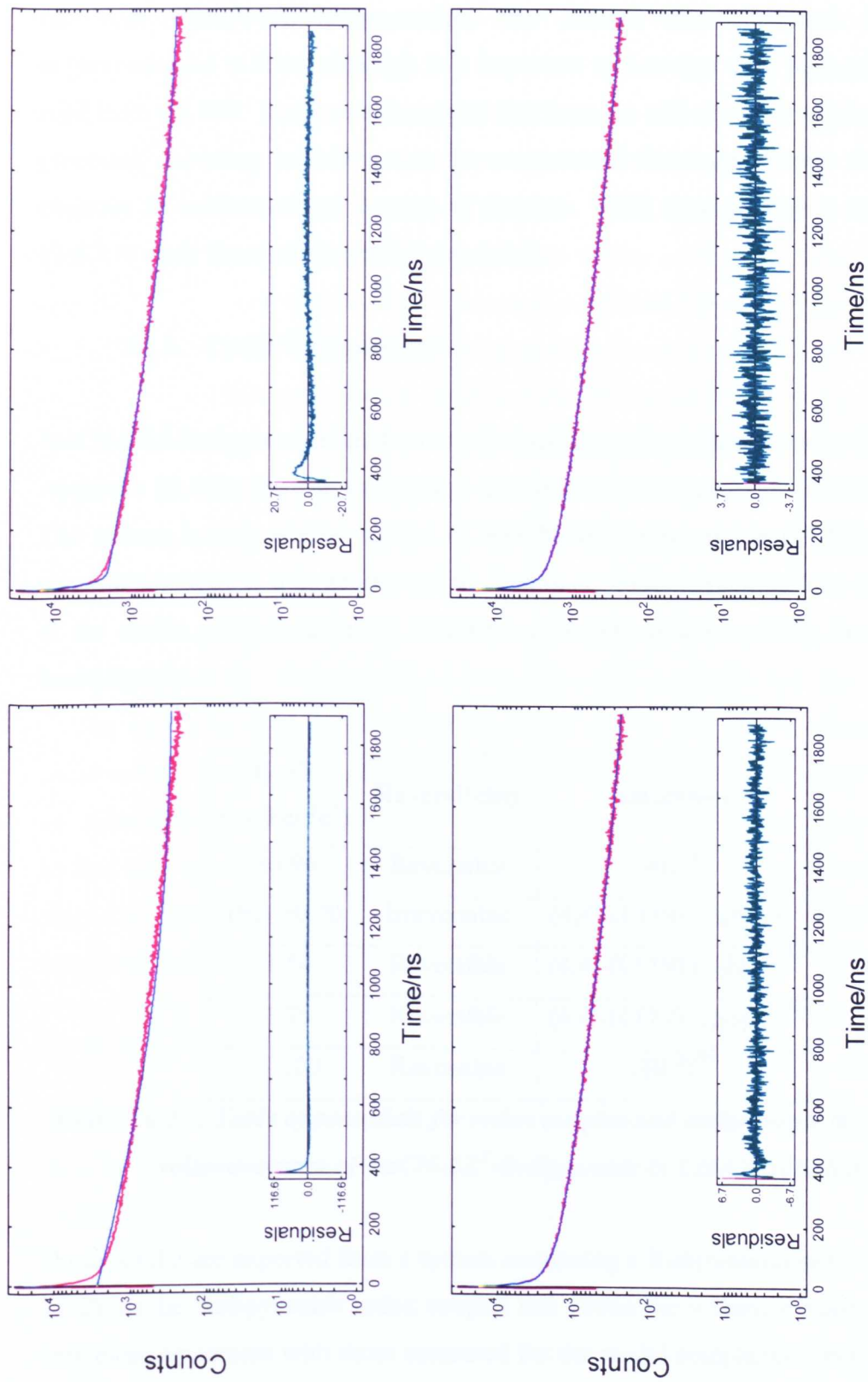


Figure 3.6.1.5: Fits to lifetime data (with residuals) for RuCN-BL²-Rubpyamide in CH₃CN. Top left: 1 exponent; top right: 2 exponents; bottom left: 3 exponents, bottom right: 4 exponents.

As with **RuCN-BL¹-Rubpyamide**, the kinetic data obtained is clearly polyexponential in form, although it is important to note that τ_1 in both solvents may arise from the IRF. These results suggest that there are still a number of photophysical processes occurring in solution on the nanosecond timescale, despite the system's decrease in conformational degrees of freedom. TRIR spectroscopy is employed in §3.6.3 to study these processes in more detail.

3.6.2. Cyclic Voltammetry

RuCN-BL²-Rubpyamide has been studied using cyclic voltammetry in CH₃CN (see Appendix §3.9 for the voltammogram) and the results are presented in Table 3.6.2.1. The picture is very similar to that of **RuCN-BL¹-Rubpyamide** (§3.5.2), with one reversible oxidation, a large irreversible feature at positive potential (due to oxidation of the amide groups) and three reversible reduction couples arising from the bpy-based ligands.

$E_{1/2}/V$ (vs. Fc/Fc ⁺)	Reversibility	Assignment
+0.96	Reversible	Ru ^{II/III}
(E _p) +0.70	Irreversible	(4,4'-(CONEt ₂) ₂ bpy) ^{0/+}
-1.54	Reversible	(4,4'-(CONEt ₂) ₂ bpy) ^{0/+}
-1.75	Reversible	(4,4'-(CONEt ₂) ₂ bpy) ^{0/+}
<-2.00	Reversible	(BL ²) ^{0/+}

Table 3.6.2.1: Table of potentials for redox couples and assignments for the cyclic voltammogram of RuCN-BL²-Rubpyamide in CH₃CN solution.

These results are expected from a system containing a **Rubpyamide-BL^x** unit (§3.3.2 3.5.2), as the **Rubpyamide** redox couples fall within the solvent window and are in very close agreement with those measured for the model complexes. Interestingly the Ru^{II/III} couple of **RuCNdmb** [$E_{1/2} = -0.03$ V (vs. Fc/Fc⁺)] is expected to be present but

isn't observed, suggesting that all its reduction processes occur outside the solvent window.

3.6.3. FTIR and Time-Resolved Infrared Spectroscopy

Luminescence spectroscopy (§3.6.1) has provided some indirect evidence for through-space PEnT between the two metal centres of **RuCN-BL²-Rubpyamide**, through the quenching of emission from the **Rubpyamide** terminus in low A. N. solvent environments. TRIR spectroscopy has been used to monitor this process directly and verify its occurrence. As with **RuCN-BL¹-Rubpyamide**, the system has two sets of IR active 'reporters' - one on either terminus - both can provide important and complementary information and it is crucial to consider them together when analysing the data.

As with **RuCN-BL¹-Rubpyamide** it is important to remember that due to the very similar nature of the chromophores appended to the two metal centres and the broadness of ¹MLCT absorption peaks, there is often a case of unselective excitation – *i.e.* either metal centre may be excited by the incident laser light and more than one excited state species may be present in solution simultaneously. This may add another degree of complexity to the study, as *bona fide* PEnT processes must be disentangled from other primary photophysical processes.

Deuterium Oxide Solution

In D₂O, SEDA interactions elevate the energy of the lowest-energy **RuCN** ³MLCT state above the corresponding state in the **Rubpyamide** terminus. Therefore **RuCN** → **Rubpyamide** PEnT is expected to take place.

The FTIR spectrum of **RuCN-BL²-Rubpyamide** in D₂O solution in the ν(CN) and amide ν(CO) region has been measured (see Appendix §3.9 for spectra). In the cyanide region there is a peak profile characteristic of the tetracyanoruthenate (II) unit with 3 resolved peak maxima at 2091, 2051 and 2032 cm⁻¹, and an additional peak is

observed at 1995 cm^{-1} . In the amide region there is a single peak present at 1615 cm^{-1} . These results are comparable with the constituent complexes **RuCNdmb** and **Rubpyamide-BL²** in D₂O solution (§3.2.5, §3.4.3).

Picosecond and nanosecond TRIR spectroscopy (with laser excitation at 400 and 355 nm respectively) were performed on **RuCN-BL²-Rubpyamide** in D₂O solution, monitoring both regions in the IR where reporter groups are present.

ps-TRIR Spectroscopy

Figure 3.6.3.1 shows the ps-TRIR spectra obtained for the **RuCN** and **Rubpyamide** termini in D₂O.

RuCN (“Donor”) terminus

The spectral profile obtained following 400 nm excitation contains several overlapped bleaches centred between 2030 and 2090 cm^{-1} and transient bands detected at lower and higher wavenumber to the bleach, centred at 2012 and 2100 cm^{-1} . The lower energy bleach is evident at *ca.* 2000 cm^{-1} . There appear to be changes in the profile on the picosecond timescale, particularly in the region where the bleaches overlap with the transient bands. Over the time range of the experiment (1-1000 ps), the majority of the $\nu(\text{CN})$ bleach and transient signals decay, indicating that there are photophysical processes occurring which facilitate the quenching of the **RuCNdmb** ³MLCT excited state. At $\Delta t = 1\text{ ns}$ only *ca.* 10% of the signal immediately after excitation remains, indicating that the majority of **RuCNdmb** excited states formed in solution have been quenched.

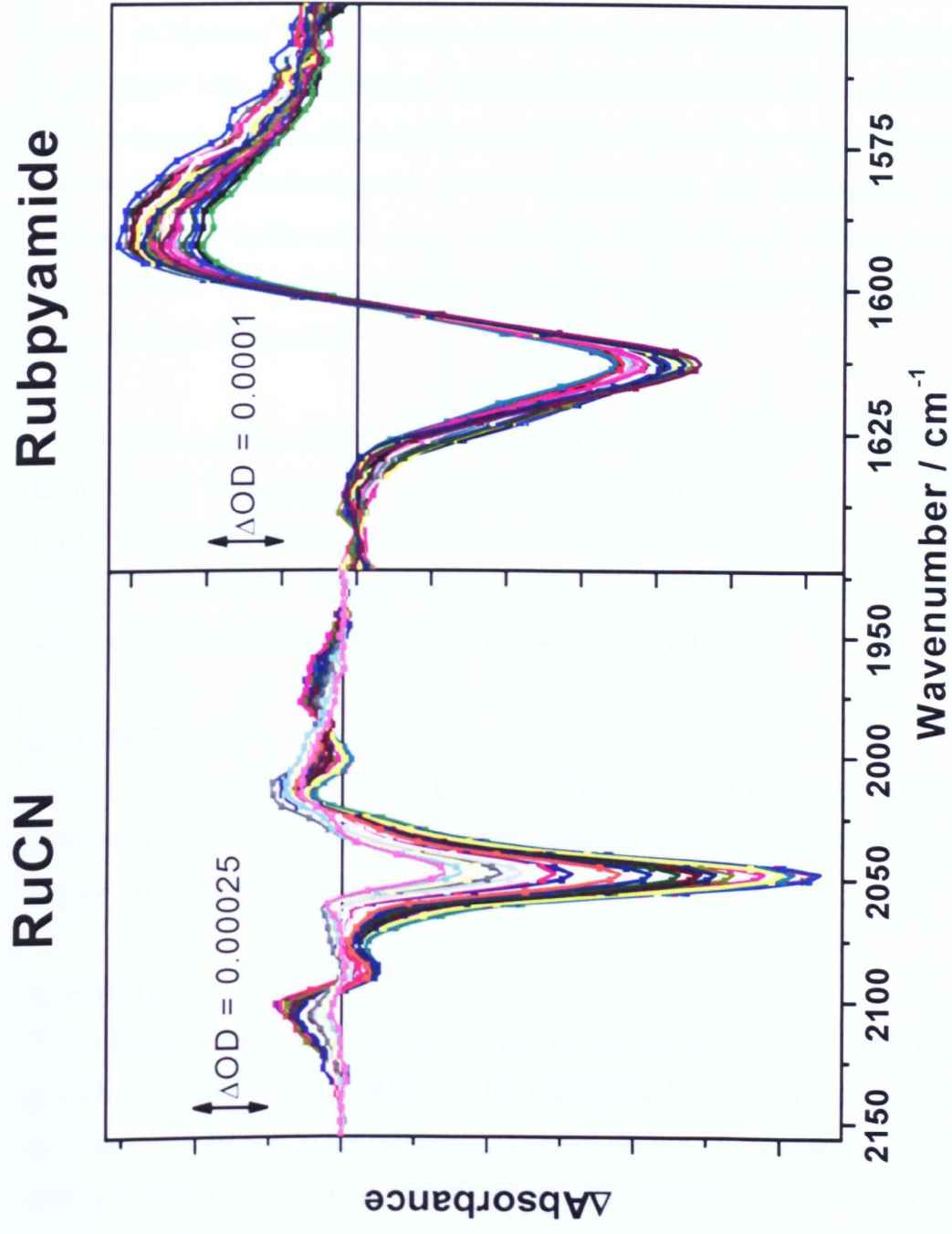


Figure 3.6.3.1: ps-TRIR spectra of RuCN-BL²-Rubpyamide in D₂O solution in the v(CN) and amide v(CO) region for $\Delta t = 0$ -2000 ps.

Rubpyamide (“Acceptor”) terminus

The spectra obtained for the **Rubpyamide** terminus in D₂O resemble the profile observed for the precursor complex **Rubpyamide-BL**², with an amide $\nu(\text{CO})$ bleach centred at 1614 cm⁻¹ and a transient at lower wavenumber centred at 1589 cm⁻¹. This is consistent with the anticipated ³MLCT lowest excited state for this terminus. The spectra show much less development over the timescale of the experiment than for the **RuCN** terminus, indicating that ultrafast processes are not contributing to excited state quenching to the same extent as in the “donor” terminus. Indeed at $\Delta t = 1$ ns there is still a strong signal remaining, indicating that excited state decay is taking place on longer timescales.

This initial result is consistent with our model, which predicts that the **RuCN** donor terminus will be quenched by efficient PEnT and have a short-lived excited state, whilst the **Rubpyamide** acceptor terminus will possess a long-lived excited state owing to it being the ultimate excited state being formed, in keeping with results observed for typical systems based on [Ru(bpy)₃]²⁺ (§1.4.1.1).

ps-TRIR Kinetics

Figures 3.6.3.2 and 3.6.3.3 show the ps-TRIR kinetics (for bleach and transient where possible) obtained for the **RuCN** and **Rubpyamide** termini in different time domains. Figure 3.6.3.2 shows $\Delta t = 0\text{-}50$ ps and 3.6.3.3 shows $\Delta t = 0\text{-}1$ ns.

$\Delta t = 0\text{-}50$ ps

This kinetics recorded during this period do not show any clear evidence for the growth in magnitude of the bleach on the **Rubpyamide** terminus over the first *ca.* 30 ps. This could be due to the offsetting of such a process by other processes occurring over a similar timescale (*e.g.* vibrational cooling) affecting the transient band width and hence affecting the bleach signal due to overlap between the two bands.

RuCN

Rubpyamide

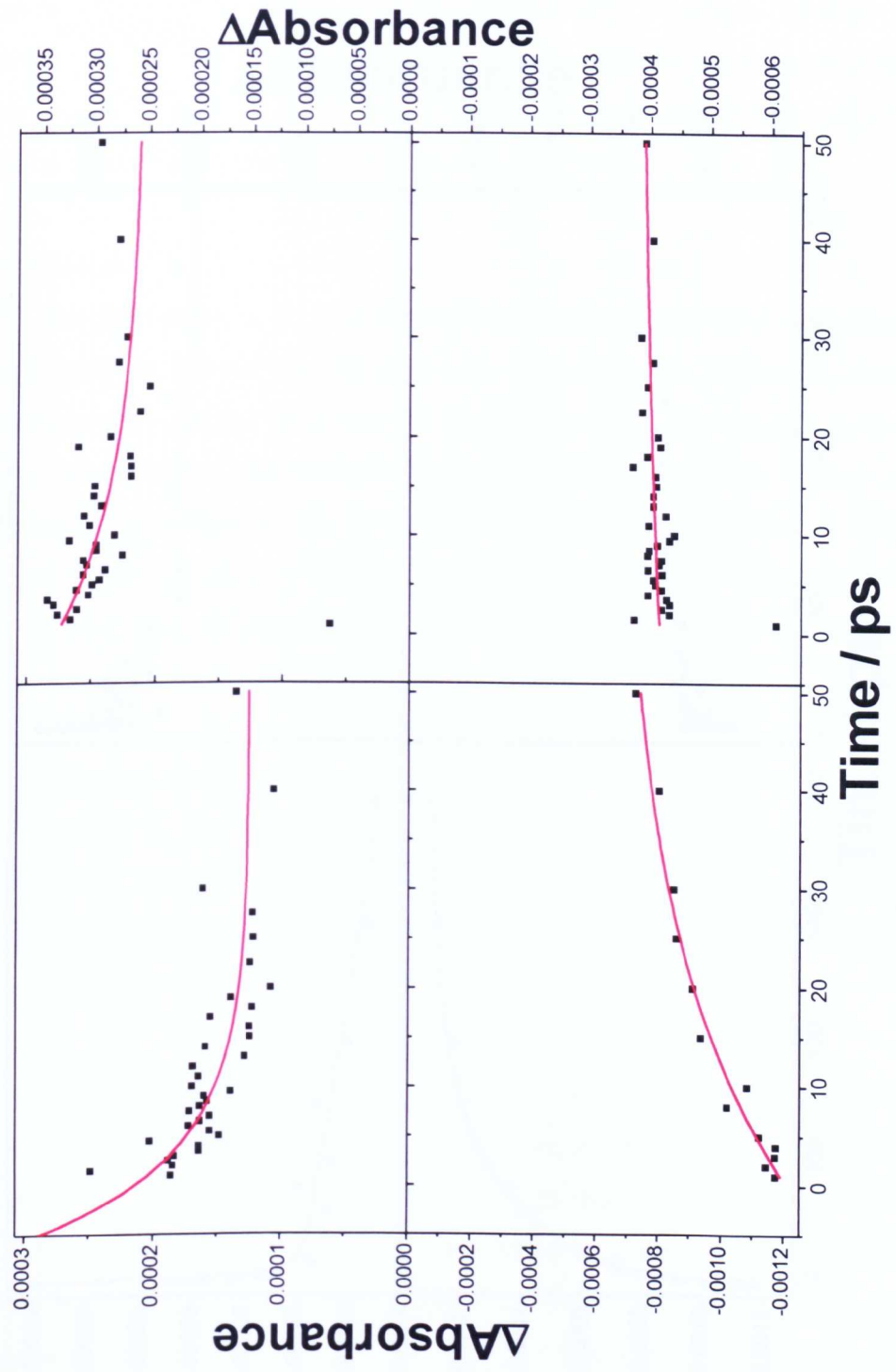


Figure 3.6.3.2: ps-TRIR kinetics of RuCN-BL²-Rubpyamide in D₂O solution for the RuCN (transient at 2103 cm⁻¹, top left and bleach at 2051 cm⁻¹, bottom left) and Rubpyamide (transient at 1592 cm⁻¹, top right and bleach at 1613 cm⁻¹, bottom right) termini for $\Delta t = 0$ -50 ps.

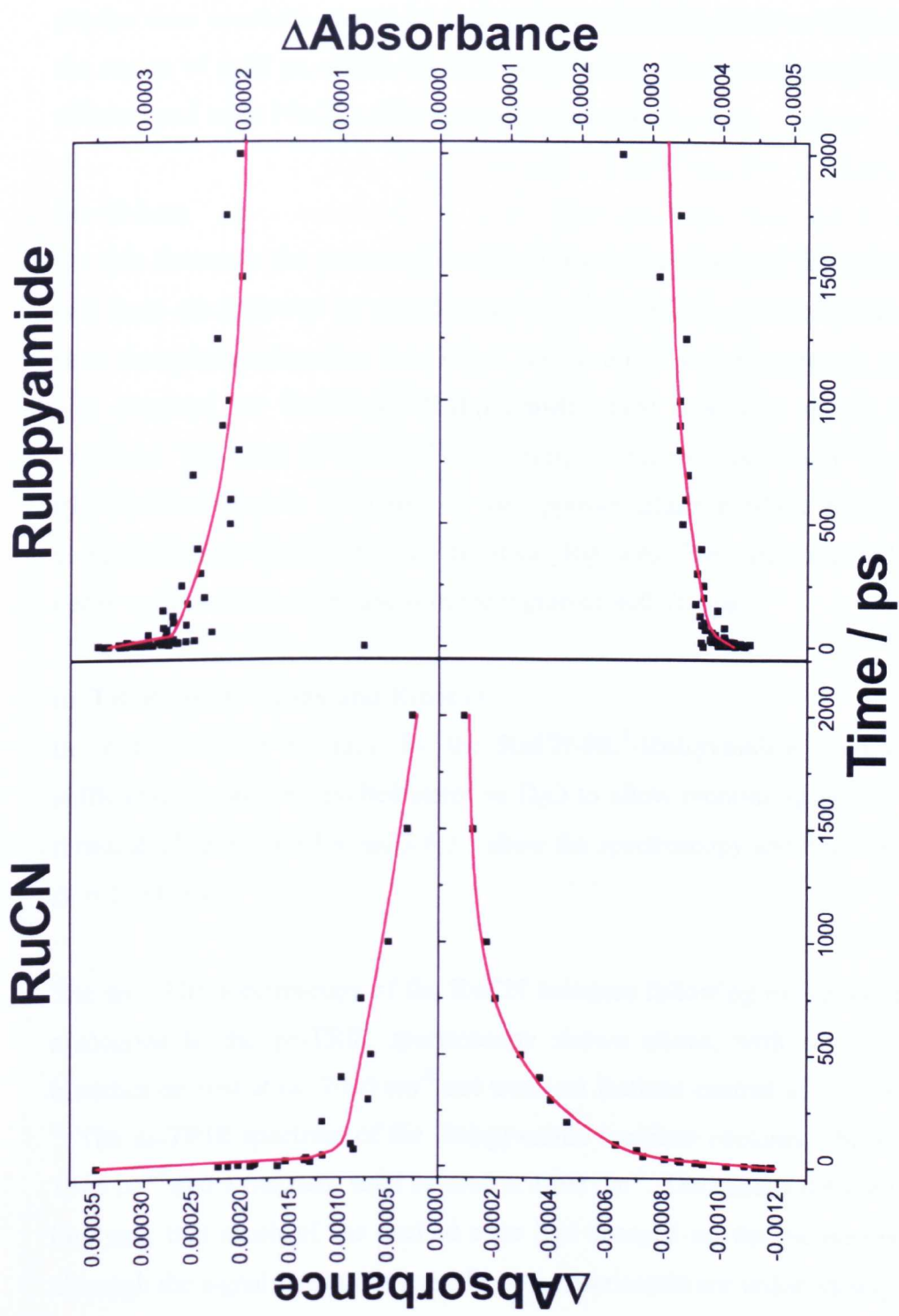


Figure 3.6.3.3: ps-TRIR kinetics of RuCN-BL²-Rubpyamide in D₂O solution for the RuCN (transient at 2103 cm⁻¹, top left and bleach at 2051 cm⁻¹, bottom left) and Rubpyamide (transient at 1592 cm⁻¹, top right and bleach at 1613 cm⁻¹, bottom right) termini for $\Delta t = 0-1$ ns.

Depletion in the magnitude of both the bleach and the transient on the **RuCN** terminus does occur over this same timescale, indicating that a quenching process, probably PEnT, is operating in this time domain. The signal intensity is such that precise time constants cannot be analysed meaningfully, however they are all within the region of 8-20 ps, which would correspond to a time constant of 12 (± 8) ps for efficient and rapid PEnT in this supramolecular system.

$\Delta t = 0-1$ ns

On this timescale the processes described above are observed following excitation, and these are followed by signal decay on both termini, indicating that the excited state decay by routes other than PEnT has become the major process occurring. As was observed for **RuCN-BL¹-Rubpyamide**, these processes appear to be multi-exponent. This may be due to the offsetting of excited state decay processes with PEnT-related grow-in of signal; or the opposite situation where there are multiple competing decay processes occurring at varying rates. The time constant for the major decay component in each case is in the region of 400-700 ps.

ns-TRIR Spectroscopy and Kinetics

In contrast to the situation for the **RuCN-BL¹-Rubpyamide**, both termini have sufficiently long-lived excited states in D₂O to allow monitoring on the nanosecond timescale. Figures 3.6.3.4 and 3.6.3.5 show the spectroscopy and kinetics measured at $\Delta t = 1-300$ ns.

The ns-TRIR spectroscopy of the **RuCN** terminus following excitation at 355 nm is analogous to the ps-TRIR spectroscopy shown above, with several overlapping bleaches centred at *ca.* 2050 cm⁻¹ and transient features centred at 2105 and 2020 cm⁻¹. The ns-TRIR spectrum of the **Rubpyamide** terminus contains a bleach centred at 1615 cm⁻¹ and a transient band centred at 1590 cm⁻¹. The signals detected were weak, implying that much of the excited state had decayed on the picosecond timescale, although the signal intensities over the two experiments are unfortunately not directly

comparable due to different laser excitation wavelengths, data collection times and sample concentrations.

Analysis of the kinetics at the bleach and transient peak maxima give multiexponent fits, with good fits obtained using 2 exponents. The **RuCN** (donor) terminus has time constants of 3.2 (± 1.8) and 19 (± 9.2) ns, and the **Rubpyamide** (acceptor) terminus has time constants of 8.4 (± 3.7), 45.1 (± 9.9) and 138 (± 50) ns. This is consistent with the luminescence data presented in §3.6.1 and confirms that there are multiple photophysical processes occurring in this system over the timescales investigated.

Acetonitrile Solution

In CH_3CN , SEDA interactions stabilise the energy of the **RuCN** $^3\text{MLCT}$ state so that it is lower than the corresponding state on the **Rubpyamide** terminus. Therefore **Rubpyamide** \rightarrow **RuCN** PEnT is expected to take place.

The FTIR spectrum of **RuCN-BL²-Rubpyamide** has been measured in CH_3CN solution in the $\nu(\text{CN})$ and amide $\nu(\text{CO})$ region (see Appendix §3.9 for spectra). 3 components to the peak are resolved at 2086, 2069 and 2058 cm^{-1} . Interestingly there appears to be an additional band present at 1989 cm^{-1} . In the amide region there is a single peak present at 1637 cm^{-1} . These results are broadly comparable with the constituent complexes **RuCNdmb** and **Rubpyamide-BL²** in CH_3CN solution (§3.2.5, §3.4.3) but there are significant differences to the corresponding **RuCN-BL¹-Rubpyamide** FTIR spectrum. The relative intensities of the components are ostensibly reversed in the two complexes, giving the spectra a ‘mirror image’ type relationship. Secondly the additional peak at lower wavenumber would be expected to bleach and give rise to transient peaks in the TRIR experiments if it is a $\nu(\text{CN})$ band.

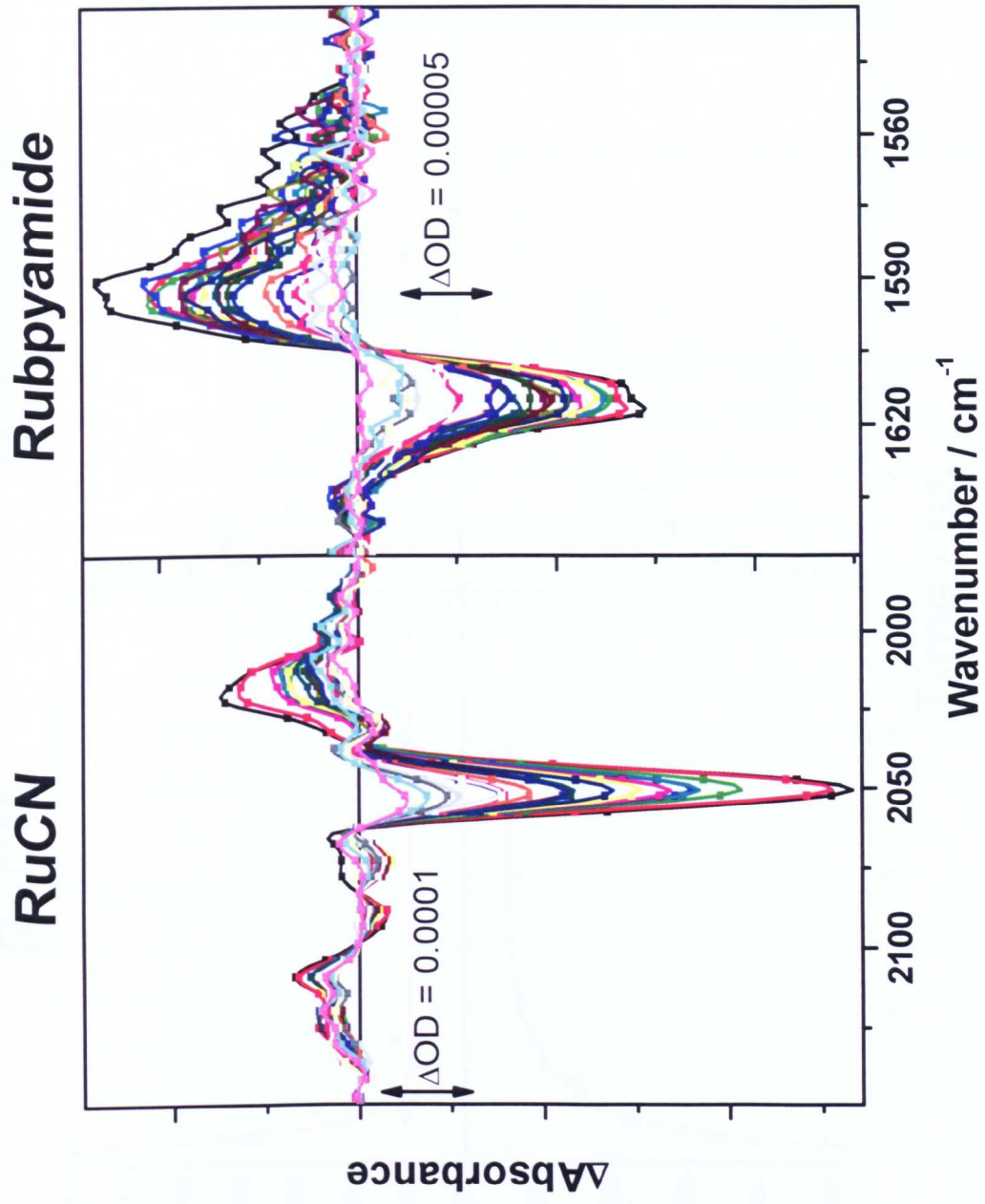


Figure 3.6.3.4: ns-TRIR spectra of RuCN-BL²-Rubpyamide in D₂O solution for both termini for $\Delta t = 0$ -300 ns.

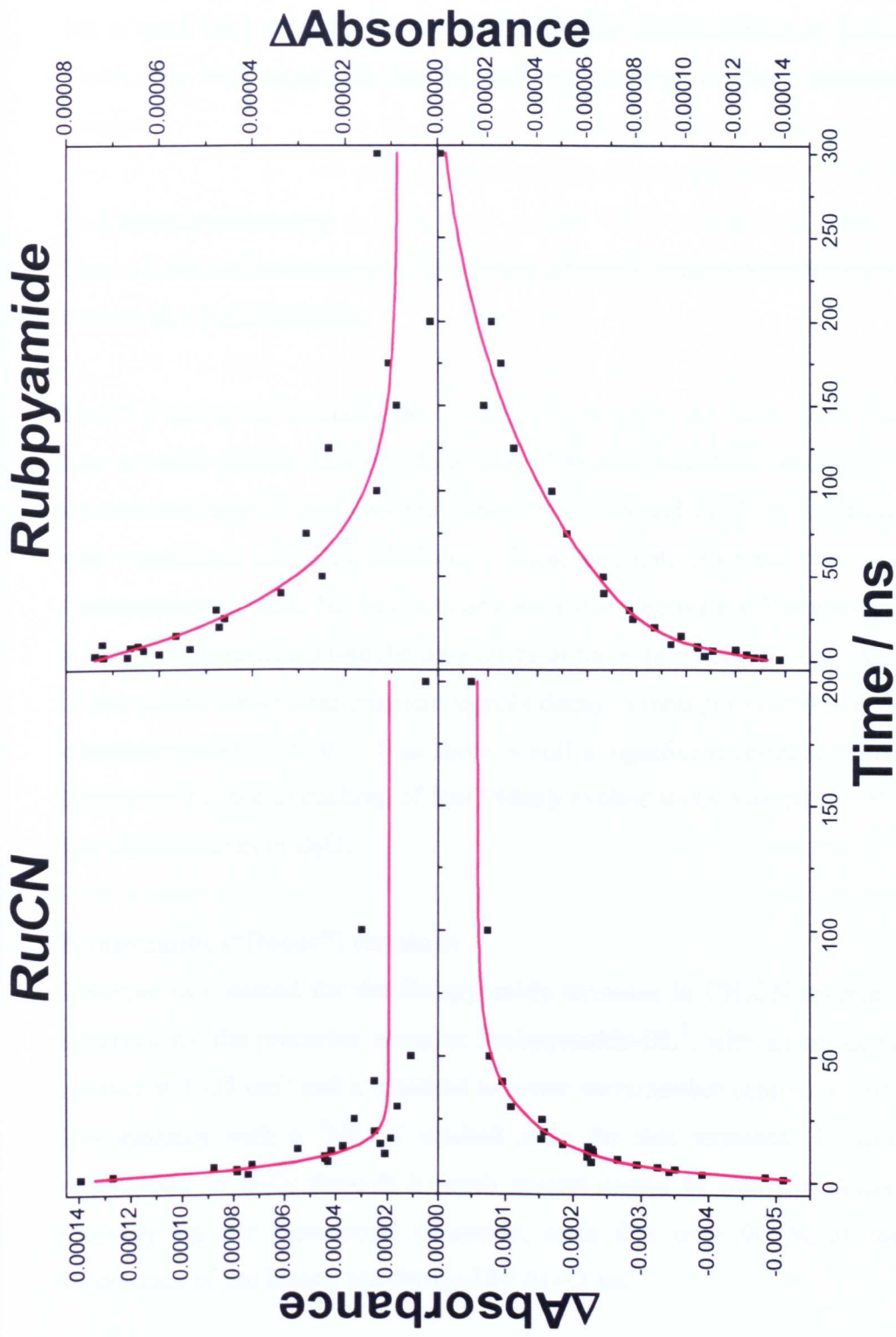


Figure 3.6.3.5: ns-TRIR kinetics of RuCN-BL²-Rubpyamide in D₂O solution for RuCN (transient at 2102 cm⁻¹, top left and bleach at 2052 cm⁻¹, bottom left) and Rubpyamide (transient at 1585 cm⁻¹, top right and bleach at 1618 cm⁻¹, bottom right) termini for $\Delta t = 0$ -300 ns.

Picosecond and nanosecond TRIR spectroscopy (with laser excitation at 400 and 355 nm respectively) were performed on **RuCN-BL²-Rubpyamide** in CH₃CN solution, monitoring both regions in the infrared spectral region where reporter groups are present.

ps-TRIR Spectroscopy

Figure 3.6.3.6 shows the ps-TRIR spectra obtained for the **RuCN** and **Rubpyamide** termini in CH₃CN solution.

RuCN (“Acceptor”) terminus

The spectral profile obtained following 400 nm excitation in CH₃CN consists of several overlapped bleaches centred between 1975 and 2100 cm⁻¹ and transient bands with maxima at 2016 and 2112 cm⁻¹. These originate from the 1989 and 2058 cm⁻¹ features respectively. No major changes in the spectral profile are apparent on the picosecond timescale. Over the time range of the experiment (1-1000 ps), the majority of the $\nu(\text{CN})$ bleach and transient signals decay, although to a lesser extent than was observed in D₂O. At $\Delta t = 1$ ns there is still a significant residual signal remaining, indicating that the quenching of **RuCNdmb** excited states formed in CH₃CN is much less efficient than in D₂O.

Rubpyamide (“Donor”) terminus

The spectra obtained for the **Rubpyamide** terminus in CH₃CN resemble the profile observed for the precursor complex **Rubpyamide-BL²**, with an amide $\nu(\text{CO})$ bleach centred at 1637 cm⁻¹ and a transient to lower wavenumber centred at 1616 cm⁻¹. This is consistent with a ³MLCT excited state for this terminus. In contrast to the observation in D₂O, there is a much greater extent of transient decay and parent recovery on the picosecond timescale, such that over 90 % of the integrated absorbance of the bleach has decayed by $\Delta t = 1$ ns.

This result is consistent with our model, which predicts that the **Rubpyamide** donor terminus will be quenched by efficient PEnT and have a short-lived excited state,

whilst the **RuCN** acceptor terminus will possess a long-lived excited state owing to it being the ultimate excited state being formed. The slight differences in the proportion of signal intensity remaining at $\Delta t = 1$ ns for the two termini between D_2O and CH_3CN can be understood by taking into account the very different natural excited state lifetimes of the two units (as measured in the model complexes **RuCNdmb** and **Rubpyamide-BL²**, §3.2.5, §3.4.3) and indeed the very significant effect that solvent composition has on the excited state properties of **RuCNdmb** in particular.

ps-TRIR Kinetics

Figures 3.6.3.7 and 3.6.3.8 show the ps-TRIR kinetics (for bleach and transient where possible) obtained for the **RuCN** and **Rubpyamide** termini in different time domains in CH_3CN solution. Figures 3.6.3.7 shows $\Delta t = 0-50$ ps and 3.6.3.8 shows $\Delta t = 0-1$ ns.

$\Delta t = 0-50$ ps

This kinetics recorded during this period are similar to those presented for **RuCN-BL¹-Rubpyamide**, as there is some evidence for the growth in magnitude of the bleach and transient on the **RuCN** terminus over the first *ca.* 30 ps, but unfortunately no data of comparable clarity for the **Rubpyamide** terminus were obtained. For the **RuCN** terminus, which as the acceptor provides the tell-tale grow-in of absorbance on both bleach and transient bands, the time constants obtained cannot be trusted precisely (owing to poor data) but they are all within the region of 0.5-3 ps. This would correspond to a time constant of $\sim 2 (\pm 1)$ ps for efficient and rapid PEnT in this supramolecular system. Analysis of the donor terminus data provides few conclusions as neither a clear grow-in or decay is observed over the $\Delta t = 0-50$ ps timescale. Possible reasons for this include offsetting of decay processes in the **Rubpyamide** terminus by peak sharpening of the amide bands due to vibrational cooling processes.

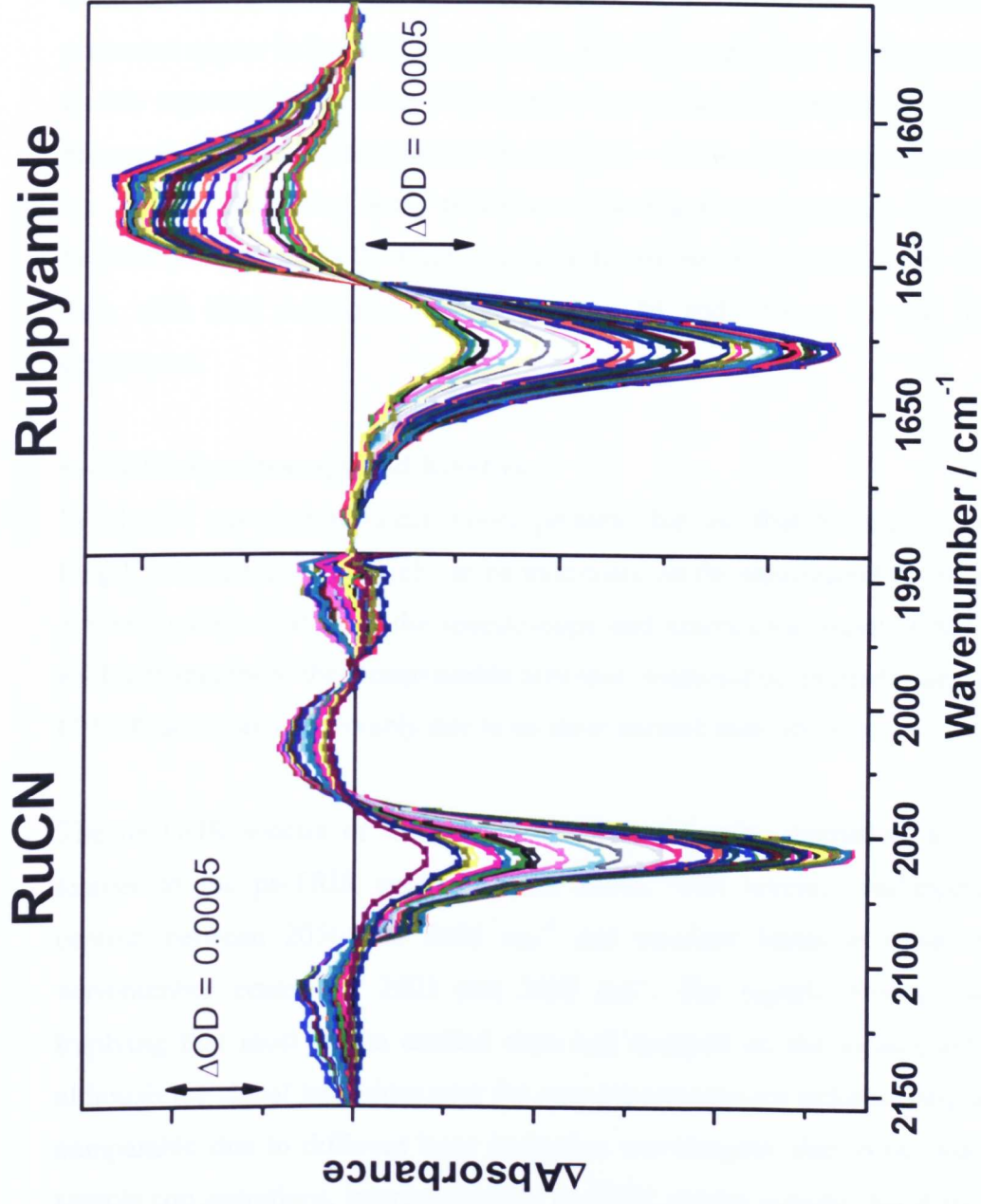


Figure 3.6.3.6: ps-TRIR spectra of RuCN-BL²-Rubpyamide in CH₃CN solution in the v(CN) and amide v(CO) region for for $\Delta t = 0\text{-}2000$ ps.

$\Delta t = 0-1$ ns

As was observed in D₂O solution, during this time domain the processes described above are followed by signal decay on both termini, indicating that the excited state decay by mechanisms other than PEnT becomes the major process occurring. These processes appear to be multi-exponential, with fits employing 1 or 2 components most closely representing the data. This may be due to the offsetting of excited state decay processes with PEnT related grow-in of signal – or the converse situation where there are multiple competing decay processes occurring at varying rates. There appears to be little consistency in the time constants determined for the fits to the experimental data, with time constants varying between 85 and 250 ps for the major decay component.

ns-TRIR Spectroscopy and Kinetics

In CH₃CN our photophysical model predicts that the **RuCN** terminus will have a long-lived excited state which can be monitored on the nanosecond timescale. Figures 3.6.3.9 and 3.6.3.10 show the spectroscopy and kinetics measured at $\Delta t = 1-500$ ns. ns-TRIR spectra of the **Rubpyamide** terminus contained no excited state signatures in CH₃CN solution, conceivably due to its short excited state lifetime.

The ns-TRIR spectra of the **RuCN** terminus following excitation at 355 nm are similar to the ps-TRIR spectra shown above, with several overlapping bleaches centred between 2050 and 2085 cm⁻¹ and transient bands at lower and higher wavenumber centred at 2023 and 2095 cm⁻¹. The signals detected were weak, implying that most of the excited state had decayed on the picosecond timescale, although the signal intensities over the two experiments are unfortunately not directly comparable due to different laser excitation wavelengths, data collection times and sample concentrations. Interestingly the ns-TRIR spectra suggest that there is a strong transient signal to lower wavenumber than the main parent bleach band (centred at 2019 cm⁻¹), however this may be an artefact arising from the poor signal-to-noise ratios obtained as the excited state decays.

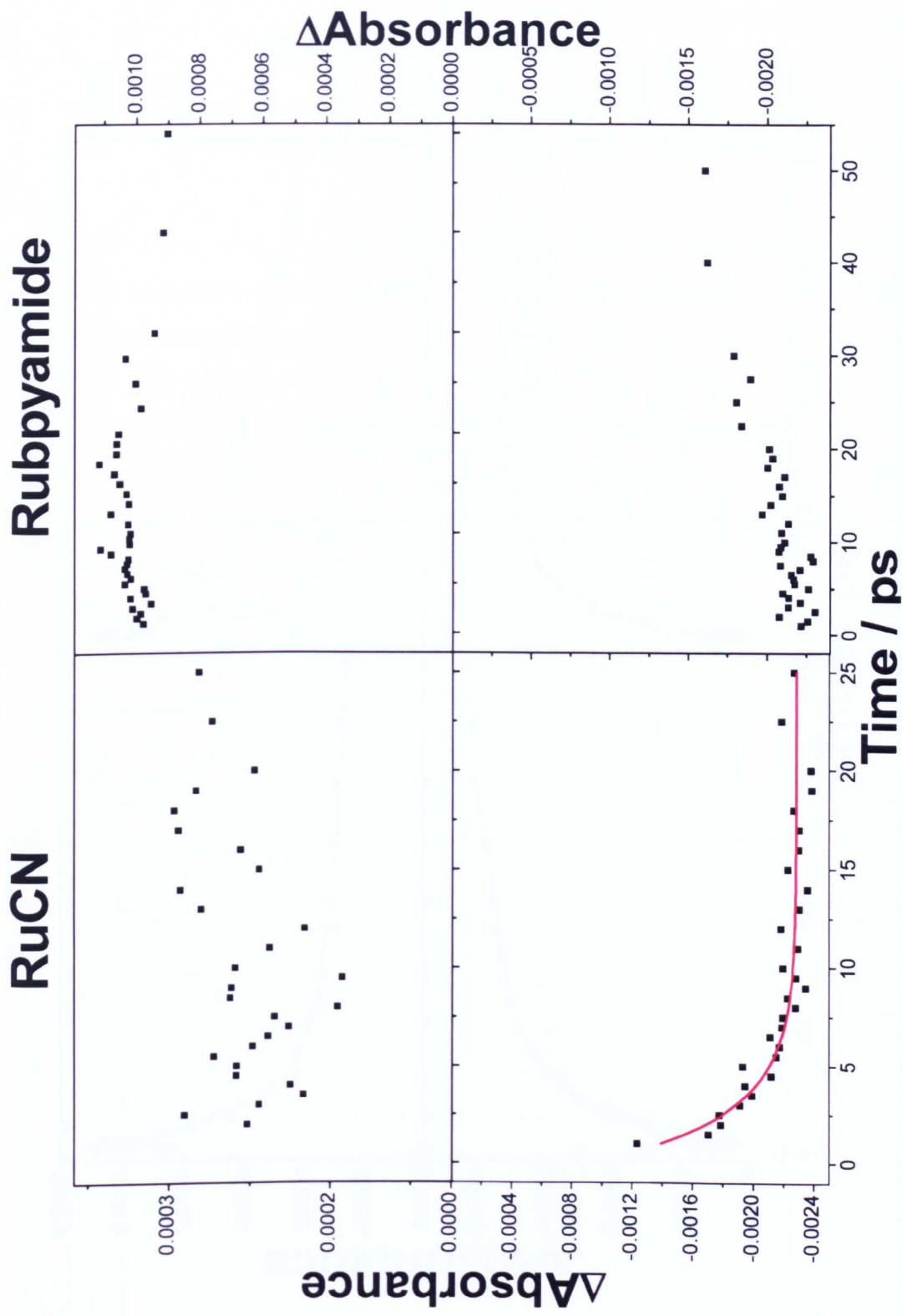


Figure 3.6.3.7: ps-TRIR kinetics of RuCN-BL²-Rubpyamide in CH₃CN solution for the RuCN (transient at 2107 cm⁻¹, top left and bleach at 2056 cm⁻¹, bottom left) and Rubpyamide (transient at 1614 cm⁻¹, top right and bleach at 1638 cm⁻¹, bottom right) termini for $\Delta t = 0$ -50 ps.

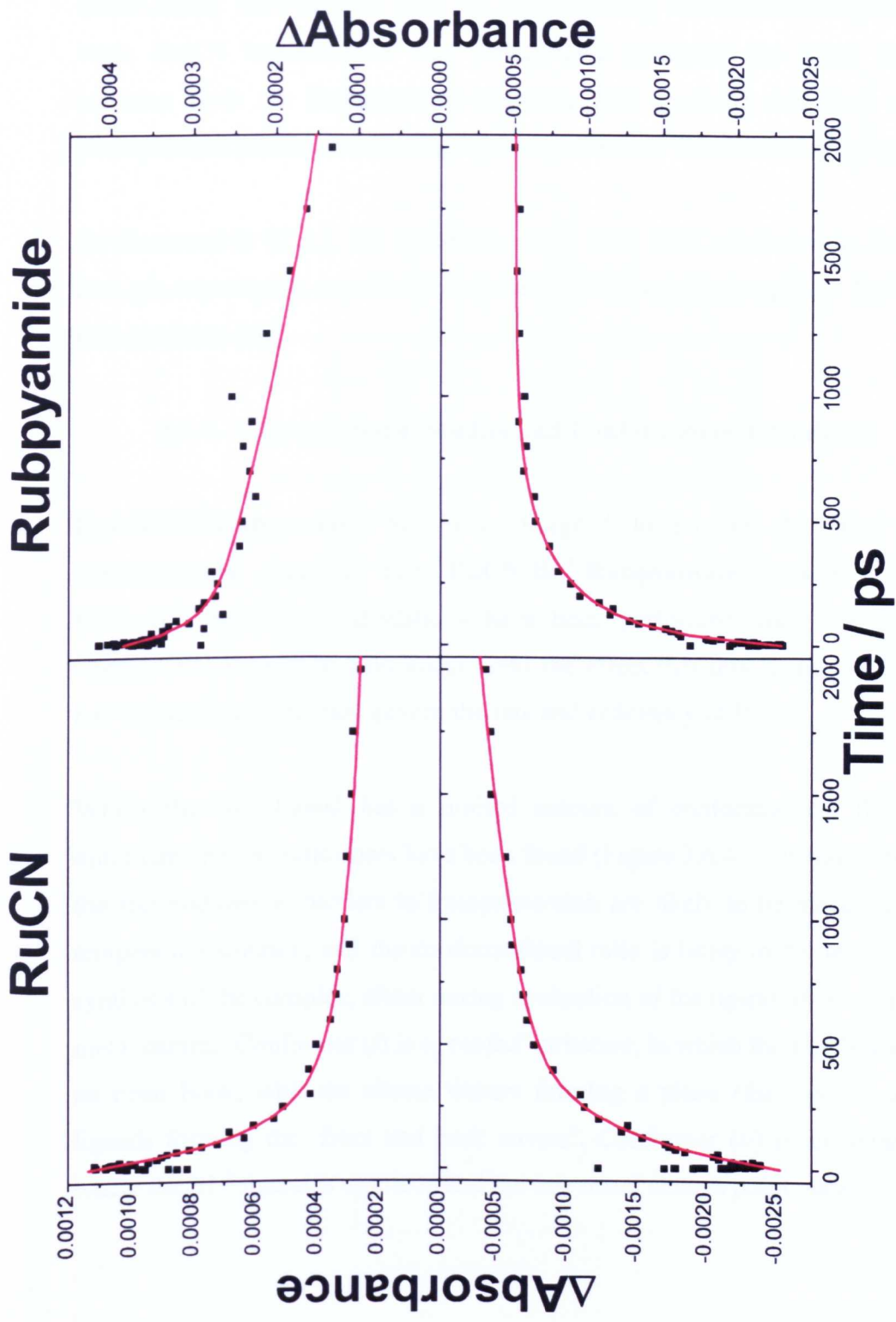


Figure 3.6.3.8: ps-TRIR kinetics of RuCN-BL²-Rubpyamide in CH₃CN solution for the RuCN (transient at 2107 cm^{-1} , top left and bleach at 2056 cm^{-1} , bottom left) and Rubpyamide (transient at 1614 cm^{-1} , top right and bleach at 1638 cm^{-1} , bottom right) termini for $\Delta t = 0-1$ ns.

Analysis of the kinetics at the bleach and transient peak maxima give biexponential fits, with components having time constants of 4.2 (± 0.9) and 110 (± 41) ns. This is unfortunately incomparable with the corresponding luminescence experiment as the weak **RuCN** luminescence was undetectable alongside the much more intense emission from the **Rubpyamide** terminus. This confirms that there are multiple photophysical processes occurring in this system over the timescales investigated.

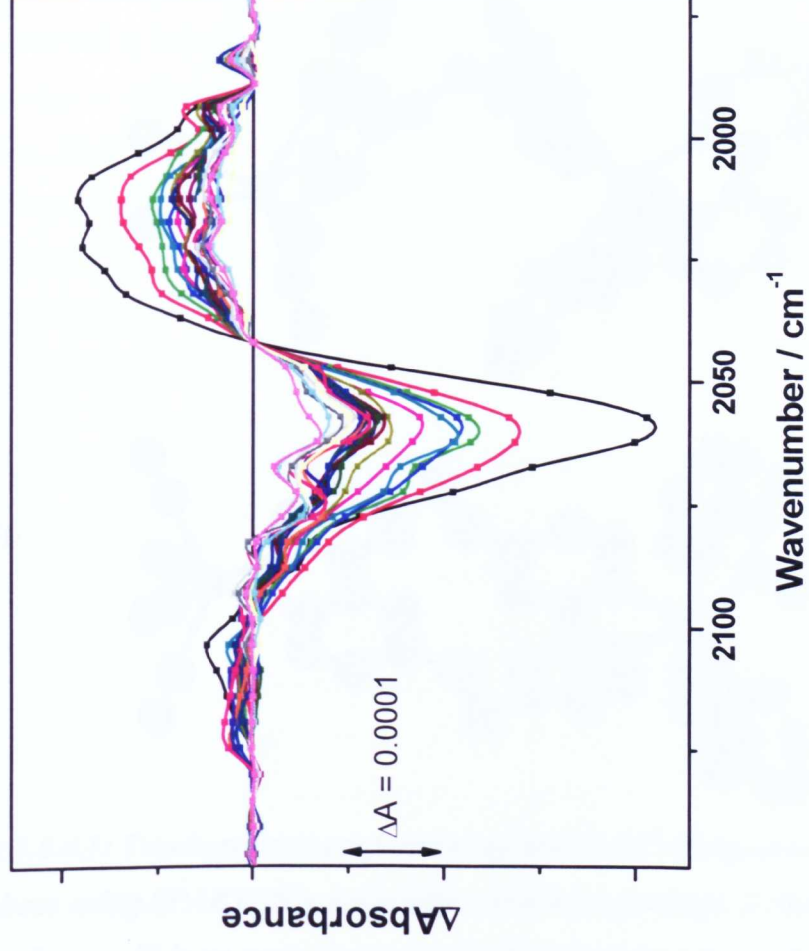
As discussed in §3.5.3, the processes above have been confirmed as intramolecular through experiments on solution mixtures of the model complexes **RuCNdmb** and **Rubpyamide-BL¹**.

3.6.4. Computational Studies and Conformational Analysis

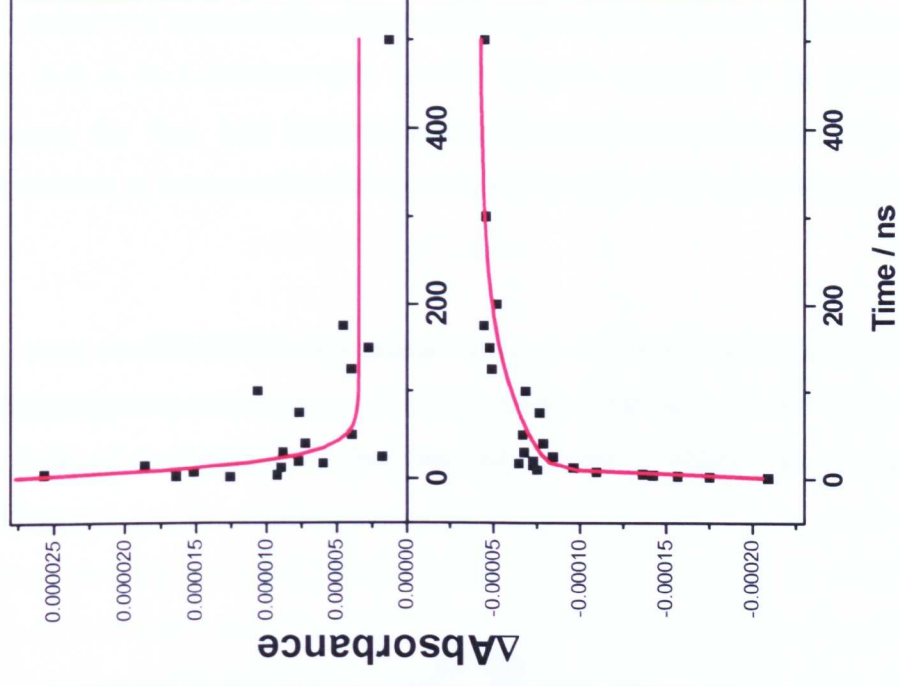
RuCN-BL²-Rubpyamide has been designed to remove the large amount of conformational freedom that **RuCN-BL¹-Rubpyamide** possesses in solution. Molecular mechanics calculations have been performed using the SPARTAN02 Computational Suite to gain insight into the effect that this change in ligand design has on the parameters that govern the rate and efficiency of PEnT.

Whilst the BL² ligand has a limited amount of conformational flexibility, two minimum energy conformers have been found (Figure 3.6.4.1). It should be noted that the thermodynamic barriers to interconversion are likely to be inaccessible in room temperature solution, and the conformational ratio is likely to be decided during the synthesis of the complex, either during cyclisation of the ligand upon complexation of metal centres. Conformer (*i*) is a ‘roofed’ structure, in which the BL² ligand resembles an open book, with the alkane linkers forming a plane (the ‘spine’) and the bpy ligands forming the ‘front and back covers’. Conformer (*ii*) is an ‘open’ structure, where the BL² ligand is unfolded and the two metal centres point outwards.

RuCN



RuCN



Figures 3.6.3.9 and 3.6.3.10: ns-TRIR spectra (left) and kinetics (transient at 2016 cm^{-1} , top left and bleach at 2054 cm^{-1} , bottom left) of RuCN-BL²-Rubpyamide in CH₃CN solution for the RuCN terminus for $\Delta t = 0\text{-}300 \text{ ns}$.

The calculated intermetallic distances in these conformers are 8.8 Å in conformer (i) and 11.9 Å in conformer (ii). As there is expected to be no interconversion between the two, and limited conformational freedom for each case, a bimodal distribution of intermetallic distances would be expected, centred around 8.8 and 11.9 Å.

As with **RuCN-BL¹-Rubpyamide** there is a significant electrostatic attraction between the two metal centres. This is of less importance in BL² bridged systems as the lack of conformational freedom reduces the likelihood of intramolecular ion-pairing.

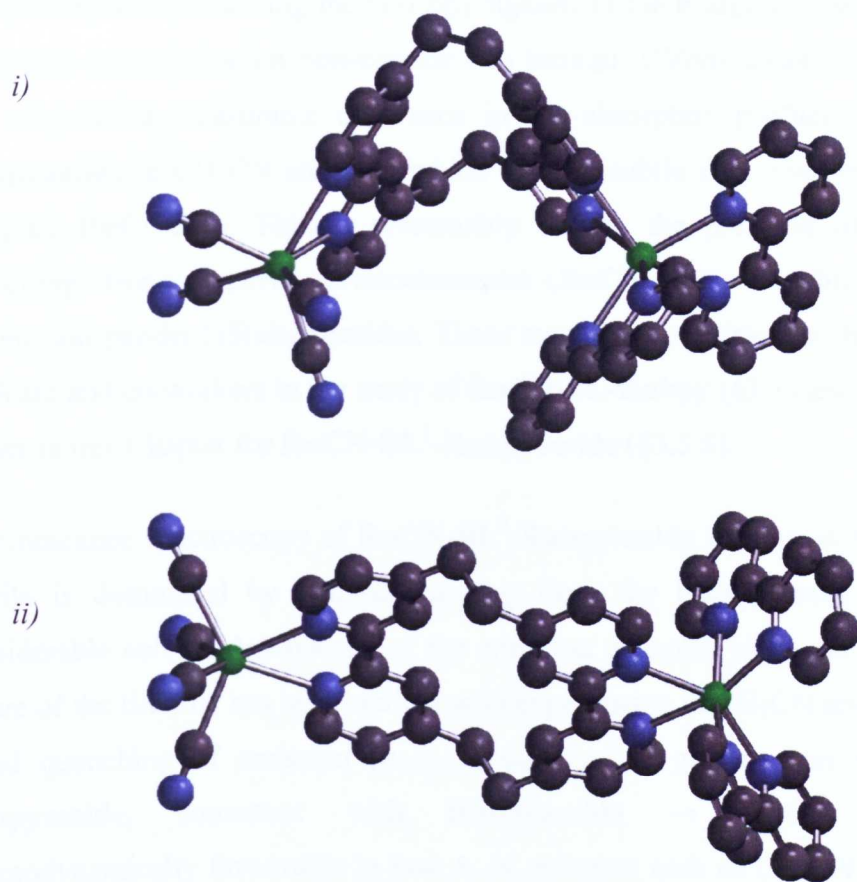


Figure 3.6.4.1: Two important conformers of **RuCN-BL²-Rubpyamide** calculated in the gas phase using SPARTAN's molecular mechanics package. i) Represents a 'roofed' conformer, ii) is an open structure with both metal centres pointing outwards.

3.6.5. RuCN-BL²-Rubpyamide: Closing Points

The bimetallic complex **RuCN-BL²-Rubpyamide** has been studied using UV/visible absorption and luminescence spectroscopy, cyclic voltammetry and TRIR spectroscopy in D₂O and CH₃CN solutions.

UV/visible spectroscopy (§3.6.1) and cyclic voltammetry (§3.6.2) of **RuCN-BL²-Rubpyamide** have shown that the ground state properties of the system are essentially a superposition of the constituent monometallic fragments most closely represented by the model complexes **RuCNdmb** and **Rubpyamide-BL²**. In an analogous manner to **RuCN-BL¹-Rubpyamide**, this supports our supposition that the saturated spacer connecting the two bpy ligands in the bridging ligand BL² prevents electronic communication between the two termini. UV/vis absorption spectroscopy has observed a measurable difference in the absorption profiles of **RuCN-BL²-Rubpyamide** in CH₃CN and D₂O which is more subtle than observed in the model complex **RuCNdmb**. This is presumably due to the presence of one terminus exhibiting strong negative solvatochromism (**RuCN**) and one which is essentially solvent-independent (**Rubpyamide**). These results are consistent with those obtained by Ward and co-workers in the study of **RuCN-BL-Rubpy** (§3.1) and those presented earlier in this Chapter for **RuCN-BL¹-Rubpyamide** (§3.5.5).

Luminescence spectroscopy of **RuCN-BL²-Rubpyamide** has shown that the spectral profile is dominated by emission arising from the **Rubpyamide** terminus. The considerable solvent-dependence of the emission quantum yield and multi-exponent nature of the lifetime has been studied with experiments in CH₃CN and D₂O. Solvent-based quenching of emission ($\phi_{(D_2O)} - \phi_{(CH_3CN)}$) is greater than in **RuCN-BL¹-Rubpyamide**, consistent with **Rubpyamide** → **RuCN** PEnT being thermodynamically favourable in low A. N. solvents such as CH₃CN, and ostensibly that the PEnT process may be more efficient in this system. The presence of multiple time constants has not been affected despite the introduction of the conformationally

restricted bridging ligand BL₂ although there are still a number of possible conformers which may be present in solution (§3.7.4, *vide infra*).

TRIR spectroscopy has been used to directly monitor the processes occurring following photoexcitation of **RuCN-BL²-Rubpyamide** on the picosecond and nanosecond timescales. As with **RuCN-BL¹-Rubpyamide** the ps and ns-TRIR data exhibits polyexponential time dependence, supporting the results from emission spectroscopy that the substantial decrease in conformational freedom has apparently not reduced the number of photophysical processes occurring. The Chapter Discussion (§3.9) contains a detailed treatment on alternative explanations for the complexity of the kinetics observed in this Chapter.

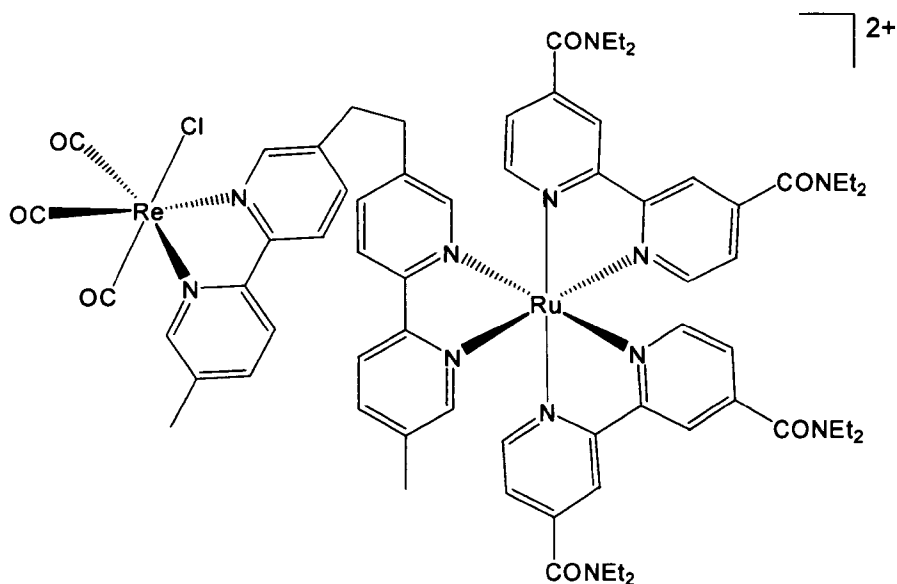
In agreement with the model presented in §3.6.3, the results presented in the same section provide some evidence for **RuCN** → **Rubpyamide** PEnT in D₂O in the Δt = 0-50 ps time range (Figure 3.6.3.2), but not as definitively as in **RuCN-BL¹-Rubpyamide** as no clear grow-in of absorbance is observed in the spectra of the **Rubpyamide** (PEnT acceptor) terminus. Evidence for **Rubpyamide** → **RuCN** PEnT in CH₃CN has also been presented (Figure 3.6.3.7) primarily on the basis of the grow-in of absorbance of the **RuCN** bleach and transient signals over the same Δt = 0-50 ps timescale. The time constants for PEnT were not precisely determined due to the low instrumental spectral resolution of the PIRATE spectrometer (*ca.* 8-9 cm⁻¹) and the limited number of spectra collected in the crucial Δt = 0-20 ps time range, but an approximate value of τ_{PEnT,CH₃CN} ~ 0.5-3 ps was obtained. It was not possible to obtain an approximate time constant for τ_{PEnT,D₂O}; ostensibly this process may be complete within the instrument response of the PIRATE apparatus (*ca.* 1 ps, see Chapter 6 for more details on the PIRATE experimental apparatus). Considering that for **RuCN-BL¹-Rubpyamide** τ_{PEnT,D₂O} ≈ 0.5 x τ_{PEnT,CH₃CN} this explanation seems plausible. These values represent a considerably higher PEnT rates than that determined for **RuCN-BL¹-Rubpyamide**, presumably due to the rigid BL² ligand pre-organising the two chromophores for PEnT with good orbital overlap. Time-resolved spectroscopic

experiments in the femtosecond time domain may provide more insight into the detailed nature and timescales of these rapid processes.

A simple conformational analysis of **RuCN-BL²-Rubpyamide** has been performed computationally (§3.6.4) and gave the structures of two important conformers of the system, based on the bridging ligand adopting either a ‘roofed’ or ‘open’ geometry (Figure 3.6.4.1). The presence of two species in solution may provide a partial explanation for the multiexponential kinetics obtained by luminescence and TRIR spectroscopy as interchromophoric distance and predicted Forster PEnT rates exhibit a sensitive interdependence (§1.3), but the substantial decrease in degrees of freedom as a result of replacing BL¹ with BL² has not been accompanied by a reduction in the complexity of the kinetics of **RuCN-BL²-Rubpyamide**. The electrostatic properties of the system are also important to consider; as was the case with **RuCN-BL¹-Rubpyamide** there may be a strong tendency to ion-pair as the termini are doubly charged with opposite polarity. In the case of **RuCN-BL²-Rubpyamide** the rigidity of BL² means that intramolecular ion-pairing is unlikely, therefore intermolecular ion-pairing might be a plausible consequence of this effect.

The success of the photophysical model in predicting the direction of PEnT in solvents of varying A. N. and the evidence for PEnT in both solvents from ps-TRIR spectroscopy has been presented and comparisons have been made between the two solvent-switchable PEnT bimetallic systems in §3.5 and §3.6. In order to study PEnT processes involving the ligand system BL¹ in more detail we have designed and studied a fixed-energy bimetallic complex **ReCO-BL¹-Rubpyamide** which is comprised of a **Rubpyamide** terminus and a [ReCl(CO)₃] unit.

3.7. $[[((4,4'-\text{CON}(\text{CH}_2\text{CH}_3)_2)_2\text{-bpy})_2\text{Ru}(\text{bpy}-4,4'-\text{CH}_2\text{CH}_2\text{-bpy})\text{ReCl}(\text{CO})_3]\text{Cl}_2, \text{ReCO-BL}^1\text{-Rubpyamide}$



ReCO-BL¹-Rubpyamide is a combination of the two mononuclear complexes *fac*-[ReCl(CO)₃(bpy)] (§1.4.1.2) and **Rubpyamide-BL¹** (§3.3) and has been designed to exploit properties of these two moieties. Both termini exhibit lowest-lying MLCT excited states as characterised by absorption, luminescence and TRIR spectroscopy. The key difference between this system and the related systems containing the **RuCN** moiety is that neither chromophore in this system is solvatochromic, enabling us to study the nuances of systems bridged by the BL¹ ligand with one of the principal variables removed. Furthermore, the electrostatic properties of this system are very different. Whilst there is an electrostatic attraction between the two chromophores in **RuCN-BL¹-Rubpyamide** (as one is doubly cationic and the other is doubly anionic) here there will be no such effect (as one is neutral whilst the other is doubly cationic). This is likely to affect the conformational dynamics of the system in solution, possibly reducing the energetic favourability of the “ion-paired” arrangement which brings the chromophores close together for optimal through-space PEnT (§3.7.4)

Due to the absence of the **RuCN** unit, the direction and gradient of PEnT in this system should not be affected by solvent. The emission wavelengths of the chromophores [ReCl(CO)₃(bpy)] (hereafter **ReCO**) and **Rubpyamide** are 612 and

641 nm respectively (§1.4.1.2),²⁵ giving an energy gradient of 740 cm⁻¹ (or 8.9 kJ mol⁻¹) for **ReCO** → **Rubpyamide** PEnT.

The $\nu(\text{CO})$ bands of the amide groups and the $\nu(\text{CO})$ bands of the carbonyl ligands provide complementary vibrational handles in different regions of the IR spectrum, enabling direct monitoring of the evolution of the excited state structure on both metal centres. As in **RuCN-BL¹-Rubpyamide**, the BL¹ bridging ligand allows the internuclear distance between the metal centres to be modulated. Efficient energy transfer *via* the Förster mechanism requires that the centres are spatially proximal and that there is little overlap in the emission energy of the donor and absorption energy of the acceptor chromophores.²⁶

3.7.1. UV/visible Absorption and Luminescence Spectroscopy

The UV/visible absorption spectrum of **ReCO-BL¹-Rubpyamide** has been measured in CH₃CN (see Appendix §3.9 for spectra) and the peak positions and assignments are presented in Table 3.7.1.1.

$\lambda^{\text{max}} / \text{nm}$	< 300	327	350	397	434	468
Assignment	IL	¹ MC	¹ MC	¹ MLCT	¹ MLCT	¹ MLCT
Terminus	π - π^*	Re	Ru	ReCO	Rubpyamide	Rubpyamide

Table 3.7.1.1: Table of peak positions and assignments for the UV/visible absorption spectrum of ReCO-BL¹-Rubpyamide in CH₃CN solution.

The profile is composed of features found in the spectra of the model complexes [ReCl(CO)₃(bpy)] (§1.4.1.2) and **Rubpyamide-BL¹** (§3.3.1), which is consistent with little or no electronic communication between the two metal centres in the ground state.

As with **RuCN-BL¹-Rubpyamide**, the two relatively solvent-invariant features (<10 nm difference between CH₃CN and D₂O) can be assigned to Ru → (4,4'-

(CONEt₂)₂bpy) ¹MLCT transitions. The weaker shorter-wavelength feature can be assigned to a Re → bpy ¹MLCT transition by comparison with the spectrum of [ReCl(CO)₃(bpy)] in CH₃CN (§1.4.1.2).

Emission spectra of **ReCO-BL¹-Rubpyamide** recorded in CH₃CN are shown in Figure 3.7.1.1. As with **RuCN-BL¹-Rubpyamide**, the complex is luminescent giving a broad, featureless spectrum with $\lambda_{\text{max}} = 645$ nm. As with the **RuCN-BL^x-Rubpyamide** systems, this is consistent with the emissive states being ³MLCT in nature, with the vast majority of the detected luminescence being derived from the **Rubpyamide** terminus (**Rubpyamide-BL²** emits at *ca.* 650 nm). The results are presented in Table 3.7.1.1.

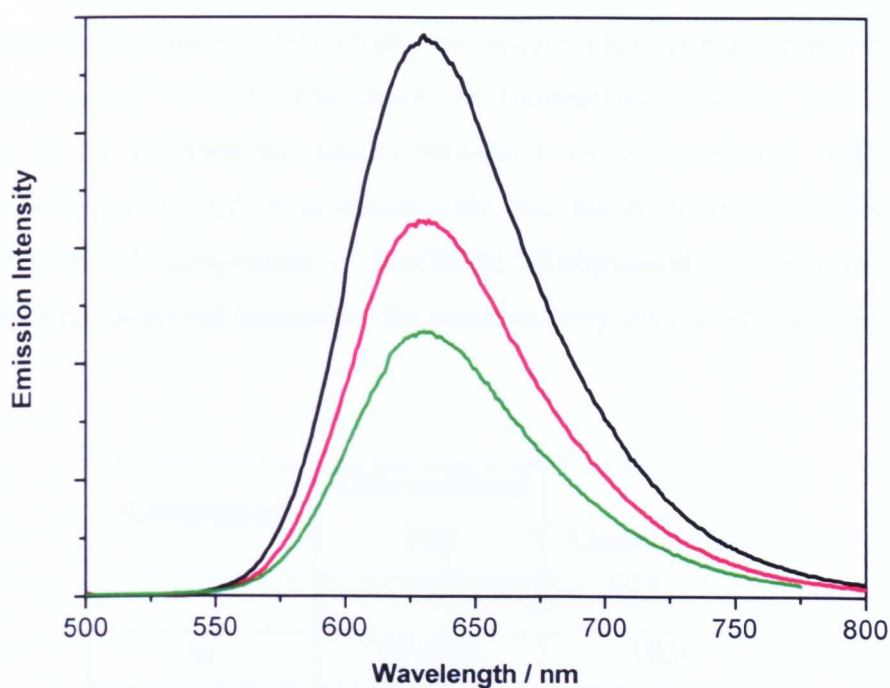


Figure 3.7.1.1: Uncorrected emission spectra of ReCO-BL¹-Rubpyamide in CH₃CN solution, with $\lambda_{\text{ex}} = 475$ nm (black), $\lambda_{\text{ex}} = 435$ nm (red) and $\lambda_{\text{ex}} = 396$ nm (green). The spectra were recorded under identical conditions.

$\lambda_{\text{ex}} / \text{nm}$	$\lambda_{\text{em}} / \text{nm}$	ϕ
475	645	0.015
435	646	0.007
396	645	0.006

Table 3.7.1.2: Table of peak positions and quantum yields from luminescence spectroscopy of ReCO-BL^1 -Rubpyamide in CH_3CN solution.

A kinetic analysis was performed on the luminescence of **ReCO-BL^1 -Rubpyamide** in CH_3CN using 405 nm excitation and registration of emission at 644 nm with an Edinburgh Instruments FLS920 spectrometer (with time resolution of *ca.* 5-7 ns). As with the **RuCN-BL^x -Rubpyamide** systems, it was found that the traces obtained could not be fitted using a simple exponential function; 3 components with time constants varying by orders of magnitude were required to obtain acceptable fits to the experimental data ($\chi^2 < 1.07$). The results are summarised in Table 3.7.1.2 and the attempts to fit the experimental data to between 1 and 3 components in CH_3CN is displayed in Figure 3.7.1.2. It is conceivable that the detection of 3 components (compared with 4/5 components in **RuCN-BL^x -Rubpyamide**) is because an IRF component is not observed because of the comparatively intense luminescence in this case.

Component	Time constant / ns	% Contribution
CH_3CN ($\chi^2 = 1.065$)		
τ_1	27 ± 1.2	19.9
τ_2	428 ± 21	25.2
τ_3	1150 ± 83	54.9

Table 3.7.1.2: Table of exponential fit components of luminescence spectra of ReCO-BL^1 -Rubpyamide in CH_3CN solution.

Further experiments were carried out to study the kinetics of **ReCO-BL¹-Rubpyamide** in CH₃CN solution using 405 nm excitation and registration of emission at 644 nm with a Edinburgh Instruments Mini-Tau spectrometer (with maximum time resolution of *ca.* 250 ps). This allows monitoring of the 0-5 ns time region (within the IRF of the FLS920 apparatus) during which PEnT is most likely to take place, by comparison with the **RuCN-BL^x-Rubpyamide** systems presented elsewhere in this Chapter. The trace is shown in Figure 3.7.1.3 and clearly demonstrates that the emission (originating from the **Rubpyamide** terminus as before) can be seen to grow in over the first few nanoseconds following the laser excitation pulse before stabilising and decaying on longer timescales (as observed in the longer timescale experiments described above). Reasonable fits to the rise and decay parts of the trace may be obtained with time constants $\tau_{\text{rise}} = 0.32 (\pm 0.04)$ ns and $\tau_{\text{decay}} = 0.15 (\pm 0.05)$ ns. τ_{rise} may correspond to the rate of **ReCO** \rightarrow **Rubpyamide** PEnT but further evidence is required to assess the validity of this hypothesis.

The results show that a much smaller degree of luminescence quenching exists in **ReCO-BL¹-Rubpyamide** than in the **RuCN-BL^x-Rubpyamide** systems discussed earlier, even after taking the effect of solvent-cyanide SEDA interactions on luminescence intensity in CH₃CN (§3.5.1, 3.6.1) into account. This could be due to efficient PEnT or because of a larger difference in the energy levels of the lowest excited states on the two chromophores reducing the likelihood of thermal deactivation of luminescent states. TRIR spectroscopy is employed to probe this further (§3.7.3). TCSPC has ostensibly monitored the PEnT process, by virtue of the use of apparatus with improved time resolution and the ostensible retardation of the energy transfer process in this heterobimetallic dyad in comparison with the homobimetallic **RuCN-BL^x-Rubpyamide** dyads previously discussed.

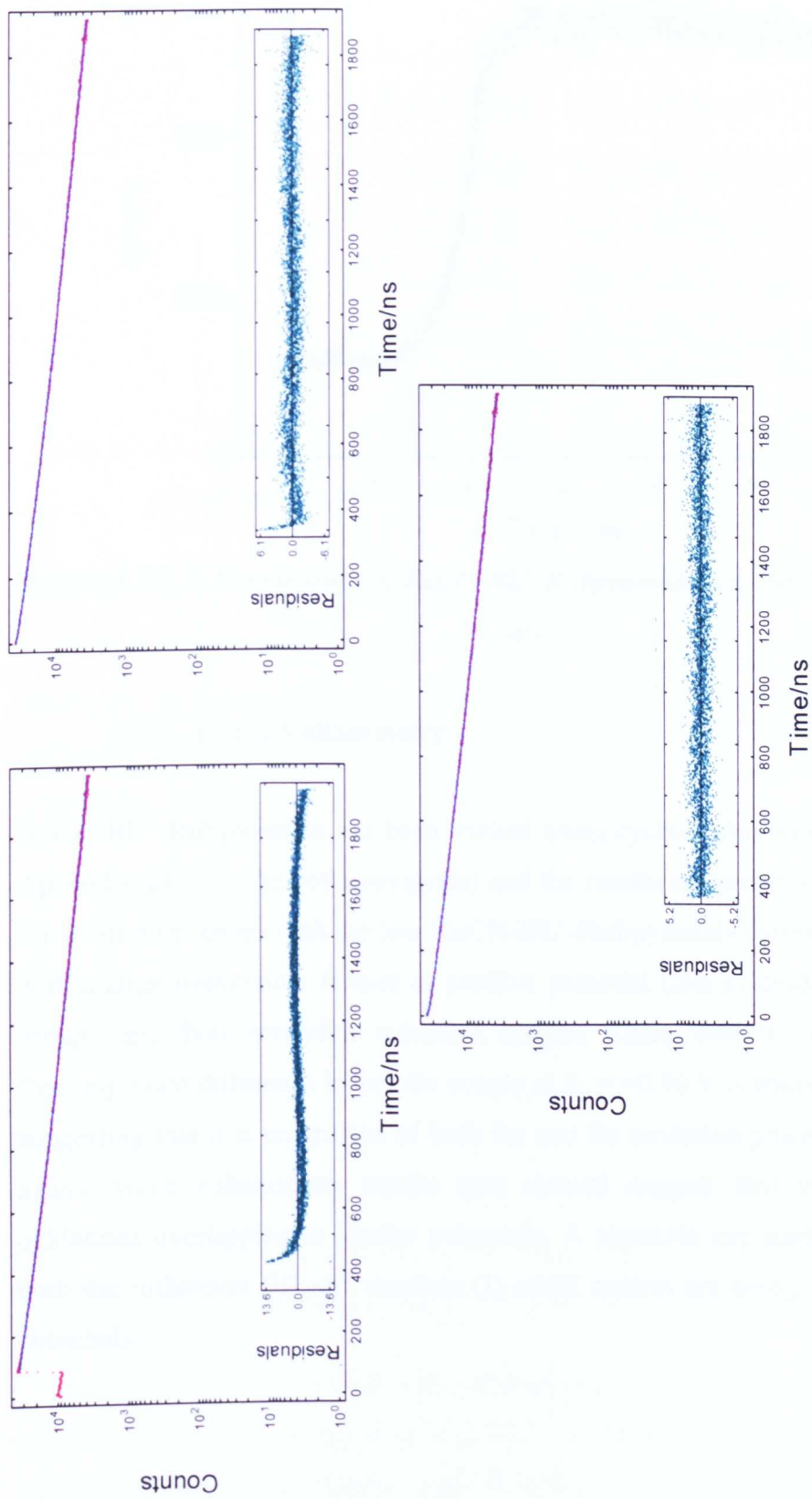


Figure 3.7.1.2: Fits to lifetime data (with residuals) for ReCO-BL¹-Rubpyamide in CH₃CN. Top left: 1 exponent; top right: 2 exponents; bottom: 3 exponents.

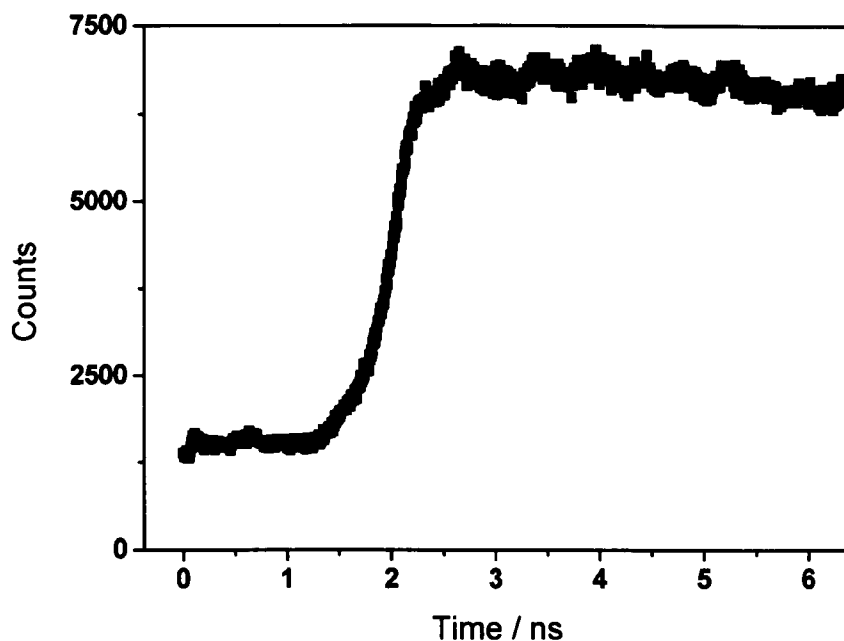


Figure 3.7.1.3: Kinetic trace of ReCO-BL¹-Rubpyamide in CH₃CN between 0 and 6 ns.

3.7.2. Cyclic Voltammetry

ReCO-BL¹-Rubpyamide has been studied using cyclic voltammetry in CH₃CN (see Appendix §3.9 for the voltammogram) and the results are presented in Table 3.7.2.1. There are similarities with the two **RuCN-BL^x-Rubpyamide** systems (§3.5.2, §3.6.2), with a large irreversible feature at positive potential (due to oxidation of the amide groups) and three reversible reduction couples arising from the bpy-based ligands. One important difference is that the couple at $E_p = +0.96$ V is irreversible in this case, suggesting that it is comprised of both Ru and Re oxidation processes. Furthermore, square wave voltammetry results (not shown) suggest that there may be two oxidations overlapping at similar potentials. A plausible explanation for this is that both the ruthenium (II) and rhenium (I) metal centres are being oxidised at similar potentials.

$E_{1/2}/V$ (vs. Fc/Fc ⁺)	Reversibility	Assignment
(E _p) +0.96	Irreversible	Ru ^{II/III} and Re ^{I/II}
(E _p) +0.70	Irreversible	(4,4'-(CONEt ₂) ₂ bpy) ^{0/+}
-1.54	Reversible	(4,4'-(CONEt ₂) ₂ bpy) ^{0/•-}
-1.75	Reversible	(4,4'-(CONEt ₂) ₂ bpy) ^{0/•-}
<-2.00	Reversible	(BL ¹) ^{0/•-}

Table 3.7.2.1: Table of potentials for redox couples and assignments for the cyclic voltammogram of ReCO-BL¹-Rubpyamide in CH₃CN solution.

These results are expected from a bimetallic complex containing a **Rubpyamide-BL^x** unit with metal centres exhibiting no ground-state interactions (§3.5.2 3.6.2), as the **Rubpyamide** redox couples fall within the solvent window and are in very close agreement with those measured for the model complex. No reduction processes originating from the **ReCO** terminus have been observed.

3.7.3. FTIR and Time-Resolved Infrared Spectroscopy

As with the other bichromophoric complexes in this Chapter, it is important to remember that due to the similar nature of the MLCT chromophores appended to the two metal centres and the broadness of ¹MLCT absorption peaks, there is often a case of unselective excitation. Either metal centre may be excited by the incident laser light and more than one excited state species may be present in solution following excitation. This adds another degree of complexity to the study, as *bona fide* PEnT processes must be disentangled from other primary photophysical processes.

Due to the insolubility of **ReCO-BL¹-Rubpyamide** in aqueous media it has not been possible to characterise this system in D₂O. However this is less crucial than in the supramolecular systems containing the **RuCN** moiety, as the lack of solvatochromism would be expected to lead to similar results being observed in different solvents.

Acetonitrile Solution

Using measurements of the excited state energies of the two chromophores (from luminescence, §1.4.2.2 and §3.2.1), in CH₃CN **ReCO** → **Rubpyamide** PEnT is expected to take place, and from emission kinetics is postulated to occur in the time range 0-2 ns (§3.7.1).

The FTIR spectrum of **ReCO-BL¹-Rubpyamide** has been measured in CH₃CN solution (see Appendix §3.9 for spectra). In the carbonyl region there is a peak profile characteristic of the rhenium (I) tricarbonyl unit with 3 peak maxima at 2023, 1916 and 1897 cm⁻¹. In the amide region there is a single peak present at 1637 cm⁻¹. These results are closely comparable with the constituent complexes [ReCl(CO)₃(bpy)] and **Rubpyamide-BL¹** in CH₃CN solution (§1.4.1.2, §3.3.5).

ReCO-BL¹-Rubpyamide was studied using ps-TRIR and ns-TRIR spectroscopy (with laser excitation at 400 and 355 nm respectively) in CH₃CN solution, monitoring both regions in the IR where reporter groups are present.

ps-TRIR Spectroscopy

Figure 3.7.3.1 shows the ps-TRIR spectra obtained for the **ReCO** and **Rubpyamide** termini in CH₃CN solution.

ReCO (“Donor”) terminus

The spectral profile obtained following 400 nm excitation resembles that of [ReCl(CO)₃(bpy)] in CH₃CN,²⁷ with three bleaches at 2023, 1916 and 1897 cm⁻¹ and three transient bands shifted to higher wavenumber at 2058, 1996 and 1959 cm⁻¹. There appear to be changes in the profile on the picosecond timescale, particularly in the region where the high energy bleach is overlapping with the transient bands. These may be partially due to vibrational cooling of initially formed $v>1$ states, but the kinetic data obtained does not show any definitive evidence for this in the appropriate timescale ($\tau \sim 10$ ps, vide infra). Over the time range of the experiment (1-

1000 ps), there is some loss of signal intensity (*ca.* 30%) of the **ReCO** $\nu(\text{CO})$ bleach and transient signals. At $\Delta t = 1$ ns there is still a significant residual signal remaining, indicating that the quenching of **ReCO** excited states formed in CH_3CN is not complete during the picosecond time domain.

Rubpyamide (“Acceptor”) terminus

The spectra obtained for the **Rubpyamide** terminus in CH_3CN resemble the profile observed for the precursor complex **Rubpyamide-BL**¹ (§4.3.5), with an amide $\nu(\text{CO})$ bleach centred at 1635 cm^{-1} and a transient to lower wavenumber centred at 1625 cm^{-1} . This is consistent with a ³MLCT excited state for this terminus. Very little change in the spectral profile occurs over the duration of the picosecond time window, such that over 90% of the initial signal intensity remains at $\Delta t = 1$ ns. This suggests that little quenching of the **Rubpyamide** excited state is occurring over this timescale. Heavy overlap between the bleach and transient bands may lead to the masking of processes, particularly when two such processes take place over a similar timescale, *e.g.* vibrational cooling and fast PEnT.

This result is consistent with our model, which predicts that the higher-energy **ReCO** terminus will be quenched by efficient PEnT and have a short-lived excited state, whilst the **Rubpyamide** acceptor terminus will possess a long-lived excited state.

ps-TRIR Kinetics

Figures 3.7.3.2 and 3.7.3.3 show the ps-TRIR kinetics (for bleach and transient where possible) obtained for the **ReCO** and **Rubpyamide** termini in different time domains in CH_3CN solution. Figures 3.7.3.2 shows $\Delta t = 0\text{-}50$ ps and 3.7.3.3 shows $\Delta t = 0\text{-}1$ ns.

$\Delta t = 0\text{-}50$ ps

This kinetics recorded during this period show some evidence for PEnT taking place, as there is a fast decay process evident in both bleach and transient on the **ReCO** terminus (with an aggregate time constant of *ca.* 30 ps), accounting for *ca.* 20% of the total signal intensity. Unfortunately the data for the **Rubpyamide** terminus is not of

comparable clarity and there is no grow-in of absorbance which would be characteristic of PEnT, by comparison with previous examples in this Chapter (§3.5.3, 3.6.3). In this case the absorbances change very little with time – this could be due to the offsetting of grown-in processes in the **Rubpyamide** terminus by other photophysical processes (*e.g.* vibrational cooling or rapid excited state decay).

As discussed above, the heavy overlap of the amide bleach and transient bands must also be considered, as this may introduce artefacts into the spectra, and hence these artefacts may propagate into the kinetic traces presented. The donor data decay could correspond to a time constant for rapid PEnT in this supramolecular system. Analysis of the donor terminus data provides few conclusions as neither a clear grow-in or decay is observed over the $\Delta t = 0\text{-}50$ ps timescale.

$\Delta t = 0\text{-}1$ ns

During this time domain the processes described above are observed at early times following excitation, and these are followed by signal decay on the **ReCO** terminus and interestingly, a growth in absorbance of the bleach and transient signals for the **Rubpyamide** terminus. This indicates that PEnT may be occurring on this timescale more efficiently than over the $\Delta t = 0\text{-}50$ ps timescale, or that the processes which masked the observation of the grow-in at early times in the **Rubpyamide** terminus may no longer be occurring. These processes appear to be multi-exponential, with adequate fits employing 1 or 2 components giving good agreement with the data for the **ReCO** terminus, with time constants averaged over the bleach and transient traces of $50 (\pm 35)$ ps and $1020 (\pm 400)$ ps.

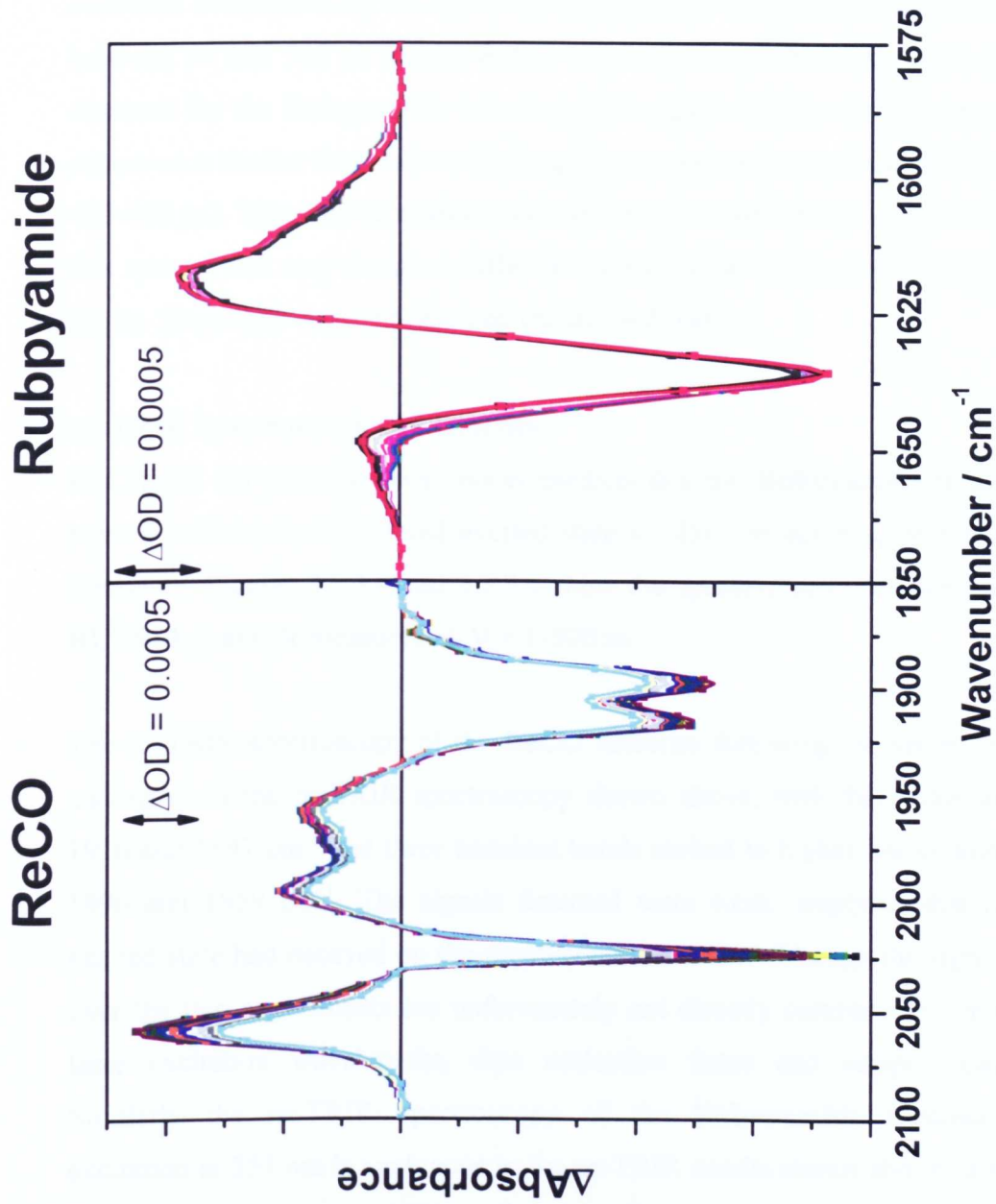


Figure 3.7.3.1: ps-TRIR spectra of ReCO-BL¹-Rubpyamide in CH₃CN solution of ReCO (left) and Rubpyamide (right) termini for $\Delta t = 0$ -2000 ps.

This may be due to the offsetting of excited state decay processes with PEnT-related grow-in of signal – or the opposite situation where there are multiple competing decay processes occurring at varying rates. There appears to be little consistency in the time constants determined for the fits to the experimental data, with time constants varying between 20 and 500 ps for the **ReCO** terminus. Good fits to the data could not be obtained for the **Rubpyamide** terminus, although it appears that the growth process occurs on a similar timescale to the long decay component on the **ReCO** terminus (*i.e.* 400-600 ps). This may represent a second time constant related to the rate of PEnT in this system, and may sample a different conformation or array of conformations than the *ca.* 30 ps time constant obtained earlier (*vide supra*).

ns-TRIR Spectroscopy and Kinetics

In CH₃CN our photophysical model predicts that the **Rubpyamide** terminus should have a sufficiently long-lived excited state to allow monitoring on the nanosecond timescale. Figures 3.7.3.4 and 3.7.3.5 show the spectroscopy and kinetics of **ReCO-BL¹-Rubpyamide** measured at $\Delta t = 1\text{-}500$ ns.

The ns-TRIR spectroscopy of the **ReCO** terminus following excitation at 355 nm is analogous to the ps-TRIR spectroscopy shown above, with three bleaches at 2023, 1916 and 1897 cm⁻¹ and three transient bands shifted to higher wavenumber at 2058, 1996 and 1959 cm⁻¹. The signals detected were weak, implying that most of the excited state had decayed on the picosecond timescale, although the signal intensities over the two experiments are unfortunately not directly comparable due to different laser excitation wavelengths, data collection times and sample concentrations. Similarly the ns-TRIR spectroscopy of the **Rubpyamide** terminus following excitation at 355 nm is analogous to the ps-TRIR results shown above, with an amide $\nu(\text{CO})$ bleach centred at 1635 cm⁻¹ and a transient to lower wavenumber centred at 1625 cm⁻¹.

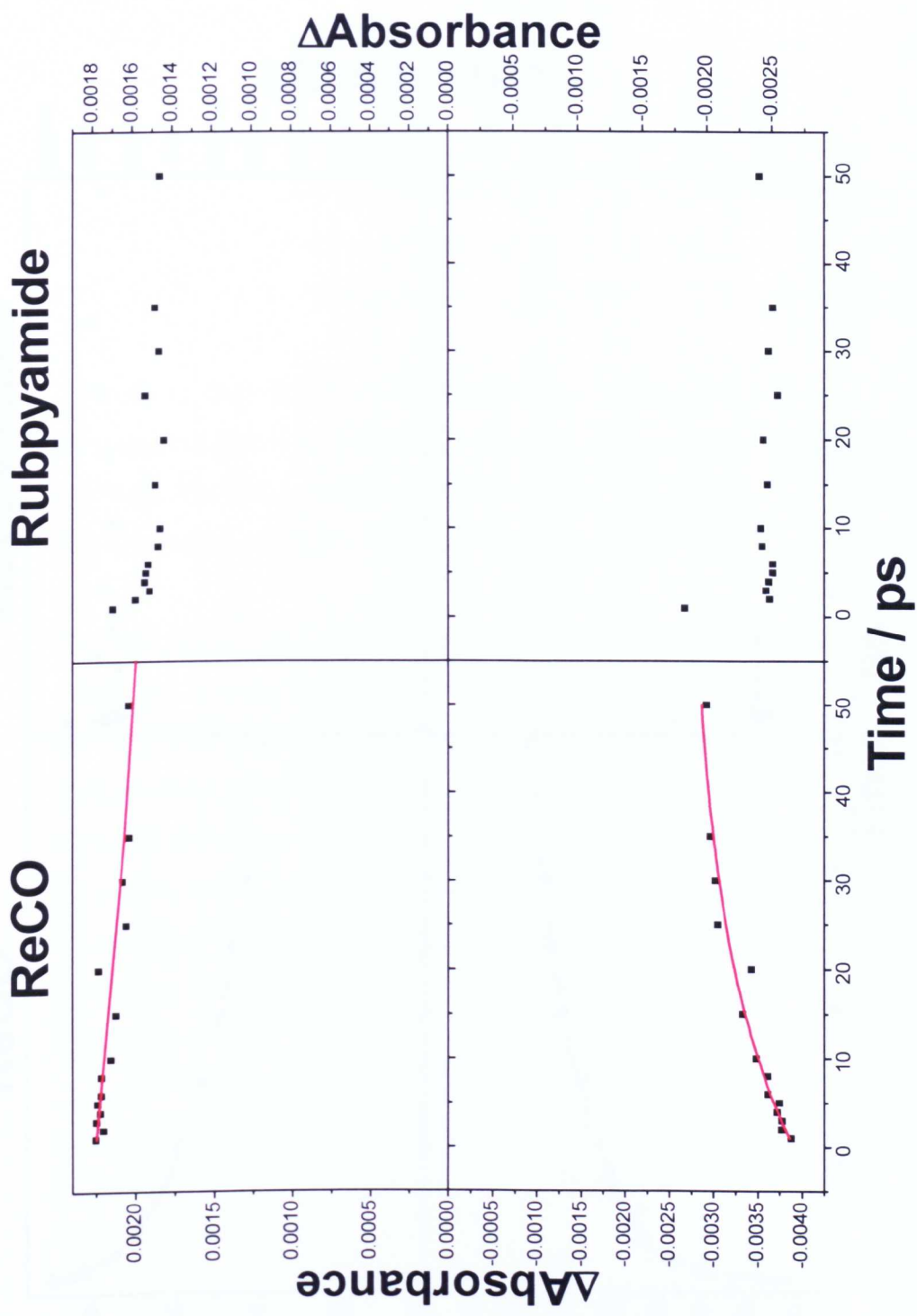


Figure 3.7.3.2: *ps-TRIR kinetics of ReCO-BL¹-Rubpyamide in CH₃CN solution for the ReCO (transient at 2056 cm⁻¹, top left and bleach at 1620 cm⁻¹, bottom left) and Rubpyamide (transient at 1620 cm⁻¹, top right and bleach at 1636 cm⁻¹, bottom right) termini for Δt = 0-50 ps.*

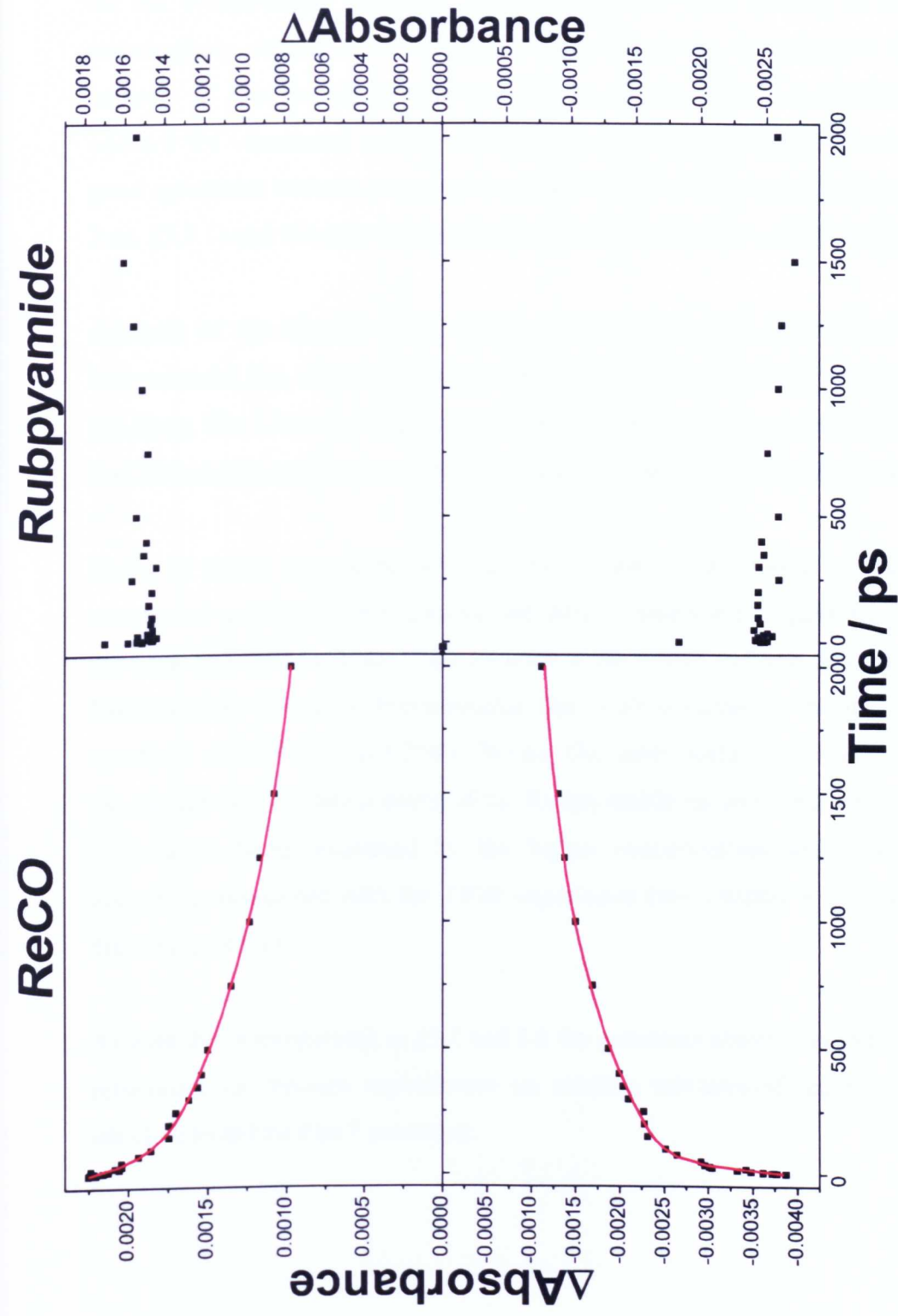


Figure 3.7.3.3: ps-TRIR kinetics of ReCO-BL¹-Rubpyamide in D₂O solution for the ReCO (transient at 2056 cm⁻¹, top left and bleach at 2024 cm⁻¹, bottom left) and Rubpyamide (transient at 1620 cm⁻¹, top right and bleach at 1636 cm⁻¹, bottom right) termini for $\Delta t = 0-2$ ns.

At first glance it is clearly evident from Figure 3.7.3.4 that there is a significant growth in the absorbance of both bleach and transient over the first few nanoseconds on the **Rubpyamide** terminus. Unfortunately the data spacing is insufficient to meaningfully subject it to a fitting routine, but it can be estimated that the time constant of this process in both cases is *ca.* 2-4 ns. This is well outside the time window for vibrational cooling and other primary photophysical processes but is in good agreement with the proposed timescale for PEnT from emission kinetics ($\Delta t = 0$ -2 ns, §3.7.1) and this may be tentatively assigned to **ReCO** \rightarrow **Rubpyamide** PEnT.

Analysis of the kinetics at the bleach and transient peak maxima of **ReCO** give biexponential fits, with the components having time constants of 1.9 (± 0.6) and 12.4 (± 3.8) ns. The 1.9 ns decay component matches well with the grow-in observed on the **ReCO** terminus and this strengthens the assignment of PEnT to this process.

There is some agreement between the values of the longer picosecond decay component and the shorter nanosecond decay component, suggesting that these are the same process. Analysis of the kinetics at the bleach and transient peak maxima of **Rubpyamide** also give biexponential fits, with components having average time constants of 7.5 (± 3.7) and 210 (± 76) ns. The latter could conceivably correspond to the natural excited state lifetime of the **Rubpyamide** excited state, with the difference in duration being explained by the higher concentrations and possibility of O₂ quenching associated with the TRIR experiment (see Chapter 6 for a more detailed discussion of this).

As with the investigations in §3.5 and 3.6 the processes above have been confirmed as intramolecular through experiments on solution mixtures of the model complexes which detected no PEnT processes.

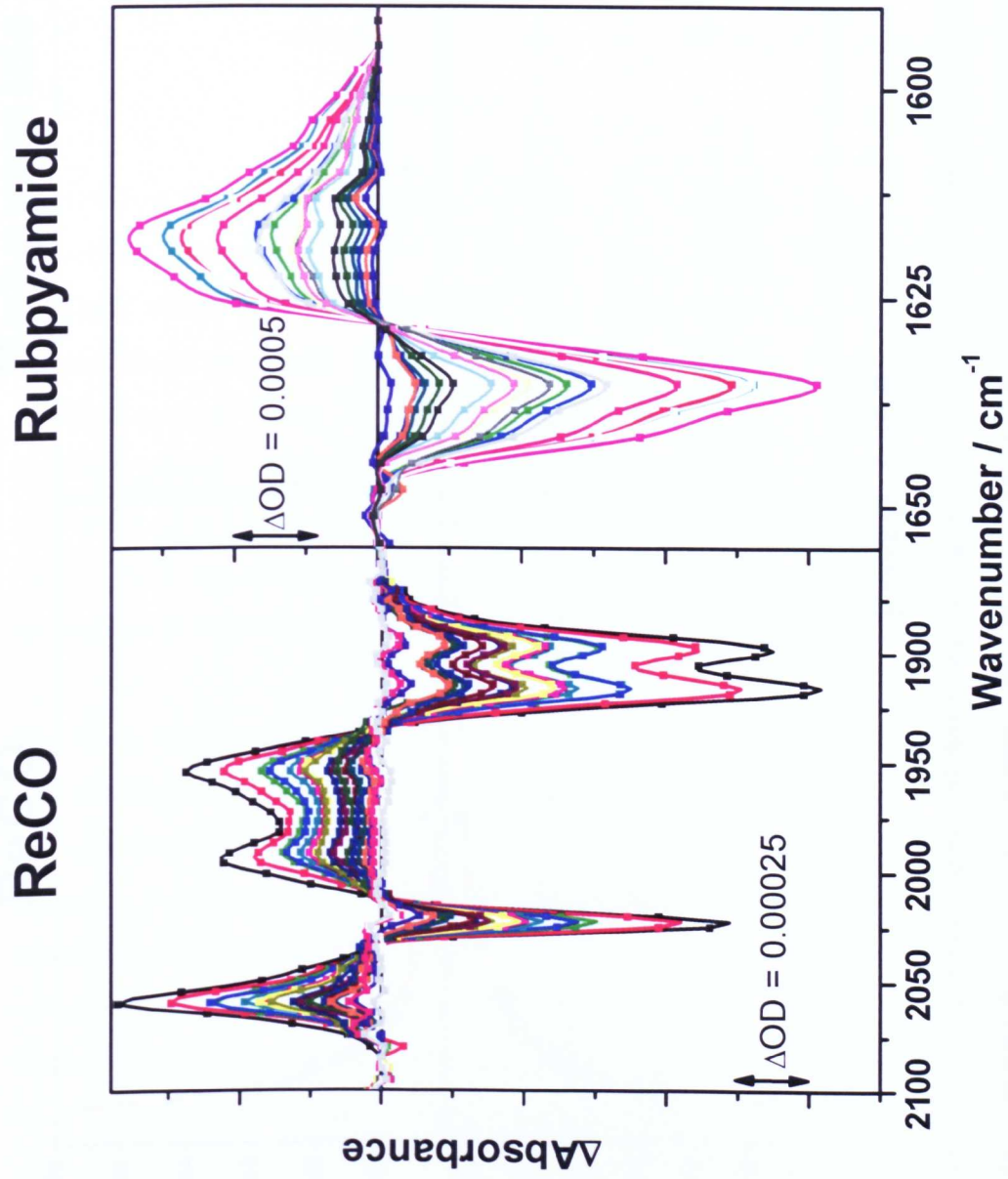


Figure 3.7.3.4: ns-TRIR spectra of ReCO-BL¹-Rubpyamide in CH₃CN solution for both termini for $\Delta t = 0-300$ ns.

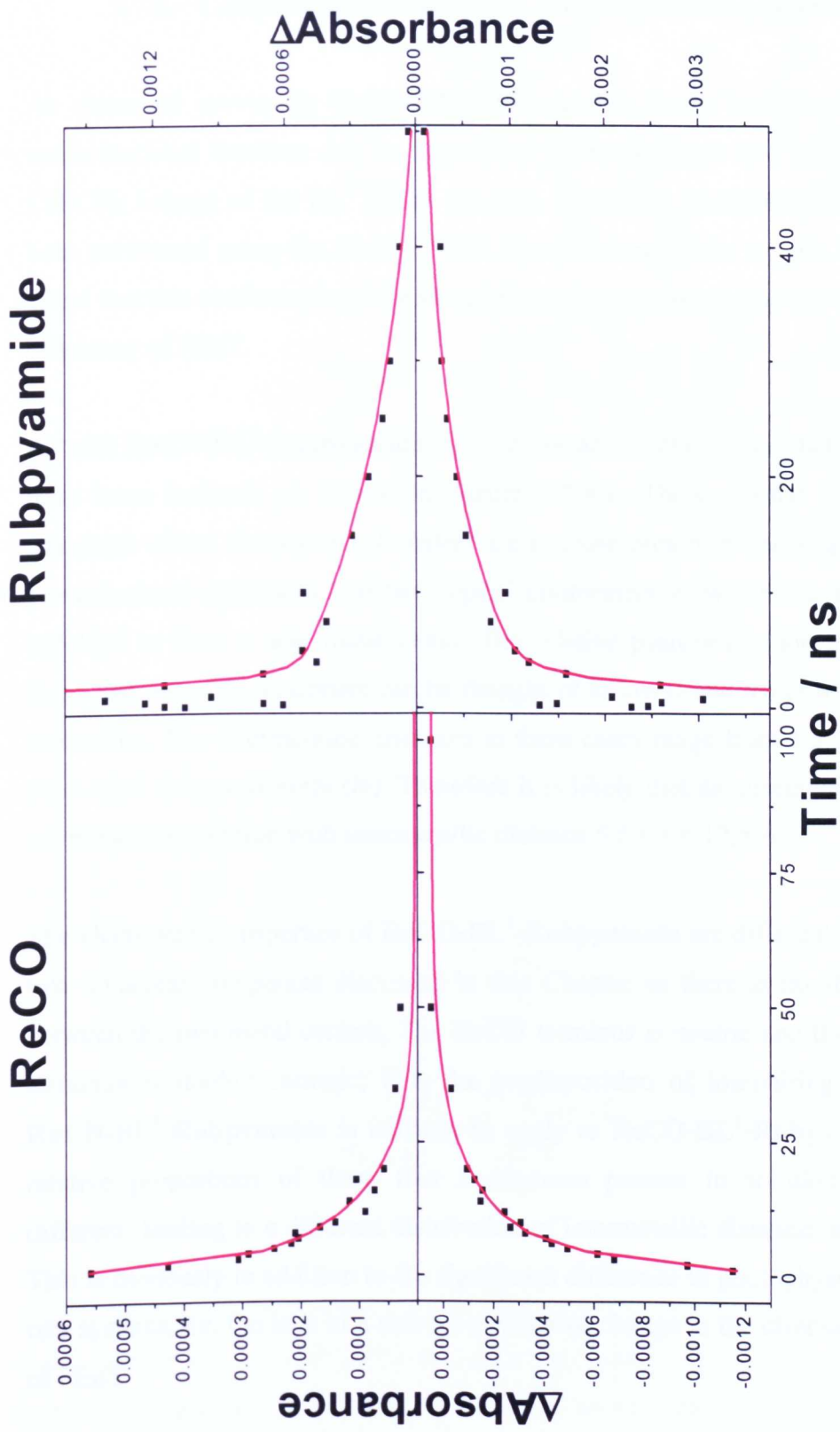


Figure 3.7.3.5: ns-TRIR kinetics of ReCO-BL¹-Rubpyamide in CH₃CN solution for ReCO (transient at 2053 cm⁻¹, top left and bleach at 2024 cm⁻¹, bottom left) and Rubpyamide (transient at 1615 cm⁻¹, top right and bleach at 1634 cm⁻¹, bottom right) termini for $\Delta t = 0$ -300 ns.

3.7.4. Computational Studies and Conformational Analysis

As discussed previously **ReCO-BL¹-Rubpyamide** has a considerable amount of conformational freedom due to the ability to freely rotate and tumble around the CH₂CH₂ linkage of the BL¹ ligand (§3.5.4). Molecular mechanics calculations have been performed using the SPARTAN02 Computational Suite to gain insight into the effect that this conformational freedom has on the parameters that govern the rate and efficiency of PEnT.

As with **RuCN-BL¹-Rubpyamide**, Four important cases of conformational behaviour have been isolated, as shown in Figure 3.7.4.1. These consist of two ‘closed’ structures where the two metal centres are in close proximity (although their ligands prevent closer approach) and two ‘open’ conformers in which the BL¹ ligand has unfolded to form a near linear chain. The relative positions of the metal centres in these two pairs of conformers can be thought of as *syn* (*i* and *iii*) or *anti* (*ii* and *iv*) to each other. The intermetallic distances in these cases range from 5.5 Å in conformer (*i*) to 12.6 Å in conformer (*iv*). Therefore it is likely that an ensemble of conformers are present in solution with intermetallic distance $5.5 < r < 12.6$ Å.

The electrostatic properties of **ReCO-BL¹-Rubpyamide** are different to the previous two dinuclear complexes discussed in this Chapter as there is no strong attraction between the two metal centres. The **ReCO** terminus is neutral and the **Rubpyamide** terminus is doubly cationic; thus the predisposition of ion-pairing postulated for **RuCN-BL¹-Rubpyamide** is unlikely to apply to **ReCO-BL¹-Rubpyamide**, and the relative proportions of these four conformers present in solution may well be different, leading to a different distribution of intermetallic distances and PEnT rates. This is obviously in addition to the significant difference in photophysics between the two systems, *i.e.* the lack of a solvent-switchable change in the direction and gradient of PEnT.

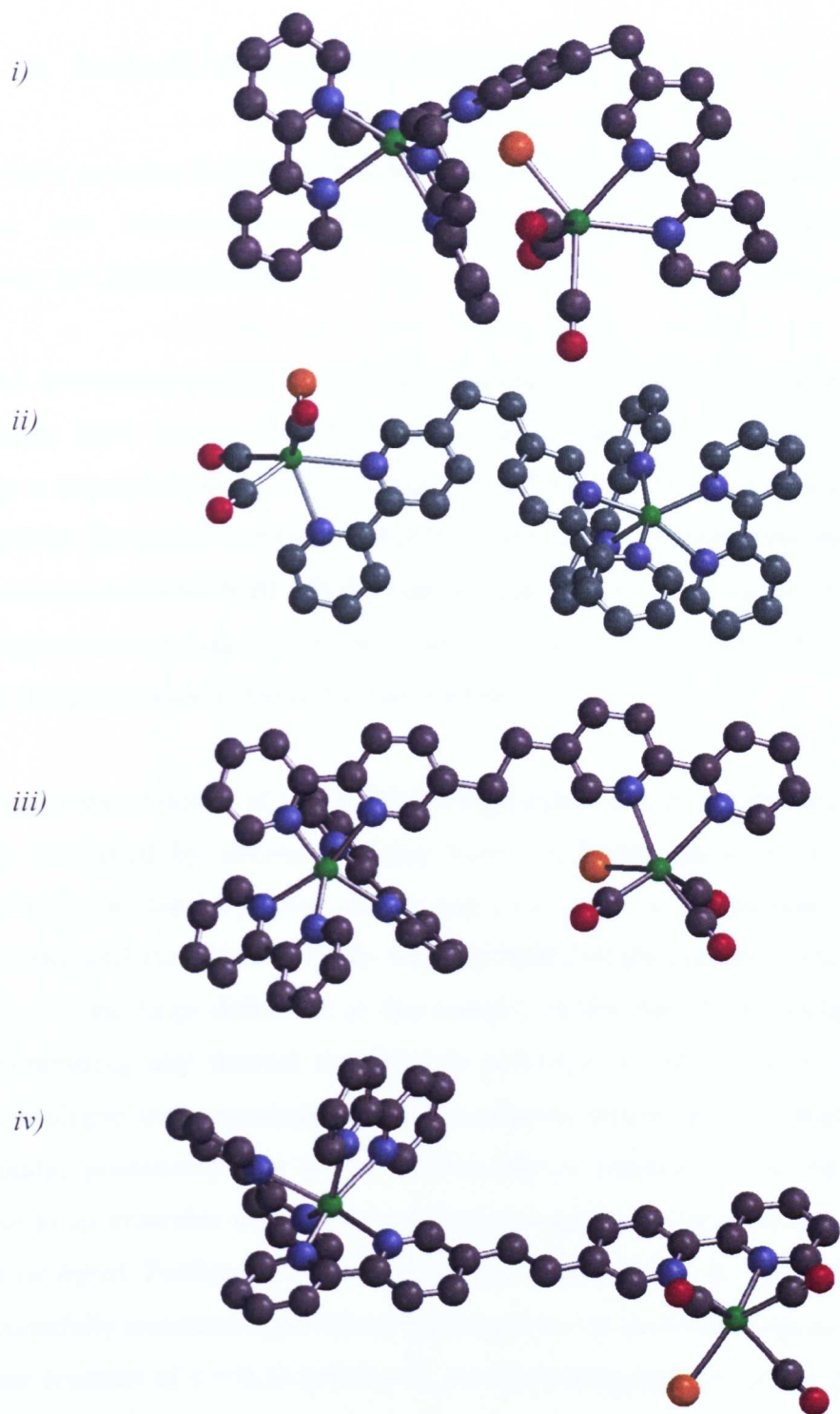


Figure 3.7.4.1: Four important conformers of ReCO-BL¹-Rubpyamide calculated in the gas phase using SPARTAN's molecular mechanics package: i) and ii) are syn and anti folded conformers of closed structures; iii) and iv) are syn and anti conformers of open structures. Amide groups and H atoms omitted for clarity.

3.7.5. ReCO-BL¹-Rubpyamide: Closing Points

The bimetallic complex **ReCO-BL¹-Rubpyamide** has been studied using UV/visible absorption and luminescence spectroscopy, cyclic voltammetry and TRIR spectroscopy in CH₃CN solution.

UV/visible spectroscopy (§3.7.1) and cyclic voltammetry (§3.7.2) of **ReCO-BL¹-Rubpyamide** have shown that the ground state properties of the system are essentially a superposition of the constituent monometallic fragments most closely represented by the model complexes [ReCl(CO)₃bpy] and **Rubpyamide-BL¹**. In an analogous manner to **RuCN-BL¹-Rubpyamide**, this supports our supposition that the saturated spacer connecting the two bpy ligands in the bridging ligand BL¹ prevents electronic communication between the two termini.

Luminescence spectroscopy of **ReCO-BL¹-Rubpyamide** has shown that the spectral profile is dominated by emission arising from the **Rubpyamide** terminus, with emission being substantially more intense (up to an order of magnitude) than the emission measured (in either solvent) the **RuCN-BL¹-Rubpyamide** systems. This may be due to the large difference in the energies of the **ReCO** and **Rubpyamide** termini minimising any thermal deactivation pathways. TCSPC experiments have measured multiple time constants on the nanosecond timescale as in **RuCN-BL¹-Rubpyamide**, presumably due to the conformational freedom of the BL¹ ligand giving rise to an ensemble of possible conformers which may be present in solution (§3.8.4, *vide infra*). Further luminescence lifetime measurements in the 0-10 ns time range successfully measured a grow-in of luminescence on the **Rubpyamide** terminus with a time constant of $\tau = 0.32 (\pm 0.04)$ ns. As the **Rubpyamide** terminus possesses the lowest energy ³MLCT excited state in the system and is the PEnT acceptor the observation of this grow-in apparently suggests that we are indeed observing the PEnT process directly.

TRIR spectroscopy has been used to directly monitor the processes occurring following photoexcitation of **ReCO-BL¹-Rubpyamide** on the picosecond and nanosecond timescales. As with **RuCN-BL¹-Rubpyamide** the ps and ns-TRIR data exhibits polyexponential time dependence, supporting the results from emission spectroscopy that a number of photophysical processes are occurring in solution. In agreement with the model presented in §3.7.3, the results presented in the same section provide some evidence for **ReCO** → **Rubpyamide** PEnT in CH₃CN in the $\Delta t = 0\text{-}2$ ns time range (Figure 3.7.3.3) as a clear grow-in of absorbance is observed in the spectra of the **Rubpyamide** (PEnT acceptor) terminus. The time constants for PEnT were not precisely determined due to the low instrumental spectral resolution of the PIRATE spectrometer (*ca.* 8-9 cm⁻¹) and noise fluctuations in the data but it may be visually estimated as $\tau_{\text{PEnT,CH}_3\text{CN}} \sim 0.5\text{-}3$ ns. This value is in good agreement with the value obtained from luminescence spectroscopy ($\tau_{\text{PEnT}} \sim 0.3$ ns).

These PEnT time constants represent considerably lower PEnT rates than that determined for the **RuCN-BL²-Rubpyamide** systems, presumably due to the difference in the energetics of the PEnT process. From ³MLCT energies, **RuCN** and **Rubpyamide** are quite closely matched in energy in high A. N. solvent environments with larger energy differences after the location of the lowest excited state reverses in lower A. N. environments ($\Delta E_{\text{D}_2\text{O}} \sim 200$ cm⁻¹ whereas $\Delta E_{\text{CH}_3\text{CN}} \sim 700$ cm⁻¹). In contrast, **ReCO** and **Rubpyamide** have an energy difference of at least 750 cm⁻¹ in CH₃CN.

A simple conformational analysis of **ReCO-BL¹-Rubpyamide** has been performed computationally (§3.7.4) and gave the structures of a number of important conformers of the flexible system, based on the metal centres being either *syn* or *anti* to each other and the structure adopting a *folded* or *open* geometry (Figure 3.7.4.1), as was the case with **RuCN-BL¹-Rubpyamide**. Due to the ease of rotation about the CH₂CH₂ axis of BL¹ it has been postulated that these structures are likely to be members of an ensemble of conformers present in solution, leading to a range of intermetallic distances between $5.5 < r < 12.6$ Å and presumably resulting in a wide variation in the

Forster PEnT rate. This provides a plausible explanation for the multiexponential kinetics obtained by luminescence and TRIR spectroscopy as interchromophoric distance and predicted Forster PEnT rates are sensitively interdependent (§1.1.3). The electrostatic properties of the system are different to those observed in the **RuCN-BL^x-Rubpyamide** systems; **Rubpyamide** is doubly cationic but **ReCO** is neutral and as a result **ReCO-BL¹-Rubpyamide** is not expected to undergo any ion-pairing in solution. This is likely to influence the conformer distribution of **ReCO-BL¹-Rubpyamide** present in solution when the spectroscopic experiments were conducted.

The luminescence and TRIR spectroscopic results obtained which have successfully observed PEnT have been presented and discussed in relation to the related **RuCN-BL^x-Rubpyamide** systems.

3.8. Discussion and Closing Points

In this Chapter a series of bimetallic complexes optimised for Förster (through-space) energy transfer have been presented and optical and vibrational spectroscopic measurements presented. This discussion will briefly compare the properties of the three bimetallic systems **RuCN-BL¹-Rubpyamide**, **RuCN-BL²-Rubpyamide** and **ReCO-BL¹-Rubpyamide** highlighting the major differences and will discuss the findings of this study with the work of Simpson *et al.* on the related complex **RuCN-BL-Rubpy**.³

One issue that has not been fully addressed thus far is that solvatochromism leads to changes in the absorption spectra of the two termini within the system, significantly for **RuCN** and less so for **ReCO** and **Rubpyamide**. For the TRIR experiments detailed in this Thesis laser excitation takes place at a single wavelength ($\lambda_{ps-TRIR} = 400$ nm and $\lambda_{ns-TRIR} = 355$ nm, see Chapter 6 for more details) and the solvent-based change in absorbance of the two termini at these wavelengths could lead to different proportions of the various excited states formed being populated in either solvent investigated. This effect adds a further degree of complexity to the unselective

excitation of either terminus by excitation at the two laser wavelengths employed in the TRIR spectra presented.

Secondly it should also be considered from an absorption cross-section perspective that the **Rubpyamide** terminus contains three "Ru → bpy" MLCT chromophores whilst **RuCN** and **ReCO** contain only one. Thus the 'relative oscillator strength' of the **Rubpyamide** terminus at 400 nm (near the absorption maximum for Ru → bpy ¹MLCT transitions) may be considerably weighted towards a greater proportion of the excitation energy going into the **Rubpyamide** terminus in most cases. This may be particularly relevant in cases where **Rubpyamide** is the lower energy terminus (*e.g.* in D₂O for the **RuCN-BL¹-Rubpyamide** systems) as a majority of the excitation energy may be channelled into a chromophore which may not undergo PEnT, thus affecting our ability to objectively probe the apparent efficiency of the PEnT process.

A further point is that a Ru → bpyamide ³MLCT excited state may be delocalised over the two bpyamide ligands, whilst the Ru_{CN} → bpy and Re_{CO} → bpy ³MLCT excited states must be localised. Such a 'localised-to-delocalised' transition may present additional energetic barriers or selection rules arising from changes in electronic structure and symmetry.²⁸

In many of the results presented in this Chapter the amount and quality of information which may be extracted from our TRIR spectra of in the $\nu(\text{CO})_{\text{amide}}$ region have not been as diagnostic as was hoped when the experiments were designed. The reasons for this are not immediately clear but the large extent of overlap between bleach and transient bands may be a contributing factor. Additionally it is important to consider that the amide reporter group is reporting on the electron density of a ligand rather than directly reporting on the electronic structure of a metal centre.

It is difficult to objectively compare the quantitative values (*e.g.* excited state lifetimes) obtained in this Chapter due to the large number of variables and unknowns in the study, mainly arising from the complexity of the supramolecular systems

presented, and this was a major reason why the Förster parameters of these systems has not been calculated. Good examples of this are the quantum yields for the bimetallic systems **RuCN-BL¹-Rubpyamide** and **RuCN-BL²-Rubpyamide**. As the two systems have slightly different termini (the **RuCN** substitution patterns on the bpy ligand vary) their absorption spectra may not match closely and there may be differing degrees of solvatochromism and as a result the excited state energetics of the two systems (in a common solvent) may be different.

As a rule of thumb it appears that using the emission spectra with $\lambda_{\text{ex}} = 400$ nm may provide most insight as this wavelength is slightly higher in energy than the two ruthenium (II) based chromophores and absorbances are comparable in the two systems. The quantum yields for the two systems at excitation wavelengths of 400 ± 10 nm are within 10% of each other in D₂O but when the **RuCN** terminus is at lower energy and luminescence quenching by PEnT is activated in CH₃CN the values are somewhat different (within 50% of each other) but the differences are much more marked if it is compared with a luminescence spectrum measured with a lower energy λ_{ex} . This is presumably because the emission spectrum reports on two processes occurring in the system following excitation; *bona fide* PEnT and simple emission from the **Rubpyamide** terminus. Finding ways to disentangle these two processes, possibly though the use of luminescence polarisation anisotropy measurements, is an interesting avenue of investigation for future extensions to this work.

In the above case the large disparity in emission quantum yields in CH₃CN of **RuCN-BL²-Rubpyamide** (when compared with **RuCN-BL¹-Rubpyamide**) may be indicative of differences in the efficiency of the quenching process as related to the identity of the bridging ligand. A more detailed study of these systems with multiple bridging ligands would provide further insight into this hypothesis.

It is also important to consider the precise differences in ³MLCT excited state energy gradients between the two termini in each system (*i.e.* $\Delta E_{\text{Donor}} - \Delta E_{\text{Acceptor}}$) and how they vary with solvent. These energy gradients undoubtedly play a significant role in

controlling the dynamics of the PEnT processes observed in this work (see Indelli *et al.*,⁴ §3.1 for an illustration of this) and an extension of this work to study solvent mixtures or Acceptor Number media intermediate between D₂O and CH₃CN would be of great utility in probing this further.

Regarding the polyexponential nature of the luminescence and TRIR kinetic data presented throughout this Chapter, it is conceivable that in some cases there may be more than four time constants present in the TCSPC fits, which is a limitation of the spectrometer control software employed for their analysis. For example the four exponent fit of TCSPC data of **RuCN-BL¹-Rubpyamide** has a χ^2 value of ~1.4. This suggests that the fit may not be statistically robust and that a greater number of time constants would be likely to improve the quality of the fit to the experimental data.

We must also attempt to contextualise this work in the frame of the proof of concept study carried out by Simpson *et al.*³ Our results are broadly comparable with theirs but this Thesis has revealed a level of depth and complexity to the primary photophysical processes occurring which was not observed in their initial study. There are a number of interesting differences between this work and their study which would provide subject matter for future work in this area.

Simpson *et al.* reported that the luminescence measured from **RuCN-BL-Rubpy** was monoexponential. This is very interesting since there is clearly a polyexponential time-dependence of all of the TCSPC traces and TRIR kinetics measured for bimetallic systems in this Chapter. A possible explanation for this may be related to conformational pre-organisation of the slightly different bridging ligand used in their study, based on a polyoxomethylene chain. Such chains are known to undergo conformational ordering in solution (with the chains aligned either *anti* or *gauche* with respect to each other depending on the solvent). This may introduce an energetic barrier to rotation which may reduce the conformational complexity of the system and thus result in a monoexponential TCSPC trace.

Additionally the longer chain length in **RuCN-BL-Rubpy** may also lead to a greater interchromophoric separation than in **RuCN-BL¹-Rubpyamide** (14 Å *c.f.* 5-12 Å) which in turn may have lowered energetic barriers to rotation and increased conformational freedom. This may have the plausible consequence of “smearing” out the polyexponential time-dependence from 4/5/10 components to hundreds or even thousands of components and have it tend towards a mean value, which may be observed as a trace fitted with a monoexponential decay by the spectrometer control software.

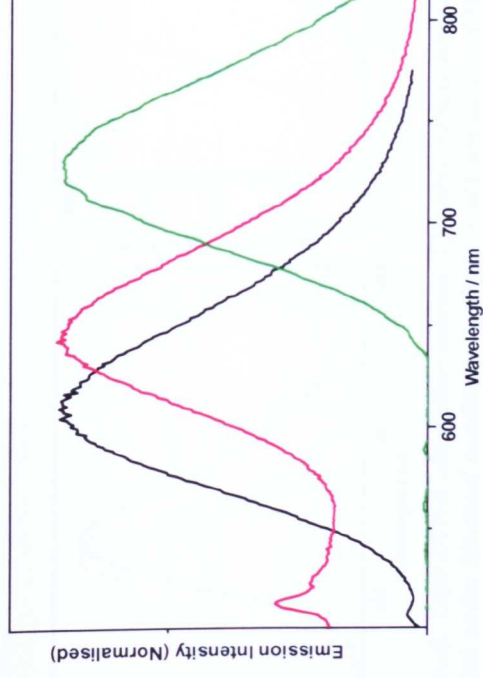
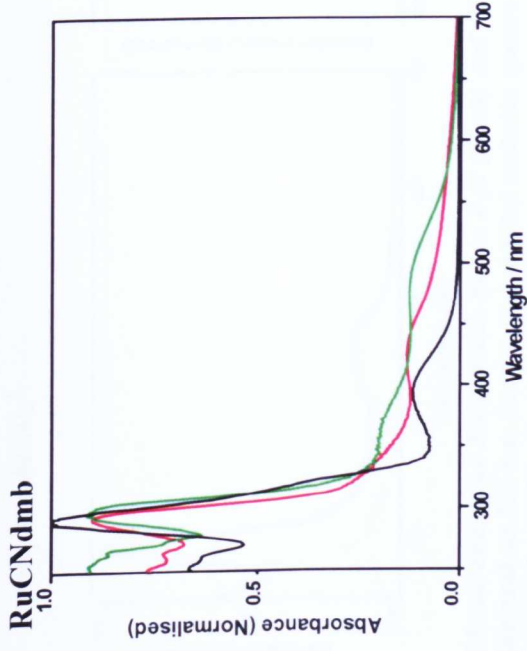
The second set of differences concern the ligand set. The absence of amide groups in **RuCN-BL-Rubpy** means that the $\text{Ru}_{\text{bpy}} \rightarrow \text{bpy}$ and $\text{Ru}_{\text{bpy}} \rightarrow \text{BL}^3\text{MLCT}$ energies would be very similar and the possibility of delocalisation of an excited state over both these ligands is a possibility (§1.3). This ligand set would possibly prevent a 2-step PEnT process from occurring, leading to a simplification of the photophysics of the system and a smaller number of photophysical processes (and hence exponents) observed. Alternatively if the energy of $(\text{Ru}_{\text{bpy}} \rightarrow \text{BL}) < (\text{Ru}_{\text{bpy}} \rightarrow \text{bpy})$ then PEnT is a localised-localised process, contrasting with the delocalised-localised process in **RuCN-BL¹-Rubpyamide**.

A comparison of Ward's systems with those in this Chapter support the notion that *intermetallic* distance may be a less suitable ‘molecular yardstick’ for PEnT and that the *interchromophoric* distance is preferable. This is due to the location of the MLCT charge density, spread over both the bipyridyl ligand *and* metal, which is the determining factor for the distance that such electron density must travel for PEnT to occur. If PEnT takes place between termini in Simpson's **RuCN-BL-Rubpy** (in which the two chromophores are ‘proximal’ to the bridging ligand *i.e.* on the near side of the bridging ligand to each other) then this represents a “direct line” whilst in this work due to the lower energy of the bpyamide ligands the excited state electron density is redistributed over more space, as the lowest energy MLCT molecular orbitals may either located proximal (**RuCN**) or distal (**Rubpyamide**) to the bridging ligand.

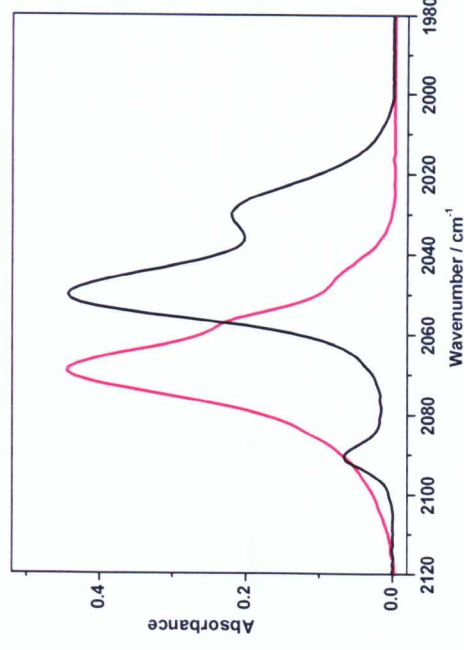
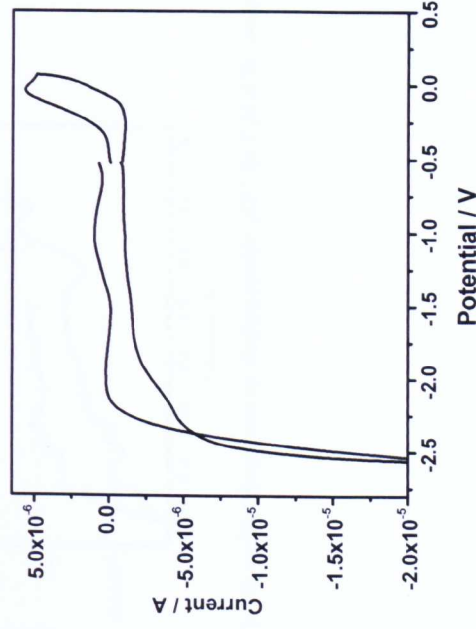
For the reasons above it would be inappropriate to give quantitative figures on the efficiency or rates of PEnT occurring in this Chapter as the detailed mechanisms and processes occurring appear too complicated to meaningfully apply the Förster treatment to. A further study involving a larger set of bichromophoric systems, a greater number of solvent environments and a great deal more experimental beamtime, preferably a combination of time-resolved UV/vis spectroscopy and TCSPC in conjunction with TRIR and Raman spectroscopy would be required to fully unravel the complexity of these systems.

The study in Chapter 4 discusses bimetallic complexes constructed from the same metal complex fragments but held together in very close proximity by a rigid, conjugated ligand. This will provide interesting material for comparison of similar metal complexes incorporated into two distinctly different classes of supramolecular system.

3.9. Appendix of Spectra and Voltammograms

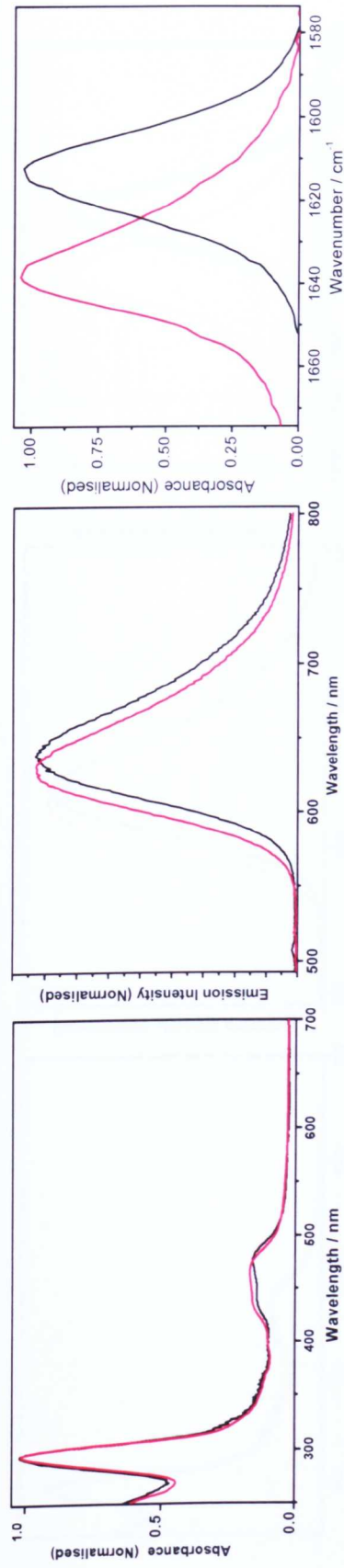


Measurements on RuCNdmb in D_2O (black), CH_3CN (red) and CH_3OH (green). The absorbances are normalised to the long-wavelength feature. Right: Uncorrected emission spectra recorded under identical conditions, with $\lambda_{ex}(H_2O) = 395$ nm, $\lambda_{ex}(CH_3OH) = 420$ nm and $\lambda_{ex}(CH_3CN) = 480$ nm.

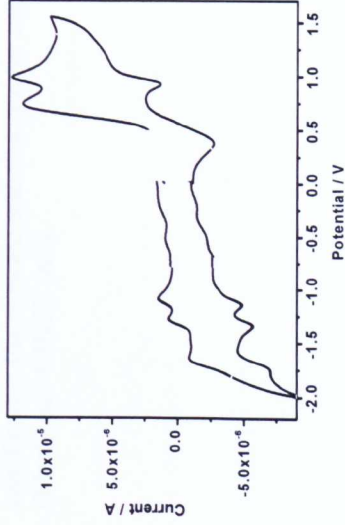


Measurements on RuCNdmb. Left: cyclic voltammogram in CH_3CN . Potentials are quoted vs. Fc/Fc^+ . The presence of features in the return wave of the reduction wave is due to decomposition of the solvent. Right: FTIR spectra of RuCNdmb in D_2O (black) and CH_3CN (red).

Rubpyamide-BL¹

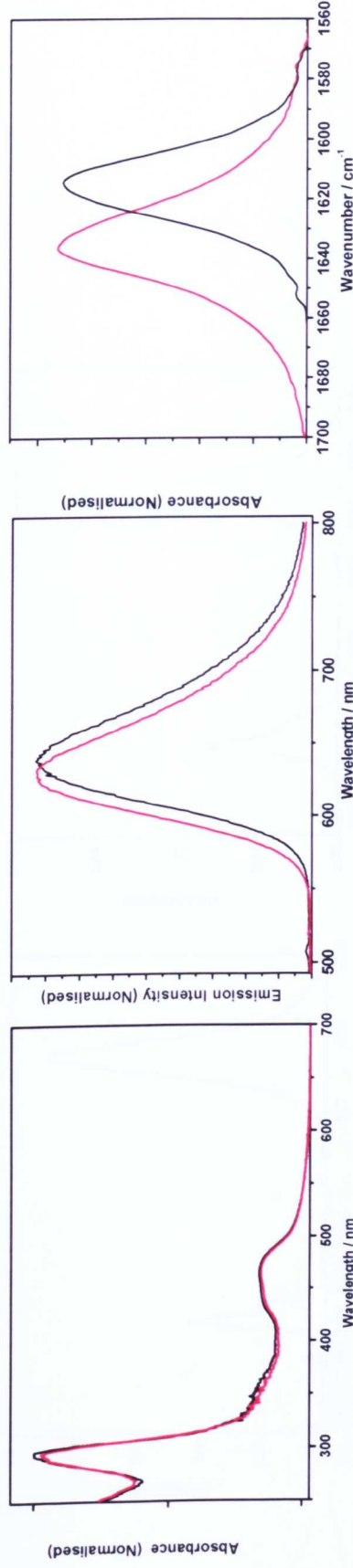


Measurements on Rubpyamide-BL¹ in D₂O (black) and CH₃CN (red). Left: UV/vis absorption spectra. The absorbances are normalised to the peak at 295 nm. Centre: Uncorrected emission spectra recorded under identical conditions $\lambda_{\text{ex}}(\text{D}_2\text{O}) = 481 \text{ nm}$ and $\lambda_{\text{ex}}(\text{CH}_3\text{CN}) = 468 \text{ nm}$. Right: FTIR spectra in D₂O (black) and CH₃CN (red).



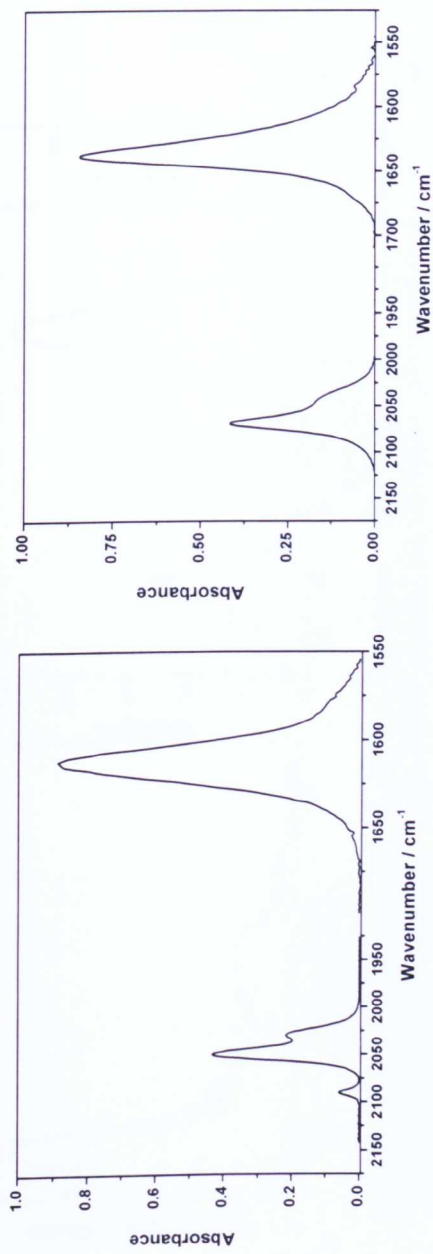
Cyclic voltammogram of Rubpyamide-BL¹ in CH₃CN. Potentials are quoted vs. Fc/Fc⁺.

Rubpyamide-BL²

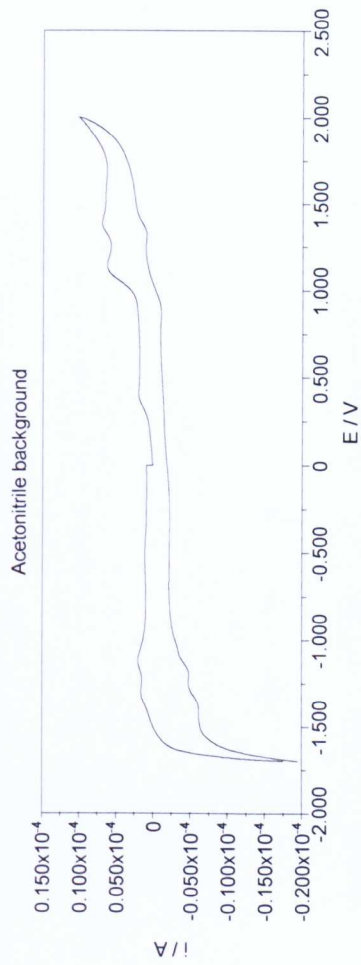


Measurements on Rubpyamide-BL² in D₂O (black) and CH₃CN (red). Left: UV/vis absorption spectra. The absorbances are normalised to the peak at 295 nm. Centre: Uncorrected emission spectra recorded under identical conditions $\lambda_{\text{ex}}(\text{D}_2\text{O}) = 476 \text{ nm}$ and $\lambda_{\text{ex}}(\text{CH}_3\text{CN}) = 474 \text{ nm}$. Right: FTIR spectra in D₂O (black) and CH₃CN (red).

RuCN-BL¹-Rubpyamide

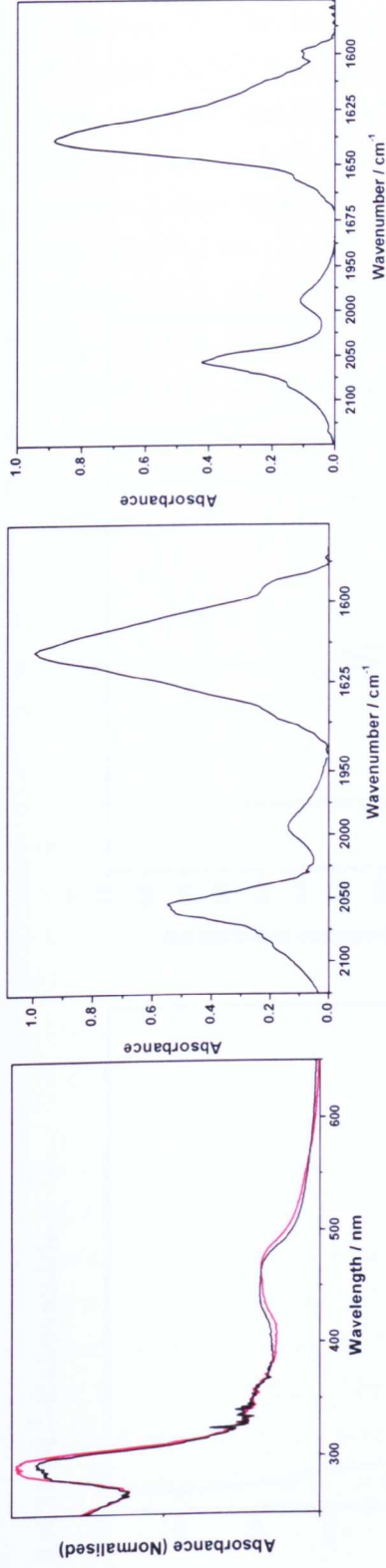


FTIR spectra of RuCN-BL¹-Rubpyamide in D₂O (left) and CH₃CN (right).

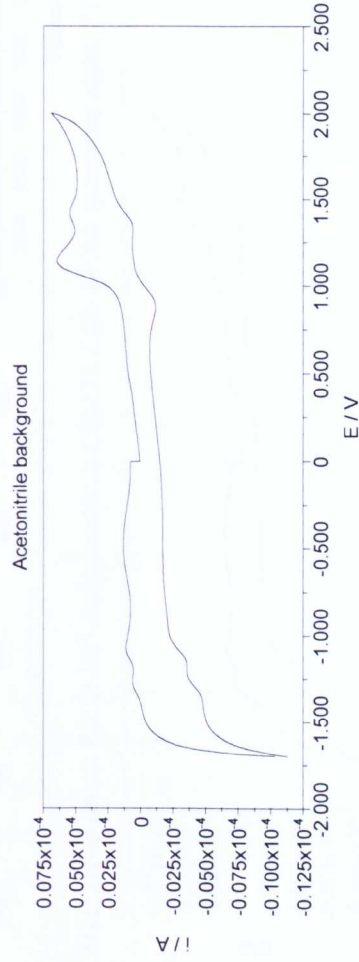


Cyclic Voltammogram of RuCN-BL¹-Rubpyamide in CH₃CN

RuCN-BL²-Rubpyamide

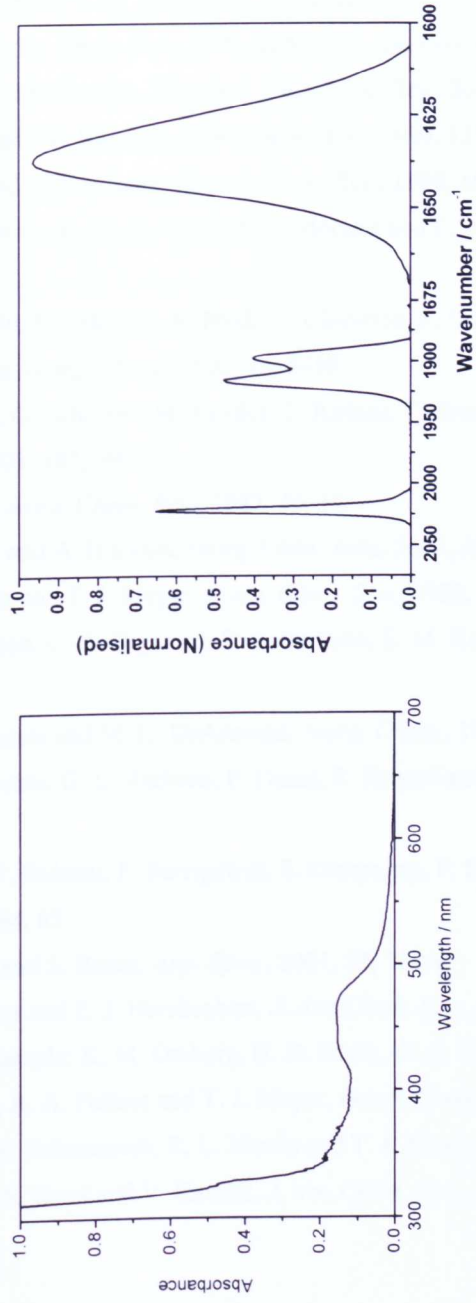


Measurements on RuCN-BL²-Rubpyamide in D₂O (black) and CH₃CN (red). Left: UV/vis absorption spectra. The absorbances are normalised to the peak at 295 nm. Centre: FTIR spectrum in D₂O. Right: FTIR spectrum in CH₃CN (red).

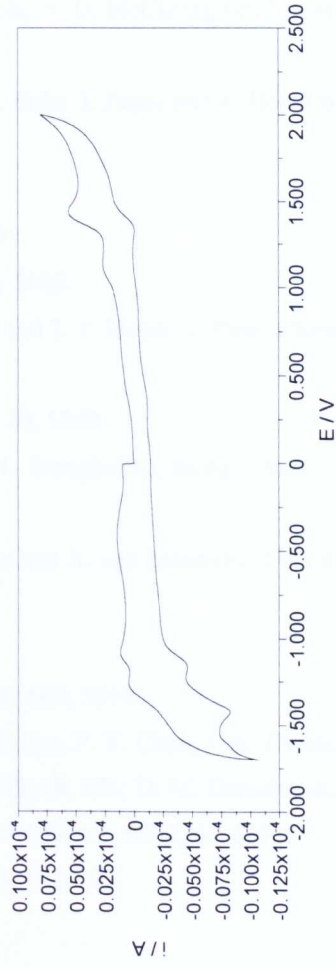


Cyclic Voltammogram of RuCN-BL²-Rubpyamide in CH₃CN

ReCO-BL¹-Rubpyamide



Measurements on ReCO-BL¹-Rubpyamide in CH₃CN. Left: UV/vis spectrum; right: FTIR spectrum.



Cyclic Voltammogram of ReCO-BL¹-Rubpyamide in CH₃CN

3.10. References

- ¹ See for example: L. Fabbri, M. Licchelli, G. Rabaioli and A. Taglietti, *Coord. Chem. Rev.*, 2000, **205**, 85; D. Parker, *Coord. Chem. Rev.*, 2000, **205**, 109; M. H. Keefe, K. D. Benkstein and J. T. Hupp, *Coord. Chem. Rev.*, 2000, **205**, 201; F. Bolletta, I. Costa, L. Fabbri, M. Licchelli, M. Montalti, P. Pallavicini, L. Prodi and N. Zaccaroni, *J. Chem. Soc., Dalton Trans.*, 1999, 1381; A. P. De Silva, H. Q. N. Gunaratne, T. Gunnlaugsson, A. J. M. Huxley, C. P. McCoy, J. Rademacher and T. E. Rice, *Chem. Rev.*, 1997, **97**, 1515.
- ² See for example: Y. H. Kim, D. H. Jeong, D. Kim, S. C. Jeoung, H. S. Cho, S. K. Kim, N. Aratani and A. Osuka, *J. Am. Chem. Soc.*, 2001, **123**, 76; L. De Cola and P. Belser, *Coord. Chem. Rev.*, 1998, **177**, 301; F. Barigelli and L. Flamigni, *Chem. Soc. Rev.*, 2000, **29**, 1; B. Schlicke, P. Belser, L. De Cola, E. Sabbioni and V. Balzani, *J. Am. Chem. Soc.*, 1999, **121**, 4207; R. Ziessel, M. Hissler, A. El-Ghayoury and A. Harriman, *Coord. Chem. Rev.*, 1998, **180**, 1251.
- ³ N. R. M. Simpson, M. D. Ward, A. F. Morales and F. Barigelli, *J. Chem. Soc. Dalton Trans.*, 2002, 2449.
- ⁴ M. T. Indelli, M. Ghirelli, A. Prodi, C. Chiorboli, F. Scandola, N. D. McClenaghan, F. Puntoriero and S. Campagna, *Inorg. Chem.*, 2003, **42**, 5489.
- ⁵ T. Meyges, G. Schubert, M. Kovács, T. Radnai, T. Grosz, I. Bako, I. Papai and A. Horváth, *J. Phys. Chem. A*, 2003, **107**, 9903.
- ⁶ A. Vlček, *Coord. Chem. Rev.*, 1982, **43**, 39.
- ⁷ M. Kovács and A. Horváth, *Inorg. Chim. Acta*, 2002, **335**, 69.
- ⁸ J. V. Caspar and T. J. Meyer, *J. Am. Chem. Soc.*, 1983, **105**, 5583.
- ⁹ C. J. Timpson, C. A. Bignozzi, B. P. Sullivan, E. M. Kober and T. J. Meyer, *J. Phys. Chem.*, 1996, **100**, 2915.
- ¹⁰ A. C. Samuels and M. K. DeArmond, *Inorg. Chem.*, 1995, **34**, 5548.
- ¹¹ S. F. A. Kettle, G. L. Aschero, E. Diana, R. Rosetti and P. L. Stanghellini, *Inorg. Chem.*, 2006, **45**, 4928.
- ¹² A. Juris, V. Balzani, F. Barigelli, S. Campagna, P. Belser and A. von Zelewsky, *Coord. Chem. Rev.*, 1988, **84**, 85.
- ¹³ S. Nigam and S. Butan, *App. Spec.*, 2001, **55**, 362A.
- ¹⁴ C. M. Elliot and E. J. Hershenhart, *J. Am. Chem. Soc.*, 1982, **104**, 7519.
- ¹⁵ See for example: K. M. Omberg, G. D. Smith, D. A. Kavaliunas, P. Y. Chen, J. A. Treadway, J. R. Schoonover, R. A. Palmer and T. J. Meyer, *Inorg. Chem.*, 1999, **38**, 951; D. M. Dattelbaum, K. M. Omberg, J. R. Schoonover, R. L. Martin and T. J. Meyer, *Inorg. Chem.*, 2002, **41**, 6071.
- ¹⁶ W. Kaim, S. Ernst and V. Kasack, *J. Am. Chem. Soc.*, 1990, **112**, 173.

-
- ¹⁷ M. K. Kuimova, D. C. Grills, P. Matousek, A. W. Parker, X-Z. Sun, M. Towrie and M. W. George, *Vib. Spec.*, 2004, **35**, 219.
- ¹⁸ See for example: D. M. Dattelbaum, C. M. Hartshorn and T. J. Meyer, *J. Am. Chem. Soc.*, 2002, **124**, 4938; D. M. Dattelbaum, M. K. Itokazu, N. Y. M. Iha and T. J. Meyer, *J. Phys. Chem. A*, 2003, **107**, 4092; K. M. Omberg, J. R. Schoonover and T. J. Meyer, *J. Phys. Chem. A*, 1997, **101**, 9531.
- ¹⁹ C. Kaes, M. W. Hosseini, R. Ruppert, A. De Cian and J. Fischer, *J. Chem. Soc. Chem. Commun.*, 1995, 1445.
- ²⁰ J.-P. Sauvage, J.-P. Collin, J.-C. Chambron, S. Guillerez, C. Coudret, V. Balzani, F. Barigelletti, L. De Cola and L. Flamigni, *Chem. Rev.*, 1994, **94**, 993.
- ²¹ J. R. Lakowicz, *Principles of Fluorescence Spectroscopy*, Kluwer Academic/Plenum Publishers, 2nd edn., 1999.
- ²² T. L. Lazarides, T. L. Easun, C. Veyne-Marti, W. Z. Alsindi, M. W. George, N. Depperman, H. Adams, G. M. Davies and M. D. Ward, *Inorg. Chem.*, submitted.
- ²³ Y. P. Kovtun, Y. O. Prostota and A. I. Tolmachev, *Dyes and Pigments*, 2003, **58**, 83; Y. J. Kubo, *J. Chem. Soc. Perkin Trans. 1*, 1994, 1787.
- ²⁴ V. Balzani, G. Bergamini, F. Marchioni and P. Ceroni, *Coord. Chem. Rev.*, 2006, **250**, 1254.
- ²⁵ K. Kalyanasundaram, *J. Chem. Soc. Faraday Trans.*, 1986, **82**, 2401.
- ²⁶ J.-P. Sauvage, J.-P. Collin, J.-C. Chambron, S. Guillerez, C. Coudret, V. Balzani, F. Barigelletti, L. De Cola and L. Flamigni, *Chem. Rev.*, 1994, **94**, 993.
- ²⁷ I. P. Clark, Ph.D. thesis, University of Nottingham, 1997.
- ²⁸ K. D. Demadis, C. M. Hartshorn and T. J. Meyer, *Chem. Rev.*, 2001, **101**, 2655.

Chapter 4:

Probing the Excited States of Ruthenium (II) and Rhenium (I) Complexes of 2,2'- Bipyrimidine using TRIR Spectroscopy

Chapter 4: Probing the Excited States of Ruthenium (II) and Rhenium (I) Complexes of 2,2'-Bipyrimidine using TRIR Spectroscopy

4.1. Introduction

4.1.1. 2,2'-Bipyrimidine As A Bridging Ligand

This chapter describes a study complementary to that discussed in Chapter 3, combining the same three d^6 transition metal building blocks *fac*-[ReCl(CO)₃], [Ru(CN)₄]²⁻ and [Ru(4,4'-CONEt₂)₂bpy]²⁺ with the potentially *bis*-chelating bridging ligand 2,2'-bipyrimidine (hereafter bpm). A series of 3 monometallic complexes, 3 homobimetallic systems (where the same d^6 unit is complexed to both sites of the bridging ligand) and 3 heterobimetallic systems (where different moieties are complexed to the bpm binding sites) have been designed and investigated using TRIR spectroscopy. This Chapter aims to provide insight into the efficacy, interplay and timescale of the photophysical processes occurring in such complexes in different solvent media; where possible the experiments have been conducted in D₂O and CH₃CN. This study provides a direct comparison of the ground and excited state electronic structure of complexes possessing metal centres held in close proximity with an estimated separation of *ca.* 5.5 Å,¹ by a conjugated bpm bridge (this Chapter) and a longer, saturated linkage terminating in two *mono*-chelating bipyridyl ligands resulting in a considerably larger intermetallic distance (up to *ca.* 13 Å, Chapter 3).

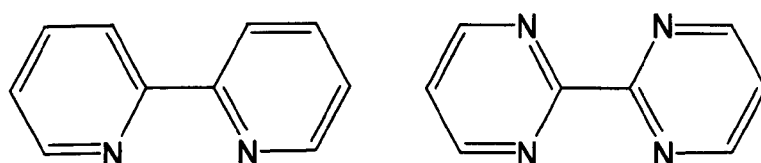


Figure 4.1.1.1: The structures of 2,2'-bipyridine (*bpy*, left) and 2,2'-bipyrimidine (*bpm*, right)

The salient properties of *bpy* and *bpm* will be compared before a discussion of previous studies of similar complexes in the scientific literature. Whilst *bpy* possesses two nitrogens which may form a chelating ring, *bpm* possesses four so that either

mono or bimetallic complexes may be prepared (Figure 4.1.1.1). At 298 K d^6 metal complexes of bpy *may be treated* as having a single low-lying $^3\text{MLCT}$ excited state (see §1.4.1.1 for a discussion of this) sometimes with thermally accessible d-d transitions, giving rise to temperature-dependent luminescence properties. Spectroscopic studies have found that the electronic structure of bpm is more complicated than that of bpy, with a number of energetically close-lying orbitals making up the frontier orbital manifold (Figure 4.1.1.2).^{2,3} This may result in several electronic transitions being thermally accessible, *i.e.* at energies within k_bT of the lowest $^3\text{MLCT}$ excited state of bpm complexes. This is because the electronic selection rules which forbid transitions between these states in the free ligand are relaxed owing to the spin-orbit coupling effect of heavy metal atoms such as rhenium (I) and ruthenium (II) (§1.1).

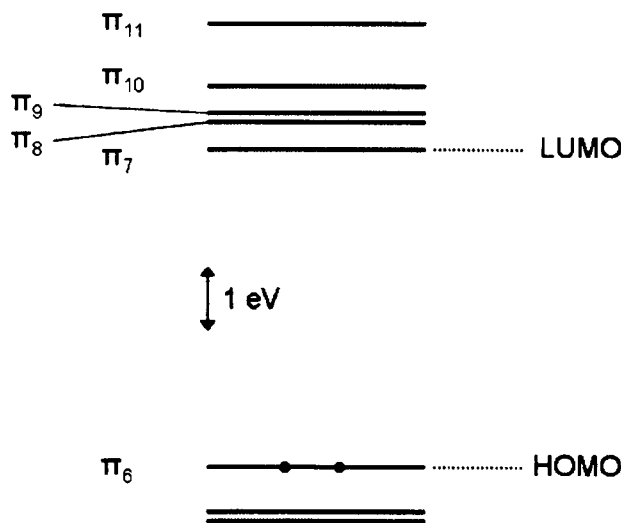


Figure 4.1.1.2: The electronic structure of frontier molecular orbitals of 2,2'-bipyrimidine. Adapted from Ref.²

A comparative study of the electrochemical properties of bpy and bpm reported that the two reductions of bpm (-2.42 and -2.94 V vs. Fc/Fc^+) occur more closely together and at less negative potentials than bpy (-2.56 and -3.20 V vs. Fc/Fc^+), presumably because of the presence of additional nitrogens in the bpm ring.³ This suggests that the

LUMOs in bpm are lower in energy and are in closer energetic proximity than the corresponding LUMO orbitals of bpy.

4.1.2. Relevant Studies of Re and Ru complexes of bpm

There have been several relevant studies incorporating the bpm ligand system into rhenium (I) and ruthenium (II) complexes, dating back to the first report of homoleptic and heteroleptic complexes of bpy and bpm by Sullivan *et al.* in 1977.⁴ This paper briefly reported the synthesis and properties of $[\text{Ru}(\text{bpm})_3]^{2+}$, $[\text{Ru}(\text{bpy})_2(\text{bpm})]^{2+}$, $\{(\text{Ru}(\text{bpy})_2)_2(\text{bpm})\}^{4+}$ and $\{((\text{Ru}(\text{bpy})_2)(\text{bpm}))_3\text{Ru}\}^{8+}$ using electronic absorption, emission and electrochemical properties in aqueous solution.

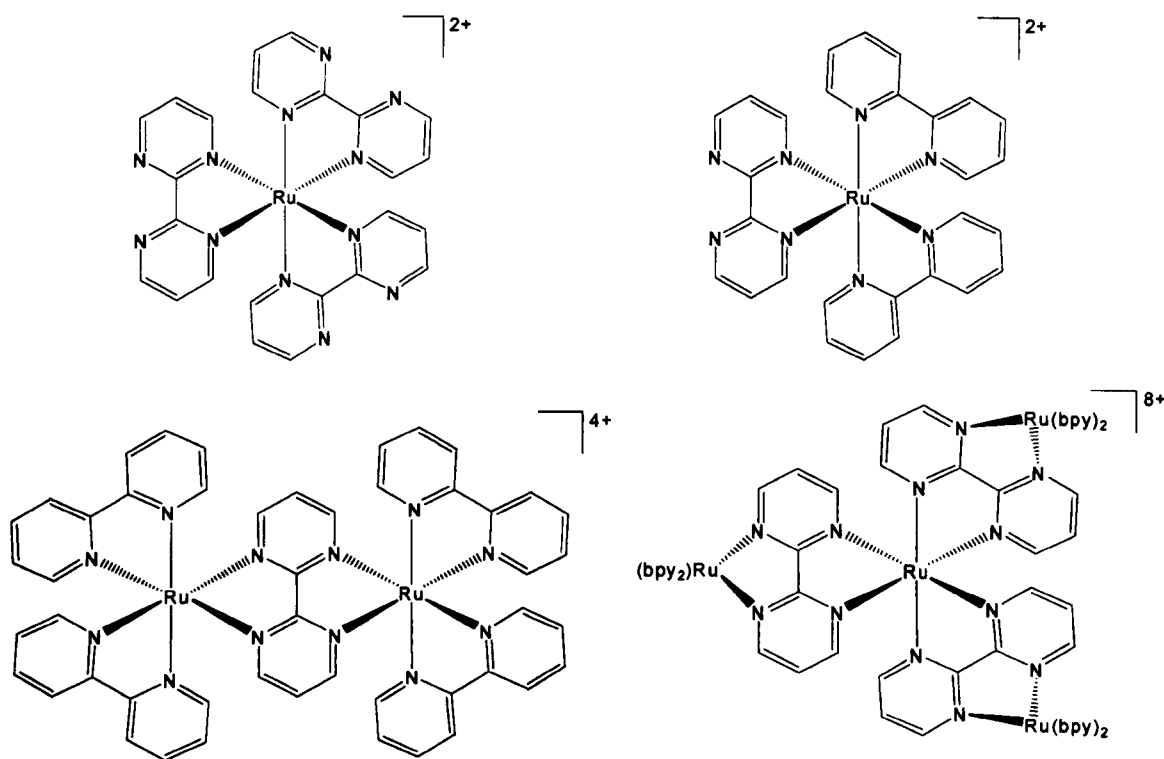


Figure 4.1.2.1: The structures of $[\text{Ru}(\text{bpm})_3]^{2+}$ (top left), $[\text{Ru}(\text{bpy})_2(\text{bpm})]^{2+}$ (top right), $\{(\text{Ru}(\text{bpy})_2)_2(\text{bpm})\}^{4+}$ (bottom left) and $\{((\text{Ru}(\text{bpy})_2)(\text{bpm}))_3\text{Ru}\}^{8+}$ (bottom right).

In comparison to $[\text{Ru}(\text{bpy})_3]^{2+}$ additional low energy absorption bands in all the complexes were observed and assigned to $\text{Ru} \rightarrow \text{bpm}^1\text{MLCT}$ transitions, with these bands shifted to considerably lower energy in polynuclear complexes containing bridging bipyrimidine (Table 4.1.2.2). This observation was rationalised in terms of the bpm LUMO energy being lowered upon complexation of a second metal centre. Interestingly the homoleptic complex $[\text{Ru}(\text{bpm})_3]^{2+}$ was found to emit strongly at room temperature (644 nm), with a quantum yield over double that of $[\text{Ru}(\text{bpy})_3]^{2+}$ under the same conditions ($\phi = 0.09$ vs. 0.042) and its emission was found to be unquenched by the presence of O_2 . The reason for this was not determined. The heteroleptic complex $[\text{Ru}(\text{bpy})_2(\text{bpm})]^{2+}$ was observed to emit weakly at 680 nm and the polynuclear systems $\{(\text{Ru}(\text{bpy})_2)_2(\mu\text{-bpm})\}^{4+}$ and $\{((\text{Ru}(\text{bpy})_2)(\mu\text{-bpm}))_3\text{Ru}\}^{8+}$ were found to be non-luminescent at 298 K and the amount of luminescence detected at <10 K (between 725 and 850 nm) decreased as the nuclearity of the complexes increased, with no emission detected for the tetranuclear complex $\{((\text{Ru}(\text{bpy})_2)(\mu\text{-bpm}))_3\text{Ru}\}^{8+}$ under any conditions. Electrochemistry in H_2O was hampered by the narrow potential (*ca.* -1 to +1 V) so full characterisation was not possible. However it was noted that the replacement of bpy with bpm shifted the first (and second, if observed) reduction couples to considerably more positive potentials.

An article by Vogler and Kisslinger conducted a study of the rhenium (I) complexes *fac*- $[\text{ReCl}(\text{CO})_3(\text{bpm})]$ and its dimer $\{(\text{ReCl}(\text{CO})_3)_2(\mu\text{-bpm})\}$ using absorption and emission spectroscopy in DMSO solution. They also reported the synthesis of the heterobimetallic d^6 complex $\{(\text{ReCl}(\text{CO})_3)(\mu\text{-bpm})(\text{Ru}(\text{bpy})_2)\}^{2+}$.⁵ The UV/vis absorption profiles of $[\text{ReCl}(\text{CO})_3(\text{bpm})]$ were reported to be comparable to other complexes of α -diimine ligands ($\lambda_{\text{max}} = 371$ nm), whilst complexation of a second $[\text{ReCl}(\text{CO})_3]$ unit to form the homobimetallic complex gave rise to a broad, lower energy absorption band (with $\lambda_{\text{max}} = 450$ nm). The heterobimetallic complex possesses a very broad spectrum with discernible maxima at $\lambda_{\text{max}} = 408$ nm and 606 nm which were assigned to $\text{Ru} \rightarrow \text{bpy}$ and $\text{Ru} \rightarrow \text{bpm}^1\text{MLCT}$ transitions respectively (Table 4.1.2.2). The authors reasoned that the absorption spectrum was dominated by charge

transfer transitions arising from the ruthenium (II) fragment due to their greater oscillator strengths and that the Re → bpm features were present but unresolved.

Strong emission at 567 nm was reported for [ReCl(CO)₃(bpm)] in DMSO at room temperature,^{*} however the homobimetallic complex {(ReCl(CO)₃)₂(μ-bpm)} was found to be non-emissive under any conditions in contrast to other homobimetallic systems studied previously (*vide supra*). The heterobimetallic complex {(ReCl(CO)₃)(μ-bpm)(Ru(bpy)₂)²⁺} was found to emit only at low temperature in the solid state at a wavelength (774 nm) similar to that reported by Sullivan *et al.* for {(Ru(bpy)₂)₂(μ-bpm)}⁴⁺.⁴ It was therefore postulated that the emitting excited state in this case was Ru → bpm ³MLCT. However the possibility of other charge-transfer transitions occurring in their bimetallic bpm-bridged systems was discussed in terms of an excited state deactivation pathway of the Re-Ru complex involving a low energy intervalence charge-transfer (IVCT) transition between the Re^I-Ru^{III} and Re^{II}-Ru^{II} redox states (Figure 4.1.2.2). Similarly, the lack of emission of the Re-Re complex was postulated to arise because of a low energy Re^I-to-Re^I IVCT transition, although no direct evidence was provided to substantiate this theory.

Sahai *et al.* published a study of Ru and Re complexes of bpm using FTIR, absorption and luminescence spectroscopy and electrochemistry.⁷ Their study re-examined many of the complexes presented by the groups of Meyer and Ludi and Vogler and Kisslinger (*vide supra*) but added valuable FTIR data (Table 4.1.2.1) for the rhenium (I) carbonyl complexes, and UV/Vis (Table 4.1.2.2) and spectroelectrochemical data (Table 4.1.2.3). The authors conducted an analysis of the relative energies of ¹MLCT and ³MLCT energies in these systems, suggesting that the energy gap between related singlet and triplet states decreases in the order: monometallic > homobimetallic > heterobimetallic, in concert with the decrease of the HOMO-LUMO energy gap. A luminescence lifetime of 76 ns was measured for [Ru(bpy)₂(bpm)]²⁺ in water. Additionally a discussion of the possible isomers of [(ReCl(CO)₃)₂(μ-bpm)] with Cl ligands oriented either *syn* or *anti* in relation to each other was explored – however it

^{*} This is inconsistent with other more recent studies, notably Kaim's in CH₂Cl₂ (λ_{em} = 724 nm)⁶ and this work in CH₃CN at 298 K, 674 nm, *vide infra*.

was concluded that neither FTIR nor any of the other techniques employed in their study would be able to differentiate between the two possible stereoisomers.

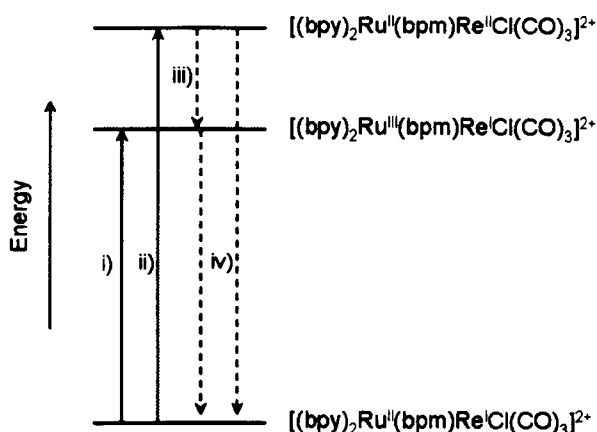


Figure 4.1.2.2: Photophysical scheme for $\{(\text{ReCl}(\text{CO})_3)(\mu\text{-bpm})(\text{Ru}(\text{bpy})_2)\}^{2+}$ in DMSO solution; i) and ii) are direct excitation, iii) is PEnT or IVCT and iv) is radiative/non-radiative relaxation to the ground state. Adapted from Ref.⁵

More recently Samuels and DeArmond have conducted a brief study of the spectroscopy, photophysics and electrochemistry of $[\text{Ru}(\text{CN})_4(\text{bpm})]^{2-}$.⁸ As observed in other tetracyanoruthenate (II) complexes (§2.1), the MLCT absorption bands show considerable negative solvatochromism in $\text{CH}_3\text{CH}_2\text{OH}$ and $(\text{CH}_3)_2\text{NCHO}$ (henceforth DMF) consistent with the effects of specific solvent-cyanide interactions (Table 4.1.2.2, §1.2.4). Cyclic voltammetry of $[\text{Ru}(\text{CN})_4(\text{bpm})]^{2-}$ showed one reversible reduction at $E_{1/2} = -2.09$ V (vs. Fc/Fc^+) in DMF. This is less negative than the value obtained in the same study for $[\text{Ru}(\text{CN})_4(\text{bpy})]^{2-}$, $E_{1/2} = -2.46$ V.⁸

Complex	Solvent	FTIR Bands / cm^{-1}		
$[\text{ReCl}(\text{CO})_3(\text{bpy})]$	CH_2Cl_2	2024	1921	1899
$[\text{ReCl}(\text{CO})_3(\text{bpm})]$	Solid	2033	1906	1899
$\{(\text{ReCl}(\text{CO})_3)_2(\mu\text{-bpm})\}$	Solid	2028	1908	
$\{(\text{ReCl}(\text{CO})_3)(\mu\text{-bpm})(\text{Ru}(\text{bpy})_2)\}^{2+}$	Solid	2034	1920	1915

Table 4.1.2.1: FTIR data for rhenium (I) bipyrimidine complexes. Adapted from Refs.^{7,9}

Complex	Solvent	$\lambda_{\text{abs}} / \text{nm}$		
$[\text{Ru}(\text{bpy})_3]^{2+}$	H_2O	452	423	
$[\text{Ru}(\text{bpm})_3]^{2+}$	H_2O	452	412	331
$[\text{Ru}(\text{bpy})_2(\text{bpm})]^{2+}$	CH_3CN	480 (sh)	422	398
$\{(\text{Ru}(\text{bpy})_2)_2(\mu\text{-bpm})\}^{4+}$	CH_3CN	594	545 (sh)	408
$[\text{ReCl}(\text{CO})_3(\text{bpm})]$	CH_3CN	384	310	
$\{(\text{ReCl}(\text{CO})_3)_2(\mu\text{-bpm})\}$	CH_3CN	480	350	
$\{(\text{ReCl}(\text{CO})_3)(\mu\text{-bpm})(\text{Ru}(\text{bpy})_2)\}^{2+}$	CH_3CN	606 (sh)	558	441
$[\text{Ru}(\text{CN})_4(\text{bpm})]^{2-}$	$(\text{CH}_3)_2\text{NCHO}$	590	425	
$[\text{Ru}(\text{CN})_4(\text{bpm})]^{2-}$	CH_3OH	490	375	

Table 4.1.2.2: Relevant UV/vis data for ruthenium (II) and rhenium (I) bipyrimidine complexes. Adapted from Refs.^{4,5,7,9}

Complex	Solvent	Redox Couples (V, vs. Fc/Fc^+)					
bpm	CH_3CN			-2.12			
$[\text{Ru}(\text{bpy})_2(\text{bpm})]^{2+}$	CH_3CN	+1.09		-1.32	-1.76	-2.14	
$\{(\text{Ru}(\text{bpy})_2)_2(\mu\text{-bpm})\}^{4+}$	CH_3CN	+1.38	+1.22	-0.10		-0.77	
$[\text{ClRe}(\text{CO})_3(\text{bpm})]$	CH_3CN	$E_p = +1.12$		-1.31		$E_p = -1.96$	
$\{(\text{ClRe}(\text{CO})_3)_2(\mu\text{-bpm})\}$	CH_3CN			-0.61		$E_p = -1.49$	
$\{(\text{ClRe}(\text{CO})_3)(\mu\text{-bpm})(\text{Ru}(\text{bpy})_2)\}^{2+}$	CH_3CN	+1.45	+1.27	-0.72	-1.41	-1.87	-2.12
$[\text{Ru}(\text{CN})_4(\text{bpm})]^{2-}$	DMF			-2.09			

Table 4.1.2.3: Redox couples for ruthenium (II) and rhenium (I) bipyrimidine complexes. Adapted from Refs.^{4,5,7}

4.1.3. Relevant Studies of Other Polynuclear Complexes

There have been a number of time-resolved spectroscopic studies of bimetallic Ru and Re complexes in solution which have investigated electronic structure and dynamics in excited states following excitation into the MLCT manifold of such complexes. The aim of these studies is usually to gain insight into excited state electronic structure and

the extent and timescale of excited state localisation/delocalisation. A particularly relevant example of this is the study of a series of bimetallic complexes constructed from $[\text{ReCl}(\text{CO})_3]$ units bridged by different polypyridyl ligands (Figure 4.1.3.1a).¹⁰ These complexes were studied using ps-TRIR spectroscopy in the $\nu(\text{CO})$ spectral region and as such provide good reference data for the carbonyl spectra presented in the remainder of this Chapter. Similar TRIR spectra were obtained for all complexes, with the three $\nu(\text{CO})$ bands observed in the ground state FTIR spectra being split into *two sets* of three bands, with one set shifted to higher wavenumber than the bleaches and the other set shifted to lower wavenumber (Figure 4.1.3.1b). This was found to be consistent with ‘asymmetry’ in the electronic structure of the excited state, with the species being formed best described as a localised excited state on the IR timescale (§1.3) with the form $[\text{Re}(\text{BL}^{\cdot-})\text{Re}^{\cdot+}]$.

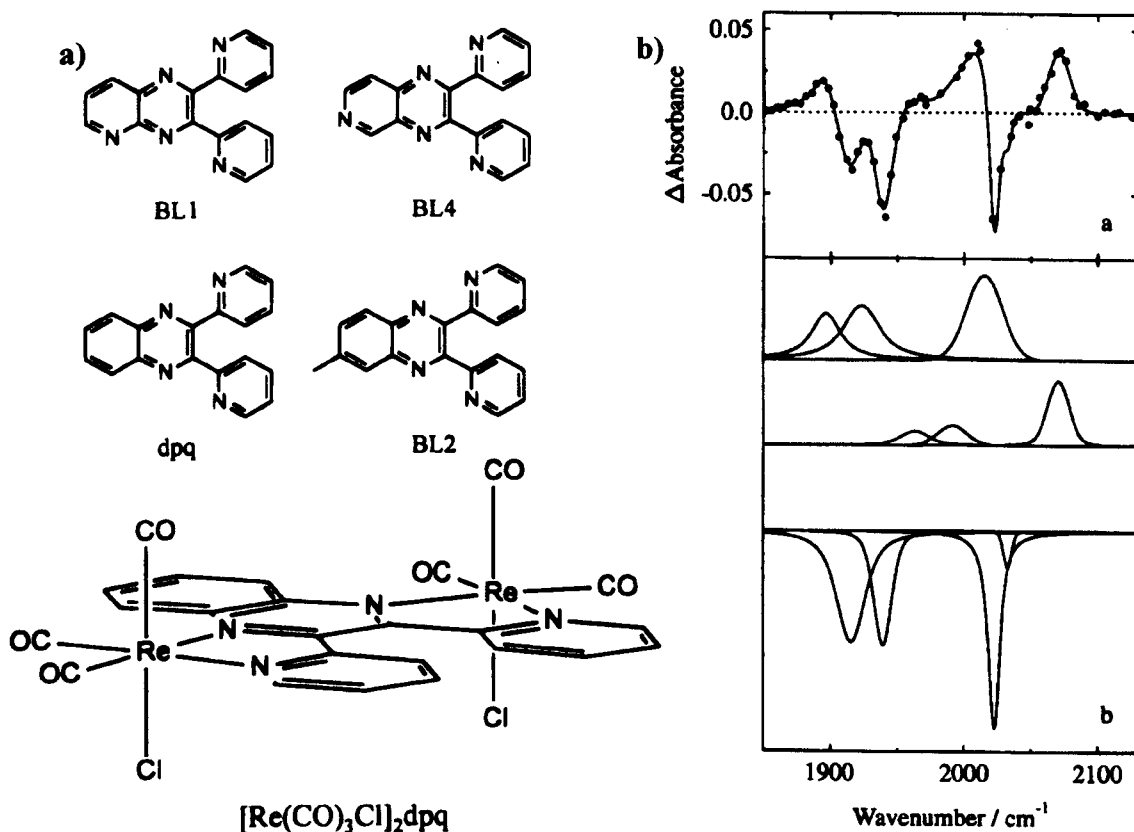


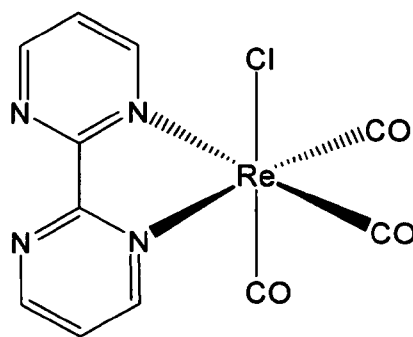
Figure 4.1.3.1: a) The bridging ligands used in the TRIR study (top) and an example of the complexes prepared (bottom); b) TRIR spectra of $[\text{Re}(\text{CO})_3\text{Cl}]_2\text{BL1}$ in CH_2Cl_2 solution following 606 nm excitation (top) and fits to the experimental bands separated into three sets of three. Adapted from Ref.¹⁰

There have been a number of more recent studies of bpm complexes of ruthenium (II), rhenium (I) and other photophysically interesting transition metals such as platinum (II),¹¹ but none of them have adequately answered the key questions posed by the studies discussed above:

- Why do rhenium (I) and ruthenium (II) complexes of 2,2'-bipyrimidine exhibit much weaker luminescence and shorter lifetimes than the corresponding 2,2'-bipyridine complexes?
- What is the electronic structure of the excited states formed upon photoexcitation of d^6 metal complexes of bpm, and how do they evolve after formation? Are they localised or delocalised on the IR timescale? Can vibrational spectroscopy be used to directly monitor these states more effectively than optical spectroscopy?
- Some bpm-bridged bimetallic systems may have several different MLCT chromophores. Considering this in combination with unselective excitation due to broad absorption bands, the rich electronic manifold of the bpm ligand and other IL/MC transitions and multiple vibrational spectroscopic signals from reporter ligands will the ultrafast dynamics of these systems be amenable to study by vibrational spectroscopy?
- Can IVCT processes occur in mixed valence homobimetallic or heterobimetallic bpm complexes? Can they be observed using vibrational spectroscopy?

In the remainder of this Chapter the results from spectroscopic and electrochemical studies will aim to address these questions.

4.2. *fac*-[ReCl(CO)₃(bpm)], ReBPM



ReBPM has been studied before using absorption, emission and FTIR spectroscopy and electrochemistry, as discussed above (§4.1.2). We have conducted these experiments in addition to IR OTTLE and TRIR experiments in order to study the electronic structure of its ground state, electrochemically generated species and its lowest-lying electronic excited state.

ReBPM is insoluble in aqueous media and has only been studied in CH₃CN. The complex is not significantly solvatochromic and thus its photophysical and electrochemical properties are expected to vary little with solvent medium.

4.2.1. UV/visible Absorption and Luminescence Spectroscopy

The UV/visible absorption spectrum of **ReBPM** has been measured in CH₃CN (see Appendix 4.12 for spectra). The results are presented in Table 4.2.1.1 and closely match literature values (Table 4.1.2.2).⁵

Solvent	$\lambda^{\max} / \text{nm}$		
	CH ₃ CN	< 300	304
Assignment	IL π - π^* (bpm)	¹ MLCT (Re)	¹ MLCT (Re)

Table 4.2.1.1: Table of peak positions and assignments for the UV/visible absorption spectrum of ReBPM in CH₃CN solution.

The luminescence spectrum of **ReBPM** was measured in CH₃CN solution (see Appendix 4.12 for spectra). Excitation into the Re → bpm MLCT manifold at 384 nm results in weak luminescence with a broad, structureless profile centred at 674 nm, in contrast to the results of Vogler’s study which reports an emission maximum of 567 nm.⁵ It is conceivable that a feature due to Raman scattering from solvent vibrations may be responsible for Vogler’s different interpretation of the emission spectrum. The luminescence is significantly red-shifted in comparison to the spectrum of [ReCl(bpy)(CO)₃], which is centred at 612 nm.¹² This has been rationalised in terms of a smaller HOMO-LUMO energy gap in bpm-containing complexes compared to bpy analogues as discussed in §4.1. In both cases the emission intensity was insufficient to perform TCSPC experiments to determine the lifetime.

4.2.2. Cyclic Voltammetry

Cyclic voltammetry of **ReBPM** in CH₃CN was performed (see Appendix 4.12 for voltammograms) and the results are presented in Table 4.2.2.1 below. Features corresponding to one reversible reduction couple and one irreversible oxidation couple are observed. The results are comparable to previous studies (Table 4.1.2.3) which also detect a second (irreversible) redox couple at more negative potentials, corresponding to a second reduction located on the bpm ligand.⁷

$E_{1/2}/V$ (vs. Fc/Fc ⁺)	Reversibility	Assignment
+1.05	Irreversible	Re ^{III}
-1.43	Reversible	(bpm) ^{0/+•-}

Table 4.2.2.1: Table of potentials for redox couples and assignments from the cyclic voltammogram of ReBPM in CH₃CN solution.

4.2.3. FTIR, IR OTTLE and Time-Resolved Infrared Spectroscopy

ReBPM has been studied using FTIR, IR OTTLE and ps-TRIR spectroscopy in CH₃CN solution. Figure 4.2.3.1 shows the FTIR and ps-TRIR spectra obtained and Figure 4.2.3.2 shows the spectra obtained from the IR-OTTLE experiment for **ReBPM** in CH₃CN solution. Figure 4.2.3.3 shows the ps-TRIR kinetics obtained for bleach and transient bands in CH₃CN.

Acetonitrile Solution

FTIR Spectroscopy

The FTIR spectrum of **ReBPM** in CH₃CN solution in the $\nu(\text{CO})$ region has been measured and is shown in Figure 4.2.3.1 (bottom). In the carbonyl region there is a peak profile characteristic of the rhenium (I) tricarbonyl unit with 3 resolved maxima at 2028, 1924 and 1909 cm⁻¹. This is in good agreement with previous studies in the literature (Table 4.1.2.1).⁷

IR OTTLE Spectroelectrochemistry

FTIR spectra were taken as the complex underwent its first reduction; the difference spectrum obtained by subtracting the starting FTIR from the final spectrum of the 1-electron reduced species is shown in Figure 4.2.3.2. Newly formed bands are evident at 2007 and 1878 cm⁻¹, which are shifted to lower wavenumber to the bands of the neutral species at 2028, 1924 and 1909 cm⁻¹. This is consistent with an increase in electron density at the metal due to the reduction of the bipyrimidine ligand.

ps-TRIR Spectroscopy

The ps-TRIR spectral profile obtained following 400 nm excitation contains three bleaches at 2028, 1924 and 1909 cm⁻¹. Three transient bands are detected at higher energy to the bleaches, which narrow and blue-shift over the first 20 ps due to vibrational cooling and settle at 2079, 2002 and 1965 cm⁻¹. This is consistent with a

decrease in electron density at the metal centre as a result of the formation of a $\text{Re} \rightarrow \text{bpm}^3\text{MLCT}$ excited state.

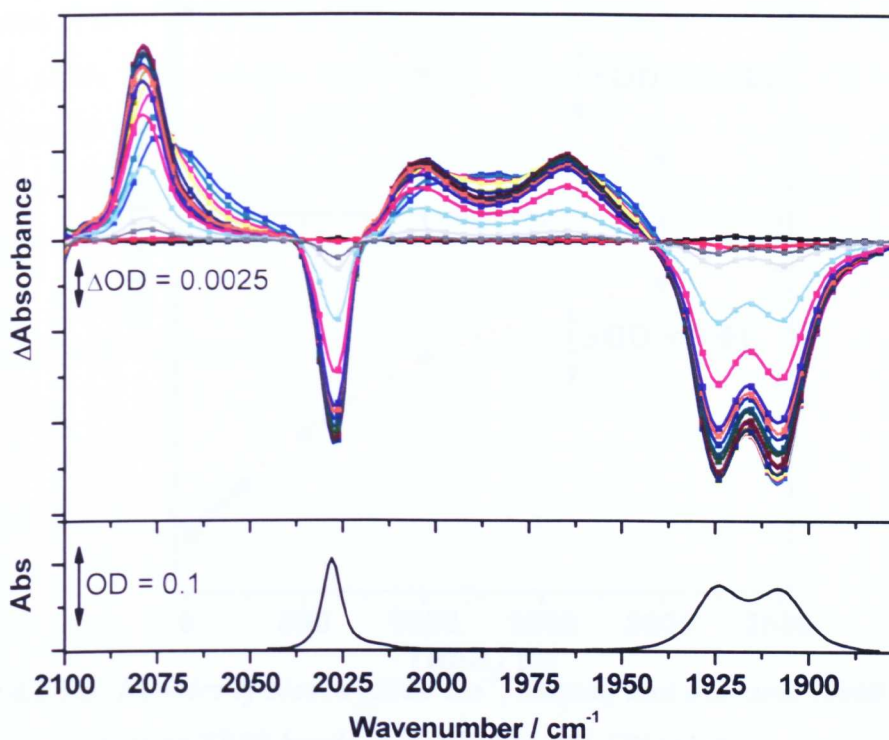


Figure 4.2.3.1: The FTIR (bottom) and ps-TRIR spectra between 1 and 2500 ps (top) of ReBPM in CH_3CN solution.

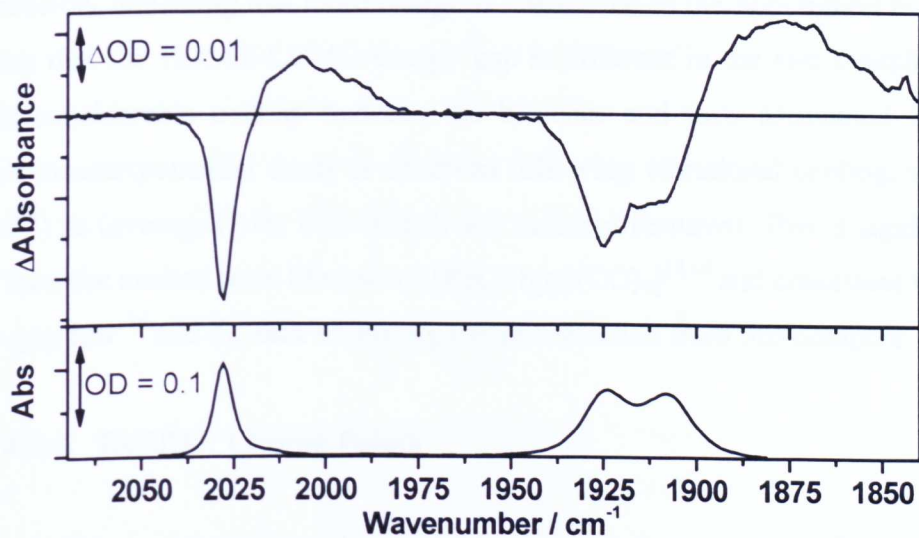


Figure 4.2.3.2: The FTIR (bottom) and IR OTTLE difference spectra [ReBPM⁻ minus ReBPM] (top) of ReBPM in CH_3CN solution.

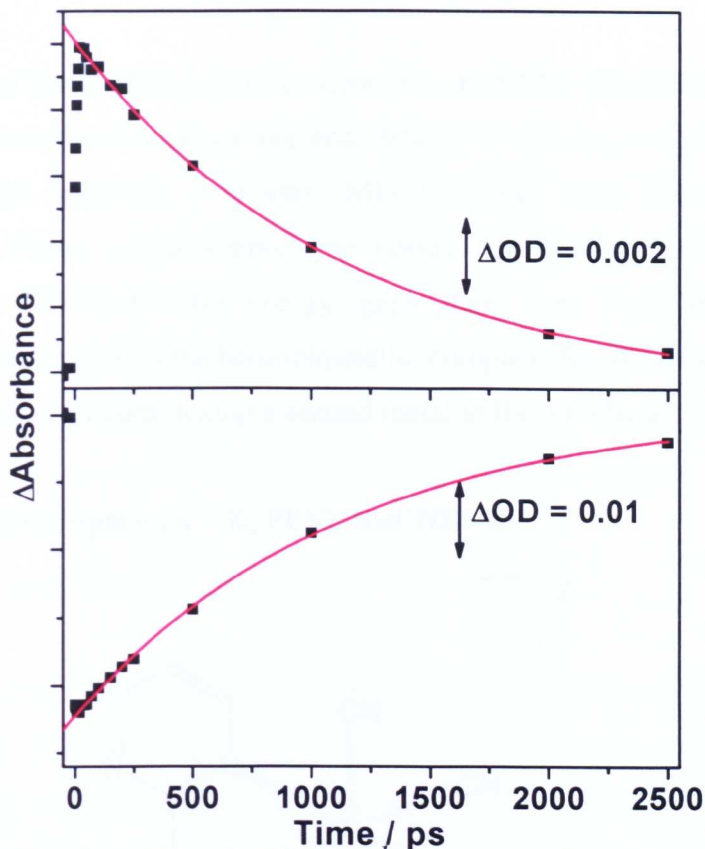


Figure 4.2.3.3: Kinetics of bleach (2026 cm^{-1} , bottom) and transient (2080 cm^{-1} , top) ps-TRIR bands of ReBPM in CH_3CN solution.

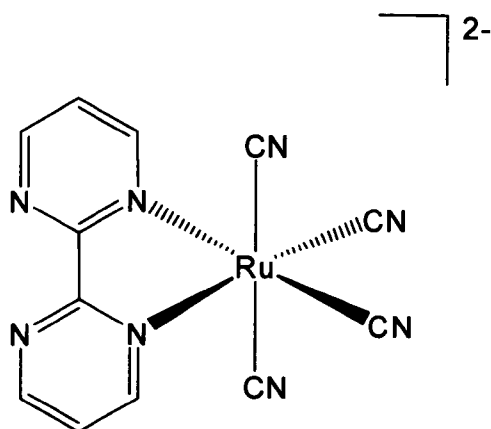
The magnitude of the band shift between ground and excited state spectra of **ReBPM** ($\Delta_{\text{ES-GS}} = 50\text{-}80\text{ cm}^{-1}$) is slightly larger than that of $[\text{ReCl}(\text{bpy})(\text{CO})_3]$ ($\Delta_{\text{ES-GS}} = 40\text{-}66\text{ cm}^{-1}$), possibly indicating that more charge is transferred to the bpm ligand as well as indicating that the HOMO-LUMO energy gap is different in the two complexes.^{9,13} There is considerable overlap between the bleaches and their associated transient bands. A monoexponential decay is observed following vibrational cooling, with $\tau = 1170 (\pm 72)\text{ ps}$ (averaged over both bleach and transient features). This is significantly shorter than the excited state lifetime of $[\text{ReCl}(\text{bpy})(\text{CO})_3]$ ^{12,14} and consistent with the ‘energy-gap law’¹⁵ and the lack of any significant emission from this complex.

4.2.4. ReBPM: Closing Points

The lowest-lying excited state of **ReBPM** is assigned to $\text{Re} \rightarrow \text{bpm}^3\text{MLCT}$ using TRIR spectroscopy, as previously reported in the literature. Upon comparison of the

results with $[\text{ReCl}(\text{bpy})(\text{CO})_3]$ it is evident that **ReBPM** possesses lower energy absorption and emission bands, a more accessible 1st reduction, a similar FTIR peak profile and TRIR spectrum, a shorter ³MLCT excited state lifetime and lower quantum yield. These results support the notion that bpm-containing complexes exhibit smaller HOMO-LUMO energy gaps than their bipyridine analogues. Interesting comparisons with the homobimetallic complex (**Re₂**)BPM (§4.5) will give insight into the effect of complexing a second metal to the bpm ligand.

4.3. $\text{X}_2[\text{Ru}(\text{CN})_4(\text{bpm})]$, (X = K, PPN), **RuCNBPM**



The spectroscopy and electrochemistry of **RuCNBPM** have been presented previously in a comparison of tetracyanoruthenate (II) complexes (§2.2) and the results will be discussed here in more detail. As with all other complexes containing the $[\text{Ru}(\text{CN})_4]^{2-}$ unit, strong negative solvatochromism is observed due to SSDA interactions between the cyanide ligands and solvent molecules. As a result **RuCNBPM** exhibits significantly different properties in D_2O and CH_3CN .

4.3.1. UV/visible Absorption and Luminescence Spectroscopy

The UV/visible absorption spectra of **RuCNBPM** have been measured in CH_3CN and D_2O (see Appendix 4.12 for spectra) and have been discussed earlier (see §2.2.1). Strong negative solvatochromism is clearly evident in the differences in peak centre between the two solvents and is typical for complexes of this type. The results are

summarised in Table 4.3.1.1 and agree well with a previous study (Table 4.1.2.2).⁸ No luminescence from **RuCNBPM** was detected at 298 K in either D₂O or CH₃CN.

Solvent	$\lambda^{\max} / \text{nm}$		
	D ₂ O	< 300	345
CH ₃ CN	< 300	416	592
Assignment	IL π - π^* (bpm)	¹ MLCT (Ru)	¹ MLCT (Ru)

Table 4.3.1.1: Table of peak positions and assignments for UV/visible absorption spectra of RuCNBPM in D₂O and CH₃CN solution.¹⁶

4.3.2. Cyclic Voltammetry

Cyclic voltammetry of **RuCNBPM** was measured in D₂O (see Appendix 4.12 for voltammograms) and the results are presented in Table 4.3.2.1 below. Features corresponding to one irreversible oxidation couple was observed – the reduction couples are ostensibly outside the narrow D₂O potential window (-1 to +1 V). The results are unfortunately incomparable with literature data (§4.1) due to differences in solvent; Samuels and DeArmond used DMF, a low A. N. solvent whereas D₂O was used here.

$E_{1/2} / \text{V}$ (vs. Fc/Fc ⁺)	Reversibility	Assignment
$E_p = +1.45$	Irreversible	Ru ^{II/III}

Table 4.3.2.1: Table of potentials for redox couples and assignments from the cyclic voltammogram of RuCNBPM in D₂O solution.

4.3.3. FTIR, IR OTTLE and Time-Resolved Infrared Spectroscopy

RuCNBPM has been studied using ps and ns-TRIR spectroscopy in D₂O and CH₃CN solution. IR OTTLE spectroelectrochemistry in CH₃CN was unsuccessful as the 1st reduction was found to be chemically irreversible on the timescale of the experiment.

Deuterium Oxide Solution

Figure 4.3.3.1 shows the FTIR and ns-TRIR spectra of **RuCNBPM** measured in D_2O solution. Figure 4.3.3.2 shows the ns-TRIR kinetics obtained for bleach and transient bands in D_2O .

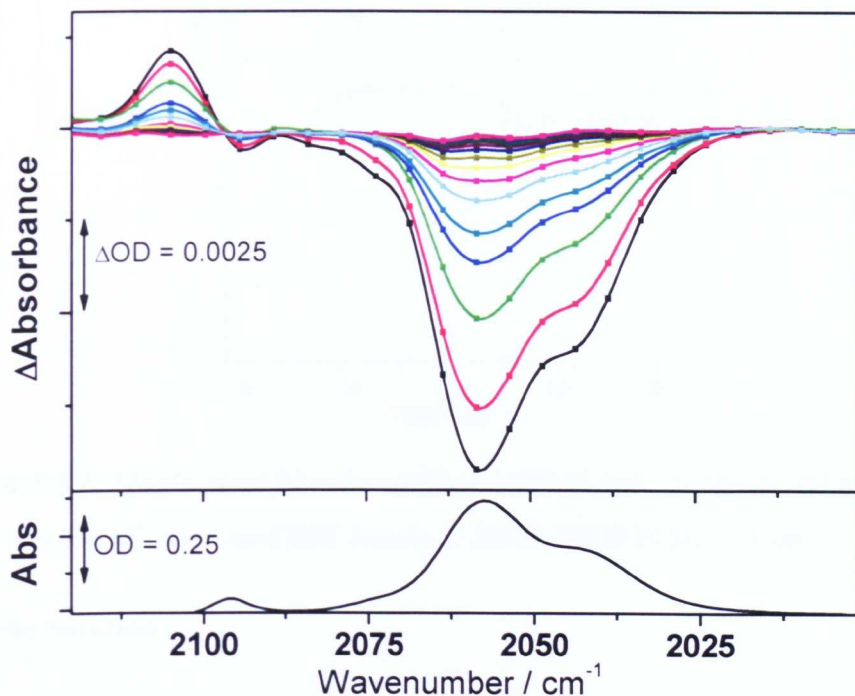


Figure 4.3.3.1: The FTIR (bottom) and ns-TRIR spectra between 1 and 50 ns (top) of RuCNBPM in D_2O solution.

The FTIR spectrum of **RuCNBPM** in D_2O solution in the $\nu(\text{CN})$ region has a peak profile characteristic of the tetracyanoruthenate (II) unit with 3 resolved maxima at 2095, 2057 and 2043 cm^{-1} . The ns-TRIR spectral profile of **RuCNBPM** following 355 nm excitation features a broad bleach with components corresponding to the band positions in the FTIR and a transient band at higher wavenumber at 2105 cm^{-1} . This is consistent with a decrease in electron density at the metal centre as a result of $\text{Ru} \rightarrow \text{bpm}^3\text{MLCT}$ excited state formation. A monoexponential decay is observed with $\tau = 3.4 (\pm 0.3)$ ns (averaged over both bleach and transient features). Although the spectral profile is similar, the lifetime is significantly shorter than that of $[\text{Ru}(\text{CN})_4(\text{bpy})]^{2-}$ (3.2 ns) and consistent with the lack of detected emission from this complex.

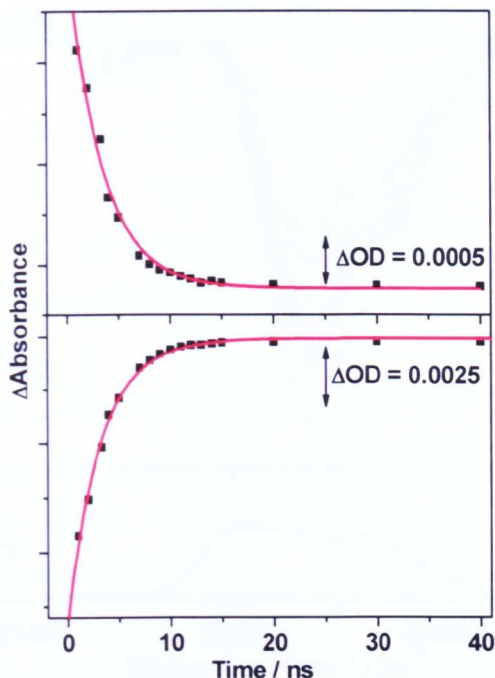


Figure 4.3.3.2: Single-pixel kinetics of bleach (2058 cm^{-1} , bottom) and transient (2106 cm^{-1} , top) ns-TRIR bands of RuCNBPM in D_2O solution.

Acetonitrile Solution

Figure 4.3.3.3 shows the FTIR and ps-TRIR spectra of **RuCNBPM** measured in CH_3CN solution. Figure 4.3.3.4 shows the ps-TRIR kinetics obtained for bleach and transient bands in CH_3CN .

The FTIR spectrum of **RuCNBPM** in CH_3CN solution in the $\nu(\text{CN})$ region has a peak profile characteristic of the tetracyanoruthenate (II) unit with 4 resolved bands at 2092 , 2074 , 2068 and 2059 cm^{-1} . The ps-TRIR spectral profile obtained following 400 nm excitation consists of a broad bleach with components corresponding to the band positions in the FTIR and a transient band at higher wavenumber centred at 2098 cm^{-1} . As in D_2O this is consistent with a decrease in electron density at the metal centre as a result of $\text{Ru} \rightarrow \text{bpm}^3\text{MLCT}$ excited state formation.

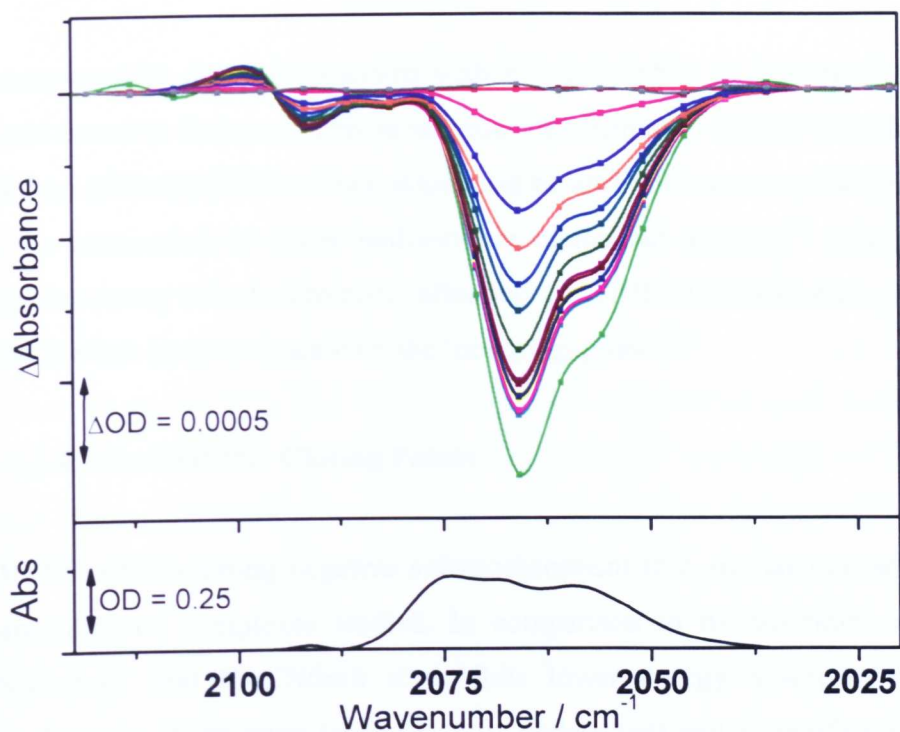


Figure 4.3.3.3: The FTIR (bottom) and ps-TRIR spectra between 1 and 1000 ps (top) of RuCNBPM in CH_3CN solution.

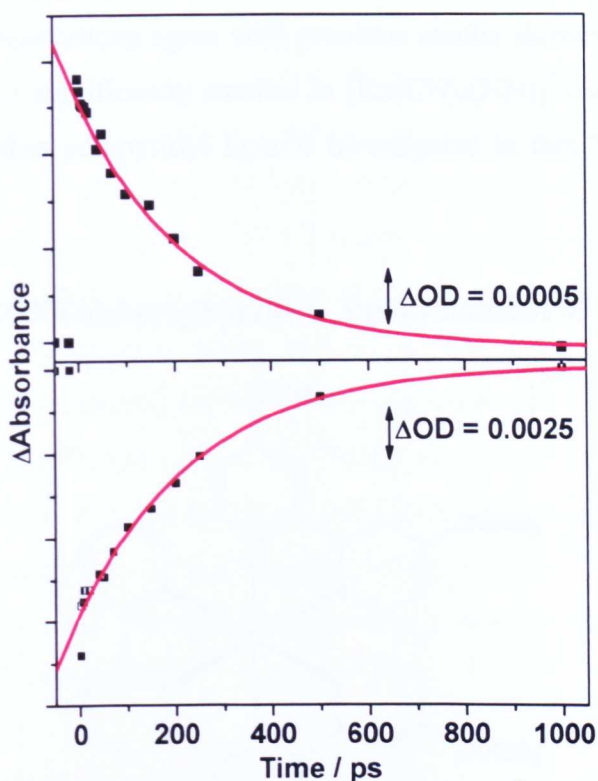


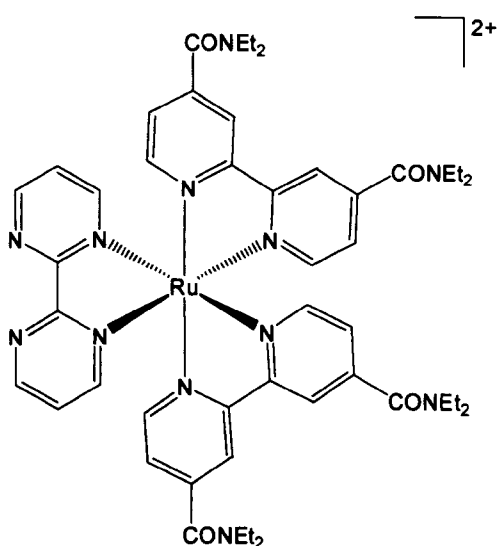
Figure 4.3.3.4: Single-pixel kinetics of bleach (2064 cm^{-1} , bottom) and transient (2099 cm^{-1} , top) ps-TRIR bands of RuCNBPM in CH_3CN solution.

A monoexponential decay is observed with $\tau = 249 (\pm 51)$ ps (averaged over both bleach and transient features). This is an order of magnitude shorter than the excited state lifetime of **RuCNBPM** in D_2O , which can be attributed to two principal reasons. Firstly, the attenuation of decay pathways in deuterated solvents¹⁷ (see §2.1) and secondly the strong solvatochromism affecting the HOMO-LUMO energy gap and hence the lifetime in accordance with the ‘energy-gap law’.¹⁵

4.3.4. RuCNBPM: Closing Points

RuCNBPM exhibits strong negative solvatochromism in a similar manner to other tetracyanoruthenate complexes studied. In comparison to its bipyridine analogues $[Ru(CN)_4(bpy)]^{2-}$ and **RuCNdmb** it exhibits lower energy absorption bands, a dramatic decrease in emission (such that it is undetected) and a significantly shorter excited state lifetime. TRIR spectroscopy in the $\nu(CN)$ spectral region facilitates direct monitoring of the excited states formed on the picosecond and nanosecond timescales. These observations agree with previous results showing that the HOMO-LUMO energy gap is significantly smaller in $[Ru(CN)_4(NN)]^{2-}$ complexes containing bipyrimidine than other polypyridyl ligands investigated in this Thesis (see Chapter 2).

4.4. $[Ru((4,4'-CONEt_2)_2bpy)_2(bpm)]Cl_2$, RubpyamideBPM



RubpyamideBPM is similar to the **RubpyamBL^x** complexes studied in Chapter 3, in that it possesses two ((4,4'-CONEt₂)₂bpy) (henceforth known as bpyamide) ligands and a third different bidentate polypyridyl ligand with vacant coordination sites available for complexation of a second metal. As there are *two* types of chromophores in the complex - Ru → bpm and Ru → bpyamide MLCT - the photophysical behaviour of the complex may be complicated; in addition to two types of possible ³MLCT excited states, there may be the possibility of interconversion between them on the ultrafast timescale. As with the **RubpyamBL^x** complexes there is little solvatochromism expected and as a result the properties of **RubpyamideBPM** are predicted to be similar in both D₂O and CH₃CN.

4.4.1. UV/visible Absorption and Luminescence Spectroscopy

The UV/visible absorption spectra of **RubpyamideBPM** have been measured in D₂O and CH₃CN (see Appendix 4.12 for spectra) and the results are summarised in Table 4.4.1.1. The absorption spectra of these complexes are only slightly affected by solvent, with differences of a few nanometres wavelength between related absorption peaks in D₂O and CH₃CN. More low energy absorption bands are observed in comparison with the other monometallic bpm complexes studied here (§4.2.1, §4.3.1), due to the presence of Ru → bpyam ¹MLCT transitions in addition to the Ru → bpm ¹MLCT transitions. There are two transitions at *ca.* 420 and 360 nm, whose positions do not vary significantly with either solvent or nuclearity (when analysed in conjunction with **(Rubpyamide)₂BPM**, §4.7.1) and hence are tentatively assigned to the Ru → bpyam ¹MLCT transitions. The bands at *ca.* 450 and 330 nm in **3** are tentatively assigned to two Ru → bpm ¹MLCT transitions, consistent with the presence of two different low-lying π* bpm orbitals giving two ¹MLCT transitions to bpm. The spectral profiles obtained are reasonably similar to those reported for [Ru(bpy)₂(bpm)]²⁺ (Table 4.1.2.2).⁷

The luminescence of **RubpyamideBPM** in CH₃CN (see Appendix 4.12 for spectra) is relatively intense for a bpm-containing complex, with a broad structureless emission

profile centred at 648 nm which decays with a time constant of 116 (± 10) ns. The quantum yield is however an order of magnitude smaller than the corresponding **Rubpyamide-BL^x** (Chapter 3) complexes, with $\phi = 0.001$. This comparatively weak luminescence is in agreement with published results for $[\text{Ru}(\text{bpy})_2(\text{bpm})]^{2+}$.⁷

Solvent	$\lambda^{\text{max}} / \text{nm}$				
	D ₂ O	< 300	330	358	424
CH ₃ CN	< 300	330	358	418	453
Assignment	IL π - π^* (bpm)	¹ MLCT (Ru-bpm)	¹ MLCT (Ru-bpyam)		¹ MLCT (Ru-bpm)

Table 4.4.1.1: Table of peak positions and assignments for UV/visible absorption spectra of RubpyamideBPM in D₂O and CH₃CN solution.

4.4.2. Cyclic Voltammetry

Cyclic voltammetry of **RubpyamideBPM** was measured in CH₃CN (see Appendix 4.12 for voltammograms) and the results are presented in Table 4.4.2.1 below. Features corresponding to three reversible reductions and one irreversible oxidation couple are observed. The redox potentials and assignments are comparable to studies of **RubpyamideBL¹** in §3.3.2, with the notable difference of the more facile reduction of bpm than bipyridine-based ligands.

$E_{1/2} / \text{V}$ (vs. Fc/Fc ⁺)	Reversibility	Assignment
$E_p = +0.81$	Irreversible	Amide oxidation
-1.30	Reversible	(bpm) ^{0/-}
-1.60	Reversible	Amide reduction
-1.81	Reversible	Amide reduction

Table 4.4.2.1: Table of potentials for redox couples and assignments from the cyclic voltammogram of RubpyamideBPM in CH₃CN solution.

4.4.3. FTIR, IR OTTLE and Time-Resolved Infrared Spectroscopy

RubpyamideBPM has been studied using ps and ns-TRIR spectroscopy in D_2O and CH_3CN solution. An IR OTTLE experiment to monitor the changes in band profile as the complex underwent its 1st reduction in CH_3CN (not shown) did not detect any significant spectral changes, ostensibly due to the lack of electronic coupling between the bipyrimidine ligand and the amide substituents on the bpy ligands.

Deuterium Oxide Solution

Figures 4.4.3.1 and 4.4.3.3 show the FTIR, ps-TRIR and ns-TRIR spectra obtained of **RubpyamideBPM** in D_2O solution. Figures 4.4.3.2 and 4.4.3.4 show the ps and ns-TRIR kinetics obtained for bleach and transient bands in D_2O .

The FTIR spectrum of **RubpyamideBPM** in D_2O solution in the amide $\nu(CO)$ region has a single amide peak present at 1617 cm^{-1} and a weak band at 1580 cm^{-1} which is assigned to a vibrational mode of bipyrimidine.

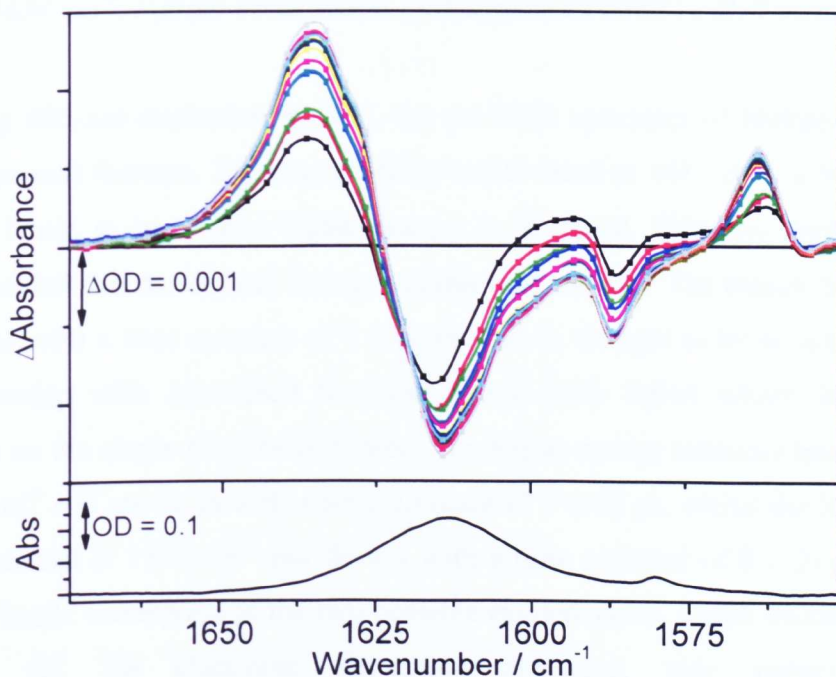


Figure 4.4.3.1: The FTIR (bottom) and ps-TRIR spectra between 1 and 1000 ps (top) of RubpyamideBPM in D_2O solution.

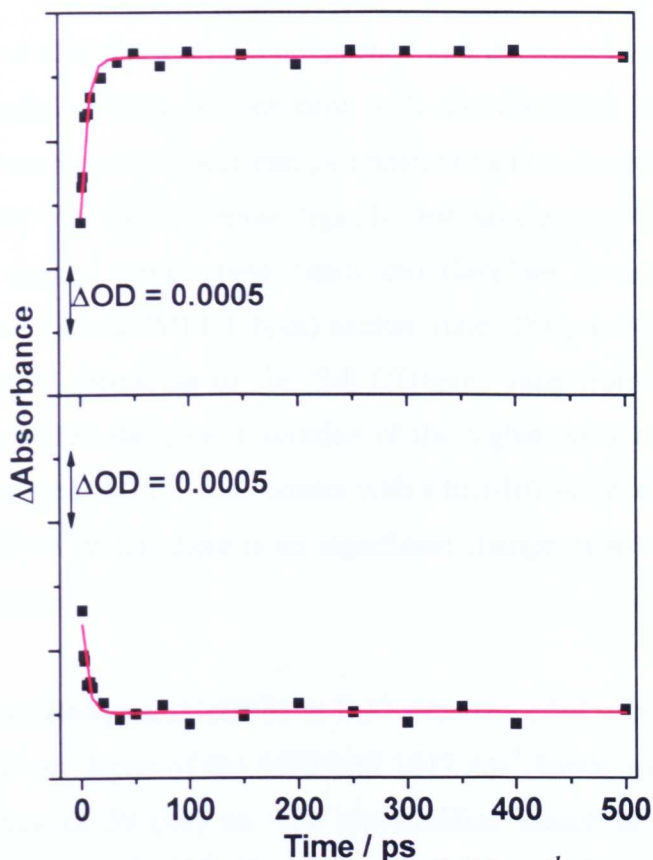


Figure 4.4.3.2: Single-pixel kinetics of bleach (1615 cm^{-1} , bottom) and transient (1634 cm^{-1} , top) ps-TRIR bands of RubpyamideBPM in D_2O solution.

Following 400 nm excitation in D_2O , the ps-TRIR spectrum of **RubpyamideBPM** exhibits several features. The parent $\nu(\text{CO})$ amide band at 1617 cm^{-1} is bleached and transient bands at lower and higher energy is observed. This has been confirmed through scaled subtraction and fitting analysis (not shown). The bleach band appears to grow in with a time constant of $7 (\pm 2)$ ps; this is thought to be an artefact due to heavy overlap with associated transient bands (*vide infra*) which imprint their dynamics on the single-pixel bleach trace. The higher energy transient band is centred at 1636 cm^{-1} and grows in with a time constant of $7 (\pm 2)$ ps, whilst the lower energy band is centred at 1593 cm^{-1} and decays with a time constant of $6 (\pm 2)$ ps. The two transient bands correspond to the two possible excited states. Initial excitation is non-selective (*cf.* the electronic absorption spectrum, *vide supra*) so both $[(\text{bpyam})(\text{bpyam}^{\bullet-})\text{Ru}^{\text{III}}(\text{bpm})]^{2+}$ (hereafter $^3\text{MLCT}(\text{bpyam})$) and $[(\text{bpyam})_2\text{Ru}^{\text{III}}(\text{bpm}^{\bullet-})]^{2+}$ (hereafter $^3\text{MLCT}(\text{bpm})$) are formed following excitation.

The transient band at higher energy corresponds to a decrease in electron density on the bpyamide ligands which is consistent with the formation of a $^3\text{MLCT}(\text{bpm})$ excited state. Conversely the lower energy transient band corresponds to an increase in electron density on the bpyamide ligands that accompany the formation of a $^3\text{MLCT}(\text{bpyam})$ excited state. These bands can therefore be used to monitor the formation and decay of the $^3\text{MLCT}(\text{bpm})$ excited state. The grow-in of the 1593 cm^{-1} band corresponds to formation of the $^3\text{MLCT}(\text{bpm})$ state from the higher-energy $^3\text{MLCT}(\text{bpyam})$ excited state, *i.e.* relaxation of the higher-lying bpyam-based to the lower-lying bpm-based $^3\text{MLCT}$ state occurs with a half-life of *ca.* 6 ps. Following this excited state interconversion there is no significant change in spectral profile on the picosecond timescale.

ns-TRIR spectra of **RubpyamideBPM** in D_2O were recorded using excitation at 355 nm. The synchronous decay of the 1593 and 1617 cm^{-1} bands was observed with a mean time constant of $59 (\pm 1)$ ns. The bipyrimidine bleach at 1580 cm^{-1} and its associated transient at 1560 cm^{-1} decay with the same (60 ns) lifetime as the higher energy amide transient band as they are also monitoring the decay of the $^3\text{MLCT}(\text{bpm})$ excited state. A rationalisation of the difference in lifetimes measured by TRIR and luminescence spectroscopy is presented in the Experimental section of this Thesis (Chapter 6).

Acetonitrile Solution

Figures 4.4.3.5 and 4.4.3.6 show the FTIR, ps-TRIR and ns-TRIR spectra obtained of **RubpyamideBPM** in CH_3CN solution. Figures 4.4.3.7 and 4.4.3.8 shows the ps and ns-TRIR kinetics obtained for bleach and transient bands in CH_3CN . The FTIR spectrum of **RubpyamideBPM** in CH_3CN solution in the amide $\nu(\text{CO})$ region has a single amide peak present at 1641 cm^{-1} and a weak band at 1581 cm^{-1} which is assigned to a vibrational mode of bipyrimidine. As in D_2O , ps-TRIR spectroscopy of **RubpyamideBPM** in CH_3CN gives a bleach of the main $\nu(\text{CO})$ amide band at 1641 cm^{-1} following 400 nm excitation.

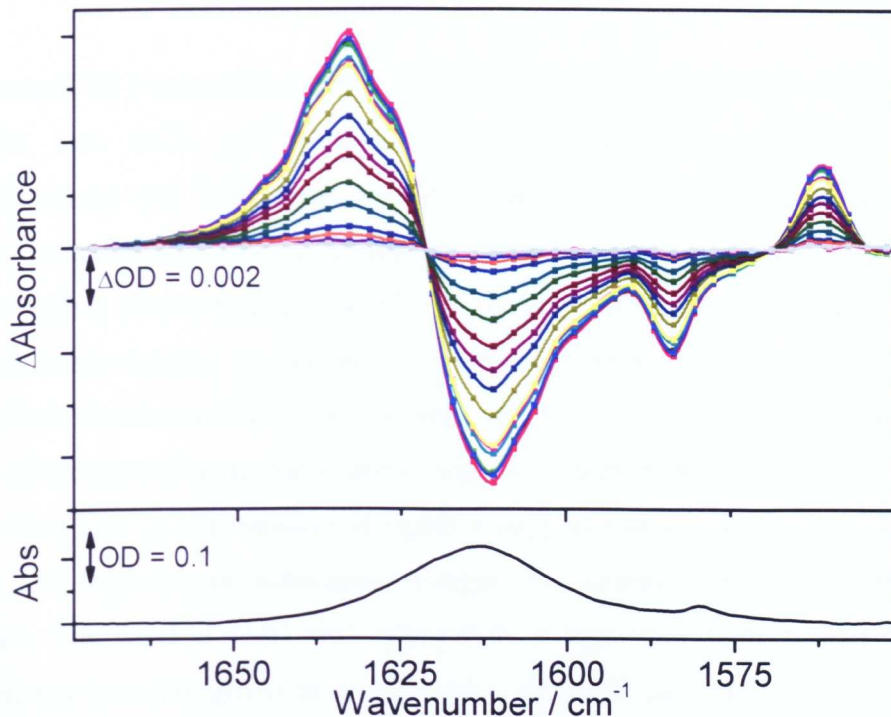


Figure 4.4.3.3: The FTIR (bottom) and ns-TRIR spectra between 1 and 750 ns (top) of RubpyamideBPM in D_2O solution.

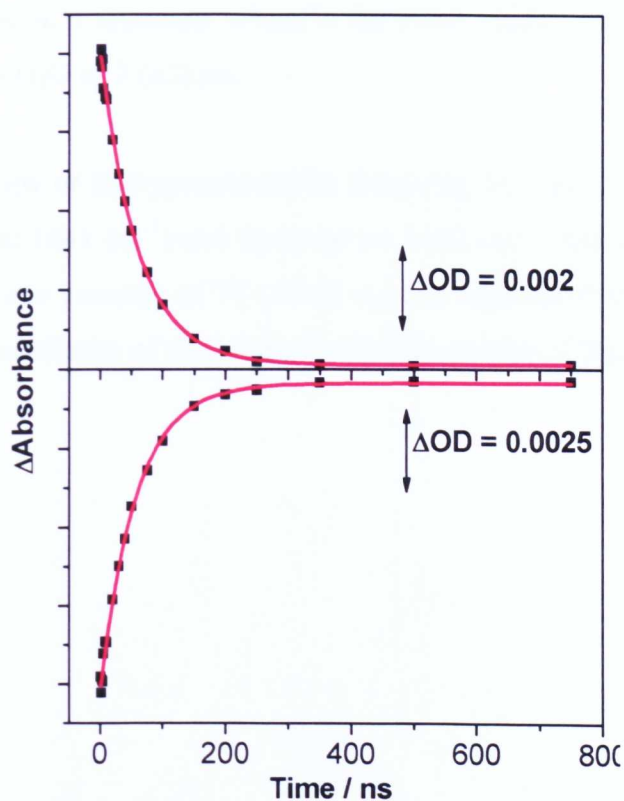


Figure 4.4.3.4: Single-pixel kinetics of bleach (1613 cm^{-1} , bottom) and transient (1635 cm^{-1} , top) ns-TRIR bands of RubpyamideBPM in D_2O solution.

Transient $\nu(\text{CO})$ bands are seen at both lower and higher energy than the ground state at 1652 and 1623 cm^{-1} respectively, consistent with population of both $^3\text{MLCT}(\text{bpyam})$ and $^3\text{MLCT}(\text{bpm})$ excited states. This has been confirmed through scaled subtraction and fitting analysis (not shown). As in D_2O , the bleach appears to grow in with a time constant of 4 (± 2) ps due to heavy overlap between bleach and transient bands leading to excited state bands ‘imprinting’ their dynamics on the single-pixel bleach trace. The lower-energy $\nu(\text{CO})$ transient overlaps heavily with the bleach of the ground-state band, preventing the straightforward extraction of kinetic information. The $\nu(\text{CO})$ transient at higher energy grows in with a time constant of 6 (± 2) ps and there are no subsequent changes in spectral profile on the picosecond timescale. The band at 1580 cm^{-1} arises from a bpm ring mode is bleached and a lower energy transient grows in at 1559 cm^{-1} , although the data was not of sufficient quality to extract kinetic information. These results indicate the observation of excited state interconversion from the higher lying $^3\text{MLCT}(\text{bpyam})$ to the lower lying $^3\text{MLCT}(\text{bpm})$ states on a timescale which is the same, within experimental error, of the rate observed in D_2O of 7 (± 2) ps.

ns-TRIR spectroscopy of **RubpyamideBPM** following 355 nm excitation shows that the amide bleach (at 1641 cm^{-1}) and transient (at 1652 cm^{-1}) bands then decay at the same rate, with a time constant of 77 (± 4.6) ns. The agreement of the two lifetimes obtained confirms similarity of the photophysical properties of **RubpyamideBPM** in the two solvents.

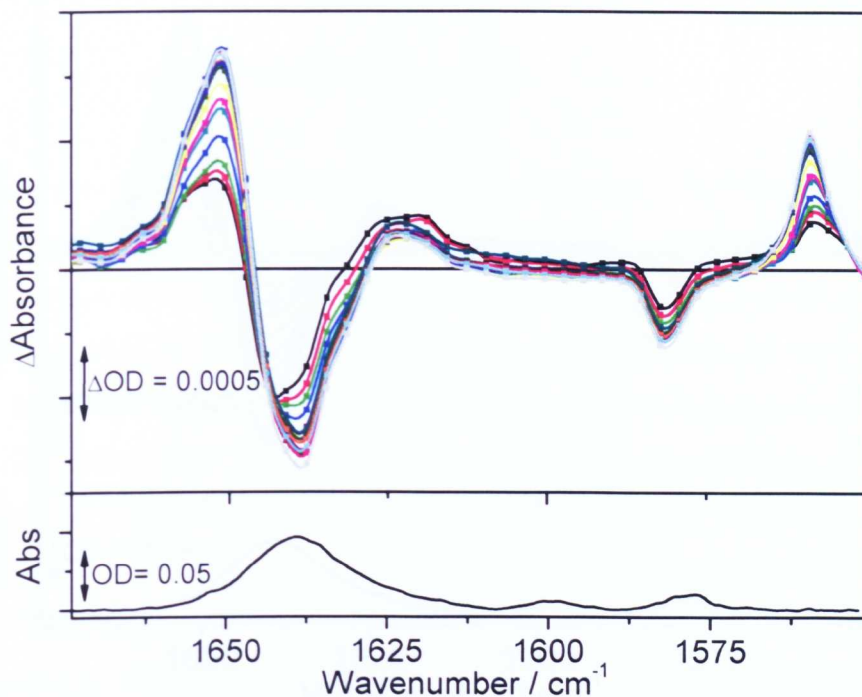


Figure 4.4.3.5: The FTIR (bottom) and ps-TRIR spectra between 1 and 1000 ps (top) of RubpyamideBPM in CH_3CN solution.

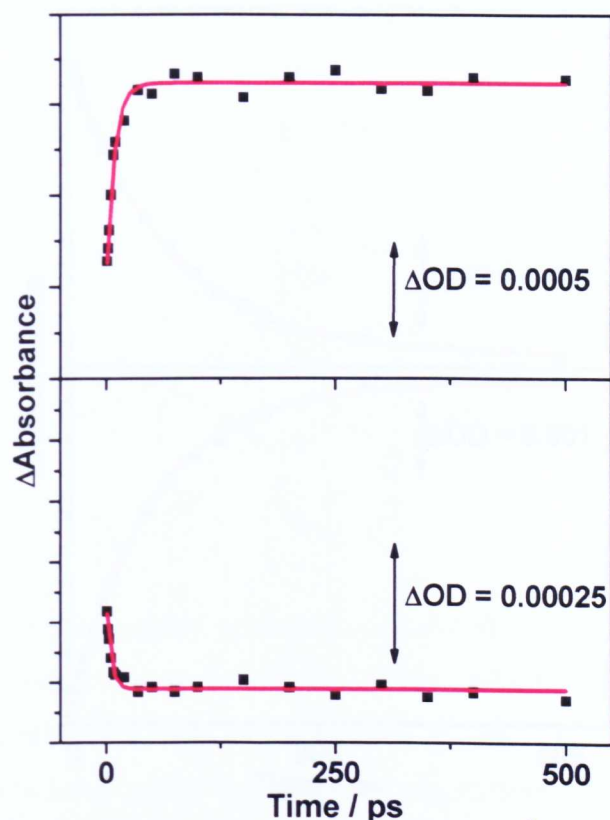


Figure 4.4.3.6: Single-pixel kinetics of bleach (1638 cm^{-1} , bottom) and transient (1652 cm^{-1} , top) ps-TRIR bands of RubpyamideBPM in CH_3CN solution.

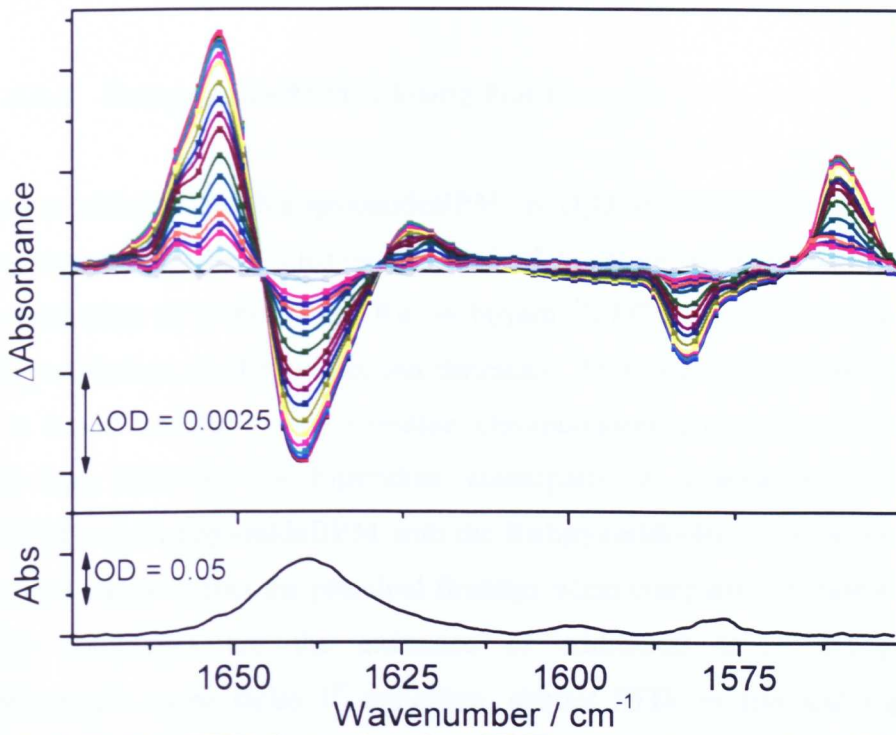


Figure 4.4.3.7: The FTIR (bottom) and ns-TRIR spectra between 1 and 500 ns (top) of RubpyamideBPM in CH_3CN solution.

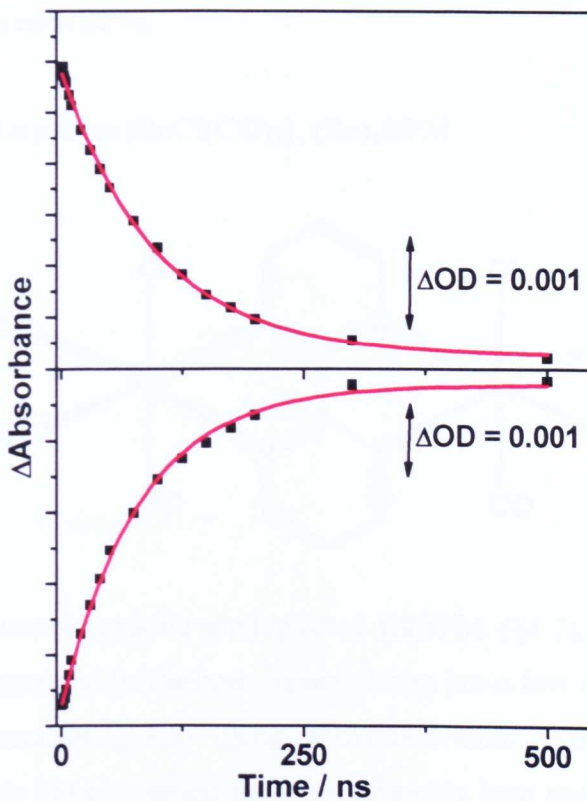
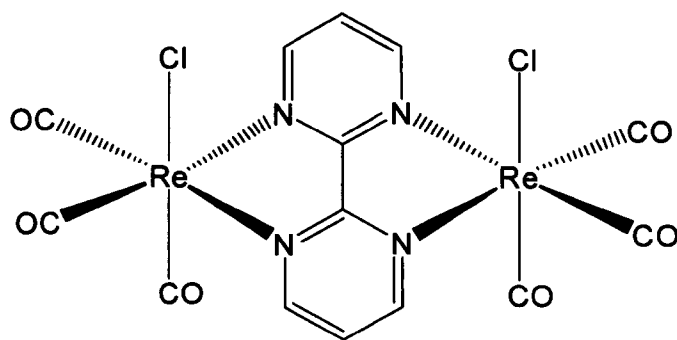


Figure 4.4.3.8: Single-pixel kinetics of bleach (1637 cm^{-1} , bottom) and transient (1652 cm^{-1} , top) ns-TRIR bands of RubpyamideBPM in CH_3CN solution.

4.4.4. RubpyamideBPM: Closing Points

The results obtained for **RubpyamideBPM** in D₂O and CH₃CN suggest that the lowest energy excited state is Ru → bpm ³MLCT in nature, although there is evidence for the formation of a short-lived Ru → bpyam ³MLCT excited state immediately following excitation on the picosecond timescale. This is consistent with our model which is based on Ru → bipyrimidine chromophores possessing lower ³MLCT energies than their Ru → bipyridine counterparts. A comparison of **ReBPM**, **RuCNBPM** and **RubpyamideBPM** with the **Rubpyamide-BL^x** complexes presented in Chapter 3 suggests that the principal findings when comparing monometallic bpm and bpy complexes are the existence of additional lower energy MLCT chromophores, a more facile 1st reduction, similar FTIR profile and significantly shorter lifetime and lower quantum yield. The results obtained for D₂O and CH₃CN are closely comparable and reiterate the lack of solvent perturbation of the electronic structure of **RubpyamideBPM**.

4.5. {(OC)₃ClRe(μ-bpm)ReCl(CO)₃}, (Re)₂BPM



(Re)₂BPM is the homobimetallic analogue of **ReBPM** (§4.2), with a second *fac*-[ReCl(CO)₃] unit appended to the bpm ligand. There are a few studies of **(Re)₂BPM** reported in the literature (§4.1) using absorption and FTIR spectroscopy and electrochemistry. We have repeated these experiments here and have conducted IR OTTL and ps-TRIR experiments in order to understand the excited state dynamics of this system. **(Re)₂BPM** is neutral and non-polar, and as such is insoluble in

aqueous media. As the complex is only slightly solvatochromic and as its properties change little with solvent the results presented in CH₃CN are taken to be representative of other solvents. Only one of the two possible configurational isomers has been drawn above – it is uncertain whether the chlorines are *syn* or *anti* to each other but this is not expected to have measurable influence on the photophysics of the system (§4.1.2).

4.5.1. UV/visible Absorption and Luminescence Spectroscopy

The UV/visible absorption spectrum of (Re)₂BPM has been measured in CH₃CN (see Appendix 4.12 for the spectrum). The results are presented in Table 4.5.1.1 and agree well with previously published results (Table 4.1.2.2).⁵ The two absorption bands are shifted to significantly longer wavelengths ($\Delta\lambda = 50\text{--}100$ nm) than in ReBPM, confirming that complexation of a second metal centre decreases the HOMO-LUMO energy gap considerably. No luminescence was detected from (Re)₂BPM in CH₃CN solution, consistent with previous observations.⁵

Solvent	$\lambda^{\max} / \text{nm}$		
	CH ₃ CN	< 300	352
Assignment	IL $\pi\text{-}\pi^*$ (bpm)	¹ MLCT (Re)	¹ MLCT (Re)

Table 4.5.1.1: Table of peak positions and assignments for UV/visible absorption spectra of (Re)₂BPM in CH₃CN solution.

4.5.2. Cyclic Voltammetry

Cyclic voltammetry of (Re)₂BPM in CH₃CN was performed (see Appendix 4.12 for voltammograms) and the results are presented in Table 4.2.2.1 below. Features corresponding to two reductions (one reversible and one irreversible) and one irreversible oxidation couple are observed. The results are comparable to previous studies of this system.⁷

$E_{1/2}/V$ (vs. Fc/Fc ⁺)	Reversibility	Assignment
$E_p = +1.30$	Irreversible	Ru ^{II/III}
-0.84	Reversible	(bpm) ^{0/+}
-1.52	Reversible	(bpm) ^{+/-2-}

Table 4.5.2.1: Table of potentials for redox couples and assignments from the cyclic voltammogram of (Re)₂BPM in CH₃CN solution.

4.5.3. FTIR, IR OTTLE and Time-Resolved Infrared Spectroscopy

(Re)₂BPM has been studied using FTIR, IR OTTLE and ps-TRIR spectroscopy in CH₃CN solution. Figure 4.5.3.1 shows the FTIR and ps-TRIR spectra obtained (Re)₂BPM in CH₃CN solution. Figure 4.5.3.2 compares the IR OTTLE (1st reduction) and TRIR difference spectra obtained in CH₃CN solution. Figure 4.5.3.3 shows the ps-TRIR kinetics obtained for bleach and transient bands in CH₃CN.

Acetonitrile Solution

FTIR Spectroscopy

The FTIR spectrum of (Re)₂BPM in CH₃CN solution in the $\nu(\text{CO})$ region has been measured. In the carbonyl region there is a peak profile characteristic of the rhenium (I) tricarbonyl unit with 3 resolved maxima at 2029, 1934 and 1921 cm⁻¹. This is in good agreement with previously published studies.⁷

Infrared Spectroelectrochemistry

The FTIR spectrum of (Re)₂BPM in CH₃CN was monitored as the complex underwent its 1st reduction. The bands originating from the neutral complex at 2029, 1934 and 1921 cm⁻¹ decrease in intensity and newly formed bands centred at 2013, 1912 and 1896 cm⁻¹ become evident. These bands at lower wavenumber correspond to an increase in electron density at the rhenium centres, consistent with the reduced electron being located on the bridging bipyrimidine ligand.

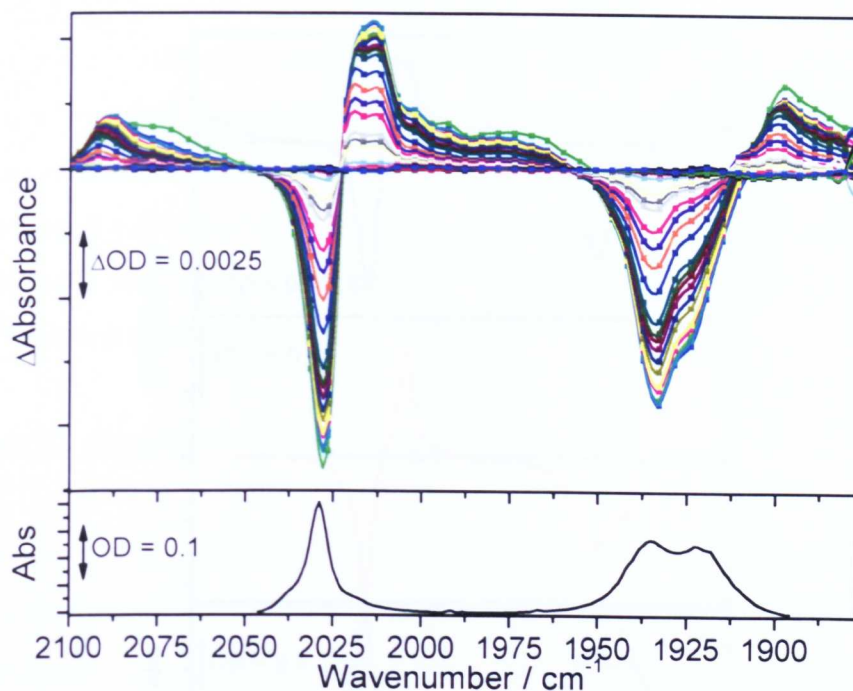


Figure 4.5.3.1: The FTIR (bottom) and ps-TRIR spectra between 1 and 1000 ps (top) of $(\text{Re})_2\text{BPM}$ in CH_3CN solution.

ps-TRIR Spectroscopy

The ps-TRIR spectral profile of $(\text{Re})_2\text{BPM}$ measured in CH_3CN following 400 nm excitation contains three bleaches at 2029, 1934 and 1921 cm^{-1} , and two sets of three transient bands are detected at lower and higher energy to the bleaches respectively. The bands to higher energy are located at 2090, 1998 and 1972 cm^{-1} and correspond to a decrease in electron density at the metal centre as a result of a $\text{Re} \rightarrow \text{bpm}^3\text{MLCT}$ transition taking place. The bands to lower energy are centred at 2015, 1900 and 1887 cm^{-1} and show good correlation with the IR bands of the reduced species $[\text{Re}(\text{bpm}^{\cdot-})\text{Re}]$ formed in the IR OTTLE experiment described above and shown in Figure 4.5.3.2. These bands are assigned to one ReCO terminus experiencing the increase in electron density at the bridging bipyrimidine (the ‘spectator’) as a result excitation of the other terminus. The $^3\text{MLCT}$ excited state is best formulated as having an asymmetric charge distribution, such that the transient structure may be written in the form $[\text{Re}(\text{bpm}^{\cdot-})\text{Re}^+]$. These results are consistent with excited state localisation on the IR timescale (§1.3), similar to other bimetallic rhenium (I) complexes previously studied using ps-TRIR spectroscopy (§4.1.3).¹⁰

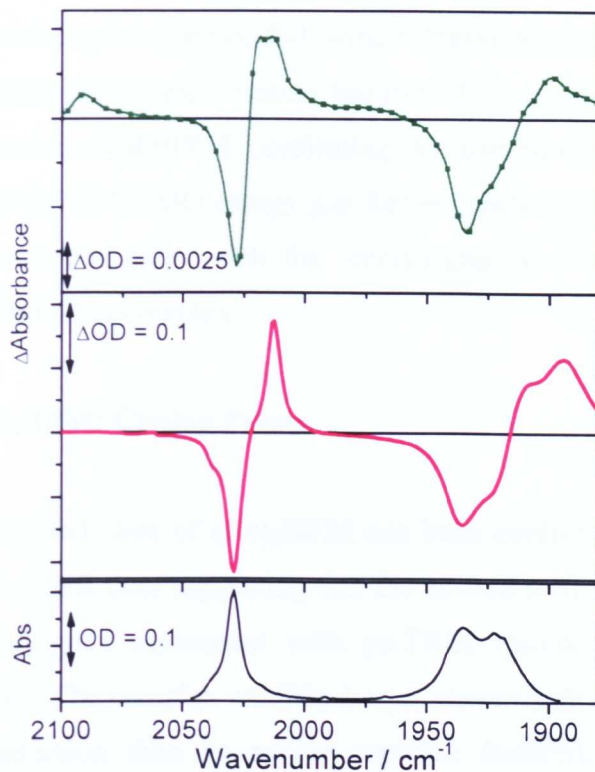


Figure 4.5.3.2: A comparison of TRIR spectrum at 100 ps (top), IR OTTLE difference spectrum (middle) and FTIR spectrum (bottom) of $(Re)_2BPM$ in CH_3CN .

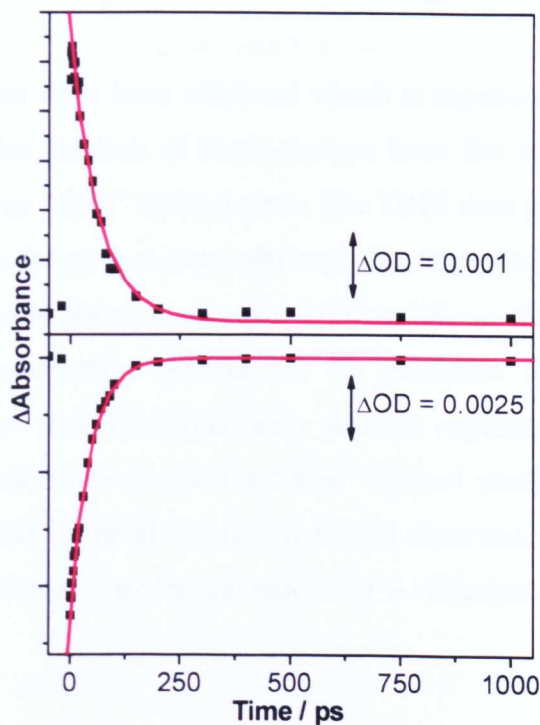


Figure 4.5.3.3: Single-pixel kinetics of bleach (2026 cm^{-1} , bottom) and transient (2013 cm^{-1} , top) ps-TRIR bands of $(Re)_2BPM$ in CH_3CN solution.

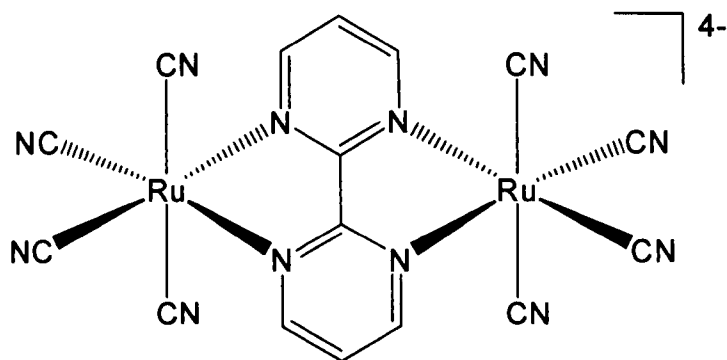
A monoexponential decay is observed following vibrational cooling, with $\tau = 46 (\pm 1)$ ps (averaged over both bleach and transient features). This is significantly shorter than the excited state lifetime of **ReBPM**, confirming that complexation of a second metal centre reduces the HOMO-LUMO energy gap further, leading to a decrease in excited state lifetime. This is consistent with the ‘energy-gap law’¹⁵ and the lack of any detected emission from this complex.

4.5.4. (Re)₂BPM: Closing Points

The lowest-lying excited state of (Re)₂BPM has been confirmed to be $\text{Re} \rightarrow \text{bpm}^3\text{MLCT}$ with the ps-TRIR data suggesting that the excited state is localised on the IR timescale (§1.3), in good agreement with ps-TRIR results reported for similar complexes (§4.1.3).¹⁰ The complex exhibits longer wavelength absorption bands and more facile 1st reduction than its model complex **ReBPM**, indicating that the complexation of a second metal to bpm reduces the HOMO-LUMO energy gap significantly through lowering of the bpm LUMO energy.

No other excited states have been observed which is significant as previous studies attempted to rationalise the lack of luminescence from this complex in terms of an unidentified low energy “dark” excited state. The TRIR data presented here does not provide any evidence for such a state, although the “snapshot-in-time” afforded by pulsed laser experiments does not provide information on the timescale of excited state localisation/delocalisation beyond the IR timescale (§1.3). In this case a delocalised-to-localised transition could be a possible explanation for the identity of the low energy absorption bands (and a “dark” excited state), but no evidence for further absorption bands in the nIR region has been observed. Such a band would be strong evidence for charge transfer transitions of a different nature *e.g.* MMCT or IVCT.

4.6. $X_4\{(\text{NC})_4\text{Ru}(\mu\text{-bpm})\text{Ru}(\text{CN})_4\}$ ($X = \text{K}, \text{PPN}$), $(\text{RuCN})_2\text{BPM}$



$(\text{RuCN})_2\text{BPM}$ is the homobimetallic analogue of RuCNBPM (§4.3), with a second $[\text{Ru}(\text{CN})_4]$ unit complexed to the bpm ligand. Unlike $(\text{Re})_2\text{BPM}$, $(\text{RuCN})_2\text{BPM}$ is highly charged, strongly solvatochromic (by virtue of its 8 cyanide ligands) and polar. It has been characterised in D_2O and CH_3CN and by analogy with other ruthenium (II) cyanide complexes is expected to display markedly different spectroscopic, photophysical and electrochemical properties in the two solvents.

4.6.1. UV/visible Absorption and Luminescence Spectroscopy

The UV/visible absorption spectra of $(\text{RuCN})_2\text{BPM}$ has been measured in CH_3CN and D_2O (see Appendix 4.12 for spectra). The strong negative solvatochromism is clearly evident in the differences in peak positions in the two solvents. The results are summarised in Table 4.6.1.1. No luminescence from $(\text{RuCN})_2\text{BPM}$ was detected in either solvent.

Solvent	$\lambda^{\text{max}} / \text{nm}$			
	D_2O	< 300	362	492
CH_3CN	< 300	400	434	478
Tentative Assignment	IL $\pi\text{-}\pi^*$ (bpm)	$^1\text{MLCT}$ (Ru)	$^1\text{MLCT}$ (Ru)	$^1\text{MLCT}$

Table 4.6.1.1: Table of peak positions and assignments for UV/visible absorption spectra of $(\text{RuCN})_2\text{BPM}$ in D_2O and CH_3CN solutions.

4.6.2. Cyclic Voltammetry

Cyclic voltammetry of $(\text{RuCN})_2\text{BPM}$ was measured in CH_3CN (see Appendix 4.12 for voltammograms) and the results are presented in Table 4.6.2.1 below. Features corresponding to one irreversible reduction and one irreversible oxidation couple are observed.

$E_{1/2}/V$ (vs. Fc/Fc^+)	Reversibility	Assignment
$E_p = +1.46$	Irreversible	$\text{Ru}^{\text{II/III}}$
$E_p = -0.43$	Irreversible	$(\text{bpm})^{0/e-}$

Table 4.6.2.1: Table of potentials for redox couples and assignments from the cyclic voltammogram of $(\text{RuCN})_2\text{BPM}$ in CH_3CN solution.

4.6.3. FTIR, IR OTTLE and Time-Resolved Infrared Spectroscopy

$(\text{RuCN})_2\text{BPM}$ has been studied using FTIR and ps-TRIR spectroscopy in D_2O and CH_3CN solution. IR OTTLE of $(\text{RuCN})_2\text{BPM}$ in CH_3CN was unsuccessful as both oxidation and reduction couples investigated were found to be chemically irreversible on the timescale of the experiment.

Deuterium Oxide Solution

Figure 4.6.3.1 shows the FTIR and ps-TRIR spectra of $(\text{RuCN})_2\text{BPM}$ measured in D_2O solution. Figure 4.6.3.2 shows the ps-TRIR kinetics obtained for bleach and transient bands in D_2O .

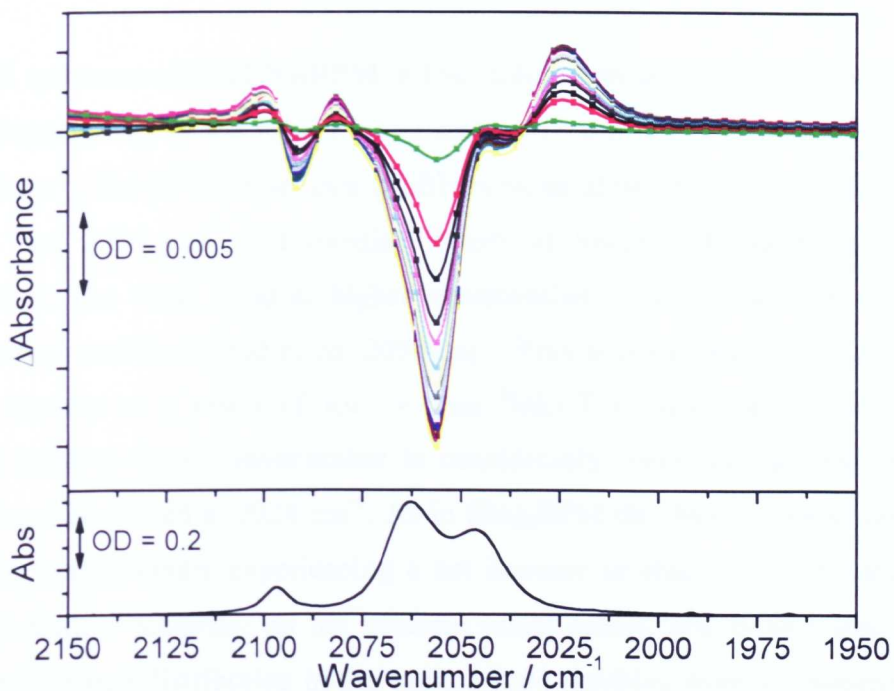


Figure 4.6.3.1: The FTIR (bottom) and ps-TRIR spectra between 1 and 1000 ps (top) of $(\text{RuCN})_2\text{BPM}$ in D_2O solution.

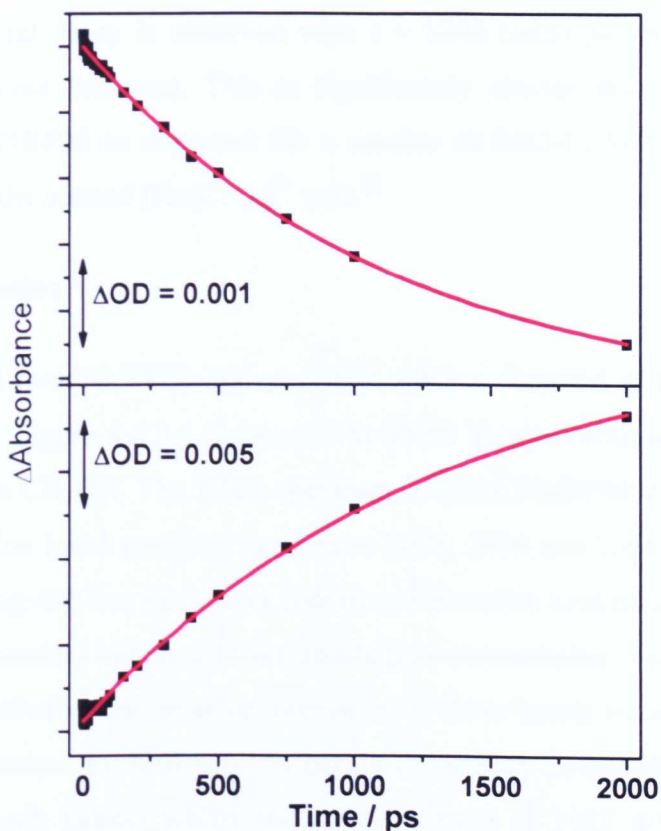


Figure 4.6.3.2: Single-pixel kinetics of bleach (2056 cm^{-1} , bottom) and transient (2022 cm^{-1} top) ps-TRIR bands of $(\text{RuCN})_2\text{BPM}$ in D_2O solution.

The FTIR spectrum of **(RuCN)₂BPM** in D₂O solution in the $\nu(\text{CN})$ region has a peak profile characteristic of the tetracyanoruthenate (II) unit with maxima at 2096, 2063 and 2046 cm⁻¹. The ps-TRIR spectral profile consists of two resolved bleaches centred at 2092 and 2056 cm⁻¹ and transient bands at lower and higher wavenumber respectively. The weak band at higher wavenumber overlaps with the small high energy bleach and is centred at *ca.* 2094 cm⁻¹. This is consistent with a decrease in electron density as a result of Ru → bpm ³MLCT excited state formation. The transient band to lower wavenumber is considerably more intense than the other transient and is centred at 2024 cm⁻¹. As in **(Re)₂BPM** this band is associated with a ‘spectating’ metal centre experiencing a net increase in electron density due to the MLCT transition occurring on the adjacent metal centre, and is thus indicative of asymmetric charge distribution in the excited state resulting from a localised excited state *viz.* **[RuCN(bpm⁻)RuCN⁺]**.

A monoexponential decay is observed with $\tau = 1200 (\pm 85)$ ps (averaged over both bleach and transient features). This is significantly shorter than the excited state lifetime of **RuCNBPM** as expected for a smaller HOMO-LUMO energy gap after complexation of the second **[Ru(CN)₄]²⁻** unit.¹⁵

Acetonitrile Solution

Figure 4.6.3.3 shows the FTIR and ps-TRIR spectra obtained of **(RuCN)₂BPM** in CH₃CN solution. Figure 4.6.3.4 shows the ps-TRIR kinetics obtained for bleach and transient bands in CH₃CN. The FTIR spectrum of **(RuCN)₂BPM** in CH₃CN solution in the $\nu(\text{CN})$ region has 3 resolved maxima at 2088, 2055 and 2038 cm⁻¹. The profile obtained following 400 nm excitation consists of bleaches centred at 2088, 2055 and 2038 cm⁻¹ and transient bands at lower and higher wavenumber, centred at 2015 and 2067 cm⁻¹ respectively. The relative intensities of these bands receive close scrutiny below as the transient at 2067 cm⁻¹ is barely detectable (presumably due to heavy overlap with bleach bands) whilst the transient band at 2015 cm⁻¹ dominates the spectrum, having a considerably larger absorbance and width than the sum total of the three bleach bands.

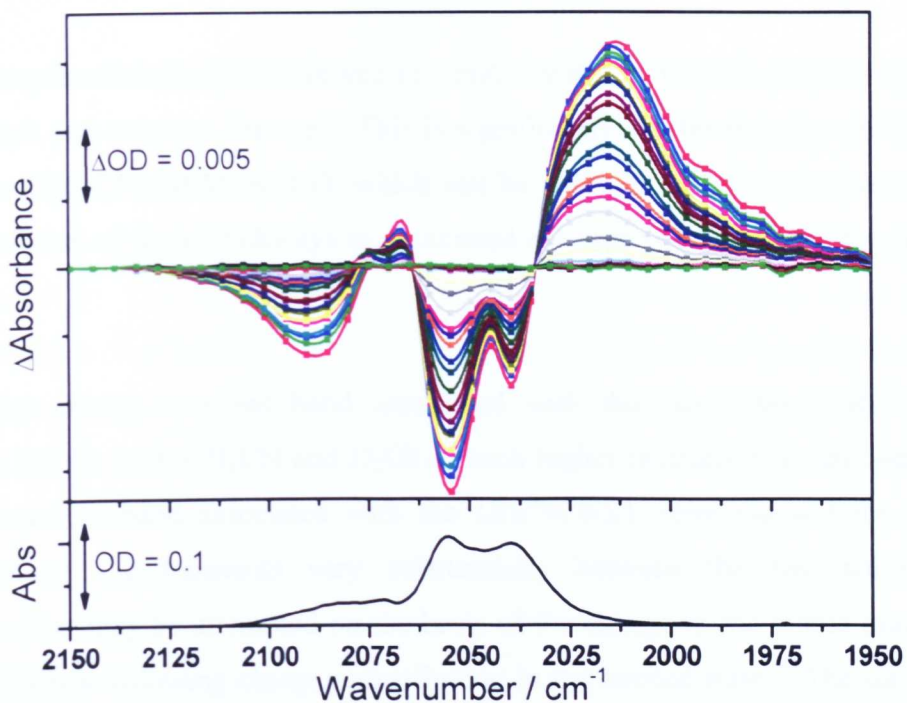


Figure 4.6.3.3: The FTIR (bottom) and ps-TRIR spectra between 1 and 1000 ps (top) of $(\text{RuCN})_2\text{BPM}$ in CH_3CN solution.

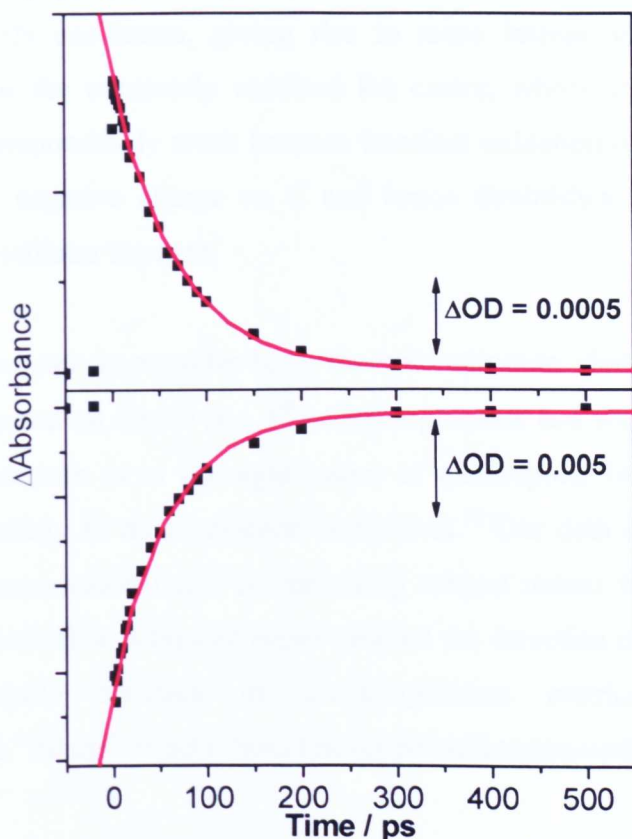


Figure 4.6.3.4: Single-pixel kinetics of bleach (2055 cm^{-1} , bottom) and transient (213 cm^{-1} , top) ps-TRIR bands of $(\text{RuCN})_2\text{BPM}$ in CH_3CN solution.

A monoexponential decay is observed in CH₃CN with $\tau = 65 (\pm 2)$ ps (averaged over both bleach and transient features). This is significantly shorter than the excited state lifetime of (RuCN)₂BPM in D₂O, which can be attributed to two principal reasons: the attenuation of decay pathways in deuterated solvents (§2.1.2),¹⁷ and the ‘energy-gap law’.¹⁵

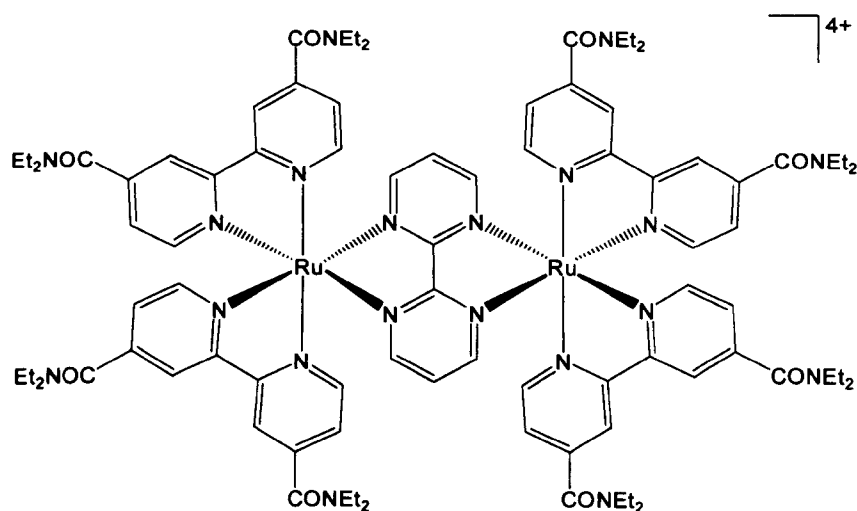
The lower energy transient band associated with the ‘spectating’ [Ru^{II}(CN)₄]²⁻ terminus has (in both CH₃CN and D₂O) a much higher intensity than the weak high energy transient band associated with the {Ru^{III}(CN)₄}⁻ terminus and the relative intensities of the transients vary substantially between the two solvents. A rationalisation may be attempted on the basis of the change in the dipole moment of the C≡N bonds following charge redistribution in the excited state.¹⁸ The increase in electron density at the spectating Ru centre in the excited state leads to an increase in the negative charge on the C atoms and hence an increase in the effective dipole moment of the C≡N oscillators, giving rise to more intense $\nu(\text{CN})$ bands. The converse is true for the transiently oxidised Ru centre, whose $\nu(\text{CN})$ band in the excited state is correspondingly weak because transient oxidation of the metal centre reduces the partial negative charge on C and hence diminishes the C-N^+ dipole, decreasing the IR oscillator strength.

There is a *caveat emptor* to consider here; the rationalisation above on IR intensity rationalisations is based on dipole (*i.e.* 1st order) arguments and there is some debate in the scientific literature as to the significance of quadrupolar (or even octupolar) interactions, particularly in metal cyanide complexes.¹⁸ Our data don’t provide any insight into this phenomenon but it is interesting subject matter for a future study. Given that the author’s first published paper detailed the detection of an unexpectedly stable dipole-octupole complex in low-temperature matrices using FTIR spectroscopy¹⁹ such “minor” effects should never be underestimated!

4.6.4. (RuCN)₂BPM: Closing Points

The lowest-lying excited state of (RuCN)₂BPM has been confirmed to be Ru → bpm ³MLCT with the ps-TRIR data suggesting that the excited state is localised on the IR timescale (§1.3). The complex exhibits longer wavelength absorption bands than its model complex RuCNBPM, reinforcing the assertion that the complexation of a second metal to bpm considerably reduces the HOMO-LUMO energy gap through lowering of the bpm LUMO energy. The system exhibits markedly different TRIR spectroscopy and kinetics in the two solvent environments used, consistent with SSDA interactions between the solvent sphere and the system's eight cyanide ligands.

4.7. {((5,5'-CONEt₂)₂bpy)₂Ru(μ-bpm)Ru((5,5'-CONEt₂)₂bpy)₂}Cl₄, (Rubpyamide)₂BPM



(Rubpyamide)₂BPM is the homobimetallic analogue of RubpyamideBPM (§4.4), with a second [Ru((5,5'-CONEt₂)₂bpy)₂] unit appended to the bpm ligand. Complexes similar to (Rubpyamide)₂BPM have been studied before in the literature, most notably [(bpy)₂Ru(μ-bpm)Ru(bpy)₂]⁴⁺ (§4.1). Comparison of the results with those of RubpyamideBPM will provide insight into the ground and excited state electronic structure of these complexes.

(Rubpyamide)₂BPM is highly charged and polar, and as such is soluble in a wide range of solvents. The results obtained in D₂O and CH₃CN will be discussed here. As the complex is only slightly solvatochromic, small differences in properties are expected between the two solvents.

4.7.1. UV/visible Absorption and Luminescence Spectroscopy

The UV/visible absorption spectra of **(Rubpyamide)₂BPM** have been measured in D₂O and CH₃CN (see Appendix 4.12 for spectra) and the results are summarised in Table 4.7.1.1. The absorption spectra of these complexes are only slightly affected by solvent, with differences of a few nanometers wavelength between related absorption maxima in D₂O and CH₃CN. As with **RubpyamideBPM** more low energy absorption bands are observed in comparison with the other homobimetallic complexes, owing to the presence of Ru → bpyamide ¹MLCT transitions in addition to the Ru → bpm ¹MLCT transitions. There are two transitions, at *ca.* 420 and 400 nm, whose positions do not vary significantly with either solvent or nuclearity (when analysed in conjunction with **RubpyamideBPM**) and hence are assigned to the Ru → bpyamide ¹MLCT transitions. The bands at *ca.* 530 and 360 nm are assigned to two Ru → bpm ¹MLCT transitions, consistent with the presence of two different low-lying π* bpm orbitals giving two ¹MLCT transitions to the bpm ligand. These results correlate well with a previous study of [(Ru(bpy)₂)₂(μ-bpm)]⁴⁺.⁷

Solvent	$\lambda^{\max} / \text{nm}$					
	D ₂ O	< 300	358	396	416	530
CH ₃ CN	< 300	360	400	424	526	581
Assignment	IL π-π* (bpm)	¹ MLCT (Ru-bpm)	¹ MLCT (Ru- bpyamide)		¹ MLCT (Ru-bpm)	¹ MLCT (Ru-bpm)

Table 4.7.1.1: Table of peak positions and assignments for UV/visible absorption spectra of (Rubpyamide)₂BPM in D₂O and CH₃CN solution.

The luminescence of **(Rubpyamide)₂BPM** in CH₃CN is much weaker than that of **RubpyamideBPM** but detectable at room temperature, with a broad structureless

emission peak centred at 774 nm (see Appendix 4.12 for spectra). The luminescence intensity was insufficient to determine the excited state lifetime or quantum yield.

4.7.2. Cyclic Voltammetry

Cyclic voltammetry of **(Rubpyamide)₂BPM** was performed in CH₃CN (see Appendix 4.12 for voltammograms) and the results are presented in Table 4.7.2.1 below. Features corresponding to four reversible reductions and one irreversible oxidation couple are observed. The results are comparable to those obtained for **RubpyamideBPM**, with the notable difference of a significantly lower 1st reduction potential. This is consistent with a lowering of the LUMO energy of the bpm ligand upon complexation of the second metal centre.

$E_{1/2}/V$ (vs. Fc/Fc ⁺)	Reversibility	Assignment
$E_p = +1.54$	Irreversible	Amide oxidation
-0.68	Reversible	(bpm) ^{0/-}
-1.35	Reversible	Amide reduction
-1.65	Reversible	Amide reduction
-1.85	Reversible	Amide reduction

Table 4.7.2.1: Table of potentials for redox couples and assignments from the cyclic voltammogram of (Rubpyamide)₂BPM in CH₃CN solution.

4.7.3. FTIR, IR OTTLE and Time-Resolved Infrared Spectroscopy

(Rubpyamide)₂BPM has been studied using FTIR and ps and ns-TRIR spectroscopy in D₂O and CH₃CN solution. An IR OTTLE experiment to monitor the changes in the FTIR spectrum of the complex in CH₃CN as it underwent its 1st reduction showed no spectral changes. As was the case with **RubpyamideBPM** this is consistent with little electronic coupling between the bipyrimidine bridging ligand and the bpyamide ligands.

Deuterium Oxide Solution

Figures 4.7.3.1 and 4.7.3.3 show the FTIR, ps-TRIR and ns-TRIR spectra obtained of **(Rubpyamide)₂BPM** in D₂O solution. Figures 4.7.3.2 and 4.7.3.4 show the ps and ns-TRIR kinetics obtained for bleach and transient bands in D₂O. The FTIR spectrum of **(Rubpyamide)₂BPM** in D₂O solution in the amide $\nu(\text{CO})$ region has a single amide peak present at 1614 cm⁻¹.

Picosecond TRIR spectra show that upon excitation the parent $\nu(\text{CO})$ band is bleached and a transient band is observed at higher energy centred at 1634 cm⁻¹. The bleach band appears to grow in with a time constant of 7 (\pm 1) ps. This is thought to be an artefact due to heavy overlap with associated transient bands (see below) which imprint their dynamics on the single-pixel bleach trace as observed in other complexes containing the bpyamide ligand in this Chapter. As with **RubpyamideBPM** initial excitation is non-selective so both [(bpyam)(bpyam^{•-})Ru^{III}(bpm)Ru^{II}(bpyam)₂]⁴⁺ (hereafter ³MLCT(bpyamide)) and [(bpyam)₂Ru^{III}(bpm^{•-})Ru^{II}(bpyam)₂]⁴⁺ (hereafter ³MLCT(bpm)) triplet excited states are expected on the picosecond timescale, the latter being significantly lower in energy (as demonstrated by UV/vis spectroscopy, *vide supra*). As with **RubpyamideBPM**, the transient $\nu(\text{CO})$ band which is shifted to higher energy can be used to monitor the formation and decay of the ³MLCT(bpm) excited state. In D₂O this transient grows in with a time constant of 9 (\pm 1) ps. In contrast to the results obtained for **RubpyamideBPM**, no transient band to lower wavenumber is observed. This has been confirmed through scaled subtraction and fitting analysis (not shown). There are no further significant changes during the picosecond timescale.

ns-TRIR spectroscopy (with excitation at 355 nm) gives an analogous profile to the ps-TRIR spectra (*vide supra*), with the parent bleach centred at 1614 cm⁻¹ and a transient centred at 1634 cm⁻¹. These bands decay synchronously with a lifetime of 6.8 (\pm 1.6) ns. This behaviour is consistent with internal conversion of the higher-lying ³MLCT(bpyamide) state to the lower-lying ³MLCT(bpm) state, formally by internal

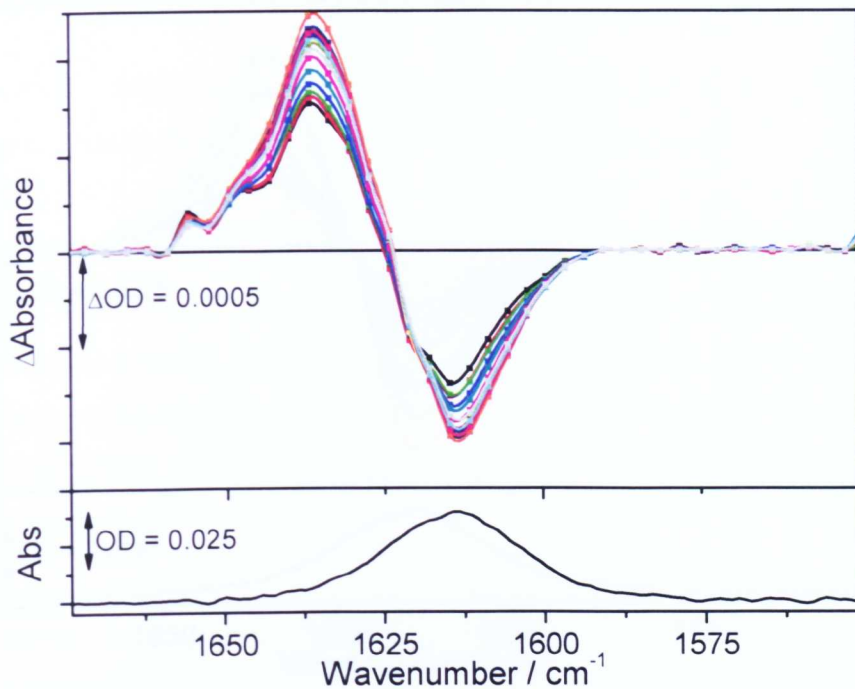


Figure 4.7.3.1: The FTIR (bottom) and ps-TRIR spectra between 1 and 1000 ps (top) of (Rubpyamide)₂BPM in D₂O solution.

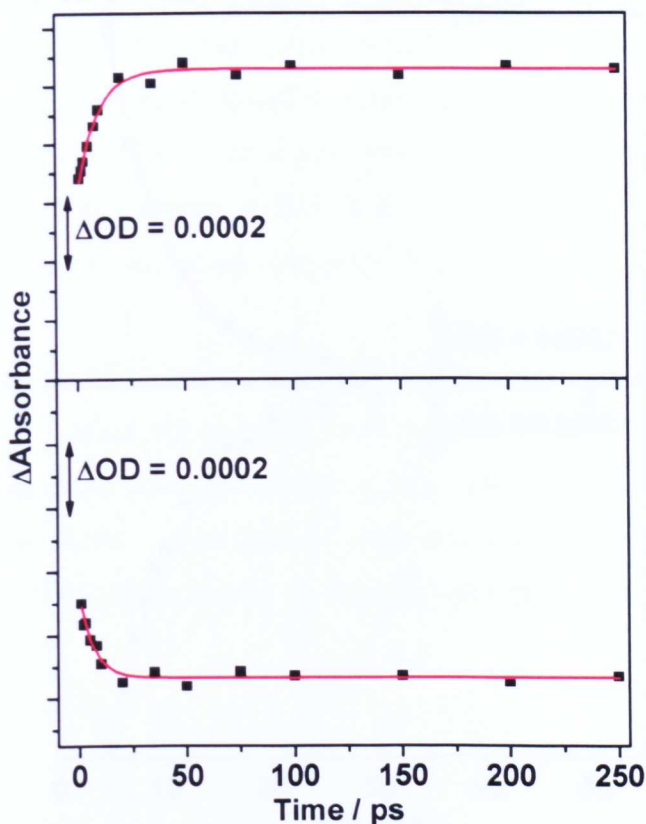


Figure 4.7.3.2: Single-pixel kinetics of bleach (1611 cm⁻¹, bottom) and transient (1635 cm⁻¹, top) ps-TRIR bands of (Rubpyamide)₂BPM in D₂O solution.

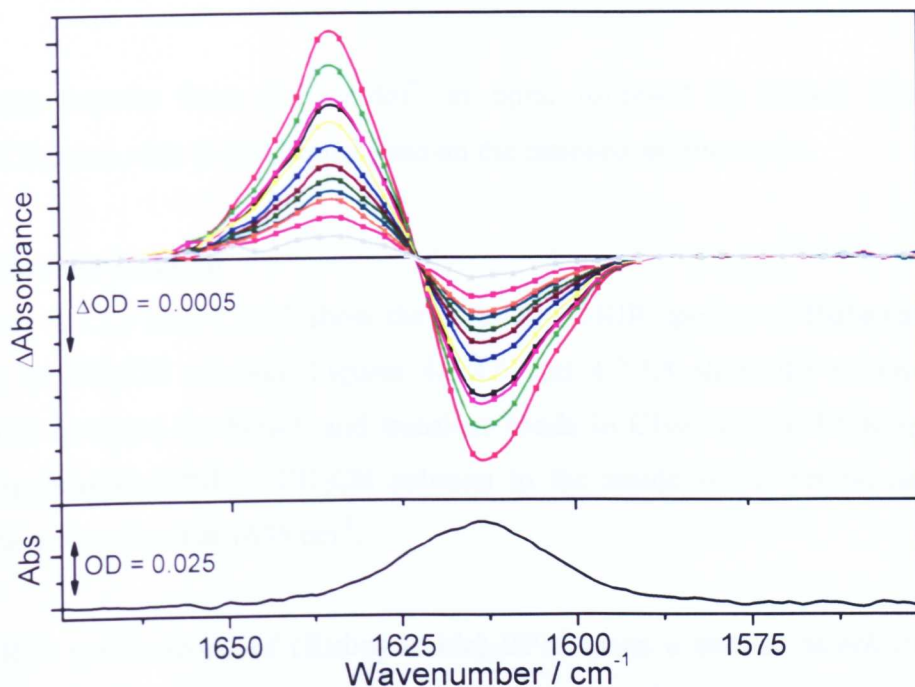


Figure 4.7.3.3: The FTIR (bottom) and ns-TRIR spectra between 1 and 100 ns (top) of (Rubpyamide)₂BPM in D₂O solution.

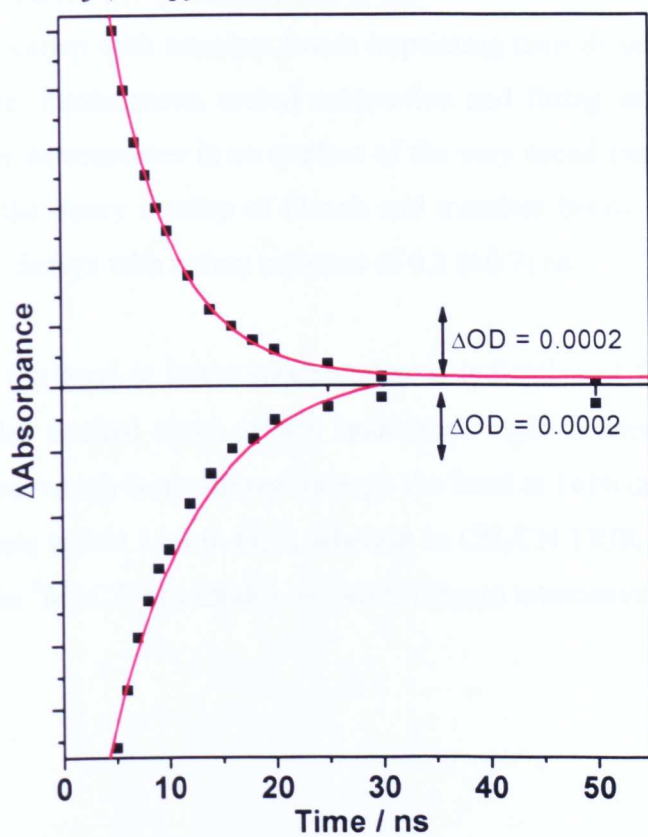


Figure 4.7.3.4: Single-pixel kinetics of bleach (1613 cm⁻¹, bottom) and transient (1637 cm⁻¹, top) ns-TRIR bands of (Rubpyamide)₂BPM in D₂O solution.

electron transfer from (bpyamide)⁻ to bpm, followed by slower decay of the ³MLCT(bpm) state to the ground state on the nanosecond timescale.

Acetonitrile Solution

Figures 4.7.3.5 and 4.7.3.7 show the ps and ns-TRIR spectra of **RubpyamideBPM** taken in CH₃CN solution. Figures 4.7.3.6 and 4.7.3.8 show the ps and ns-TRIR kinetics obtained for bleach and transient bands in CH₃CN. The FTIR spectrum of **(Rubpyamide)₂BPM** in CH₃CN solution in the amide ν(CO) region has a single amide peak present at 1635 cm⁻¹.

ps-TRIR spectroscopy of **(Rubpyamide)₂BPM** gives a similar bleach of the main ν(CO) amide band following 400 nm excitation as in D₂O, but interestingly transient bands to lower and higher wavenumber are observed, centred at 1616 and 1646 cm⁻¹ respectively. As in D₂O, the bleach appears to grow in with a time constant of 4 (± 2) ps due to heavy overlap with transient bands imprinting their dynamics on the single-pixel kinetic trace. Furthermore, scaled subtraction and fitting analysis showed that this peak to lower wavenumber is an artefact of the very broad transient at 1646 cm⁻¹ compounded by the heavy overlap of bleach and transient bands. The ³MLCT(bpm) excited state then decays with a time constant of 6.2 (±0.7) ns.

The presence of the band at lower wavenumber is indicative of the detection of the ³MLCT(bpyamide) excited state, which undergoes rapid interconversion into the ³MLCT(bpm) state which is monitored through the band at 1616 cm⁻¹. Ostensibly this process is complete within 1 ps in D₂O, whereas in CH₃CN TRIR spectroscopy gives a time constant for ³MLCT(bpyamide) → ³MLCT(bpm) interconversion of 14 (±3) ps.

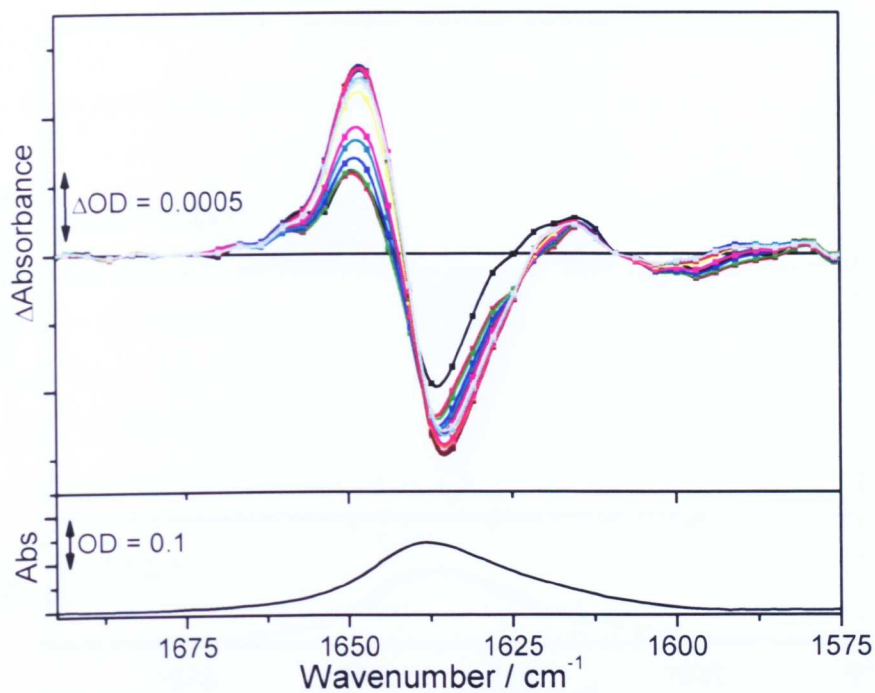


Figure 4.7.3.5: The FTIR (bottom) and ps-TRIR spectra between 1 and 1000 ps (top) of (Rubpyamide)₂BPM in CH₃CN solution.

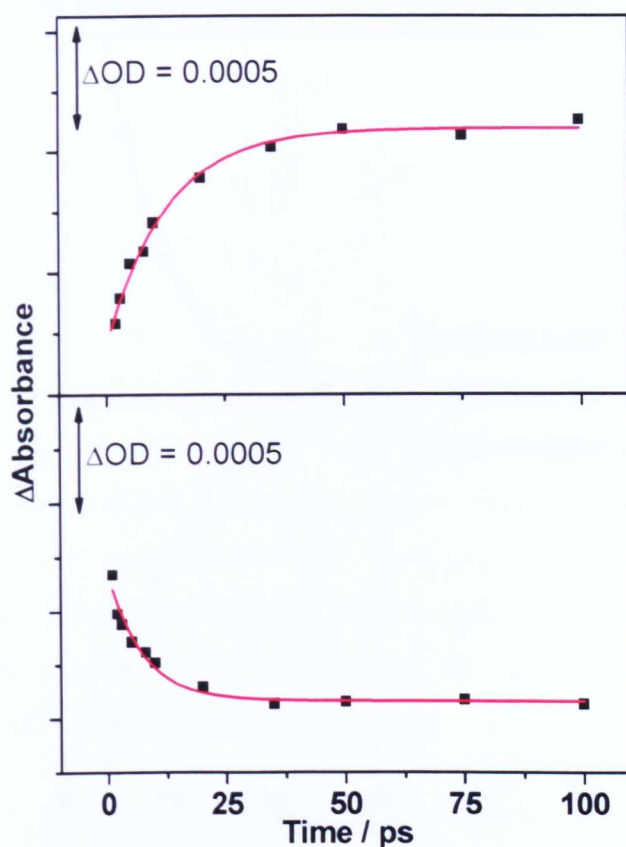


Figure 4.7.3.6: Single-pixel kinetics of bleach (1635 cm^{-1} , bottom) and transient (1648 cm^{-1} , top) ps-TRIR bands of (Rubpyamide)₂BPM in CH₃CN solution.

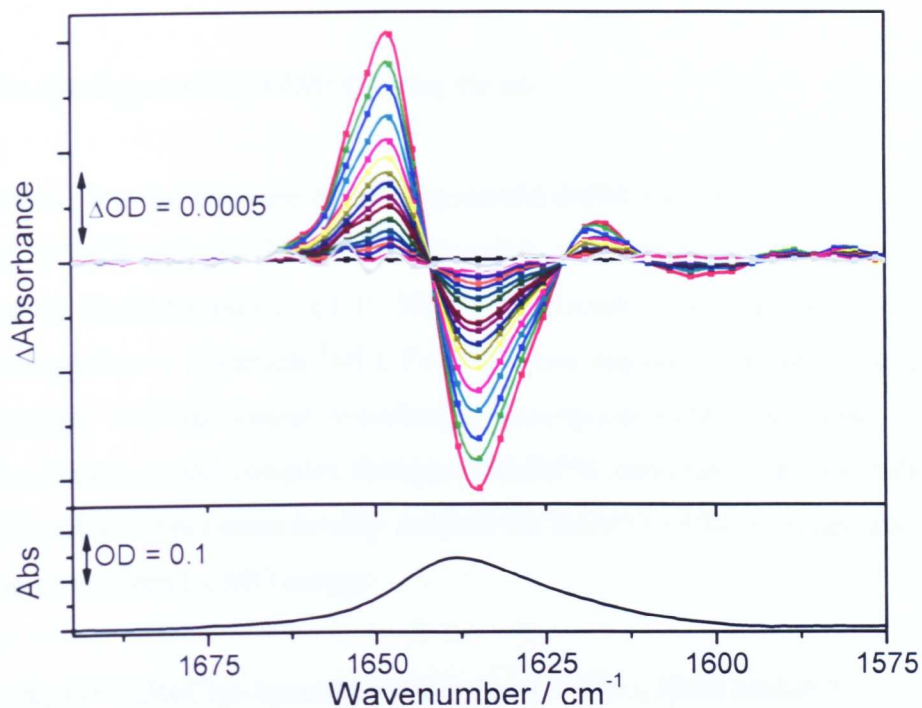


Figure 4.7.3.7: The FTIR (bottom) and ns-TRIR spectra between 1 and 100 ns (top) of (Rubpyamide)₂BPM in CH₃CN solution.

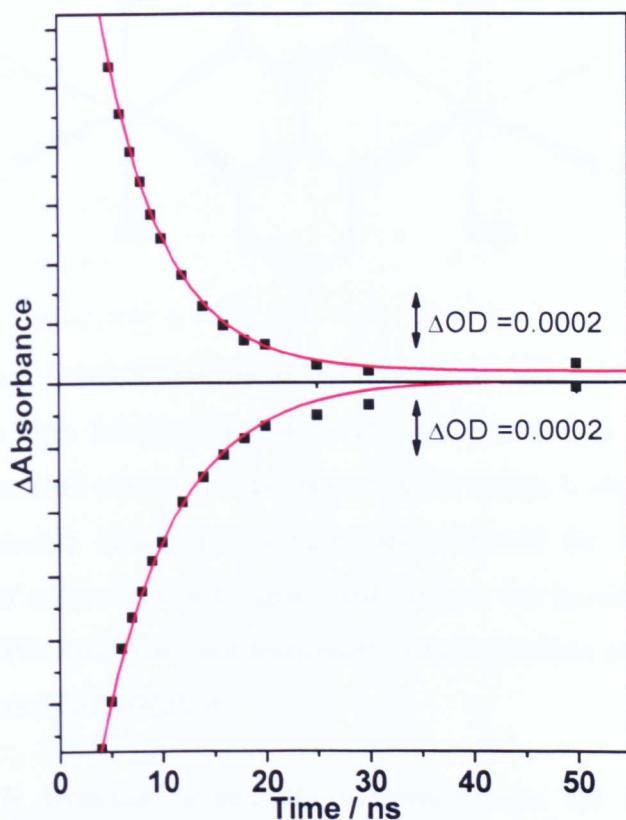
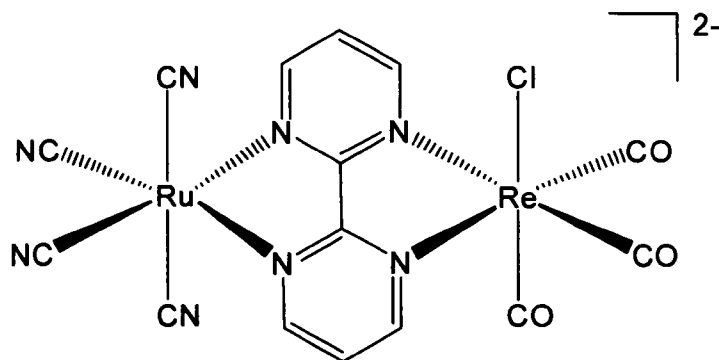


Figure 4.7.3.8: Single-pixel kinetics of bleach (1636 cm⁻¹, bottom) and transient (1648 cm⁻¹, top) ns-TRIR bands of (Rubpyamide)₂BPM in CH₃CN solution.

4.7.4. (Rubpyamide)₂BPM: Closing Points

The lowest-lying excited state of (Rubpyamide)₂BPM has been confirmed to be Ru → bpm ³MLCT with the TRIR data ostensibly suggesting that the excited state is localised on the IR timescale (§1.3). The initial formation and subsequent decay of a higher energy Ru → bpyamide ³MLCT excited state has been observed in some cases. The complex exhibits longer wavelength absorption bands and more facile 1st reduction than its model complex RubpyamideBPM, reiterating that complexation of a second metal to bpm considerably reduces the HOMO-LUMO energy gap through lowering of the bpm LUMO energy.

4.8. X₂{(OC)₃ReCl(μ-bpm)Ru(CN)₄} (X = K, PPN), ReBPMRuCN



ReBPMRuCN is a heterobimetallic complex with ReCO and RuCN termini on either side of the bpm bridging ligand. Each terminus has an M → bpm MLCT chromophore associated with it. As the bipyrimidine bridge is conjugated and strong intermetallic electronic coupling has been demonstrated for the homobimetallic complexes studied earlier in this Chapter (*vide supra*) the ground and excited state properties of ReBPMRuCN are not necessarily a superposition of those observed for ReBPMRe and RuCNBPMRuCN.

Whilst the RuCN terminus is strongly solvatochromic, the ReCO terminus is essentially solvent-independent. This will ostensibly lead to differences in the photophysical and spectroscopic properties of ReBPMRuCN in D₂O and CH₃CN,

although the differences in $^1\text{MLCT}$ transition energies of **ReBPM** and **RuCNBPM** ($\Delta^1_{\text{MLCT}} = 3300\text{-}9150\text{ cm}^{-1}$ depending on solvent; calculated from absorption spectra) are of sufficient magnitude to render solvent-based switching of the location of the excited state unlikely; $\text{Ru} \rightarrow \text{bpm } ^3\text{MLCT}$ is expected to be the lowest energy excited state in both CH_3CN and D_2O .

4.8.1. UV/visible Absorption and Luminescence Spectroscopy

The UV/visible absorption spectra of **ReBPMRuCN** have been measured in D_2O and CH_3CN (see Appendix 4.12 for spectra). It is difficult to discern peak maxima in the spectra as very broad features dominate the spectrum across the visible region. The peaks maxima extracted are reported in Table 4.8.1.1. The emission spectrum of **ReBPMRuCN** has been measured in CH_3CN solution. No luminescence was detected.

Solvent	$\lambda^{\text{max}} / \text{nm}$		
	D_2O	< 300	384
CH_3CN	< 300	328	434
Tentative Assignment	IL $\pi\text{-}\pi^*$	$^1\text{MLCT}$	$^1\text{MLCT}$
Location	bpm	ReCO	RuCN

*Table 4.8.1.1: Table of peak positions and assignments for UV/visible absorption spectra of **ReBPMRuCN** in D_2O and CH_3CN solutions.*

4.8.2. Cyclic Voltammetry

Cyclic voltammetry of **ReBPMRuCN** in D_2O has been measured (see Appendix 4.12 for voltammograms) and the results are presented in Table 4.8.2.1 below. Features corresponding to one reversible reduction and two oxidation couples (one reversible and one irreversible) are observed. It is noteworthy to mention the ease of reduction of the bipyrimidine ligand in this case – the redox couple's proximity to 0 V indicates that this redox process may be accessible in the absence of electrical current, which

could have important implications for the electrochemical equilibrium mixture of electronic structures of the ground and excited states of **ReBPMRuCN** in solution.

$E_{1/2}/V$ (vs. Fc/Fc^+)	Reversibility	Tentative Assignment
$E_p = +1.17$	Irreversible	Re^{II}
+0.87	Reversible	$Ru^{II/III}$
$E_p = +0.23$	Reversible	$(bpm)^{0/+}$

Table 4.8.2.1: Table of potentials for redox couples and assignments from the cyclic voltammogram of **ReBPMRuCN in CH_3CN solution.**

4.8.3. FTIR, IR OTTLE and Time-Resolved Infrared Spectroscopy

ReBPMRuCN has been studied using FTIR and ps and ns-TRIR spectroscopy in D_2O and CH_3CN solutions. As a result of the negative solvatochromism of the **RuCN** terminus differences in the two solvents are expected, but the identity of the lowest energy excited is predicted to be $Ru \rightarrow bpm^3MLCT$ in either case.

IR OTTLE of **ReBPMRuCN** in CH_3CN was unsuccessful as the 1st reduction couple was found to be chemically irreversible on the timescale of the experiment.

Deuterium Oxide Solution

The FTIR spectrum of **ReBPMRuCN** has been measured in D_2O solution (Figure 4.8.3.1). In the cyanide region there is a peak profile characteristic of the tetracyanoruthenate (II) unit with resolved maxima at 2071 and 2045 cm^{-1} . In the carbonyl region there are peaks present at 2022 and 1908 cm^{-1} . These results are broadly comparable with the FTIR spectra of the model complexes **ReBPM** and **RuCNBPM** (§4.2.3, §4.3.3).

Picosecond and nanosecond TRIR spectroscopy (with laser excitation at 400 and 355 nm respectively) were performed on **ReBPMRuCN** in D₂O solution, monitoring both regions in the IR where reporter groups are present.

ps-TRIR Spectroscopy

Figure 4.8.3.1 shows the ps-TRIR spectra obtained for the **ReCO** and **RuCN** termini in D₂O. Figure 4.8.3.2 shows the ps-TRIR kinetics obtained for bleach and transient bands in D₂O. It is immediately apparent that the features arising from the two termini overlap, giving rise to a dense, feature-rich spectrum between 2100 and 1800 cm⁻¹. By analogy with **(Re)₂BPMRe** and **(RuCN)₂BPM** (§4.5.3, §4.6.3) we would expect TRIR spectroscopy to detect a localised excited state (on the IR timescale) with one set of transient bands shifted to higher energy than their bleach, and one set shifted lower. Combining this with the unselective (400 nm) excitation used for the ps-TRIR experiments, this would give bands at higher and lower wavenumber to the parent bleaches for both termini. This has important implications for the following analysis.

RuCN (Lower Energy) terminus

The parent bleach of the **RuCN** terminus is barely visible at 2051 cm⁻¹ as it is surrounded by a small transient to higher wavenumber centred at 2092 cm⁻¹ and a broad, intense transient to lower energy centred at about 1979 cm⁻¹, which dominates the spectrum. These two transient features can be assigned to Ru → bpm and Re → bpm ³MLCT excited states respectively. In the latter case the **RuCN** terminus is sensing the increase in electron density on the bpm bridging ligand as a result of a MLCT transition involving the other metal centre. There are strong similarities to the spectra of **(RuCN)₂BPM** and the reasons for the low energy feature's intensity are explained in detail in §4.6.3.

The **RuCN** bands decay polyexponentially with a very fast component [$\tau_1 < 1$ ps] and a slower component $\tau_2 = 135 (\pm 15)$ ps. At $\Delta t = 1$ ns less than *ca.* 5% of the signal at $\Delta t = 1$ ps remains, indicating that quenching of the excited state is almost complete during the picosecond time domain.

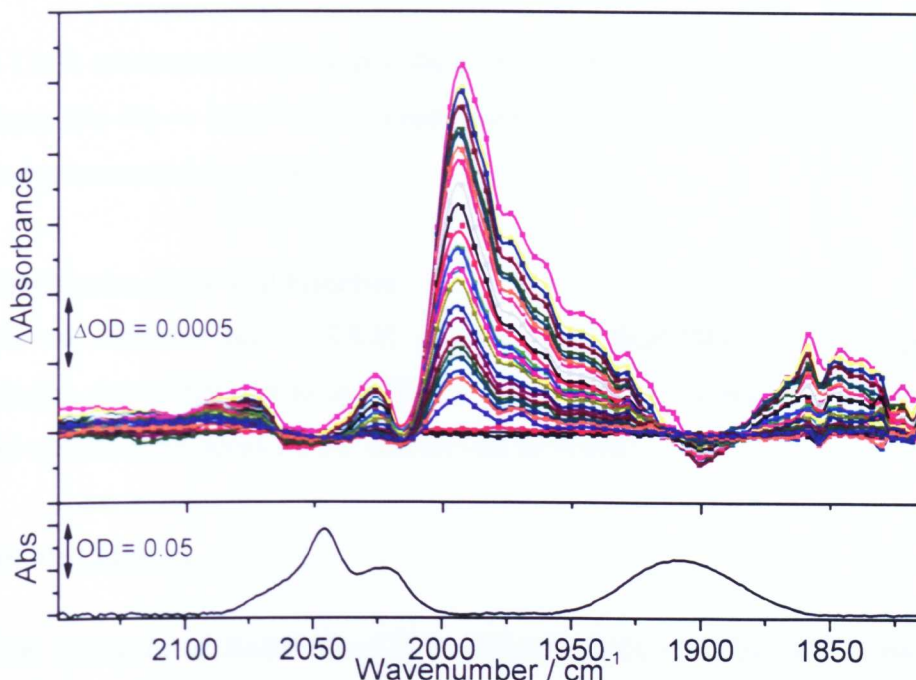


Figure 4.8.3.1: The FTIR (bottom) and ps-TRIR spectra between 1 and 1000 ps (top) of ReBPMRuCN in D₂O solution.

ReCO (Higher Energy) terminus

The **ReCO** parent bleaches are apparent at 2011 and 1905 cm⁻¹, with the former being detected as a sharp depletion in the large **RuCN** transient band which dominates the spectrum (*vide supra*). Transient bands are clearly evident at 1990 and 1854 cm⁻¹, which are at lower wavenumber to the bleaches and correspond to the Re centre experiencing a net increase in electron density on the bridging ligand arising from Ru → bpm ³MLCT. There is the distinct possibility that transients to *higher* wavenumber than the bleaches may also be present but are obscured by the numerous features detected.

The **ReCO** bands decay polyexponentially with a very fast component ($\tau_1 < 2$ ps) and a slower component with $\tau_2 = 34 (\pm 10)$ ps (averaged over bands at 1993, 1901 and 1855 cm⁻¹). Due to the overlap of the bleach at 2011 cm⁻¹ with **RuCN** features no meaningful kinetics could be obtained in that region. At $\Delta t = 1$ ns there are barely detectable signals remaining. This adds further evidence to the earlier supposition that quenching of the excited state is almost complete during the picosecond time domain.

The ps-TRIR spectra recorded do not show any evidence for conversion between the $\text{Re} \rightarrow \text{bpm}$ and $\text{Ru} \rightarrow \text{bpm}^3\text{MLCT}$ excited states, but this process may be occurring on the sub-picosecond timescale.

ns-TRIR Spectroscopy and Kinetics

Attempts to measure the ns-TRIR spectrum of **ReBPMRuCN** in D_2O were unsuccessful, ostensibly due to insufficient signal-to-noise ratios obtained following the rapid excited state decay on the picosecond timescale.

Acetonitrile Solution

The FTIR spectrum of **ReBPMRuCN** in CH_3CN solution in the $\nu(\text{CN})$ and $\nu(\text{CO})$ regions has been measured. In the cyanide region there is a broad peak profile centred at 2067 cm^{-1} . In the carbonyl region there are peaks present at 2015 and 1899 cm^{-1} . These results show a degree of similarity to the FTIR spectra of the model complexes **ReBPM** and **RuCNBPM** (§4.2.3, §4.3.3). Picosecond and nanosecond TRIR spectroscopy (with laser excitation at 400 and 355 nm respectively) were performed on **ReBPMRuCN** in CH_3CN solution, monitoring both regions in the IR where reporter groups are present.

ps-TRIR Spectroscopy

Figure 4.8.3.4 shows the ps-TRIR spectra obtained for the **ReCO** and **RuCN** termini in CH_3CN and Figure 4.8.3.5 shows the ps-TRIR kinetics for bleach and transient bands in CH_3CN . The features arising from the two termini overlap, giving rise to a very feature-rich spectrum between 2100 and 1800 cm^{-1} , is a similar scenario to that observed in D_2O . Excited state localisation and unselective excitation should result in transient bands at higher and lower wavenumber to the parent bleaches for both termini. This has important implications for the following analysis.

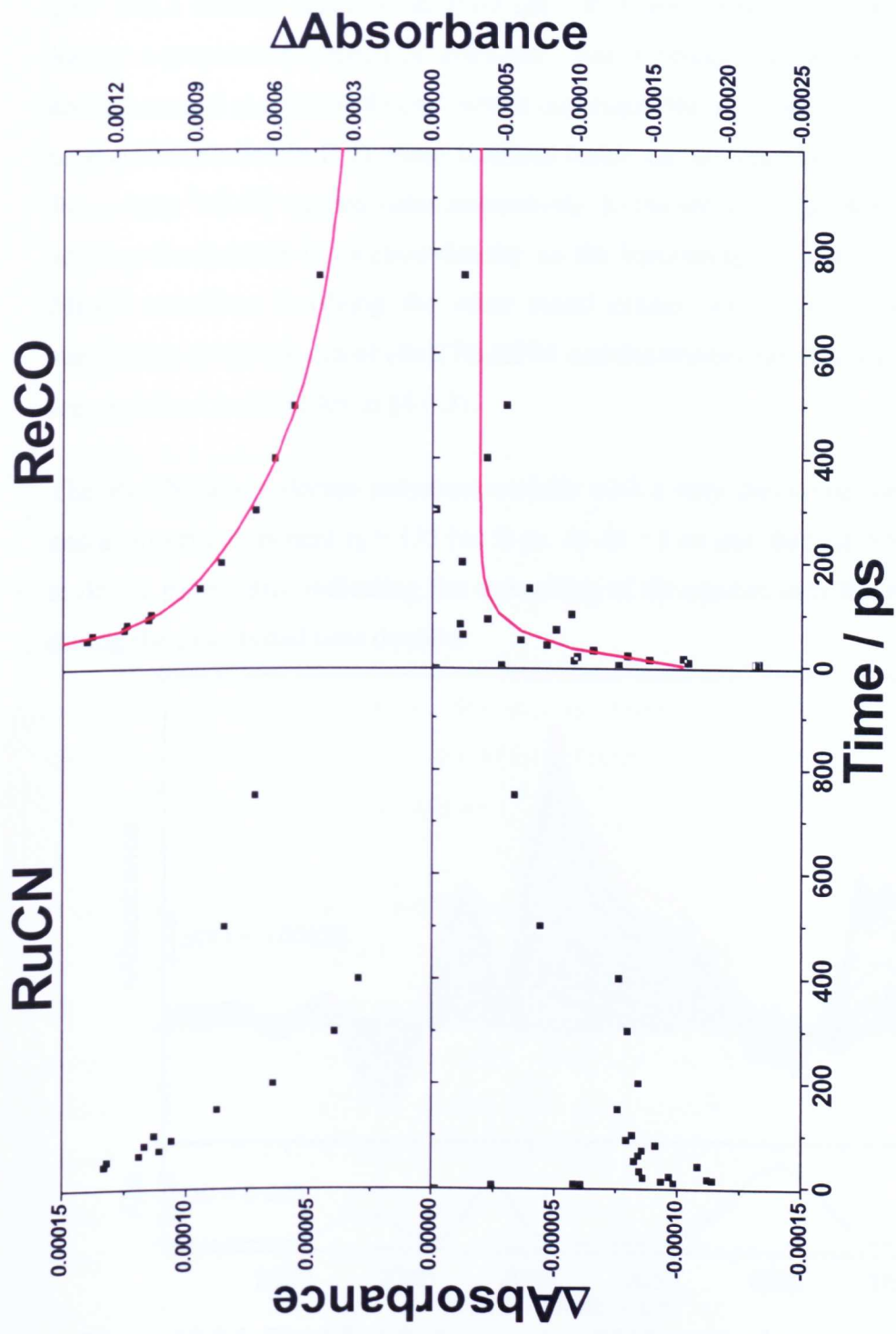


Figure 4.8.3.2: ps-TRIR kinetics of ReBPMRuCN in D_2O solution for RuCN (transient at 2077 cm^{-1} , top left and bleach at 2056 cm^{-1} , bottom left) and ReCO (transient at 1993 cm^{-1} , top right and bleach at 1901 cm^{-1} , bottom right) termini for $\Delta t = 0\text{-}1000\text{ ps}$.

RuCN (Lower Energy) terminus

The parent bleach of the **RuCN** terminus is evident as a broad feature centred at 2058 cm^{-1} and a smaller depletion at 2100 cm^{-1} . It is surrounded by a small transient to higher wavenumber centred at 2089 cm^{-1} and a broad, intense transient to lower energy centred at about 1985 cm^{-1} which dominates the spectrum. In a similar manner to spectra recorded in D_2O , these transient bands can be assigned to $\text{Ru} \rightarrow \text{bpm}$ and $\text{Re} \rightarrow \text{bpm}^3\text{MLCT}$ excited states respectively. In the latter case the **RuCN** terminus is sensing the increase in electron density on the bpm bridging ligand as a result of a MLCT transition involving the other metal centre. As in D_2O there are strong similarities to the spectra of **(RuCN)₂BPM** and the reasons for this feature's intensity are explained in detail for in §4.6.3).

The **RuCN** bleach decays polyexponentially with a very fast component ($\tau_1 < 1$ ps) and a slower component $\tau_2 = 135 (\pm 15)$ ps. At $\Delta t = 1$ ns less than *ca.* 5% of the signal at $\Delta t = 1$ ps remains, indicating that quenching of the excited state is almost complete during the picosecond time domain.

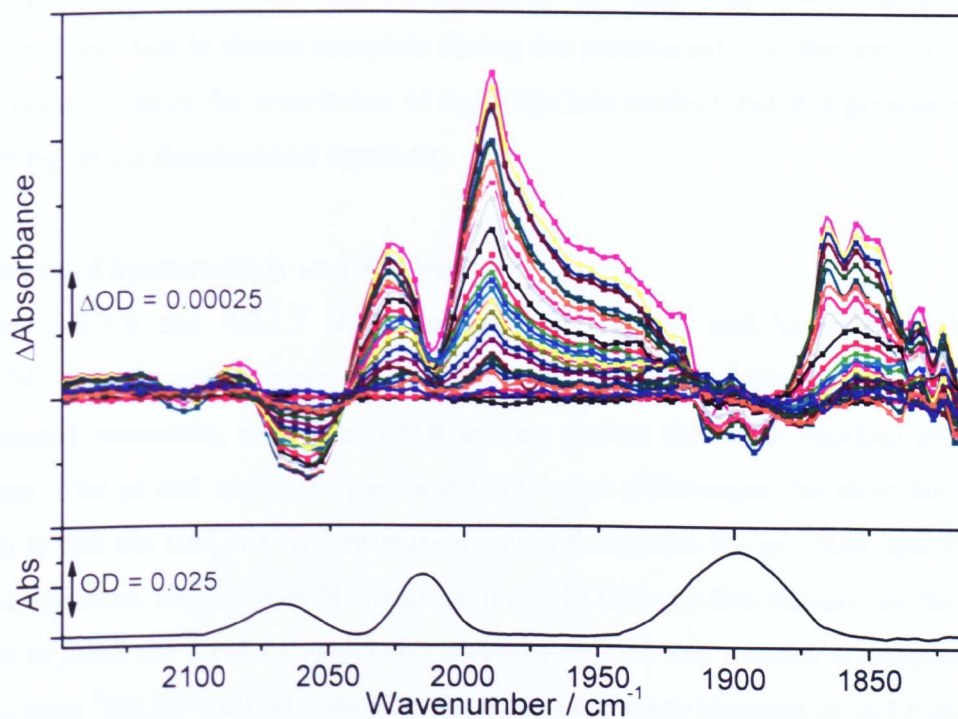


Figure 4.8.3.3: The FTIR (bottom) and ps-TRIR spectra between 1 and 1000 ps (top) of **ReBPMRuCN in CH_3CN solution.**

ReCO (Higher Energy) terminus

The **ReCO** parent bleaches are apparent at 2012 and 1901 cm^{-1} , with the former being detected as a sharp depletion in the large **RuCN** transient band which dominates the spectrum (Figure 4.8.3.3). Transient bands are clearly evident at 1990 and 1855 cm^{-1} , which are at lower wavenumber to the bleaches and correspond to the **ReCO** terminus experiencing a net increase in electron density on the bridging ligand arising from the formation of a $\text{Ru} \rightarrow \text{bpm}^3\text{MLCT}$ excited state. It is conceivable that transients to *higher* wavenumber than the bleaches may also be present but may be obscured by transient features. The similarity of the peak positions in both solvents indicates that the electronic structures of the excited states are ostensibly similar.

The **ReCO** bands decay polyexponentially with a very fast component ($\tau_1 < 1$ ps) and a slower component with $\tau_2 = 26 (\pm 6)$ ps (averaged over bands at 1990, 1893 and 1855 cm^{-1}). Due to the overlap of the bleach at 2012 cm^{-1} with **RuCN** features no meaningful kinetics could be obtained. At $\Delta t = 1$ ns less than *ca.* 5% of the signal at $\Delta t = 1$ ps remains. This adds further evidence to the earlier supposition that quenching of the excited state is almost complete during the picosecond time domain. As in D_2O there is no evidence for conversion of one state into another, but this process may be occurring on the femtosecond timescale.

Nanosecond Spectroscopy and Kinetics

Figures 4.8.3.6 and 4.8.3.7 show the ns-TRIR spectra and kinetics obtained in CH_3CN . As discussed above, most of the excited state bands decay within the picosecond timescale, so the ns-TRIR spectra probes the weak residual remaining features. The ps and ns-TRIR spectra exhibit major differences, the most striking of which is that the **RuCN** transient feature which dominates the ps-TRIR spectra is no longer apparent. On the **RuCN** terminus, the only features that remain are the parent bleach at 2068 cm^{-1} and its associated transient at 2094 cm^{-1} , which corresponds to a $\text{Ru} \rightarrow \text{bpm}^3\text{MLCT}$ excited state. On the **ReCO** terminus bleaches at 2012 and 1893 cm^{-1} and transient peaks at 1990 and 1924 cm^{-1} are observed. The results are consistent with one excited state persisting into the nanosecond timescale, in contrast

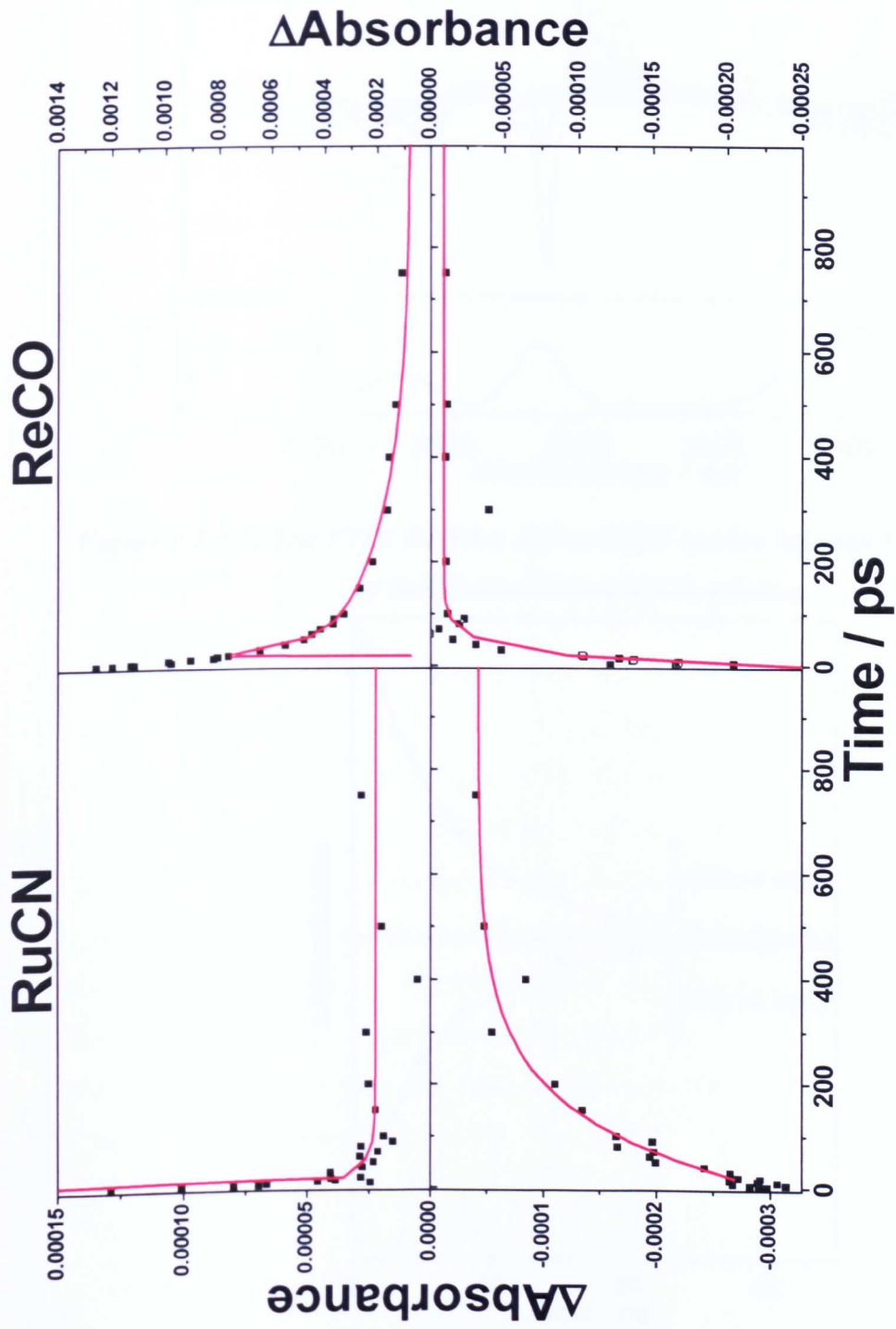


Figure 4.8.3.4: ps-TRIR kinetics of ReBPMRuCN in CH₃CN solution for RuCN (transient at 2083 cm⁻¹, top left and bleach at 2058 cm⁻¹, bottom left) and ReCO (transient at 1893 cm⁻¹, top right and bleach at 1893 cm⁻¹, bottom right) termini for Δt = 0-1000 ps.

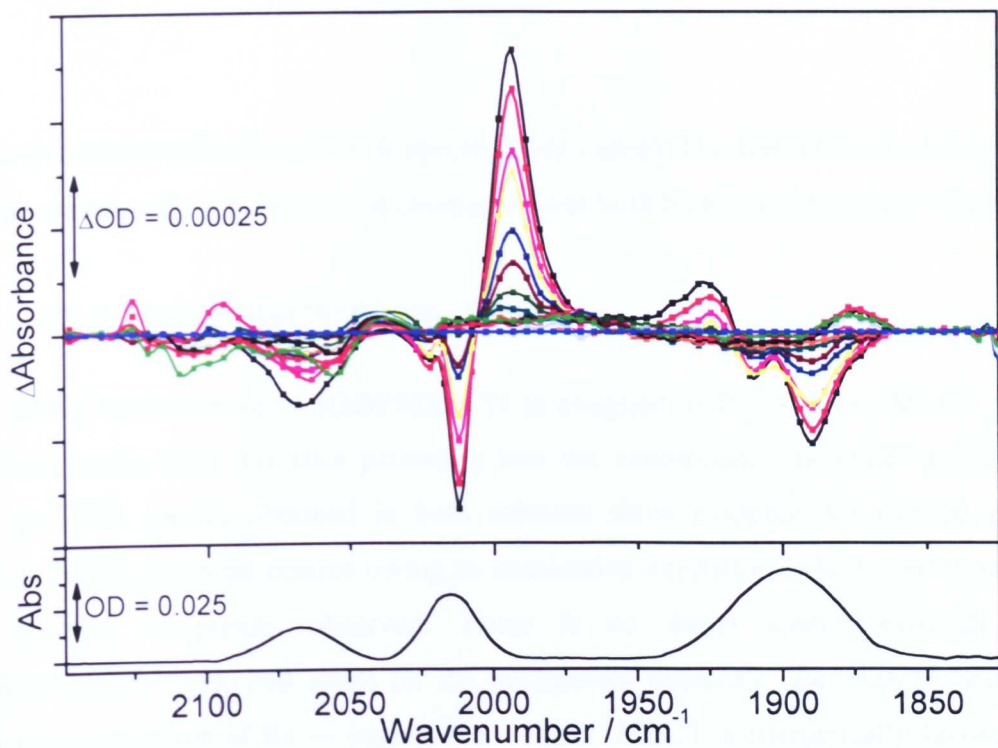


Figure 4.8.3.5: The FTIR (bottom) and ns-TRIR spectra between 1 and 40 ns (top) of ReBPMRuCN in CH₃CN solution.

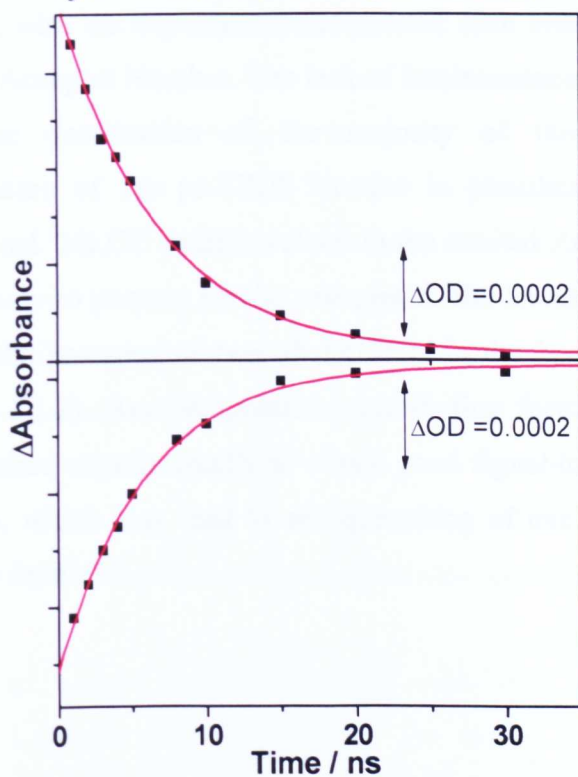


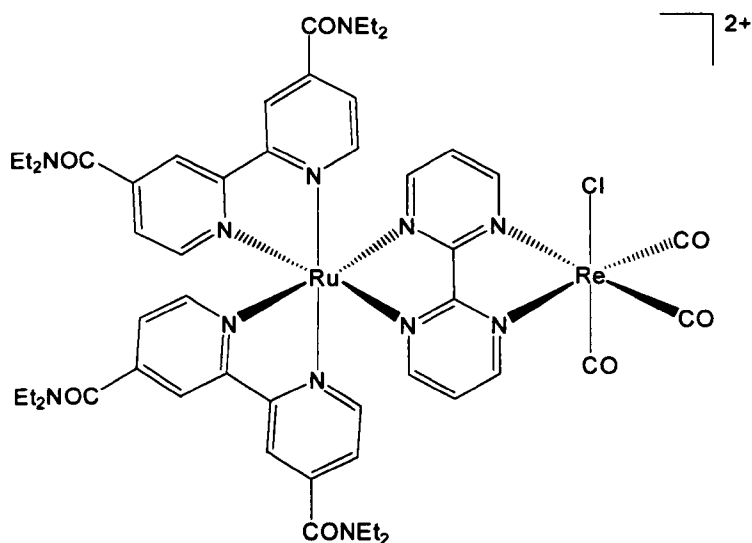
Figure 4.8.3.6: Single-pixel kinetics of bleach (2010 cm^{-1} , bottom) and transient (1995 cm^{-1} , top) ns-TRIR bands of ReBPMRuCN in CH₃CN solution.

to the two observed in the ps-TRIR spectra (*vide supra*). The **ReCO** bands decay with a time constant of $\tau = 6.2 (\pm 0.4)$ ns (averaged over both bleach and transient values).

4.8.4. **ReBPMRuCN: Closing Points**

The lowest excited state of **ReBPMRuCN** is assigned to $\text{Ru} \rightarrow \text{bpm}^3\text{MLCT}$, with transient bands from this state persisting into the nanosecond timescale in CH_3CN . The ps-TRIR spectra obtained in both solvents show evidence for excited states arising from both metal centres owing to unselective excitation, which contributes to the spectral complexity observed. There is no direct kinetic evidence for interconversion of excited states on the picosecond timescale; for example excited state interconversion of $\text{Re} \rightarrow \text{bpm}$ to $\text{Ru} \rightarrow \text{bpm}^3\text{MLCT}$ is energetically favourable in D_2O and CH_3CN . However such processes may feasibly be complete within 1 ps, particularly in conjugated systems.²⁰ The spectral profiles observed are similar in both solvents, consistent with the expectation that excited state ordering is unaffected by changes in solvent Acceptor Number. The lack of luminescence is consistent with the rapid excited state deactivation of the majority of the TRIR signal. The polyexponential nature of the ps-TRIR kinetics is postulated to arise from the presence of additional $^3\text{MLCT}$ states involved in the excited state relaxation process. These states are likely to possess similar energies to the lowest-lying excited $\text{Ru} \rightarrow \text{bpm}$ state due to the presence of two π^* LUMOs in the bpm ligand with similar energies (Figure 4.1.1.2). Another possible contributing factor is the high sample concentrations required experimentally to obtain good signal-to-noise ratios with the PIRATE apparatus, which may lead to self-quenching of excited state species (see Chapter 6 for more details).

4.9. $\{(OC)_3ReCl(\mu\text{-bpm})Ru((5,5'\text{-CONEt}_2)_2bpy)_2\}Cl_2$, ReBPMRubpyamide



ReBPMRubpyamide is a heterobimetallic complex with **ReCO** and **Rubpyamide** termini on either side of the bpm bridging ligand. Each terminus has an $M \rightarrow bpm$ MLCT chromophore associated with it, and the **Rubpyamide** terminus possesses an additional $Ru \rightarrow bpyamide$ chromophore. This may complicate the photophysical dynamics of the system in a similar manner to other **Rubpyamide**-containing complexes in this Chapter (§4.4 and §4.7) and could be an issue in the event of unselective excitation in the TRIR experiments. Neither terminus is strongly solvatochromic and as a result no significant differences in the spectroscopic properties of **ReBPMRubpyamide** are expected between D_2O and CH_3CN . $Ru \rightarrow bpm$ 3MLCT is expected to be the lowest energy excited state (and hence the longest-lived) in both CH_3CN and D_2O .

4.9.1. UV/visible Absorption and Luminescence Spectroscopy

UV/visible absorption spectra of **ReBPMRubpyamide** have been measured in D_2O and CH_3CN (see Appendix 4.12 for spectra). The results are presented in Table 4.9.1.1. The spectral profile obtained is similar to that reported for $[(ReCl(CO)_3)(\mu\text{-bpm})(Ru(bpy)_2)]^{2+}$ in CH_3CN .⁵

Solvent	$\lambda^{\max} / \text{nm}$					
	D ₂ O	< 300	323	358	394	418
CH ₃ CN	< 300	325	355	401	426	544
Tentative Assignment	IL π - π^*	¹ MC	¹ MC	¹ MLCT	¹ MLCT	¹ MLCT
Location	bpy/bpm	Re	Ru	Re	Ru	Ru

Table 4.9.1.1: Table of peak positions and assignments for UV/visible absorption spectra of ReBPMRubpyamide in D₂O and CH₃CN solutions.

The luminescence spectrum of **ReBPMRubpyamide** was measured in CH₃CN solution (see Appendix 4.12 for spectra). The results are presented in Table 4.9.1.2. Excitation directly into the Ru → ((4,4'-CONEt₂)₂bpy) MLCT chromophore at 426 nm results in weak luminescence with a broad, structureless profile centred at 646 nm, strongly resembling the emission observed in **RubpyamideBPM**. Excitation (at 550 nm) into the low energy charge transfer band gives barely detectable emission also centred at 646 nm. In both cases the emission intensity was insufficient to perform TCSPC experiments to determine the lifetime.

$\lambda_{\text{ex}} / \text{nm}$	$\lambda_{\text{em}} / \text{nm}$	Φ
426	646	0.0006
550	646	0.0003

Table 4.9.1.2: Table of peak positions and assignments for emission spectra of ReBPMRubpyamide in CH₃CN solution.

4.9.2. Cyclic Voltammetry

Cyclic voltammetry of **ReBPMRubpyamide** was measured in D₂O (see Appendix 4.12 for the voltammogram) and the results are presented in Table 4.9.2.1 below. Features corresponding to three reversible reductions and three oxidation couples (one reversible and two irreversible) are observed. As with **RebpmRuCN**, the ease of reduction of the bipyrimidine ligand may be significant. The redox couple's proximity

to 0 V indicates that this couple may be accessible in the absence of electrical current, which could have important implications for the electronic structure of the ground and excited states of **ReBPMRubpyamide** in solution. The voltammogram obtained is similar to that reported for $[(\text{ReCl}(\text{CO})_3)(\mu\text{-bpm})(\text{Ru}(\text{bpy})_2)]^{2+}$ in CH_3CN .⁵

$E_{1/2}/\text{V}$ (vs. Fc/Fc^+)	Reversibility	Tentative Assignment
$E_p = +1.71$	Irreversible	Re^{VII}
$E_p = +1.17$	Irreversible	$\text{Ru}^{\text{IV/III}}$
$E_p = +0.70$	Irreversible	Amide Oxidation
-0.60	Reversible	$(\text{bpm})^{0/\bullet-}$
-1.37	Reversible	Amide Reduction
-1.65	Reversible	Amide Reduction

Table 4.9.2.1: Table of potentials for redox couples and assignments from the cyclic voltammogram of **ReBPMRubpyamide in CH_3CN solution.**

4.9.3. FTIR, IR OTTLE and Time-Resolved Infrared Spectroscopy

ReBPMRubpyamide has been studied using ps and ns-TRIR spectroscopy in D_2O and CH_3CN solutions.

IR OTTLE of **ReBPMRubpyamide** in CH_3CN was unsuccessful as the 1st reduction couple was found to be chemically irreversible on the timescale of the experiment.

Deuterium Oxide Solution

The FTIR spectrum of **ReBPMRubpyamide** in D_2O solution in the $\nu(\text{CO})$ and amide $\nu(\text{CO})$ region has been measured. In the carbonyl region there is a peak profile characteristic of the rhenium (I) tricarbonyl unit with 3 resolved maxima at 2015, 1997 and 1925 cm^{-1} . There are also smaller ‘satellite’ peaks visible at 1874, 1835 and 1810 cm^{-1} . In the amide region there is a single peak present at 1616 cm^{-1} . These

results are broadly comparable with the FTIR spectra of the model complexes **ReBPM** and **RubpyamideBPM** (§4.2.3, §4.4.3), although **ReBPM** is insoluble in aqueous media and hence was only studied in CH₃CN. One significant difference from the model complexes' spectra (also observed in the FTIR spectra of other bimetallics in this Chapter) is the presence of satellite peaks, at lower wavenumber to the carbonyl bands. This suggests that the 1st reduction of **ReBPMRubpyamide** ($E_{1/2} = -0.598$ V vs. Fc/Fc⁺) is partially accessible in D₂O solution without any potential difference applied, and the peaks correspond to the FTIR spectrum of the partially reduced complex (with the electron residing on the bipyrimidine ligand). It is reasonable to suggest that the absence of such a satellite feature from the amide $\nu(\text{CO})$ region is due to the comparatively small amount of electronic coupling between the amide groups (situated on the bpy ligands) and the bipyrimidine bridge.

Picosecond and nanosecond-TRIR spectroscopy (with laser excitation at 400 and 355 nm respectively) were performed on **ReBPMRubpyamide** in D₂O solution, monitoring both regions in the IR where reporter groups are present.

ps-TRIR Spectroscopy

Figure 4.9.3.1 shows the ps-TRIR spectra obtained for the **ReCO** and **Rubpyamide** termini in D₂O. Figure 4.9.3.2 shows the ps-TRIR kinetics obtained for bleach and transient bands in D₂O.

ReCO (“Donor” / Higher Energy) terminus

The spectral profile obtained following 400 nm excitation is dominated by two bleaches at 2027 and 1936 cm⁻¹. Two transient bands are formed at lower energy to the bleaches, centred at 2015 and 1925 cm⁻¹. This is consistent with the **ReCO** terminus experiencing an increase in electron density as a result of a MLCT transition involving the **Rubpyamide** terminus (*vide infra*). There is considerable overlap between the bleaches and their associated transient bands. These bands narrow and blue-shift over the first 25 ps of the experiment, indicating that vibrational cooling takes place during this period. A biexponential decay is observed with $\tau_1 = 120 (\pm 75)$

and $\tau_2 = 1060 (\pm 195)$ ps (averaged over both bleach and transient features). At $\Delta t = 1$ ns only *ca.* 10% of the signal present at $\Delta t = 1$ ps remains, indicating that quenching of the excited state is almost complete during the picosecond time domain.

Rubpyamide (“Acceptor” / Lower Energy) terminus

The ps-TRIR spectra obtained are comprised of a parent bleach centred at 1616 cm^{-1} and a transient band to higher wavenumber at 1636 cm^{-1} . This is consistent with a decrease in electron density on the bpy ligands, as expected during the formation of a $\text{Ru} \rightarrow \text{bpm}^3\text{MLCT}$ excited state. Additionally a small bleach is present at 1582 cm^{-1} and is accompanied by a transient at 1560 cm^{-1} . By comparison with **RubpyamideBPM** and **(Rubpyamide)₂BPM** this can be assigned to a vibrational mode of the bipyrimidine ligand, directly reporting on the increase in electron density on the bridging ligand. Examination of the kinetics of the amide bands shows evidence for a grow-in of absorbance over the first 100 ps on both bleach and transient features. The duration of this growth and its manifestation in both bleach and transient spectra indicates that vibrational cooling is not responsible for this observation and there is a good case for it matching up with the fast decay process τ_1 on the **ReCO** terminus.

After this grow-in has ended, the signal decays with a time constant (averaged over both bleach and transient features) of $1050 (\pm 350)$ ps. This is in very good agreement with the slow decay process τ_2 on the **ReCO** terminus (*vide supra*). At $\Delta t = 1$ ns *ca.* 25% of the signal at $\Delta t = 1$ ps remains, indicating that a long-lived component persists into the nanosecond time domain.

ns-TRIR Spectroscopy

Figures 4.9.3.3 and 4.9.3.4 show the ns-TRIR spectra and kinetics obtained respectively for the **Rubpyamide** terminus in D_2O . As with the ps-TRIR spectra, the spectrum is dominated by a bleach centred at 1616 cm^{-1} with a transient band at 1633 cm^{-1} . A bleach band arising from a vibrational mode of bipyrimidine is detected at 1583 cm^{-1} and its associated transient is centred at 1561 cm^{-1} . All the bands decay

synchronously with a biexponential time constants (averaged over both bleach and transient features) of $\tau_1 = 1.7 (\pm 0.1)$ and $\tau_2 = 63.2 (\pm 2.5)$ ns. The τ_1 decay component from ns-TRIR spectroscopy shows relatively good agreement with τ_2 in the picosecond spectra (*vide supra*), considering that neither the ps nor ns-TRIR experimental setups are well suited to measuring lifetimes of a few nanoseconds.

Acetonitrile Solution

The FTIR spectrum of **ReBPMRubpyamide** in CH₃CN solution in the $\nu(\text{CO})$ and amide $\nu(\text{CO})$ region has been measured. In the carbonyl region there is a peak profile characteristic of the rhenium (I) tricarbonyl unit with 3 resolved maxima at 2034, 1936 and 1919 cm⁻¹. There are also smaller 'satellite' peaks visible at 2017, 1903 and 1879 cm⁻¹. In the amide region there is a single peak present at 1639 cm⁻¹.

These results are comparable with the model complexes **ReBPM** and **RubpyamideBPM** in CH₃CN solution (§4.2.3, §4.4.3). As in D₂O, the presence of satellite peaks in CH₃CN in addition to D₂O suggests that the 1st reduction of **ReBPMRubpyamide** is partially accessible in both solvents studied without any potential difference applied. As before, it is reasonable to assume that the absence of such a satellite feature from the amide $\nu(\text{CO})$ region is due to the comparatively small amount of electronic coupling between the amide groups (situated on the bpy ligands) and the bipyrimidine bridge.

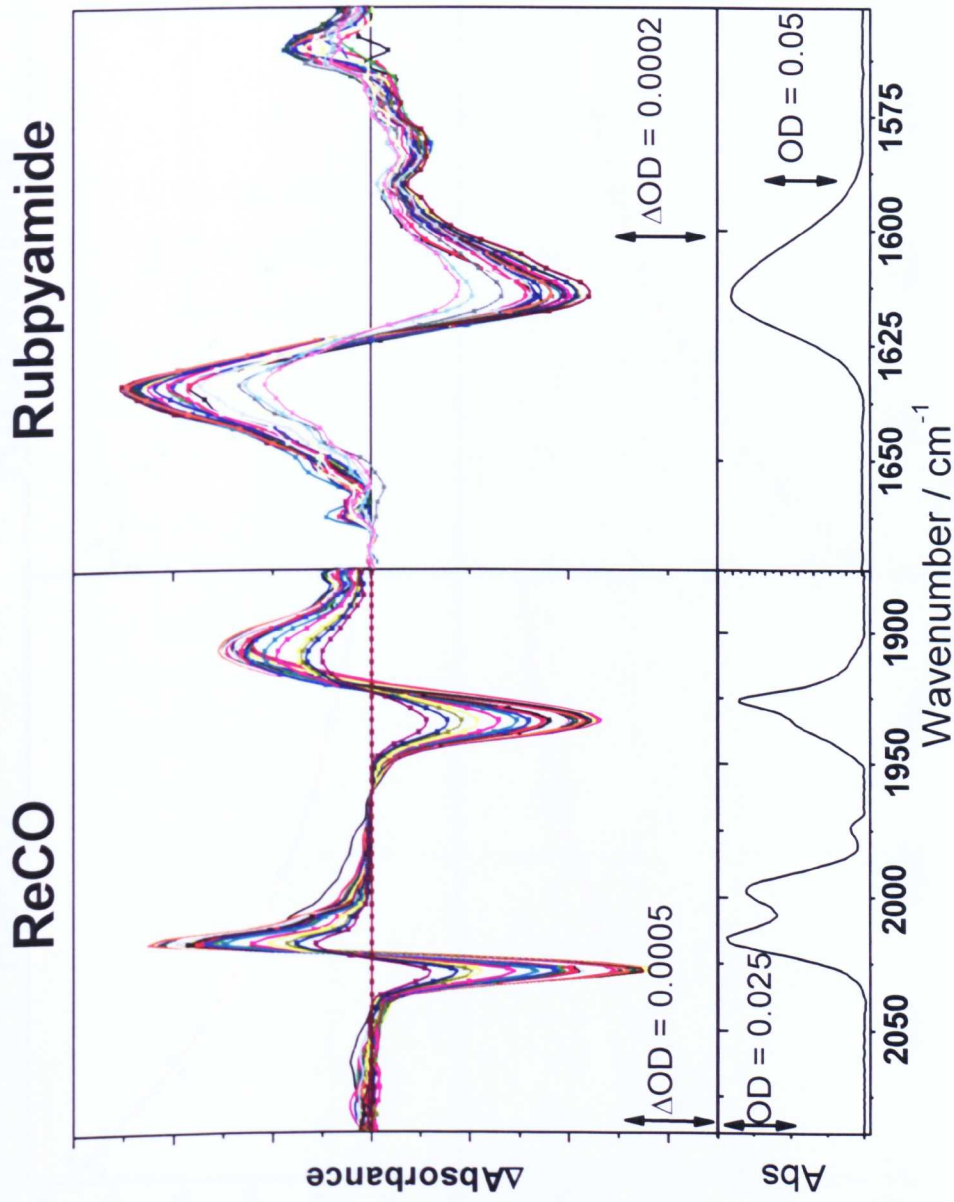


Figure 4.9.3.1: The FTIR (bottom) and ps-TRIR spectra (top) between 1 and 1000 ps (top) of the ReCO (left) and Rubpyamide (right) termini of ReBPMRubpyamide in D_2O solution.

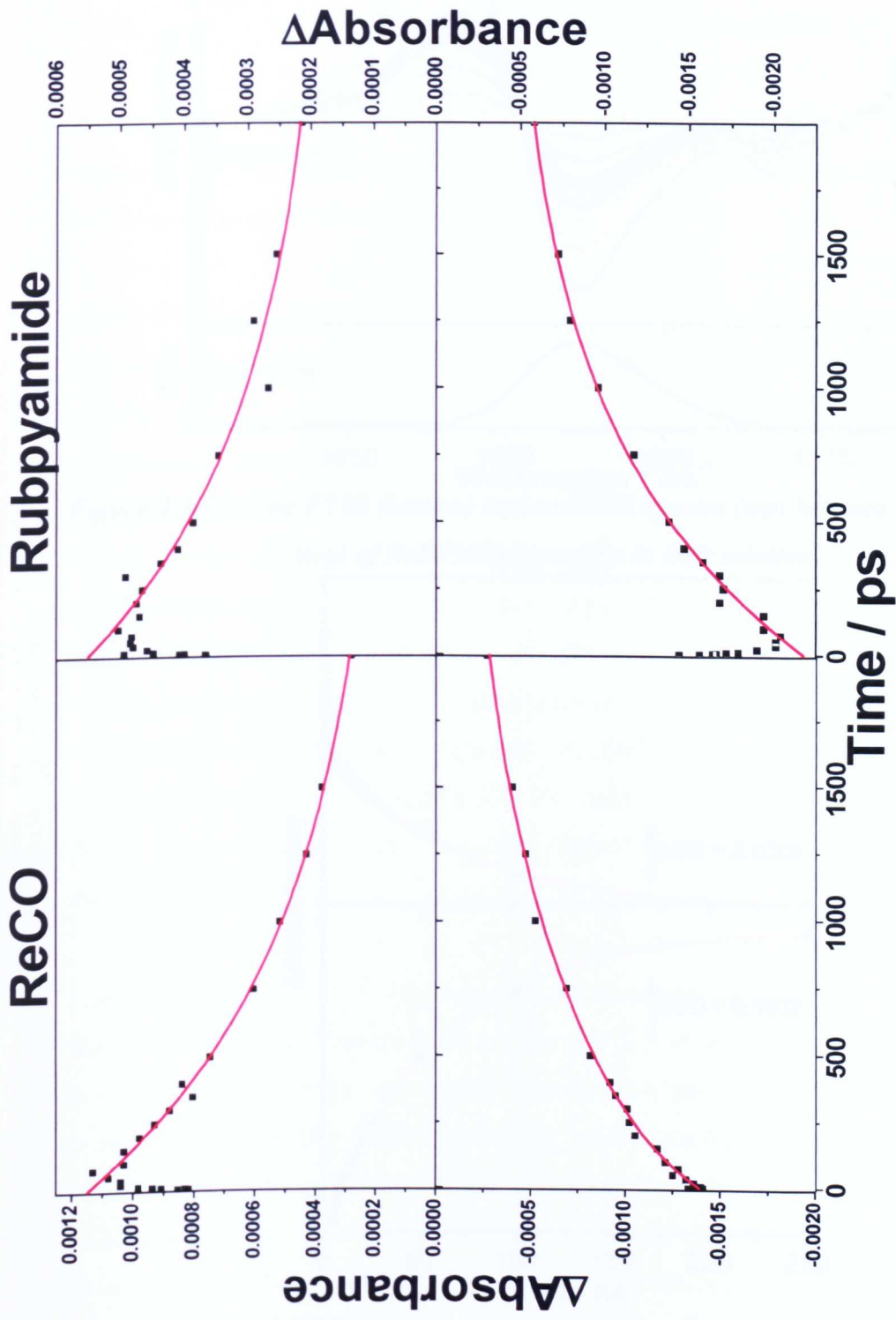


Figure 4.9.3.2: ps-TRIR kinetics of ReBPMRubpyamide in D₂O solution for ReCO (transient at 2023 cm⁻¹, top left and bleach at 2028 cm⁻¹, bottom left) and Rubpyamide (transient at 1614 cm⁻¹, top right and bleach at 1635 cm⁻¹, bottom right) termini for $\Delta t = 0$ -2000 ps.

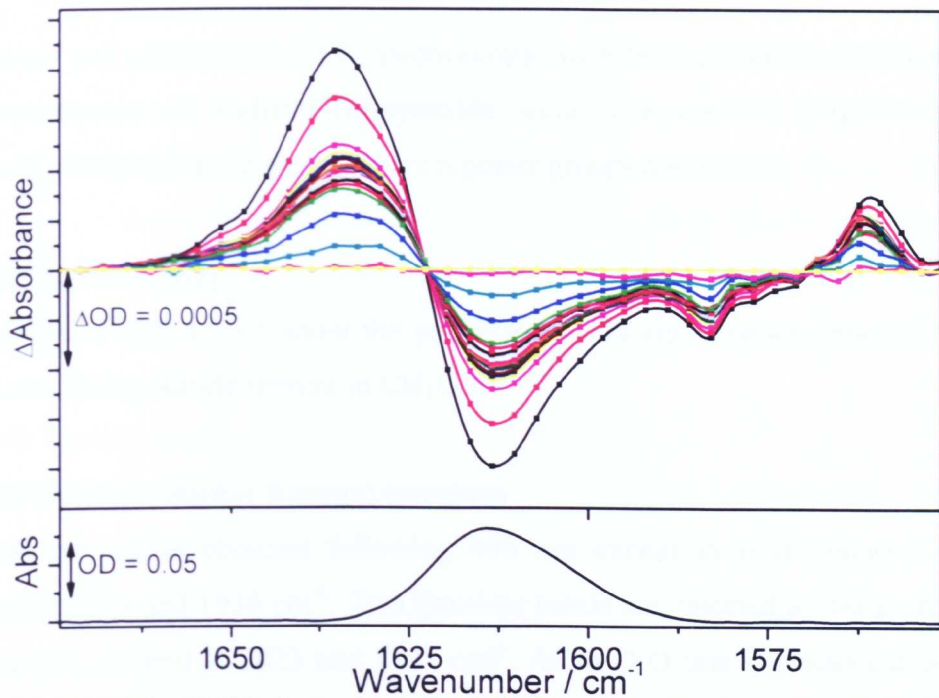


Figure 4.9.3.3: The FTIR (bottom) and ns-TRIR spectra (top) between 1 and 250 ns (top) of ReBPMRubpyamide in D_2O solution.

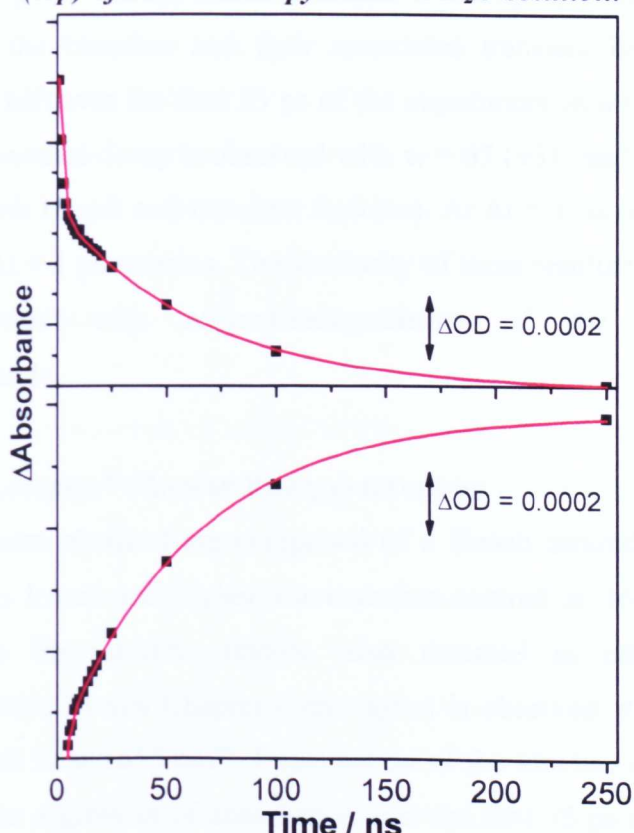


Figure 4.9.3.4: ns-TRIR kinetics of bleach (1632 cm^{-1} , bottom) and transient (1614 cm^{-1} , top) bands of ReBPMRubpyamide in D_2O solution.

Picosecond and nanosecond-TRIR spectroscopy (with laser excitation at 400 and 355 nm respectively) of **ReBPMRubpyamide** were measured in CH₃CN solution, monitoring both regions in the IR where reporter groups are present.

ps-TRIR Spectroscopy

Figures 4.9.3.5 and 4.9.3.6 show the ps-TRIR spectra and kinetics obtained for the **ReCO** and **Rubpyamide** termini in CH₃CN.

ReCO (“Donor” / Higher Energy) terminus

The spectral profile obtained following 400 nm excitation is dominated by two bleaches at 2034 and 1936 cm⁻¹. Two transient bands are detected at lower energy to the bleaches, centred at 2023 and 1931 cm⁻¹. As in D₂O this is consistent with the **ReCO** terminus experiencing an increase in electron density as a result of a MLCT transition involving the **Rubpyamide** terminus (*vide infra*). There is considerable overlap between the bleaches and their associated transient bands. These bands narrow and blue-shift over the first 25 ps of the experiment as a result of vibrational cooling. A biexponential decay is observed with $\tau_1 = 67 (\pm 31)$ and $\tau_2 = 970 (\pm 150)$ ps (averaged over both bleach and transient features). At $\Delta t = 1$ ns only *ca.* 10% of the signal present at $\Delta t = 1$ ps remains. The similarity of these results to those obtained in D₂O is consistent with solvent-independence of the photophysics of **ReBPMRubpyamide**.

Rubpyamide (“Acceptor” / Lower Energy) terminus

The ps-TRIR spectra obtained are comprised of a bleach centred at 1639 cm⁻¹ and transient bands to lower and higher wavenumber centred at 1621 and 1650 cm⁻¹ respectively. The bipyrimidine feature, also detected in other **Rubpyamide**-containing complexes in this Chapter (*vide supra*) is observed at 1577 cm⁻¹ and its associated transient is at 1555 cm⁻¹. Examination of the kinetics of the amide bands shows evidence for a grow-in of absorbance over the first 75 ps on both bleach and transient features. As in D₂O, the timescale of this transient signal's growth and its manifestation in both bleach and transient spectra indicates that vibrational cooling is

not responsible and there is a correlation with the fast decay process τ_1 on the **ReCO** terminus (*vide supra*). After this growth has halted, the signal decays with a time constant (averaged over both bleach and transient features) of 917 (± 88) ps. This is in very good agreement with the slow decay process τ_2 on the **ReCO** terminus (*vide supra*). At $\Delta t = 1$ ns *ca.* 25% of the signal at $\Delta t = 1$ ps remains, indicating that a long-lived transient species persists into the nanosecond time domain.

ns-TRIR Spectroscopy

Figures 4.9.3.7 and 4.9.3.8 show the ns-TRIR spectra and kinetics obtained respectively for the **Rubpyamide** terminus in D₂O (no signal was detected in for the **ReCO** terminus). As with the ps-TRIR spectra (*vide supra*), the spectrum is dominated by a bleach centred at 1639 cm⁻¹ with transient bands at 1649 and 1621 cm⁻¹. The bipyrimidine mode bleach is detected at 1579 cm⁻¹ and its associated transient is centred at 1556 cm⁻¹. All the bands decay synchronously with a biexponential time constants (averaged over both bleach and transient features) of $\tau_1 = 1.4$ (± 0.1) and $\tau_2 = 84.5$ (± 4.2) ns. The τ_1 ns-TRIR decay component shows relatively good agreement with τ_2 in the **Rubpyamide** picosecond spectra (*vide supra*), considering that neither time domain is well calibrated for measuring lifetimes of a few nanoseconds.

4.9.4. ReBPMRubpyamide: Closing Points

The lowest energy excited state of **ReBPMRubpyamide** has been shown to be Ru \rightarrow bpm ³MLCT, with transient bands from this state persisting into the nanosecond time domain. The spectral profiles observed are similar in both solvents, consistent with the expected lack of solvatochromism in the system. In contrast to **ReBPMRuCN** there is evidence in the picosecond TRIR kinetics for interconversion of Re \rightarrow bpm into Ru \rightarrow bpm ³MLCT excited states in both D₂O and CH₃CN. The satellite bands observed in the FTIR suggest that the 1st redox couple near 0 V is accessible and this may provide a mechanism with which to switch on additional photoprocesses such as IVCT although there is no definitive evidence for this in this complex.

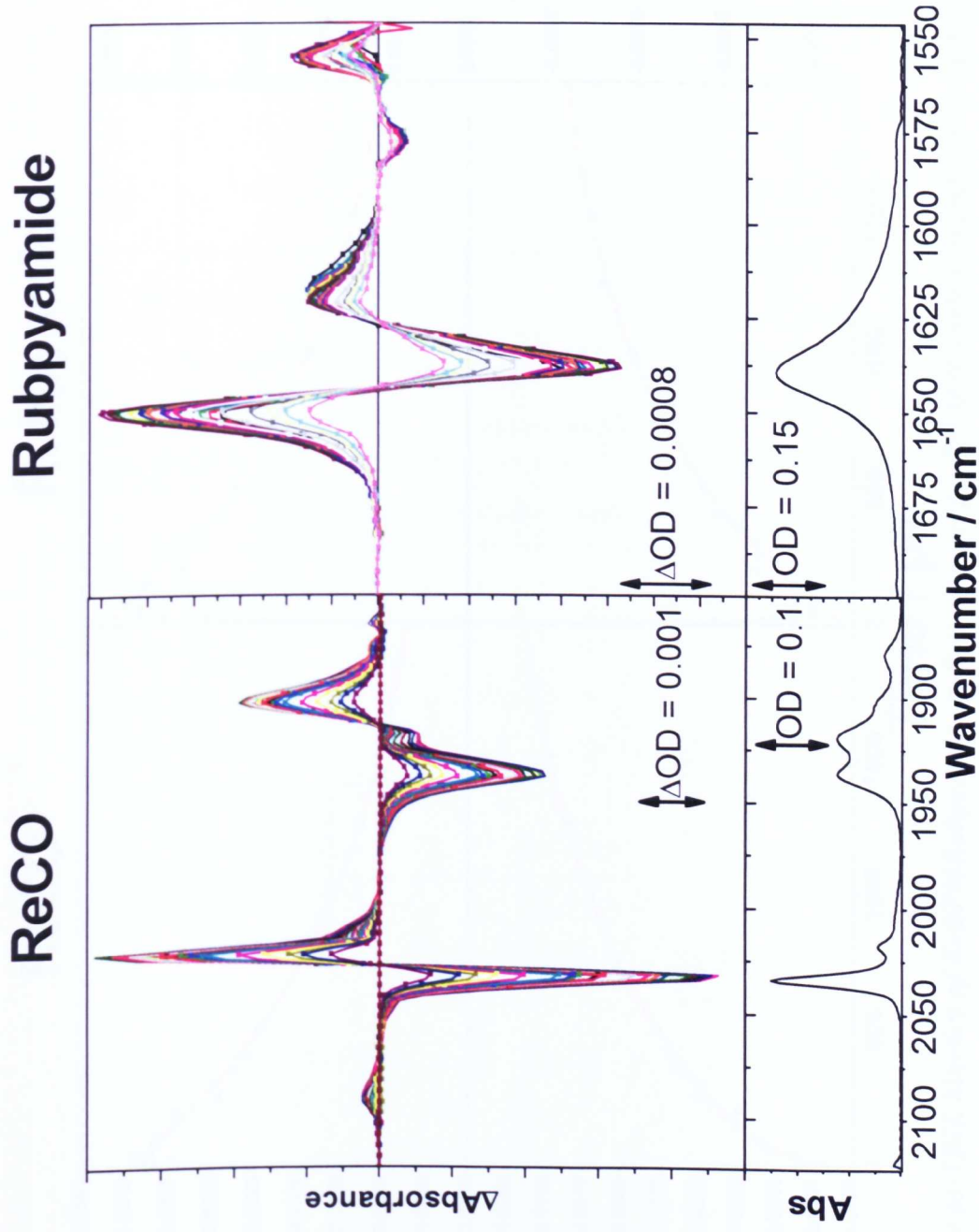


Figure 4.9.3.5: The FTIR (bottom) and ps-TRIR spectra (top) between 1 and 1000 ps (top) of the ReCO (left) and Rubpyamide (right) termini of ReBPMRubpyamide in CH₃CN solution.

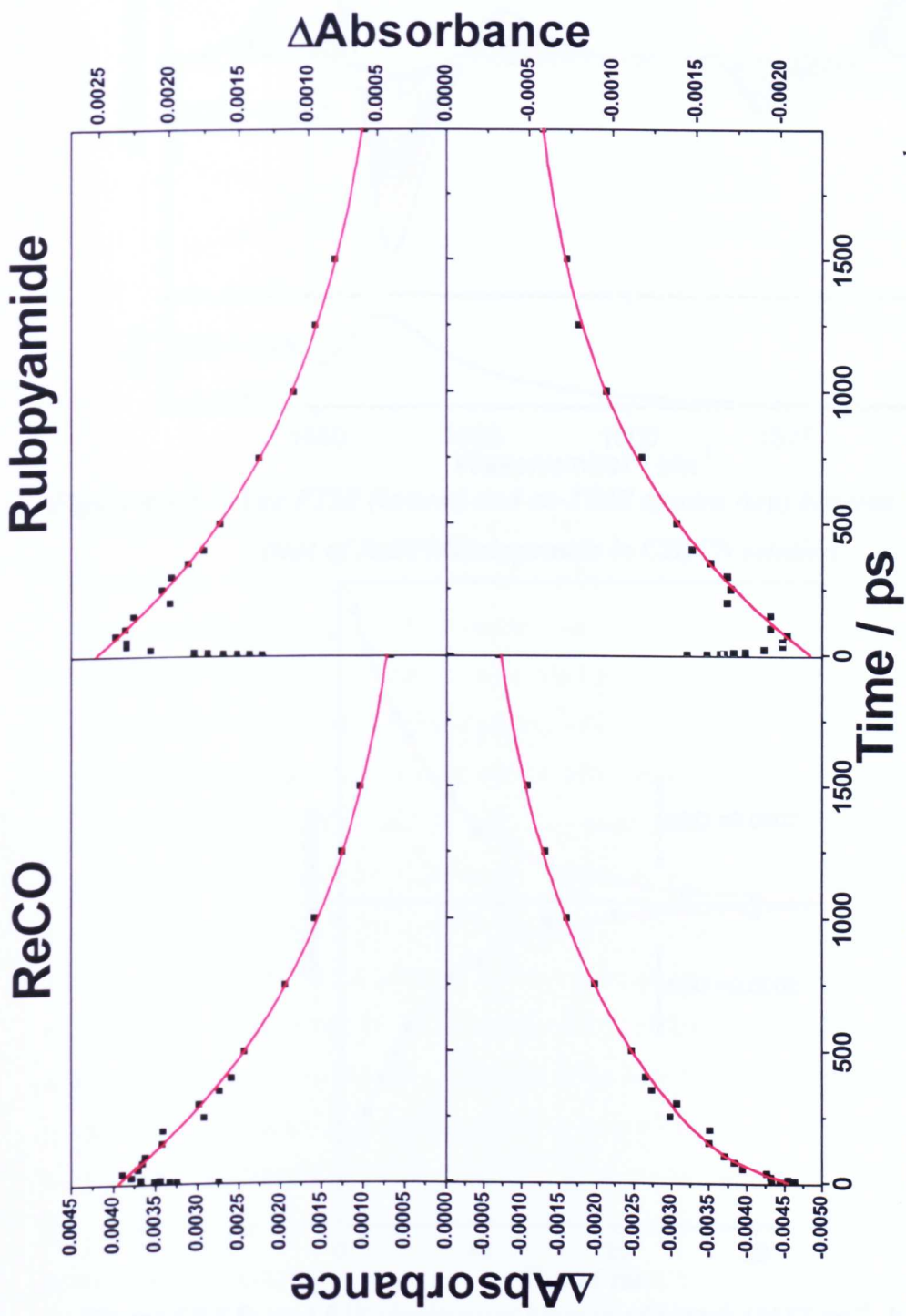


Figure 4.9.3.6: ps-TRIR kinetics of ReBPMRubpyamide in D₂O solution for ReCO (transient at 2022 cm⁻¹, top left and bleach at 2032 cm⁻¹, bottom left) and Rubpyamide (transient at 1650 cm⁻¹, top right and bleach at 1637 cm⁻¹, bottom right) termini for $\Delta t = 0$ -2000 ps.

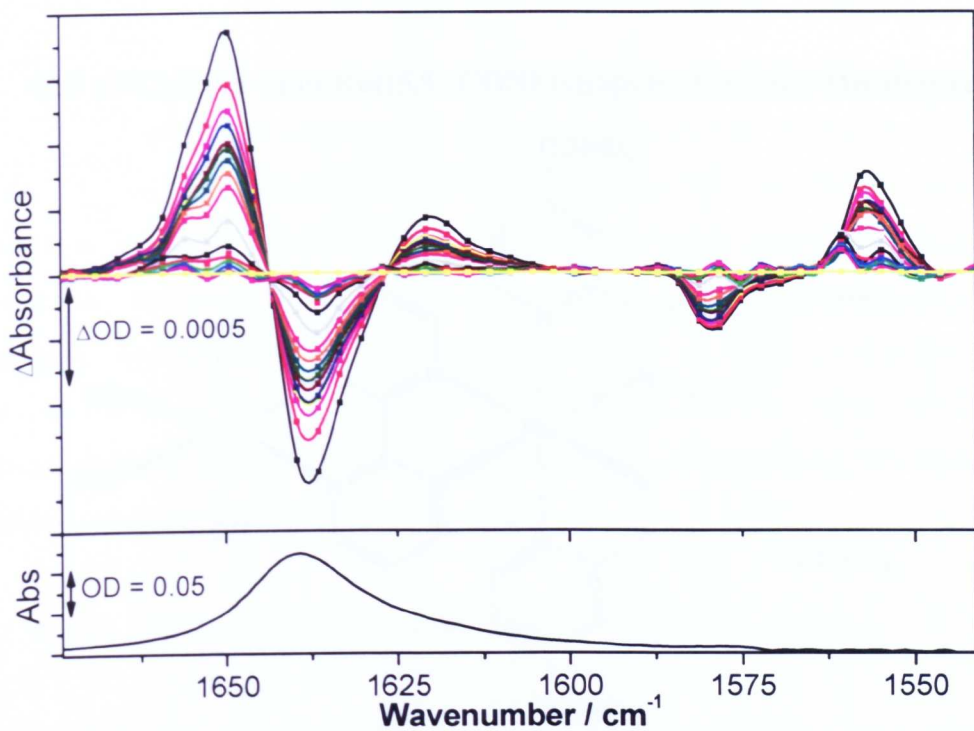


Figure 4.9.3.7: The FTIR (bottom) and ns-TRIR spectra (top) between 1 and 250 ns (top) of ReBPMRubpyamide in CH_3CN solution.

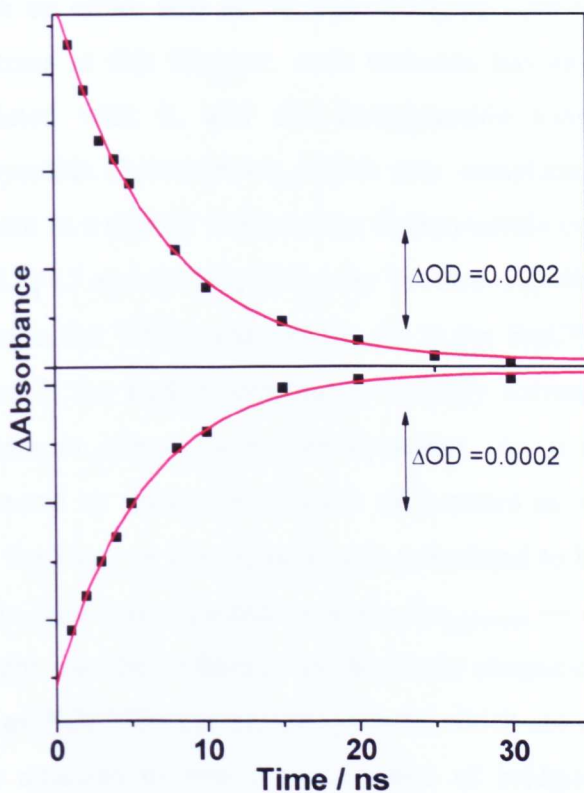
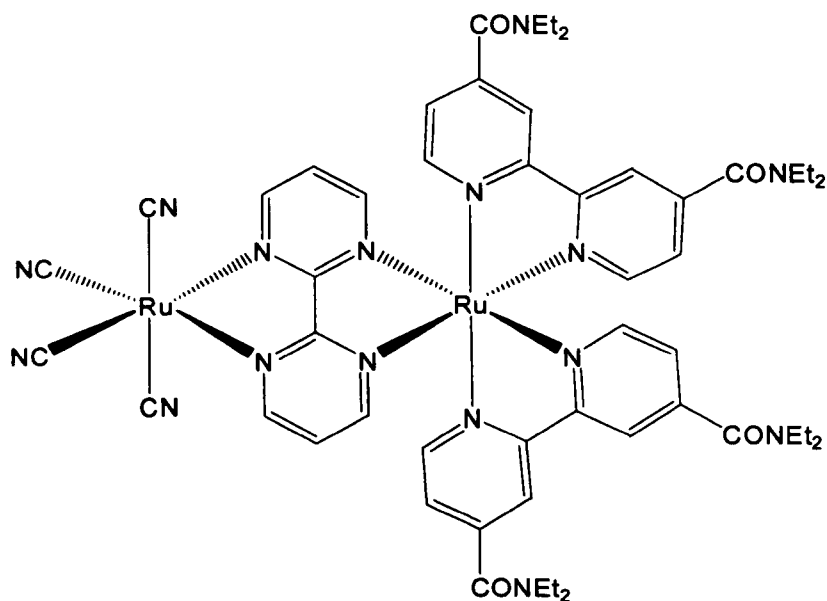


Figure 4.9.3.8: ns-TRIR single-pixel kinetics of bleach (1637 cm^{-1} , bottom) and transient (1651 cm^{-1} , top) bands of ReBPMRubpyamide in CH_3CN solution.

4.10 $\{(\text{NC})_4\text{Ru}(\mu\text{-bpm})\text{Ru}((5,5'\text{-CONEt}_2)_2\text{bpy})_2\}$, RuCNBPMRubpyamide



RuCNBPMRubpyamide is a heterobimetallic complex with **RuCN** and **Rubpyamide** termini on either side of the bpm bridging ligand. As with the other heterobimetallic systems in this Chapter, each terminus has an $\text{M} \rightarrow \text{bpm}$ MLCT chromophore associated with it, and the **Rubpyamide** terminus possesses an additional $\text{Ru} \rightarrow \text{bpyamide}$ chromophore, which may complicate the photophysical dynamics of the system in a similar way to other **Rubpyamide**-containing complexes in this Chapter (§4.4, §4.7 and §4.10). This may become significant in the event of unselective excitation in the TRIR experiments. As in the **RuCN-BL^x-Rubpyamide** complexes in Chapter 3, the **RuCN** terminus is strongly solvatochromic whilst the **Rubpyamide** terminus is almost solvent-independent. As a result the system's photophysics is expected to show considerable differences in low and high A. N. solvents. In CH_3CN the $\text{Ru}_{\text{CN}} \rightarrow \text{bpm}$ transition is postulated to be the lowest energy excited state whilst in D_2O it is expected to be the $\text{Ru}_{\text{bpyamide}} \rightarrow \text{bpm}$ transition. This may provide an insight into the difference in electronic structure of the **RuCN-BL^x-Rubpyamide** and **RuCNBPMRubpyamide** systems, which are constructed from the same chromophores attached to two extreme cases of bridging ligands; strongly conjugated bpm and saturated BL^1 and BL^2 .

Towards the end of the project it became apparent that the sample of **RuCNBPMRubpyamide** used in the experiments performed using the PIRATE apparatus at RAL (particularly affecting TRIR spectra collected in CH₃CN) contained a significant amount of NaCl impurity. Given other work in this thesis (§3.5.1) demonstrating the profound effect that alkali and alkaline earth metals have upon binding to the cyanide groups of the tetracyanoruthenate (II) unit it is conceivable that the bound Na⁺ ions have affected the Ru → bpm and Ru → bpyamide MLCT transition energies and the subsequent photophysics. We interpret the following anomalous results in terms of such metal binding.

4.10.1. UV/visible Absorption and Luminescence Spectroscopy

The UV/visible absorption spectra of **RuCNBPMRubpyamide** have been measured in D₂O and CH₃CN (see Appendix 4.12 for spectra). The results are presented in Table 4.10.1.1.

Solvent	$\lambda^{\max} / \text{nm}$					
	D ₂ O	< 300	362	394	422	494
CH ₃ CN	< 300	364	402	457	494	750
Assignment	IL π - π^*	¹ MC	¹ MLCT	¹ MLCT	¹ MLCT	¹ MLCT
Location	bpy/bpm	RuCN	Rubpyamide	Rubpyamide	RuCN	RuCN

Table 4.10.1.1: Table of peak positions and assignments for UV/visible absorption spectra of RuCNBPMRubpyamide in D₂O and CH₃CN solutions.

The emission spectrum of **RuCNBPMRubpyamide** was measured in CH₃CN solution at room temperature. No luminescence was detected.

4.10.2. Cyclic Voltammetry

Cyclic voltammetry of **RuCNBPMRubpyamide** was measured in CH₃CN (see Appendix 4.12 for voltammograms) and the results are presented in Table 4.10.2.1

below. Features corresponding to three reversible reductions and three oxidation couples (one reversible and two irreversible) are present. As with the other heterobimetallics in this Chapter (§4.8, §4.9), the ease of reduction of the bipyrimidine ligand in this case could be significant as the redox couple's proximity to 0 V indicates that this couple may be accessible in the absence of current, which could have important implications for the electronic structure of the ground and excited states of **RuCNBPMRubpyamide** in solution.

$E_{1/2}/V$ (vs. Fc/Fc ⁺)	Reversibility	Tentative Assignment
$E_p = +1.38$	Irreversible	Re ^{IV/III}
$E_p = +1.17$	Irreversible	Amide Oxidation
$E_p = +0.38$	Irreversible	Ru ^{II/III}
-0.38	Reversible	(bpm) ^{0/+•}
-0.84	Reversible	Amide Reduction
-1.02	Reversible	Amide Reduction

Table 4.10.2.1: Table of potentials for redox couples and assignments from the cyclic voltammogram of **RuCNBPMRubpyamide** in CH₃CN solution.

4.10.3. FTIR, IR OTTLE and Time-Resolved Infrared Spectroscopy

RuCNBPMRubpyamide has been studied using ps and ns-TRIR spectroscopy in D₂O and CH₃CN solutions. As a result of the negative solvatochromism of the **RuCN** terminus we expect the excited state ordering to differ in the two solvents, as in the **RuCN-BL[±]-Rubpyamide** complexes in Chapter 3.

IR OTTLE of **RuCNBPMRubpyamide** in CH₃CN was unsuccessful as the 1st reduction couple was found to be chemically irreversible on the timescale of the experiment.

Deuterium Oxide Solution

The FTIR spectrum of **RuCNBPMRubpyamide** in D₂O solution in the $\nu(\text{CN})$ and amide $\nu(\text{CO})$ region has been measured. In the cyanide region there is a peak profile characteristic of the tetracyanoruthenate (II) unit with 3 resolved maxima at 2099, 2064 and 2054 cm⁻¹. There is also a smaller ‘satellite’ peak visible at 2014 cm⁻¹, which may be composed of a number of unresolved bands. In the amide region there is a single peak present at 1613 cm⁻¹. These results are comparable with the FTIR spectra of the model complexes **RuCNBPM** and **RubpyamideBPM** (§4.2.3, §4.4.3). Satellite peaks at lower wavenumber to the cyanide bands has been observed and these are thought to be due to the partial accessibility of the complex’s 1st reduction in D₂O solution at 0 V. The peaks correspond to the FTIR spectrum of the partially reduced complex with the electron residing on the bipyrimidine ligand. No satellite bands have been observed in the amide $\nu(\text{CO})$ region of the spectrum for reasons discussed in §4.9.3.

Picosecond and nanosecond TRIR spectroscopy (with laser excitation at 400 and 355 nm respectively) were performed on **RuCNBPMRubpyamide** in D₂O solution, monitoring both regions in the IR where reporter groups are present. Each timescale will be discussed in turn and then the validity of the photophysical model will be evaluated.

ps-TRIR Spectroscopy

Figure 4.10.3.1 shows the ps-TRIR spectra obtained for the **RuCN** and **Rubpyamide** termini in D₂O. Figure 4.10.3.2 shows the ps-TRIR kinetics obtained for bleach and transient bands in D₂O.

RuCN (Higher Energy) Terminus

The spectral profile obtained following 400 nm excitation is dominated by a broad bleach with components centred at 2099, 2064 and 2054 cm⁻¹. A transient band is formed at higher energy to the bleaches, centred at 2102 cm⁻¹. This is consistent with

$\text{Ru}_{\text{CN}} \rightarrow \text{bpm } ^3\text{MLCT}$ being the lowest energy excited state, as predicted by the photophysical model. A very weak transient band is also detected to lower wavenumber than the bleach at 1986 cm^{-1} . By invoking the dipole moment and IR oscillator strength arguments presented in §4.6.3, it is possible that this band may represent a very small population of molecules but does suggest that the excited state electronic charge resides on bpm and therefore that $\text{Ru} \rightarrow \text{bpm MLCT}$ is occurring. The bands decay monoexponentially with $\tau = 181 (\pm 24) \text{ ps}$ (averaged over bleach and transient features). At $\Delta t = 1 \text{ ns}$ only *ca.* 5% of the signal at $\Delta t = 1 \text{ ps}$ remains. This indicates that quenching of the excited state is almost complete during the picosecond time domain.

Rubpyamide (Lower Energy) Terminus

The ps-TRIR spectra obtained are comprised of a parent bleach centred at 1613 cm^{-1} and a transient band to lower wavenumber at 1601 cm^{-1} . This is consistent with an increase in electron density on the bpy ligands, expected during the formation of a $\text{Ru} \rightarrow ((4,4'\text{-CONEt}_2)_2\text{bpy}) ^3\text{MLCT}$ excited state. This is in contradiction to the earlier statement in §4.1 that $\text{Ru} \rightarrow \text{bpm } ^3\text{MLCT}$ transitions are always at lower energy than $\text{Ru} \rightarrow \text{bpy } ^3\text{MLCT}$ transitions. Additionally a transient is observed at 1545 cm^{-1} , although no accompanying bleach is detected. This feature can be assigned to a ring mode of the bipyrimidine ligand, directly reporting on the increase in electron density on the bridging ligand.

Examination of the kinetics of the amide bands gives a biexponential relationship with decay constants $\tau_1 = 8 (\pm 3)$ and $\tau_2 = 190 (\pm 13) \text{ ps}$. There is good agreement of τ_2 with the decay of the **RuCN** terminus. Interestingly the kinetics of the bipyrimidine transient band at 1545 cm^{-1} exhibit a growth over the first 20 ps followed by decay with $\tau = 150 (\pm 15) \text{ ps}$. This growth gives good agreement with the fast decay component of the **Rubpyamide** terminus and strongly suggests that (as expected) the $\text{Ru} \rightarrow ((4,4'\text{-CONEt}_2)_2\text{bpy}) ^3\text{MLCT}$ excited state is converting into the $\text{Ru} \rightarrow \text{bpm } ^3\text{MLCT}$ excited state.

If this was the case, then we would expect to observe transient features at higher wavenumber to the bleach in the amide spectrum (as in **ReBPMRubpyamide**, §4.9.3). However these bands are not observed. This anomalous result may be a consequence of NaCl impurity in the sample perturbing the electronic structure and photophysical behaviour of the complex *via* Na^+ binding to the cyanide ligands.

Acetonitrile Solution

ps-TRIR Spectroscopy

Figure 4.10.3.3 shows the ps-TRIR spectra obtained for the **ReCO** and **Rubpyamide** termini in CH_3CN . Figure 4.10.3.4 shows the ps-TRIR kinetics obtained for bleach and transient bands in CH_3CN .

RuCN (Lower Energy) Terminus

The spectral profile obtained following 400 nm excitation is dominated a bleach with components centred at 2099, 2075 and 2065 cm^{-1} . A broad transient band is detected at lower energy to the bleach, centred at 2033 cm^{-1} . This is consistent with the **RuCN** terminus experiencing an increase in electron density due to $^3\text{MLCT}$ excited state formation on the other terminus. No transient band was detected to higher wavenumber, although the data obtained suffer from noise due to instability of the probe laser at RAL and weak bands may be indistinguishable from baseline fluctuations. The reader is reminded of the *caveat* with this system (particularly in CH_3CN) as a result of sample impurity (§4.10.1). A biexponential decay is observed with $\tau_1 = 16 (\pm 8)$ and $\tau_2 = 96 (\pm 13)$ ps (averaged over both bleach and transient features). At $\Delta t = 1$ ns less than 5% of the signal at $\Delta t = 1$ ps remains, reiterating the very short lifetime of the excited state formed.

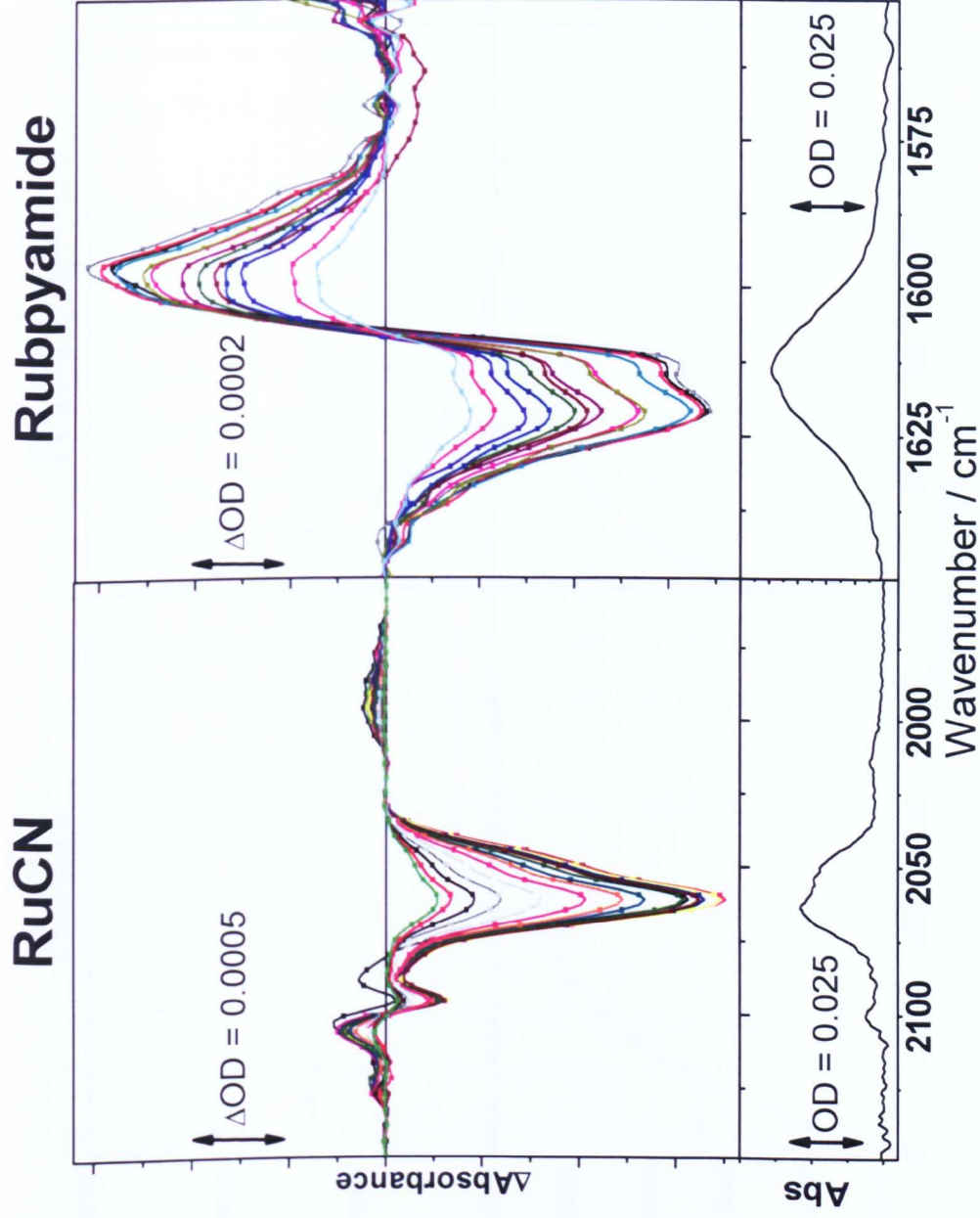


Figure 4.10.3.1: The FTIR (bottom) and ps-TRIR spectra (top) of the RuCN (left) and Rubpyamide (right) termini of ReBPMBRubpyamide in D_2O solution.

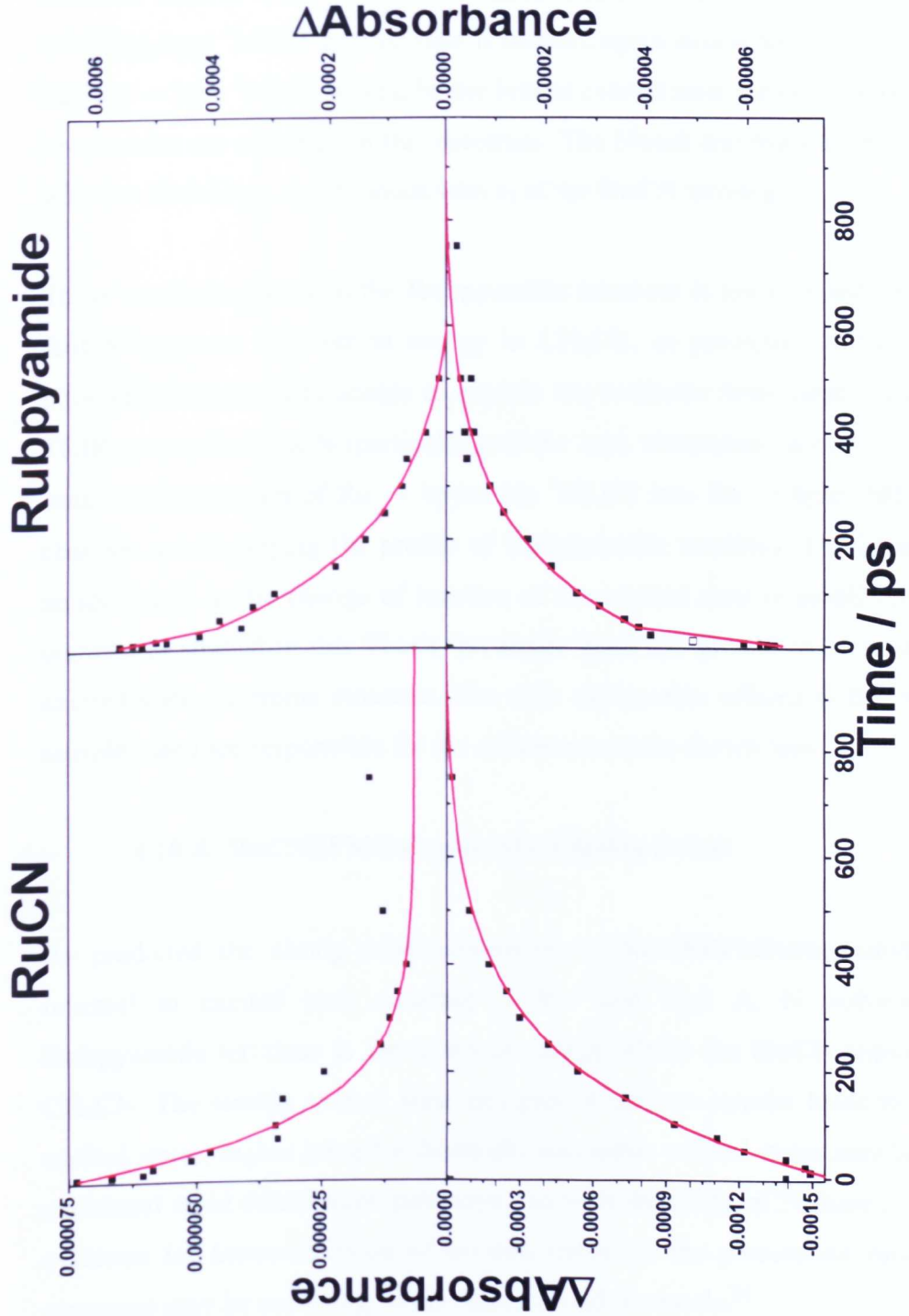


Figure 4.10.3.2: ps-TRIR kinetics of RuCNBPMBRubpyamide in D₂O solution for RuCN (transient at 2001 cm⁻¹, top left and bleach at 2065 cm⁻¹, bottom left) and Rubpyamide (transient at 1599 cm⁻¹, top right and bleach at 1618 cm⁻¹, bottom right) termini for $\Delta t = 0$ -1000 ps.

Rubpyamide (Higher Energy) Terminus

The ps-TRIR spectra obtained are comprised of a bleach centred at 1637 cm^{-1} and a transient band to lower wavenumber centred at 1623 cm^{-1} , implying that a $\text{Ru} \rightarrow ((4,4'\text{-CONEt}_2)_2\text{bpy})^3\text{MLCT}$ excited state is formed, again in contrast to the model's prediction that $\text{Ru} \rightarrow \text{bpm}^3\text{MLCT}$ would be the lowest excited state formed. No bands arising from bpm modes are observed in this spectrum. The bleach and transient bands decay rapidly with $\tau = 13 (\pm 1)\text{ ps}$, synchronous with τ_1 of the **RuCN** terminus.

These results suggest that the **Rubpyamide** terminus is lower in energy in D_2O and the **RuCN** terminus is lower in energy in CH_3CN , as predicted by the model. But our photophysical model is unable to explain the evidence from kinetic analysis of the ps-TRIR spectra in CH_3CN (particularly of the bpm vibrational mode) the apparent excited state interconversion of $\text{Ru} \rightarrow \text{bpyamide}^3\text{MLCT}$ into $\text{Ru} \rightarrow \text{bpm}^3\text{MLCT}$ without any changes accompanying the profile of **Rubpyamide** terminus. The insensitivity of the amide bands to the change of location of the excited state is perplexing as in all other complexes studied in this Thesis the amide band has proved to be a sensitive probe of excited state electronic structure. The only explanation offered is that impurities in the samples used are responsible for the erroneous results shown here.

4.10.4. RuCNBPMRubpyamide: Closing Points

As predicted the strong solvatochromism of **RuCNBPMRubpyamide** has led to a reversal in excited state ordering in low and high A. N. solvents. In D_2O the **Rubpyamide** terminus is the lower in energy whilst the **RuCN** terminus is lowest in CH_3CN . The similar excited state energies of the two termini leads to very short-lived excited states; higher lying but thermally accessible excited states may be responsible for additional rapid deactivation pathways. As with **ReBPMRuCN** there is no direct kinetic evidence for interconversion of excited states on the picosecond timescale but these processes may be occurring on the femtosecond timescale.²¹

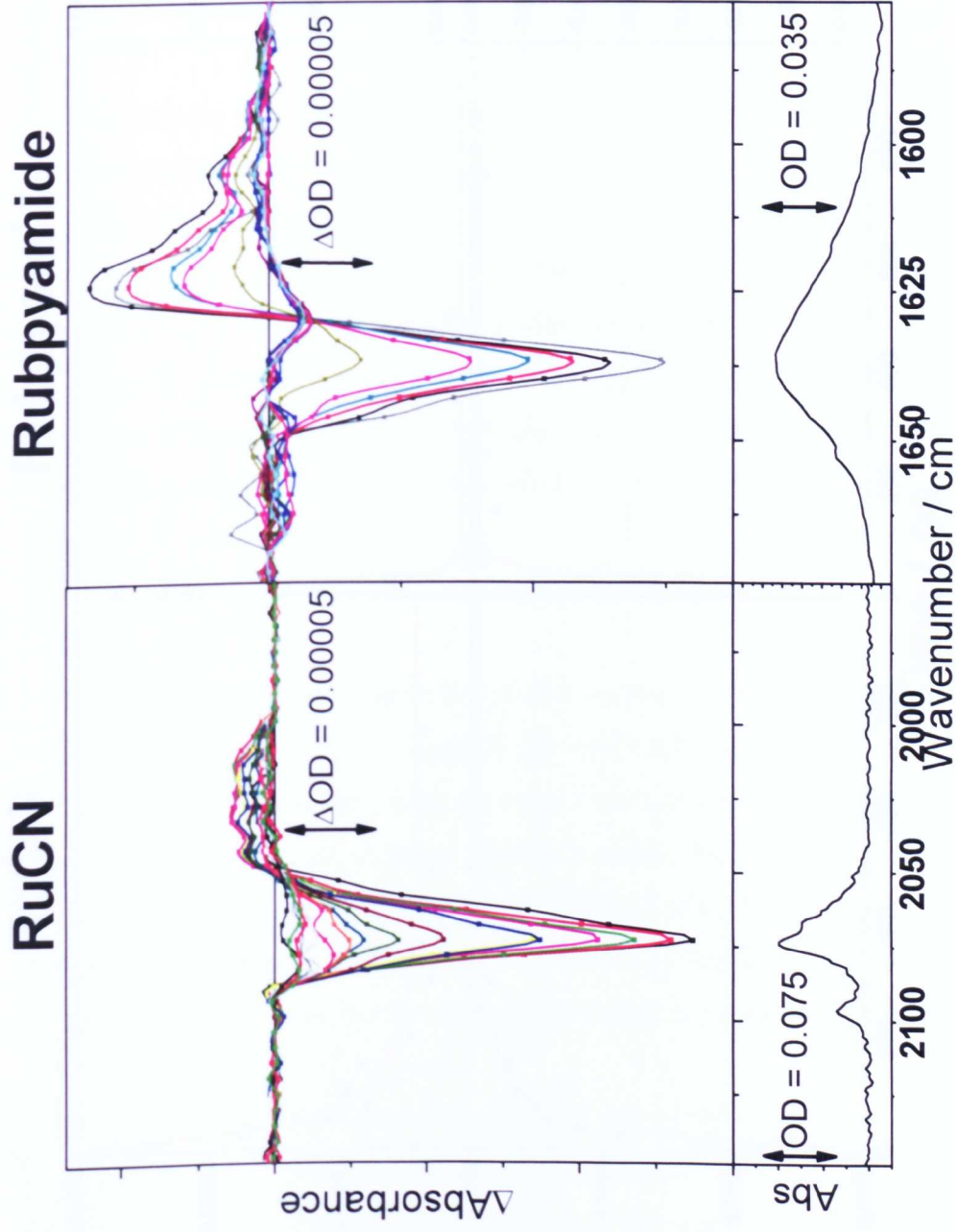


Figure 4.10.3.3: The FTIR (bottom) and ps-TRIR spectra (top) between 1 and 1000 ps (top) of the RuCN (left) and Rubpyamide (right) termini of ReBPMRubpyamide in CH₃CN solution.

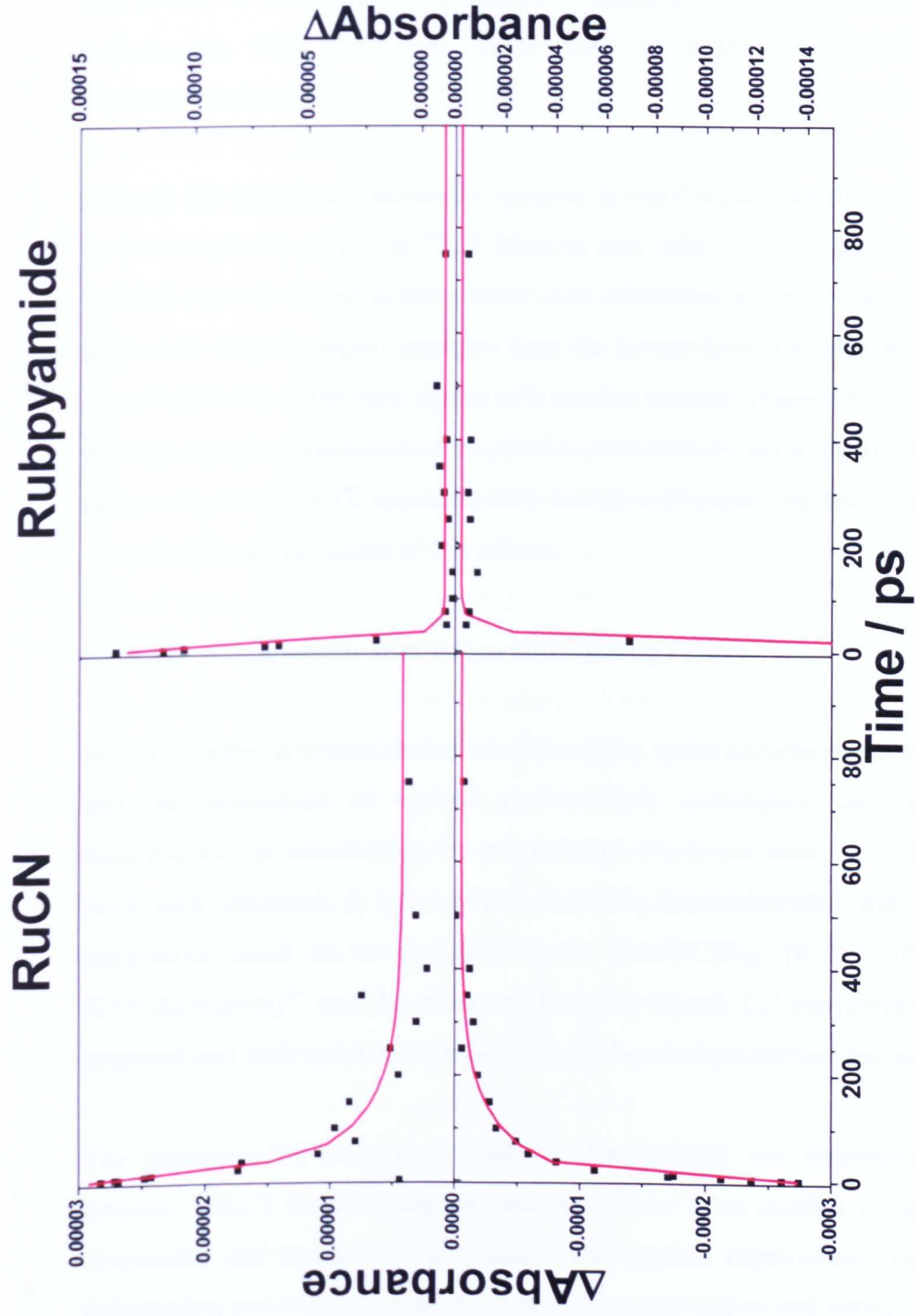


Figure 4.10.3.4: *ps-TRIR kinetics of RuCNBPMRubpyamide in CH₃CN solution for RuCN (transient at 2033 cm⁻¹, top left and bleach at 2073 cm⁻¹, bottom left) and Rubpyamide (transient at 1624 cm⁻¹, top right and bleach at 1637 cm⁻¹, bottom right) termini for $\Delta t = 0$ -1000 ps.*

Many of the TRIR spectra and kinetic traces measured for **RuCNBPMRubpyamide** give inconsistent or anomalous results compared to other complexes in this Chapter. The reader is reminded of the sample contamination that was discovered after the experiments were conducted which may be responsible for the unexplained phenomena observed.

As with the other heterobimetallic systems in this Chapter, another contributing factor to the complexity of the ps-TRIR kinetics may arise from the presence of additional $^3\text{MLCT}$ states involved in the excited state relaxation process. These states are likely to possess slightly higher energies than the lowest-lying one due to the presence of two π^* LUMOs in the bpm ligand with similar energies (Figure 4.1.1.2). Additionally the high sample concentrations required experimentally to obtain good signal-to-noise ratios with the PIRATE apparatus may lead to self-quenching and/or aggregation (see Chapter 6 for a discussion of this effect).

4.11. Chapter Discussion and Closing Points

In this Chapter, previous studies of d^6 transition metal complexes have been presented and the limitations of optical spectroscopic techniques such as UV/vis and luminescence in determining the excited state electronic structure of bpm complexes have been discussed. A series of monometallic, homobimetallic and heterobimetallic complexes based on the building blocks $[\text{ReCl}(\text{CO})_3]$, $[\text{Ru}(\text{CN})_4]^{2-}$ and $[\text{Ru}(4,4\text{-}(\text{CONEt}_2)_2\text{bpy})_2]^{2+}$ and the bidentate bridging ligand 2,2'-bipyrimidine (bpm) were prepared and their spectroscopic and electrochemical properties studied.

The monometallic complexes **ReBPM**, **RuCNBPM** and **RubpyamideBPM** each possess $^3\text{MLCT}$ lowest-lying excited states and were studied using TRIR on the picosecond and nanosecond timescales, a substantial improvement on the amount of information previously available using UV/vis absorption and emission spectroscopy. The excited state energies of these complexes are found to be lower than corresponding complexes of 2,2'-bipyridine, in agreement with previous reports and

this may be a contributing factor to the inherently weak luminescence of bpm-containing complexes. In the case of **RubpyamideBPM** the presence of two polypyridyl chromophores gives rise to more complicated photophysical dynamics, with excited state interconversion of $\text{Ru} \rightarrow \text{bpy}^3\text{MLCT}$ into $\text{Ru} \rightarrow \text{bpm}^3\text{MLCT}$ observed using the amide $\nu(\text{CO})$ bands and vibrational modes of the bpm ligand. The results obtained were found to be similar to those in the literature for identical or related complexes.

The homobimetallic complexes **(Re)₂BPM**, **(RuCN)₂BPM** and **(Rubpyamide)₂BPM** display more complex photophysics than their monometallic precursors. For the pair **(Re)₂BPM** and **(RuCN)₂BPM** whose IR reporters are ligands directly connected to the metal centre, the ps-TRIR spectra collected indicate that there is electronic asymmetry in the excited state; one metal centre is undergoing MLCT excitation to the bridging bpm and the other is sensing it, giving rise to two sets of excited state bands. These are located either side of the ground state bleach, such that one set of bands are shifted to higher wavenumber and the other set are shifted to lower wavenumber relative to the parent bands. These results indicate that the excited states probed are localised on the IR timescale (§1.3), in keeping with similar studies in the literature (§4.1.3).¹⁰ **(Rubpyamide)₂BPM**'s IR reporter groups are attached to pendant bpy ligands and as such return less detailed spectroscopic information on the electron density at the metal centre, however insights on excited state interconversion have been gleaned from the kinetic data collected and investigation of the lineshapes of the spectra (*vide infra*). The results obtained for **(Re)₂BPM** and **(Rubpyamide)₂BPM** were found to be similar to those in the literature for identical or related complexes.

It is interesting to compare the lifetimes of **ReBPM** and **(Re)₂BPM** vs. **RuCNBPM** and **(RuCN)₂BPM** in CH_3CN . Although in both cases the dinuclear complexes have a shorter lifetime than the corresponding mononuclear complexes, the difference is significantly less between **RuCNBPM** and **(RuCN)₂BPM** ($\tau_{\text{Mono}} \approx 3 \times \tau_{\text{Bimetallic}}$) than between **ReBPM** and **(Re)₂BPM** ($\tau_{\text{Mono}} \approx 26 \times \tau_{\text{Bimetallic}}$). Secondly, although the

lifetimes of both **RuCNBPM** and **(RuCN)₂BPM** in D₂O are much longer than in CH₃CN, the same ratio of lifetimes is observed ($\tau_{\text{Mono}} \approx 3 \times \tau_{\text{Bimetallic}}$). This can be ascribed to the fact that addition of a second [ReCl(CO)₃] centre (on changing from **ReBPM** to **(Re)₂BPM**) reduces the lowest ¹MLCT absorption by 5400 cm⁻¹, whereas addition of a second [Ru(CN)₄]²⁻ centre (on changing from **RuCNBPM** to **(RuCN)₂BPM**) has a smaller effect on the lowest MLCT state, reducing the lowest ¹MLCT absorption by only 3300 cm⁻¹ in water. Consequently there is a bigger difference between the LUMO energies of **ReBPM** and **(Re)₂BPM** than between **RuCNBPM** and **(RuCN)₂BPM**, and the energy-gap law will result in a bigger drop in the excited state lifetimes between **ReBPM** and **(Re)₂BPM**. It is likely that the weaker stabilising effect on the bpm LUMO of an additional [Ru(CN)₄]²⁻ unit compared to an additional [ReCl(CO)₃] is because the former is a poorer π -acceptor on account of its doubly negative charge.

Lineshape analysis of the ps-TRIR spectra of **RubpyamideBPM** and **(Rubpyamide)₂BPM** determined that there is an obscured transient feature at lower energy to the bleach for **RubpyamideBPM** but not for **(Rubpyamide)₂BPM**. This suggests that the Ru \rightarrow bpy into Ru \rightarrow bpm ³MLCT excited state conversion process occurs on the picosecond timescale in the monometallic complex but on the femtosecond timescale in the homobimetallic complex.

The heterobimetallic complexes **ReBPMRuCN**, **ReBPMRubpyamide** and **RuCNBPMRubpyamide** each possess two different chromophores and IR reporter groups, generally resulting in more complicated photophysical dynamics than the homobimetallic complexes. In the case of **ReBPMRuCN** there is substantial overlap between the IR bands of the **RuCN** and **ReCO** termini, resulting in a very convoluted spectrum which is difficult to meaningfully analyse. The spectra obtained for **ReBPMRubpyamide** indicate that excited state conversion from Re \rightarrow bpm ³MLCT into Ru \rightarrow bpm ³MLCT is observed on the picosecond timescale. **RuCNBPMRubpyamide** has an interesting relationship with the **RuCN-BL^x-Rubpyamide** systems in Chapter 4. The replacement of the saturated bridging ligand

BL^1/BL^2 for the conjugated bpm ought to have provided an interesting comparison, but the spectra collected for **RuCNBPMRubpyamide** are somewhat anomalous and provide limited insight due to a problem with NaCl impurity. However this is ostensibly a testament to the strong binding of alkali and alkali earth metals to cyanide ligands, an effect which is deliberately exploited in Chapter 3!

In both heterobimetallic complexes containing a **ReCO** terminus the initial laser excitation is unselective, populating 3MLCT excited states on either terminus. Internal relaxation processes then facilitate $Re \rightarrow bpm$ to $Ru \rightarrow bpm$ 3MLCT excited state interconversion, with evidence for this from the grow-in of absorbance of the **Rubpyamide** terminus of **ReBPMRubpyamide** in D_2O and CH_3CN . The polyexponential time dependence of heterobimetallic ps-TRIR has been rationalised in terms of the presence of (at least) two independent 3MLCT states involved in the excited state relaxation process. These states are likely to possess similar energies due to the presence of two π^* LUMOs in the bpm ligand with similar energies (Figure 4.1.1.2).

In the complex **RuCNBPMRubpyamide** which presented some anomalous results, ps-TRIR suggests a similar scenario occurs with unselective excitation and subsequent excited state relaxation to the lowest-energy 3MLCT . The unusually short lifetimes of the excited states formed may be in part due to a number of factors, discussed in §4.10.4. These include the projected proximity of the energies of the lowest 3MLCT excited states located on the **RuCN** and **Rubpyamide** termini leading to additional thermally-accessible excited state deactivation pathways, multiple close-lying 3MLCT excited states on each terminus (due to the electronic structure of bpm, *vide supra*) and the contamination of the sample with NaCl impurity. The latter is likely to result in the binding of Na^+ ions to the cyanide ligands – an effect which demonstrably alters the electronic structure of the **RuCN** terminus to the extent that excited state ordering may be affected (§3.5.1).

Although the possibility of IVCT transitions in these complexes has been mentioned at several points throughout the Chapter on account of the extent of electronic communication between the two metal centres in such bimetallic systems, no evidence for such a process has been identified. The ground state structures of these complexes are unlikely to exhibit IVCT – a redox event may be required to generate a mixed-valence species (*e.g.* Ru^{II}-bpm-Ru^{III}) which may then undergo IVCT processes. It was postulated that the presence of a redox couple in the cyclic voltammograms of some bimetallic complexes near 0 V (see §4.12 for the voltammograms obtained) may have provided the necessary ‘switching’ event to activate IVCT but no evidence has been observed for this in terms of low energy UV/Vis absorption bands or nIR luminescence features.

Finally, returning to the questions posed at the start of this Chapter:

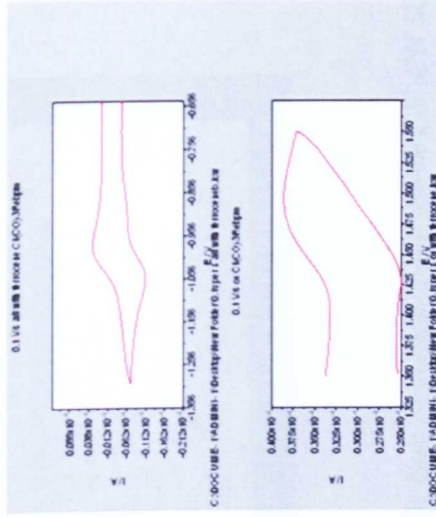
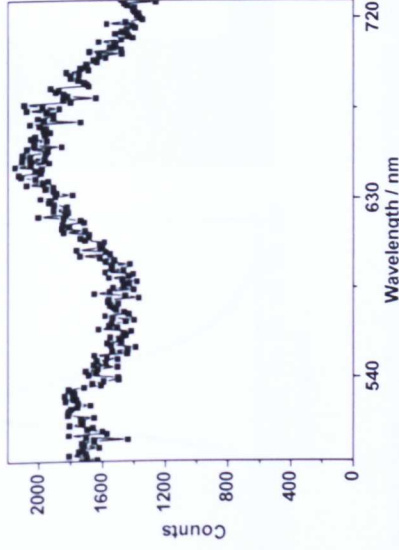
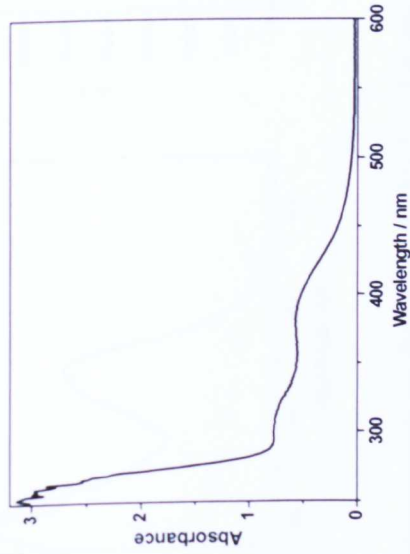
- Rhenium (I) and ruthenium (II) complexes of bpm exhibit weaker luminescence and shorter excited state lifetimes than the corresponding bpy complexes because the bpm ligand possesses multiple low energy LUMOs which in accordance with the energy-gap law the smaller HOMO-LUMO energy difference leads to short-lived excited states and more efficient non-radiative decay.
- All of the bimetallic complexes have been shown to possess excited states which are localised on the IR timescale. In many cases there are multiple excited state species present in solution and efficient interconversion to form the lowest energy ³MLCT excited state occurs on the femtosecond or picosecond timescales. The observation of many of these ‘dark’ (non-luminescent) states would not be possible using emission spectroscopy.
- The consequences of unselective excitation of MLCT chromophores have been observed with some convoluted spectra (*e.g.* **ReBPMRuCN**) from which it has been difficult to extract information from. It is conceivable that higher

resolution TRIR spectroscopy would be useful to understand such systems further.

- No evidence for IVCT processes has been observed using UV/vis absorption, luminescence or TRIR spectroscopy or electrochemistry.

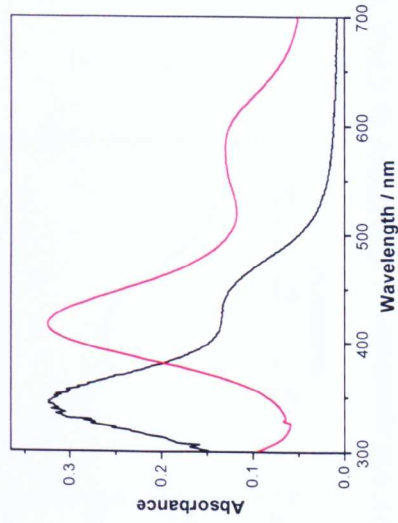
4.12. Appendix of Spectra and Voltammograms

ReBPM



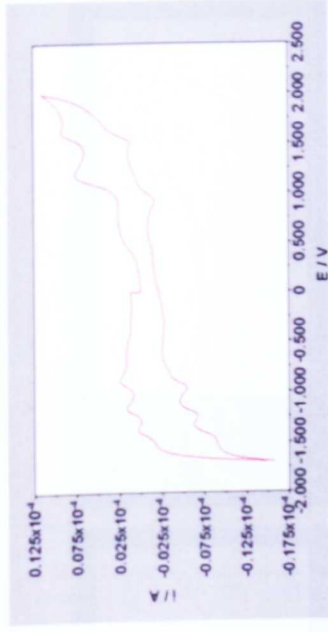
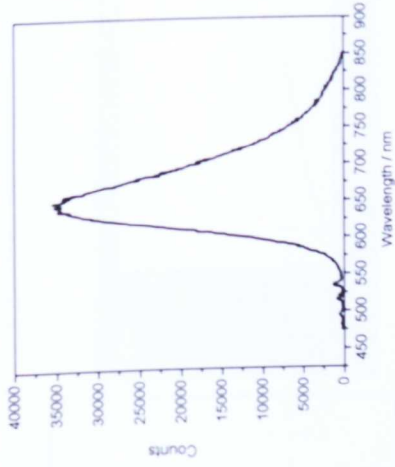
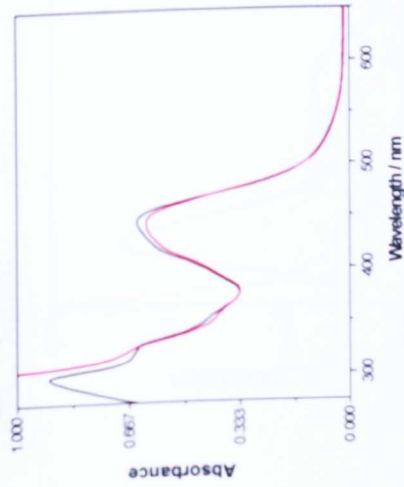
Measurements on ReBPM in CH₃CN: UV/Vis spectrum (left); luminescence spectrum ($\lambda_{ex} = 375$ nm, centre); cyclic voltammograms (right).

RuCNBPM



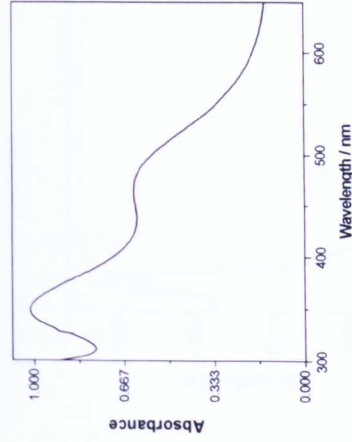
UV/Vis spectrum of RuCNBPM in D₂O (black) and CH₃CN (red).

RubpyamBPM



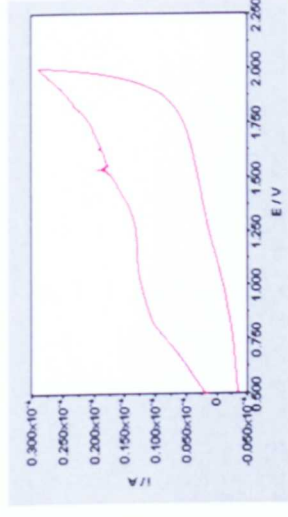
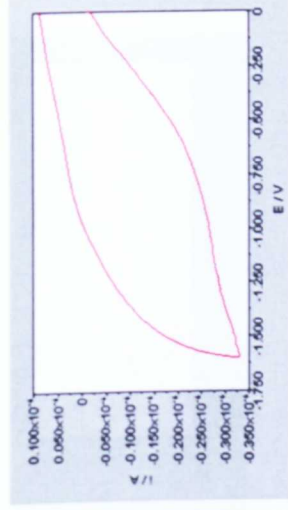
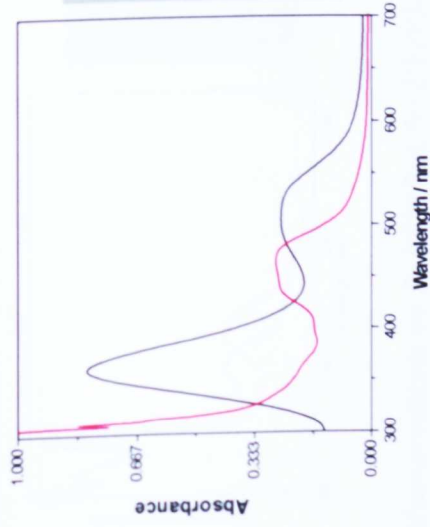
Measurements on RubpyamBPM: UV/Vis spectrum (left) in D_2O (black) and CH_3CN (red); luminescence spectrum in CH_3CN (I_{ex}) = 461 nm, centre) (left); cyclic voltammogram in CH_3CN (right).

(Re)₂bpm



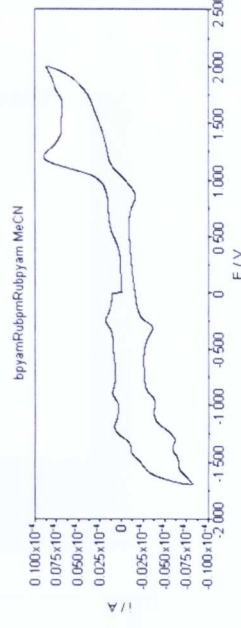
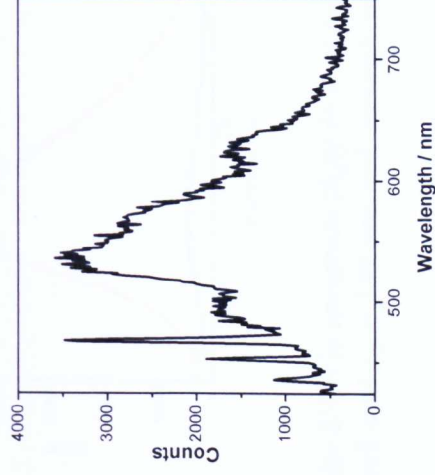
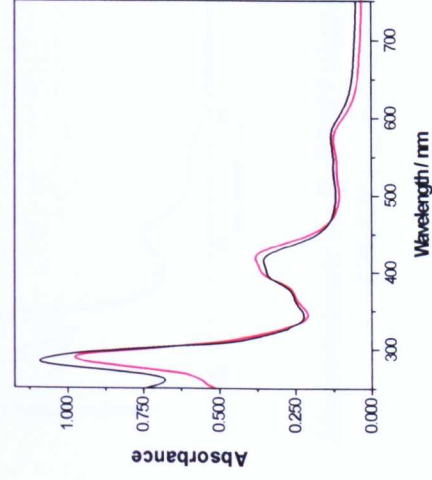
UV/Vis spectrum of $(Re)_2bpm$ in CH_3CN .

(RuCN)₂BPM



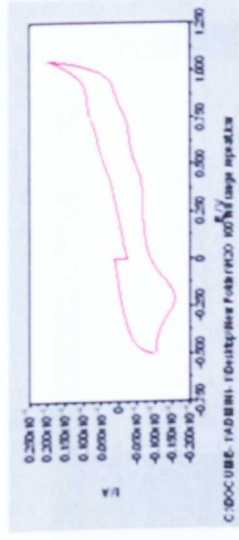
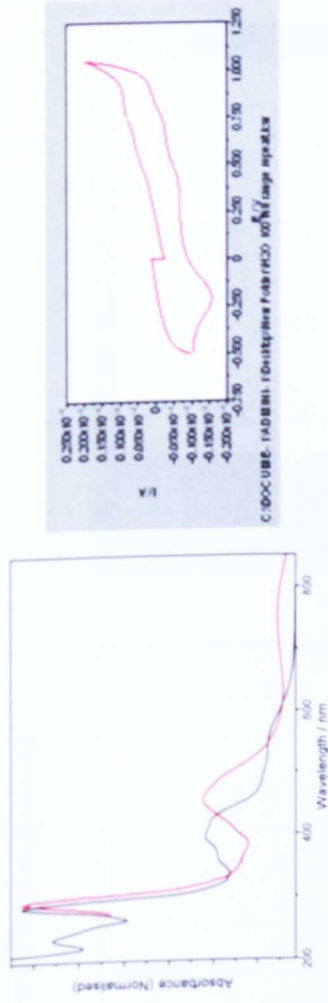
Measurements on (RuCN)₂BPM: UV/Vis spectrum (left) in D₂O (black) and CH₃CN (red); cyclic voltammogram in CH₃CN (middle and right).

(Rubpyam)₂BPM



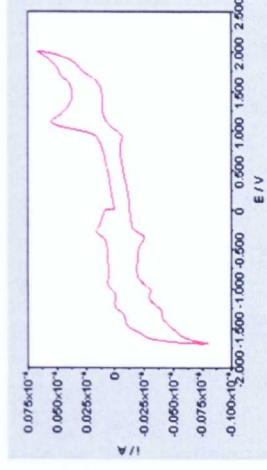
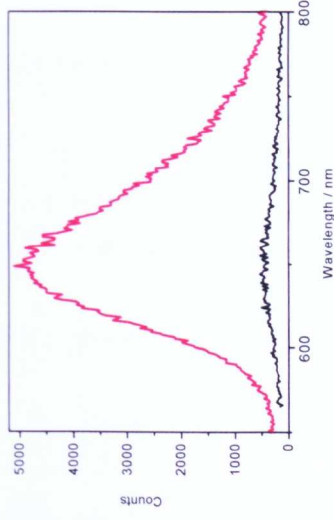
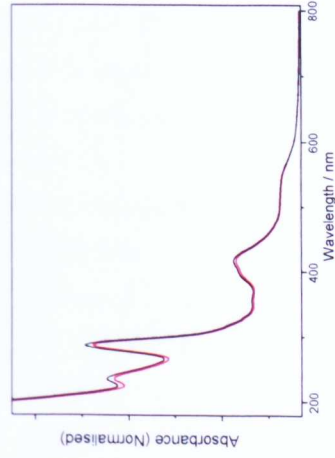
Measurements on (Rubpyam)₂BPM: UV/Vis spectrum (left) in D₂O (black) and CH₃CN (red); luminescence spectrum in CH₃CN ($\lambda_{ex} = 550$ nm, black and $\lambda_{ex} = 550$ nm, red, centre); cyclic voltammogram in CH₃CN (right).

ReBPMRuCN



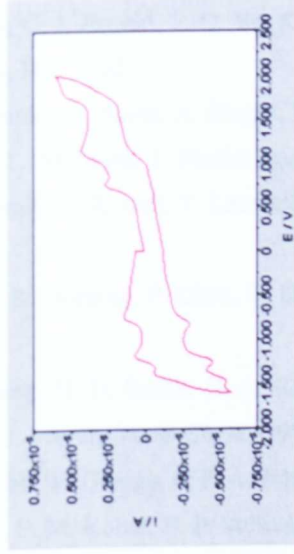
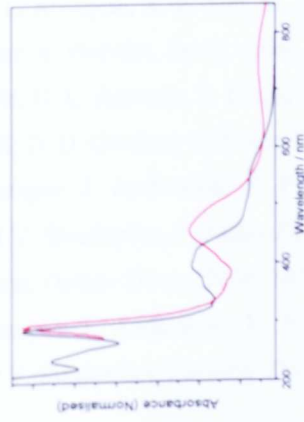
Measurements on ReBPMRuCN: UV/Vis spectrum (left) in D₂O (black) and CH₃CN (red); cyclic voltammogram in CH₃CN (right).

ReBPMRubpyamide



Measurements on ReBPMRubpyamide: UV/Vis spectrum (left) in D₂O (black) and CH₃CN (red); luminescence spectrum in CH₃CN ($\lambda_{ex} = 550$ nm, black and $\lambda_{ex} = 550$ nm, red, centre); cyclic voltammogram in CH₃CN (right).

RuCNBPMRubyamide



Measurements on RuCNBPMRubyamide: UV/Vis spectrum (left) in D₂O (black) and CH₃CN (red); cyclic voltammogram in CH₃CN (right).

4.13. References

- ¹ W. Matheis and W. Kaim, *Inorg. Chim. Acta*, 1991, **181**, 15.
- ² P. S. Braterman, J.-I. Song, S. Kohlmann, C. Vogler and W. Kaim, *J. Organomet. Chem.*, 1991, **411**, 207.
- ³ P. S. Braterman and J.-I. Song, *J. Org. Chem.*, 1991, **56**, 4678.
- ⁴ B. P. Sullivan, J. A. Baumann, T. J. Meyer, D. J. Salmon, H. Lehmann and A. Ludi, *J. Am. Chem. Soc.*, 1977, 7370.
- ⁵ A. Vogler and J. Kisslinger, *Inorg. Chim. Acta*, 1986, **115**, 193.
- ⁶ W. Kaim, H. E. A. Kramer, C. Vogler and J. Rieku, *J. Organomet. Chem.*, 1989, **367**, 107.
- ⁷ R. Sahai, D. P. Rillema, R. Shaver, S. van Wallendael, D. C. Jackman and M. Boldaji, *Inorg. Chem.*, 1989, **28**, 1022.
- ⁸ A. C. Samuels and M. K. DeArmond, *Inorg. Chem.*, 1995, **34**, 5548.
- ⁹ M. W. George, F. P. A. Johnson, J. R. Westwell, P. M. Hodges and J. J. Turner, *J. Chem. Soc. Dalton Trans.*, 1993, 2977.
- ¹⁰ L. C. Abbott, C. J. Arnold, T.-Q. Ye, K. C. Gordon, R. N. Perutz, R. E. Hester and J. N. Moore, *J. Phys. Chem. A*, 1998, **102**, 1252.
- ¹¹ See for example: W. Kaim, A. Dogan, M. Wanner, A. Klein, I. Tiritiris, T. Schleid, D. J. Stufkens, T. L. Snoeck, E. J. L. McInnes, J. Fiedler and S. Zalis, *Inorg. Chem.*, 2002, **41**, 4139; N. M. Shavaleev, G. Accorsi, D. Virgili, Z. R. Bell, T. Lazarides, G. Calogero, N. Amaroli and M. D. Ward, *Inorg. Chem.*, 2005, **44**, 61.
- ¹² L. A. Worl, R. Duesing, P. Chen, L. Della Ciana and T. J. Meyer, *J. Chem. Soc., Dalton Trans.*, 1991, 849.
- ¹³ K. M. Omberg, G. D. Smith, D. A. Kavaliunas, P. Y. Chen, J. A. Treadway, J. R. Schoonover, R. A. Palmer and T. J. Meyer, *Inorg. Chem.*, 1999, **38**, 951.
- ¹⁴ J. J. Turner, M. W. George, F. P. A. Johnson and J. R. Westwell, *Coord. Chem. Rev.*, 1993, **125**, 101;
- ¹⁵ J. V. Caspar, E. M. Kober, B. P. Sullivan and T. J. Meyer, *J. Am. Chem. Soc.*, 1982, **104**, 630.
- ¹⁶ H. Adams, W. Z. Alsindi, G. M. Davies, M. B. Duriska, T. L. Easun, H. E. Fenton, J.-M. Herrera, M. W. George, K. L. Ronayne, X.-Z. Sun, M. Towrie and M. D. Ward, *Dalton Trans.*, 2006, 39.
- ¹⁷ M. Kovács and A. Horváth, *Inorg. Chim. Acta*, 2002, **335**.
- ¹⁸ S. F. A. Kettle, G. L. Aschero, E. Diana, R. Rosetti and P. L. Stanghellini, *Inorg. Chem.*, 2006, **45**, 4928.
- ¹⁹ W. Z. Alsindi, D. O. Gardner, E. F. van Dishoeck and H. J. Fraser, *Chem. Phys. Lett.*, 2003, **378**, 178.
- ²⁰ See for example: J. Andersson, F. Puntoriero, S. Serroni, A. Yartsev, T. Pascher, T. Polivka, S. Campagna and V. Sundström, *Faraday Discuss.*, 2004, **127**, 295; S. Ott, M. Borgström, L. Hammarström and O. Johansson, *Dalton Trans.*, 2006, 1434.
- ²¹ See for example: J. Andersson, F. Puntoriero, S. Serroni, A. Yartsev, T. Pascher, T. Polivka, S. Campagna and V. Sundström, *Faraday Discuss.*, 2004, **127**, 295.

Chapter 5:

Closing Points and Future Work

Chapter 5: Closing Points and Future Work

5.1. Introduction

In this Thesis, “Solvent Based Switching of the Photophysical Properties of Polynuclear Complexes” two different types of photophysically active supramolecular system have been designed and studied using a variety of spectroscopic, electrochemical and theoretical techniques, in low and high Acceptor Number solvents (CH₃CN and D₂O respectively). The transition metal moieties used as modular building blocks, [Ru(CN)₄]²⁻, [Ru((4,4’-CONEt₂)₂bpy)₂]²⁺ and [ReCl(CO)₃] were combined with the bridging ligands BL¹ and BL² (Chapter 3) and bpm (Chapter 4) to construct monometallic,¹ homobimetallic² and heterobimetallic³ complexes containing zero, one or two strongly solvatochromic [Ru(CN)₄]²⁻ moieties. This has enabled the study of ‘solvent-switchable’ systems (*e.g.* **RuCN-BL¹-Rubpyamide**, §3.5) to be carried out alongside bimetallic complexes which exhibit strong negative solvatochromism but no solvent dependence in the location of their lowest ³MLCT excited state (*e.g.* **(RuCN)₂BPM**, §4.6) and also complexes which exhibit strong solvatochromism but the same excited state ordering regardless of solvent environment (*e.g.* **ReBPMRuCN**, §4.8).

A study of tetracyanoruthenate (II) complexes with a series of polypyridyl ligands was presented in Chapter 2, providing a valuable dataset for the scientific community with UV/vis, luminescence and TRIR spectroscopies, crystallography* and electrochemistry. This study has demonstrated the utility of the ν(CN) bands of the [Ru(CN)₄]²⁻ unit to act as a sensitive reporter of ground and excited state electron density.

Furthermore an additional mechanism for modulating the ³MLCT excited state energy of the [Ru(CN)₄]²⁻ unit was also briefly demonstrated by way of a luminescence titration of **RuCN-BL¹-Rubpyamide** with Ba²⁺ ions (§3.5.1). This study has recently

* Performed at the University of Sheffield by Mr. T. L. Easun and co-workers and not shown in this Thesis.

been expanded upon by Prof. M. D. Ward and co-workers through spectroscopic monitoring of titrations with a variety of metal ions and tetracyanoruthenate (II) complexes and is the subject of a recent publication.⁴ This article (in conjunction with the luminescence titration detailed in §3.5.1) demonstrates the ability of the cyanide ligands of the $[\text{Ru}(\text{CN})_4]^{2-}$ unit to strongly and reversibly bind metal ions which modulate the $^3\text{MLCT}$ excited state energies of the $[\text{Ru}(\text{CN})_4(\text{NN})]^{2-}$ moiety.

The ps and ns-TRIR spectra shown throughout this Thesis which have been central to probing the photophysical processes occurring in Chapters 2, 3 and 4 were recorded using the PIRATE spectrometer at the Rutherford Appleton Laboratory. This meant that the amount of time which could be devoted to collecting spectra and designing experiments based on the results obtained was largely determined by our success (or otherwise) in being awarded experimental time at the Central Laser Facility and various experimental issues such as the performance of the pump and probe lasers, detectors and data acquisition software. Our proposals to study our solvent-switchable bimetallic systems (Chapters 3 and 4) using ultrafast transient UV/vis and Raman spectroscopies were unsuccessful, restricting us to focus on ultrafast TRIR spectroscopy as our primary time-resolved technique.

With the imminent completion of a custom-built picosecond time-resolved IR, UV/vis, Raman and fluorescence spectroscopic suite in the School of Chemistry, University of Nottingham more detailed and complete investigations will be possible. Such investigations could include more advanced experiments such as t2D-IR hole-burning and labelling experiments (§1.4.1.3). With this in mind one hopes that the next generation of Nottingham spectroscopists will be able to use these state-of-the-art facilities to design and execute more complete ultrafast spectroscopic studies of transition metal excited states.

5.2. Closing Points and Future Work

In Chapter 2 “Tetracyanoruthenate (II) Complexes With α -Diimine Ligands” a family of $[\text{Ru}(\text{CN})_4(\text{NN})]^{2-}$ complexes was presented and studied. The dataset presented (and also those in Chapters 3 and 4) would benefit from study of the photophysical properties (and hence the effect of SSDA interactions) in a greater number of solvent environments. A good candidate for such an environment might be CH_3OH . This would be a suitable choice as its A. N. (41.3) is approximately midway between that of D_2O (54.8) and CH_3CN (19.3).⁵ Unfortunately several strong solvent peaks in the $\nu(\text{CN})$ region of the infrared spectrum of CH_3OH precluded its use as a solvent in our TRIR investigations. It is interesting to note that Indelli *et al.* used CH_3OH to demonstrate an interesting case of equilibrium between the excited states of two chromophores in a supramolecular system based on $[\text{Ru}(\text{CN})_4(\text{bpy})]^{2-}$ and pyrene (§3.1) using luminescence spectroscopy.⁶ As an aside, some ps-TRIR experiments were attempted on ‘Indelli-type’ complexes but were unsuccessful due to insufficient solubility for TRIR experiments. An alternative approach could be to use an equimolar solvent mixture of D_2O and CH_3CN to give an Acceptor Number intermediate between those of the pure solvents (37.1).

The close proximity of the four $\nu(\text{CN})$ ground state bands of $[\text{Ru}(\text{CN})_4(\text{NN})]^{2-}$ complexes (typically within 50 cm^{-1} of each other) and the heavy overlap between bleach and transient bands, limited the amount of information which could be extracted from the cyanide region of TRIR spectra of systems incorporating the $[\text{Ru}(\text{CN})_4]^{2-}$ unit. This was further compounded by the low spectral resolution of the PIRATE spectrometer (*ca.* $8 - 9\text{ cm}^{-1}$) when configured for a wide enough spectral range to collect the entire $\nu(\text{CN})$ spectrum over the 64 detector pixels. An attempt was made to simulate a higher resolution TRIR spectrum by splicing together two low resolution spectra (§2.3). However no major insights were gained, and it is unclear if this is because of feature obscuration as a result of spectral overlap or imprecision in the combination of the constituent spectra. In either case the acquisition of higher resolution TRIR ($2 - 4\text{ cm}^{-1}$) spectra in the $\nu(\text{CN})$ region would no doubt further

spectroscopic understanding of the relative ordering of excited state $\nu(\text{CN})$ bands in systems containing the $[\text{Ru}(\text{CN})_4]^{2-}$ unit.

An interesting point was also raised following the discussion of the recent publication by Kettle *et al.* regarding the possible significance of quadrupolar interactions in affecting the analysis of vibrational spectra of metal cyanide complexes, in addition to the well-known effect of dipole moment changes on vibrational spectra.⁷ At this stage it is not clear how such second-order interactions could best be studied and quantified, but this effect may be associated with the wide variations in IR band intensity observed for different metal centres in the ps-TRIR spectra of **(RuCN)₂BPM** (§4.6.3). Perhaps the combination of high-resolution FTIR, ps-TRIR and Levenberg-Marquardt lineshape fitting routines, similar to those used in a previous investigation by the author to detect dipole-octupole interactions in thin solid films might offer some insight.⁸

In Chapter 3 “Solvent Based Switching of the Gradient and Direction of Förster Photoinduced Energy Transfer in Polynuclear Complexes”, two termini based on ruthenium (II) and rhenium (I) centres were linked *via* a saturated CH_2CH_2 bridge connecting bipyridyls ligated on either metal centre. The complexity of the kinetics obtained from TCSPC and TRIR spectroscopy suggested that there were multiple photophysical processes occurring in solution, including through-space PEnT.⁹ A more rigorous data fitting procedure might reveal more precisely (or at least give a ‘ballpark’ estimate of) the number of discrete components present in the multiexponential traces obtained.

In the systems designed to exhibit solvent-switchable photophysics (**RuCN-BL^x-Rubpyamide**) the ps-TRIR kinetic information on the $\Delta t = 0\text{-}50$ ps timescale provided direct evidence supporting the photophysical model proposed by Simpson *et al.* (§3.1).¹⁰ A major triumph of this work is the *direct* observation of PEnT using vibrational spectroscopy *in real time* in the picosecond timescale.

However the kinetic data from TRIR spectroscopy were not totally consistent over both termini in many cases; in particular some (single-pixel) traces from the **Rubpyamide** terminus were ambiguous and exhibited neither a grow-in or a decay. It is conceivable that longer data acquisition times and improved band fitting could lead to better quality TRIR spectra and kinetics and it would be interesting for these systems to be reinvestigated using the new apparatus in Nottingham. In combination with a ps-TRIR study of Simpson's complex **RuCN-BL-Rubpy** a more detailed picture of the similarities and differences between the two systems (discussed in §3.8) might emerge.

There is some evidence from ps-TRIR spectroscopy for a 2-step PEnT process in **RuCN-BL¹-Rubpyamide** in D₂O (§3.5.3). However, more evidence is required to gain a better understanding of this effect, in particular the reasons for its absence in **RuCN-BL²-Rubpyamide** in D₂O, which is thought to possess termini with almost identical energetics. The key differences between these two complexes are ostensibly conformational, however only a rudimentary conformational analysis was conducted in Chapter 3. A possible avenue for future extensions to this work could involve experimental studies of the luminescence anisotropy in conjunction with a thorough computational study of the conformations likely present in solution. Sophisticated algorithms used for protein folding, such as Stanford's recent distributed computation project 'Folding@Home',¹¹ could provide a weighted distribution of the ensemble of supramolecular conformers likely to be present for the different systems in various solvents, taking into account the electrostatic properties of the two termini.

More generally an in-depth ground and excited state Density Functional Theory (DFT) study of $[\text{Ru}(\text{CN})_4(\text{bpy})]^{2-}$, which to date has only been studied in brief,¹² and polynuclear complexes based on it would add considerable gravitas to the analysis of the spectroscopic results presented in this Thesis. Such a study was attempted using the GAUSSIAN03 computational suite.¹³ However, the complexity of the polynuclear systems studied and the unusual nature of the SSSA interactions (which are responsible for these complexes' interesting photophysical behaviour) could not be

satisfactorily modelled using the simple ‘out-of-the-box’ algorithms and the author’s limited knowledge of DFT and computational chemistry. The University of Nottingham has recently installed the GAUSSIAN software on its supercomputer and an interesting avenue for future work in this area would be to complement the experimental ground and excited state spectroscopic results with a comprehensive DFT study.

It is interesting to consider that the perceived reduction in conformational degrees of freedom from BL¹ to BL² (*i.e.* from an infinite ensemble to two fairly rigid conformers) did not in fact result in a reduction in the number of exponents in the kinetics obtained by luminescence and TRIR spectroscopy. The reasons for this are unclear but the possibility of additional mono and bimetallic species’ presence as impurities produced as a result of the synthesis of the BL² ligand was raised in §3.4. The difference in photophysical behaviour between the solvatochromic **RuCN-BL^x-Rubpyamide** and **ReCO-BL¹-Rubpyamide** which is a solvent-independent system, is also not fully understood. The timescale of PEnT in the solvent-switchable systems containing a **RuCN** terminus (§3.5.3, 3.6.3) was on the $\Delta t = 0\text{-}10$ ps timescale, whilst in the system containing a **ReCO** terminus (§3.7.3) this process took place on the $\Delta t = 0\text{-}5$ ns timescale. Energy differences between the ³MLCT excited states on the **ReCO** and **Rubpyamide** termini are thought to be important factors in addition to the different electrostatic properties of the two termini. However the ³MLCT energies of the two termini in each of the systems was calculated to be relatively similar based on luminescence energies of the model complexes **RuCNdmb**, **Rubpyamide-BL^x** and **[ReCl(CO)₃(bpy)]** (§1.4.1.2, 3.2.1, 3.3.1, 3.4.1).

The rates of interchromophoric PEnT in Chapter 3 were not measured sufficiently accurately to calculate meaningful Förster parameters, in particular κ^2 , the orientational term. There is scope for the collection of more complete datasets to explore and calculate these parameters, possibly also using ultrafast time-resolved UV/vis. Such datasets might include more ps-TRIR time delays, higher resolution spectra and more advanced fitting routines. This might facilitate the calculation of the

rate of through-space PEnT and the 'effective' interchromophoric distance, often used as a 'molecular yardstick' to gauge distances between chromophores in non-rigid systems.¹⁴

In Chapter 4 "Probing the Excited States of Ruthenium (II) and Rhenium (I) Complexes of 2,2'-Bipyrimidine using TRIR Spectroscopy", two metal centres were linked *via* the conjugated bpm ligand, with the two metal centres held in close proximity and with electronic interaction between them in the ground and excited states. One of the key properties of the systems studied was the timescale of excited state delocalisation, and TRIR spectroscopy is perhaps not the most suitable technique to probe this as the characteristic timescale of IR spectroscopy is on the femtosecond timescale. The use of additional spectroscopic techniques such as femtosecond and picosecond time-resolved UV/vis spectroscopy might facilitate direct investigation of the timescale of excited state localisation/delocalisation, and would also enable observation of the interconversion of Ru → bpy into Ru → bpm ³MLCT in bimetallic complexes in the cases when this process was apparently complete within 1 ps. Time-resolved UV/vis might also allow further study of IVCT processes in the heterobimetallic complexes **ReBPMRuCN**, **ReBPMRubpyamide** and **RuCNBPMRubpyamide**.

The TRIR spectra obtained for **ReBPMRuCN** (§4.8.3) were somewhat convoluted due to the presence of approximately twenty $\nu(\text{CN})$ and $\nu(\text{CO})$ bands between 2100 and 1850 cm^{-1} , arising from the two excited state species present in solution following excitation. A proposal for experimental time at RAL to study these systems using time-resolved UV/vis and Raman spectroscopies was unsuccessful but these experiments could be carried out using the new facility in Nottingham.

A possible extension to the study of bipyrimidine-linked systems in Chapter 4 is to synthesise and study polynuclear complexes linked by cyanide ligands using ultrafast TRIR spectroscopy. There are a number of reports describing such systems in the

literature (§1.4.2.2) and would provide an interesting comparison with bipyrimidine-linked systems.

The apparently anomalous results obtained for **RuCNBPMRubpyamide**, which was explained in terms of Na⁺ binding to the cyanide ligands, requires further study to verify the cause. In an analogous manner to the Ba²⁺ titrations in §3.5.1, a ps-TRIR titration experiment with Na⁺ ions and a macrocycle with appropriate cavity size to sequester the ions *e.g.* a cryptahemispherand¹⁵, might be helpful in confirming the nature of the impurity/anomaly more precisely. Atomic absorption spectrometry may also be of use in this case to directly measure the sodium ion concentration. Unfortunately a luminescence titration would not be suitable due to the absence of significant emission from the system (§4.11.1).

Further studies are required to investigate the significance of the redox processes apparently occurring at 0 V observed in cyclic voltammograms of homobimetallic and heterobimetallic bpm complexes. A combination of UV/vis OTE and EPR may prove useful in conclusively verifying whether these processes are occurring, and if they have any effect on the ground and excited state properties of the complexes studied in Chapter 4.

The particularly strong solvatochromism of **(RuCN)₂BPM**, which results from its eight cyanide ligands (§4.6), provides scope for studies designed to exploit this. Potential applications include incorporating the complex into a moisture, solvent or metal ion sensor (directly exploiting the colour change in the presence of solvent molecules or ions) or as a photosensitiser and charge injector into nanocrystalline TiO₂, taking advantage of its broad ¹MLCT absorption profile (covering most of the visible spectrum) and strongly variable ³MLCT excited state energies.

An interesting consideration is that the intercomponent photophysical processes occurring in bimetallic complexes of bipyrimidine may be described with equal validity as excited state electron *or* energy transfer. As the process occurring is

identical in either case, it is a semantic argument as to which describes the process most accurately. This has been discussed in a previous study.¹⁶

Taking a wider view of the project, this Thesis, and possible future directions, a long-term goal of the scientific community is to incorporate systems such as the ones discussed in Chapters 3 and 4 into proto-devices like those envisioned by proponents of 'supramolecular machines' such as Lehn, Balzani and Stoddart.¹⁷ Considering the systems described in this Thesis as potential device components one can foresee the construction of light-driven supramolecular machines¹⁸ whereby intercomponent energy and electron transfer processes may occur in the same system. The dominant excited state deactivation pathway would then depend on some external stimulus *e.g.* solvent or atmospheric environment or the presence of metal ions which might reversibly bind to the cyanide ligands of the $[\text{Ru}(\text{CN})_4(\text{NN})]^{2-}$ unit, modulating the energetics of the lowest energy ³MLCT excited state.

Systems incorporating the $[\text{Ru}(\text{CN})_4(\text{bpy})]^{2-}$ unit and a cobaltocene moiety (**RuCN-Cob**, see Figure 5.2.1) were designed to study solvent-dependent PET and were analysed using luminescence and TRIR spectroscopy. However, no meaningful results were obtained. A more detailed study of such systems would be of considerable interest for the molecular electronics community, as the facile control of direction and thermodynamic gradient of PET would be an important step towards the construction of supramolecular device components acting as electronic switches (*i.e.* molecular transistors).¹⁹

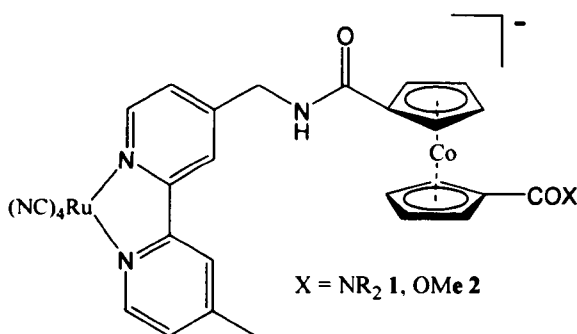


Figure 5.2.1: The RuCNbpy-Cob complexes studied unsuccessfully.

The construction of higher nuclearity transition metal cyanide complexes, which was explored briefly during the course of this project using the ligand HAT (not shown in this Thesis) would offer additional benefits over the systems described here. These include a higher degree of connectivity to a single node and a potentially greater degree of modulation of their photophysical properties *via* solvatochromism and metallochromism phenomena, since these depend on the number of cyanide ligands present.

We recently studied the series of complexes $[\text{Ru}(\text{CN})_4(\text{HAT})]^{2-}$, $\{(\text{Ru}(\text{CN})_4)_2(\mu_2\text{-HAT})\}^{4-}$ and $\{(\text{Ru}(\text{CN})_4)_3(\mu_3\text{-HAT})\}^{6-}$ in which one, two or three $[\text{Ru}(\text{CN})_4]^{2-}$ units are connected to the bidentate sites of the tridentate ligand hexaaza-triphenylene (HAT).^{20,21} These systems would be expected to show a near-linear relationship with degree of solvatochromism and number of cyanide ligands (§2.1.3). Therefore $\{(\text{Ru}(\text{CN})_4)_3(\mu_3\text{-HAT})\}^{6-}$ would be expected to exhibit the most marked degree of negative solvatochromism yet observed in complexes of this type owing to its twelve cyanide ligands. This would suggest that this complex would show even greater promise as a solvent/moisture/metal ion sensor than the bimetallic complex **(RuCN)₂BPM**.

Another potentially interesting avenue of research identified is the broadening of the scope of the metal centres used in this Thesis. Extending the study to metals such as osmium (II), rhodium (I/III) and iridium (I/III) and platinum (II) would not only increase the potential synthetic functionalisation, design flexibility and utility of such systems, but would also ostensibly open up the possibility of device components exploiting a 'two-tier' solvatochromic effect. Two different metal cyanide supramolecular building blocks in the same system could exhibit varying degrees of negative solvatochromism such that there may be more than one Acceptor Number switching point in the photophysical properties of the complex. Such an effect might occur in systems incorporating identical metal centres with varying numbers of cyanide ligands attached to them, *e.g.* $[\text{Ru}(\text{CN})_4(\text{bpy})]^{2-}$ and $[\text{Ru}(\text{CN})_2(\text{bpy})_2]$ (§2.1.3), although to a lesser extent. The latter case might however suffer from spectral

congestion in ground and excited state TRIR spectroscopy in the $\nu(\text{CN})$ region, which might limit the insights which could be gained from spectroscopic study.

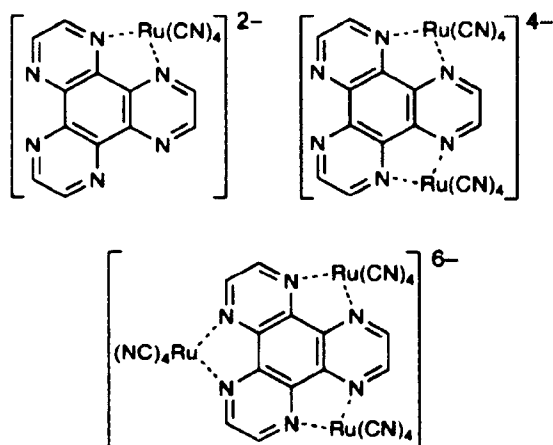


Figure 5.2.2: $(\text{RuCN})_x\text{HAT}$ complexes.

In conclusion a number of supramolecular systems have been designed, studied and analysed in conjunction with the photophysical models presented. The solvent-based nature of the switching of photophysical properties of polynuclear complexes incorporating the strongly solvatochromic $[\text{Ru}(\text{CN})_4(\text{bpy})]^{2-}$ unit has been demonstrated using UV/vis, luminescence and TRIR spectroscopies and electrochemistry. The utility of the $\nu(\text{CN})$ bands of the $[\text{Ru}(\text{CN})_4(\text{bpy})]^{2-}$ unit as a sensitive reporter of ground and excited state electron density in FTIR and TRIR spectra and as an efficient metal ion binder has also been shown. Possible applications and future extensions to the work in this Thesis have been presented.

5.3. References

-
- ¹ H. Adams, W. Z. Alsindi, G. M. Davies, M. B. Duriska, T. L. Easun, H. E. Fenton, J.-M. Herrera, M. W. George, K. L. Ronayne, X.-Z. Sun, M. Towrie and M. D. Ward, *Dalton Trans.*, 2006, 1, 39.
- ² W. Z. Alsindi, T. L. Easun, X.-Z. Sun, K. L. Ronayne, M. Towrie, J.-M. Herrera, M. W. George and M. D. Ward, *Inorg. Chem.*, accepted; T. L. Easun, M. D. Ward, W. Z. Alsindi, X.-Z. Sun and M. W. George, *Central Laser Facility Ann. Rep.*, 2006, 169.
- ³ W. Z. Alsindi, T. L. Easun, X.-Z. Sun, K. L. Ronayne, M. Towrie, J.-M. Herrera, M. W. George and M. D. Ward, in prep.
- ⁴ T. Lazarides, T. L. Easun, C. Veyne-Marti, W. Z. Alsindi, M. W. George, N. Deppermann, H. Adams, G. M. Davies and M. D. Ward, *J. Am. Chem. Soc.*, 2007, **129**, 4014.
- ⁵ C. J. Timpson, C. A. Bignozzi, B. P. Sullivan, E. M. Kober and T. J. Meyer, *J. Phys. Chem.*, 1996, **100**, 2915.
- ⁶ M. T. Indelli, M. Ghirotti, A. Prodi, C. Chiorboli, F. Scandola, N. D. McClenaghan, F. Puntoriero and S. Campagna, *Inorg. Chem.*, 2003, **42**, 5489.
- ⁷ S. F. A. Kettle, G. L. Aschero, E. Diana, R. Rosetti and P. L. Stanghellini, *Inorg. Chem.*, 2006, **45**, 4928.
- ⁸ W. Z. Alsindi, D. O. Gardner, E. F. van Dishoeck and H. J. Fraser, *Chem. Phys. Lett.*, 2003, **378**, 178.
- ⁹ T. L. Easun, M. D. Ward, W. Z. Alsindi, X.-Z. Sun and M. W. George, *Central Laser Facility Ann. Rep.*, 2005, 125; W. Z. Alsindi, T. L. Easun, X.-Z. Sun, K. L. Ronayne, M. Towrie, M. W. George and M. D. Ward, in prep.
- ¹⁰ N. R. M. Simpson, M. D. Ward, A. F. Morales and F. Barigelletti, *J. Chem. Soc. Dalton Trans.*, 2002, 2449.
- ¹¹ See for example J. Chodera, N. Singhal, V. S. Pande, K. Dill and W. Swope, *J. Chem. Phys.*, in press.
- ¹² T. Meyges, G. Schubert, M. Kovács, T. Radnai, T. Grosz, I. Bako, I. Papai and A. Horváth, *J. Phys. Chem. A*, 2003, **107**, 9903.
- ¹³ Gaussian 03, Revision C.02, M. J. Frisch, G. W. Trucks, H. B. Schlegel, G. E. Scuseria, M. A. Robb, J. R. Cheeseman, J. A. Montgomery, Jr., T. Vreven, K. N. Kudin, J. C. Burant, J. M. Millam, S. S. Iyengar, J. Tomasi, V. Barone, B. Mennucci, M. Cossi, G. Scalmani, N. Rega, G. A. Petersson, H. Nakatsuji, M. Hada, M. Ehara, K. Toyota, R. Fukuda, J. Hasegawa, M. Ishida, T. Nakajima, Y. Honda, O. Kitao, H. Nakai, M. Klene, X. Li, J. E. Knox, H. P. Hratchian, J. B. Cross, V. Bakken, C. Adamo, J. Jaramillo, R. Gomperts, R. E. Stratmann, O. Yazyev, A. J. Austin, R. Cammi, C. Pomelli, J. W. Ochterski, P. Y. Ayala, K. Morokuma, G. A. Voth, P. Salvador, J. J. Dannenberg, V. G. Zakrzewski, S. Dapprich, A. D. Daniels, M. C. Strain, O. Farkas, D. K. Malick, A. D. Rabuck, K. Raghavachari, J. B. Foresman, J. V. Ortiz, Q. Cui, A. G. Baboul, S. Clifford, J. Cioslowski, B. B. Stefanov, G. Liu, A. Liashenko, P. Piskorz, I. Komaromi, R. L. Martin, D. J. Fox, T. Keith, M. A. Al-Laham, C. Y. Peng, A.

Nanayakkara, M. Challacombe, P. M. W. Gill, B. Johnson, W. Chen, M. W. Wong, C. Gonzalez, and J. A. Pople, Gaussian, Inc., Wallingford CT, 2004.

¹⁴ J. R. Lakowicz, *Principles of Fluorescence Spectroscopy*, Kluwer Academic/Plenum Publishers, 2nd edn., 1999.

¹⁵ D. J. Cram, S. P. Ho, C. B. Knobler, E. Maverick and K. N. Trueblood, *J. Am. Chem. Soc.*, 1986, **108**, 2998.

¹⁶ A. Vogler and J. Kisslinger, *Inorg. Chim. Acta*, 1986, **115**, 193.

¹⁷ V. Balzani and F. Scandola, *Supramolecular Photochemistry*, Ellis Horwood, 1991.

¹⁸ See for example: T. Muraoka, K. Kinbara, Y. Kobayashi and T. Aida, *J. Am. Chem. Soc.*, 2003, **125**, 5612; A. M. Brouwer, C. Frochot, F. G. Gatti, D. A. Leigh, L. Mottier, F. Paolucci, S. Roffia and G. W. H. Wurpel, *Science*, 2001, 2124.

¹⁹ V. Balzani, G. Bergamini, F. Marchioni and P. Ceroni, *Coord. Chem. Rev.*, 2006, **250**, 1254.

²⁰ J.-M. Herrera, M. D. Ward, H. Adams, S. J. A. Pope and S. Faulkner, *Chem. Commun.*, 2006, 1851.

²¹ J.-M. Herrera, T. L. Easun, W. Z. Alsindi, , X.-Z. Sun, K. L. Ronayne, M. Towrie, M. W. George and M. D. Ward, in prep.

Chapter 6:

Experimental Procedures

Chapter 6: Experimental Procedures

6.1. Materials, Measurements and Analysis

Materials

Chemicals were purchased from Sigma-Aldrich at the highest available purity. CH₃CN and CH₃OH were distilled over calcium hydride under an atmosphere of argon.

All complexes were synthesised by Mr. T. L. Easun and co-workers under the supervision of Prof. M. D. Ward at the University of Sheffield.¹

All experiments were conducted at room temperature (23 ± 2 °C) and atmospheric pressure unless otherwise indicated.

Spectroscopic Measurements

FTIR Spectroscopy

FTIR spectra were recorded in standard CaF₂ solution cells (Specac) using a Nicolet Avatar 360 FTIR spectrometer, recording 128 scans at a typical resolution of 2 cm⁻¹ with two levels of zero filling. For measurements in D₂O solution a pathlength of 50-100 μm was normally used and in CH₃CN solution a pathlength of 0.5 mm was normally used. During the collection of spectra in the 1500-1900 cm⁻¹ spectral region it was necessary to purge the spectrometer sample compartment with nitrogen or dry air due to strong absorptions of atmospheric water vapour in this region until no further spectral changes were observed, typically for 30-60 minutes.

UV/visible Absorption Spectroscopy

UV/visible absorption spectra were obtained in quartz cuvettes using a UNICAM UV-2 Spectrophotometer, typically with a data spacing of 1 nm using cuvettes of either 1 mm or 10 mm pathlength, depending on the absorbance of sample and solvent in the spectral regions of interest.

Luminescence Spectroscopy

Emission measurements were performed on a combined fluorescence lifetime and steady state spectrometer (Edinburgh Instruments FLS920). Non-aqueous solutions were thoroughly degassed using the freeze-pump-thaw technique, in specially modified 10 mm x 10 mm quartz cuvettes. Aqueous solutions were degassed using the same technique with care taken to ensure that the solidifying water did not rapidly expand and shatter the measuring vessel. The optical density was adjusted to *ca.* 0.2 at the excitation wavelength, which corresponds to a concentration of *ca.* 1×10^{-5} M. Steady state emission and excitation spectra were obtained with a xenon arc lamp as the excitation source and were corrected for detector sensitivity. The emission monochromator wavelength was stepped in 1 nm increments. Emission lifetime measurements were performed using time-correlated single-photon counting (TCSPC), with a nanosecond H₂ flash lamp (repetition rate 40 Hz and pulse width *ca.* 2 ns) as the excitation source. The uncertainties quoted for emission lifetimes have been taken from the uncertainty of the fitted decay traces from Levenberg-Marquardt Non-Linear Least Squares Fitting.²

Quantum yields, Φ_{em} were calculated from the following equation, using a solution of [Ru(bpy)₃]Cl₂ in H₂O as an emission standard,

$$\phi_{em} = \phi_r \cdot \frac{I}{I_r} \cdot \frac{OD_r}{OD} \cdot \frac{n^2}{n_r^2}$$

Where:

Φ_r = quantum yield of emission standard (0.028 for [Ru(bpy)₃]²⁺ in H₂O at 298 K³),

I = integrated emission intensity of the sample,

I_r = integrated emission intensity of the emission standard,

OD = optical density of the sample at the excitation wavelength,

OD_r = optical density of the emission standard at the excitation wavelength,

n = refractive index of the solvent used for the sample,

n_r = refractive index of the solvent used for the emission standard.

The fractional uncertainty in emission quantum yield is estimated as ± 10 %.

A second apparatus was used for faster TCSPC experiments, the Edinburgh Instruments Mini-Tau Lifetime Spectrometer based at the Department of Chemistry, University of Sheffield. This enabled the undertaking of TCSPC experiments with an excitation wavelength of 405 nm with time resolution of below 1 ns. All other aspects of the experiments were identical.

Time-resolved Infrared (TRIR) Spectroscopy

For TRIR measurements of transition metal complexes concentrations ranging from 1×10^{-4} to 5×10^{-3} M were typically used. The choice of pathlength was dependent of the concentration of the solute and of solvent absorption in the spectral region under study. Typically, the pathlengths were 50-60 μm for D_2O and 500-1000 μm for CH_3CN and CH_2Cl_2 . It should be noted that apparent discrepancies between time constants obtained using luminescence and TRIR spectroscopy may be rationalised in terms of the different experimental conditions required for the experiments. Two likely contributing factors are worth noting. The much higher analyte concentrations required for TRIR experiments may lead to self-quenching which is an effect that has been observed previously in TRIR spectra.⁴ Another possible reason for this is the inferior degassing protocol that is used during the PIRATE TRIR experiments and both of these factors would result in shorter ³MLCT lifetimes under the conditions of TRIR measurements compared to luminescence measurements. It should also be noted that in most cases the TRIR kinetic traces shown are ‘single-pixel’ in nature, in that a single detector pixel’s $\Delta\text{Absorbance}$ signal is plotted versus time. In all traces, $\Delta\text{Absorbance} = 0$ is defined as the X-axis.

Picosecond TRIR Spectroscopy

The picosecond TRIR experiments were carried out on the PIRATE apparatus at the Central Laser Facility of the CCLRC Rutherford Appleton Laboratory. This apparatus has been described in detail previously.⁵ Briefly part of the output from a 1 kHz, 800 nm, 150 fs, 2 mJ Ti-Sapphire oscillator/regenerative amplifier (Spectra Physics Tsunami/Spitfire) was used to pump a white light continuum seeded $\beta\text{-BaB}_2\text{O}_4$ (BBO) optical parametric amplifier (OPA). The signal and idler produced by this OPA were

difference frequency mixed in a type I AgGaS₂ crystal to generate tuneable mid-infrared pulses (*ca.* 150 cm⁻¹ FWHM, 1 μJ), which were split to give probe and reference pulses. Second harmonic generation of the residual 800 nm light provided 400 nm pump pulses which were used for all ps-TRIR experiments described in this Thesis. Both the pump and probe pulses were focused to a diameter of 200-300 μm and co-linearly overlapped in the sample. Changes in infrared absorption at various pump-probe time delays were recorded by normalising the outputs from a pair of 64-element MCT infrared linear array detectors each monitoring independently the probe and reference pulses on a shot-by-shot basis. Data were collected in pump-on/pump-off pairs in order to minimise the effect of long-term drift in the laser intensity. Data points are spaced approximately 4-5 cm⁻¹ apart, giving a spectral resolution of *ca.* 8-9 cm⁻¹. Optical effects due to pump and probe laser interference are present in spectra recorded earlier than 1 picosecond, which is taken as the instrument response time (or IRF).

In all TRIR experiments dry, degassed solutions were saturated with argon and flowed through a home-built flow system incorporating an IR cell (Harrick Scientific Corp.) and a Teflon peristaltic pump (Cole Palmer). In the case of D₂O solutions the static samples were sealed inside the IR cell. The cell was rapidly oscillated in the plane perpendicular to the direction of the laser beams in order to minimise the potential build-up of decomposition products on the windows. All the samples were checked for the formation of decomposition products by on-line FTIR (*vide supra*) after each experiment.

Nanosecond TRIR Spectroscopy

The nanosecond TRIR spectra shown in this Thesis were obtained using the PIRATE apparatus at the Central Laser Facility of the CCLRC Rutherford Appleton Laboratory using a Nd:YAG laser (Advanced Optical Technology ACE) as the excitation source ($\lambda = 355$ nm) and the detection system detailed above.⁶

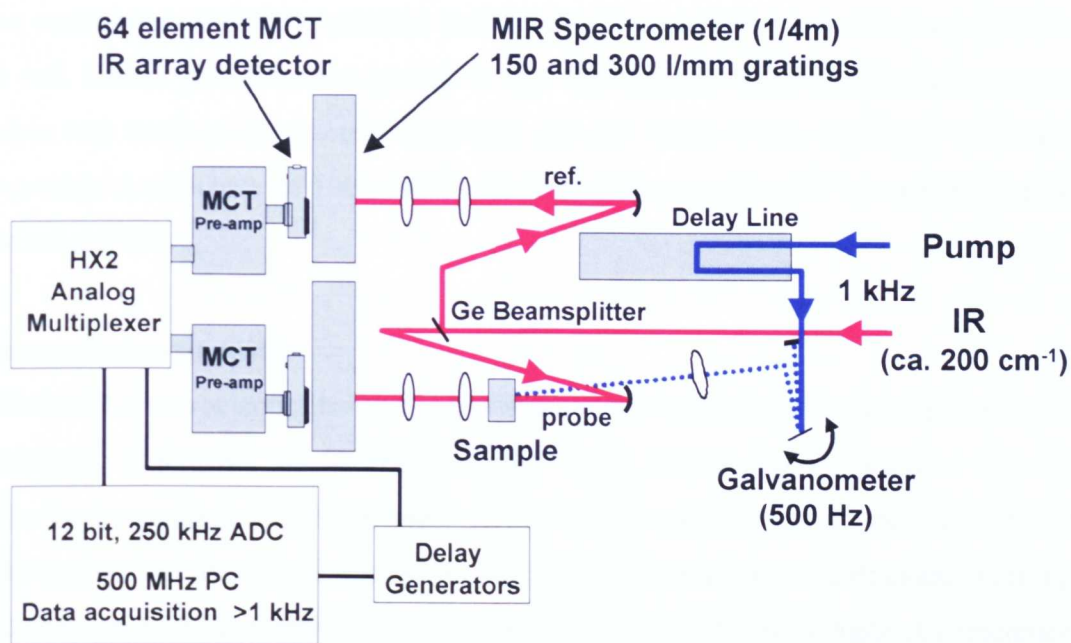


Figure 6.1: A schematic of the PIRATE apparatus. Adapted from Ref.⁴

The Nottingham step-scan FTIR apparatus used in the early stages of this project has been described in detail elsewhere.⁷ Briefly the apparatus comprises of a commercially available step-scan FTIR spectrometer (Nicolet Magna 860) equipped with a 100 MHz 12-bit digitizer and a 50 MHz MCT detector interfaced to a Nd:YAG laser (Spectra Physics GCR-12). Synchronization of the Nd:YAG laser with data collection was achieved using a pulse generator (Stanford DG535). A commercially available IR cell (Harrick, 1 to 3 mm pathlength) was used with a home built flow system to minimise the build-up of decomposition products on the cell windows.

Electrochemistry

Cyclic Voltammetry

Cyclic voltammetric studies were carried out in anhydrous CH_3CN solutions (*ca.* 1×10^{-3} M, with $[\text{nBu}_4][\text{BF}_4]$ as the supporting electrolyte) using a potentiostat (EG & G Model 362) and a digitiser (EG & G Condecon 310). Cyclic voltammetry was carried out under an atmosphere of argon using a three-electrode arrangement in a single compartment cell. A Pt wire working electrode, a Pt wire secondary electrode and a

Ag/AgCl reference electrode, chemically isolated from the test solution *via* a bridge tube containing electrolyte solution and fitted with a porous vycor frit, were used in the cell. Redox potentials are quoted *vs.* the ferrocenium-ferrocene (Fc/Fc⁺) couple, which was used as an internal reference (at *ca.* +0.45 V *vs.* Ag/AgCl reference electrode). A scan rate of 100 mVs⁻¹ was used. Compensation for internal resistance was not applied.

Spectroelectrochemistry

UV/vis/nIR spectroelectrochemical experiments were carried out at the Department of Chemistry, University of Sheffield by Mr T. L. Easun and co-workers with an optically transparent electrochemical (OTE) cell (modified quartz cuvette, optical pathlength 0.5 mm). A three-electrode configuration, consisting of a Pt gauze working electrode (in a PTFE sheath), a Pt wire secondary electrode and a Ag/AgCl reference electrode, chemically isolated from the test solution *via* a bridge tube containing electrolyte solution and terminated in a porous frit, was used in the cell.

The potential at the working electrode was controlled by a Princeton Applied Research 273A potentiostat. The UV/vis/nIR spectra were recorded using a Varian Cary 5000 UV/vis/nIR spectrophotometer. The spectrometer cavity was purged with dry N₂ gas and temperature control at the sample was achieved by flowing cooled N₂ gas across the surface of the cell.

FTIR spectroelectrochemical experiments were carried out with an optically transparent thin-layer electrochemical (OTTLE) cell.^{8,9} The cell consisted of a modified IR solution cell (Specac, optical pathlength *ca.* 200 μm) equipped with CaF₂ windows and a three-electrode configuration; Pt/Rh minigrad working and (unbridged) secondary electrodes and a twisted Ag wire pseudo-reference electrode. The cell was positioned so that the beam passed through the centre of the working electrode; all other electrodes were masked from the IR beam. Potentials were controlled by a potentiostat (EG&G Model 362) and spectra were recorded at ambient temperature on an FTIR spectrometer (Nicolet Avatar) that was purged with dry air.

For UV/vis/nIR and FTIR spectroelectrochemical experiments the metal complex in solution was either electrolysed at constant potential (UV/vis) or the potential was stepped across the redox event (FTIR). For the single potential step experiments a potential typically 100 mV more positive than E_p^a for an oxidation experiment and 100 mV more negative than E_p^c for a reduction was applied to the working electrode. The redox process was considered complete when consecutive spectra were identical. The chemical reversibility of the process was investigated by applying a potential at the working electrode sufficient to re-oxidise or re-reduce the electrogenerated product. These potentials were typically 100 mV more negative than E_p^c to reverse an oxidation process or 100 mV more positive than E_p^a to reverse a reduction process. The process was considered to be reversible under the conditions of the experiment if the spectroscopic profile of the starting material was reproduced. The kinetics of the redox process may not allow full return to the starting material within the timescale of the experiment. In such cases isosbestic points were taken to indicate reversibility of the spectral profile.

Analysis of TRIR Data

The basic methodology employed for the initial analysis of the raw data, generated in the ps-TRIR experiments in the PIRATE facility at the Central Laser Facility of the Rutherford Appleton Laboratory has been described previously.¹⁰

In each experiment up to 100 pump-probe time delays could be measured. The experiment could be accumulated for any number of cycles and for each cycle the computer randomised the order in which the time delays were measured. The acquisition time at each time delay was determined by the user prior to the experiment on the basis of the signal-to-noise ratio in the spectra. This in turn was determined by the signal strength (sample concentration) and solvent absorption in the spectral region of interest. For ps-TRIR spectra for CH_3CN or CH_2Cl_2 solutions of metal carbonyl or cyanide complexes in the metal carbonyl region, 20 time delays measured over 2 cycles with 15 s data acquisition time at each time delay was usually sufficient to provide a good signal-to-noise ratio. For ps-TRIR spectra of solutions of transition

metal complexes in D₂O typically 15-25 time delays measured over 4-6 cycles with 15-30 s data acquisition time at each time delay was used.

Custom software (EMToF and FeTian, written by Dr. Xue-Zhong Sun, University of Nottingham) was used to automatically generate the “ Δ Absorbance Difference” TRIR spectra from the .dao data files for each time delay. The spectra contain 64 data points, representing the 64 pixels of the linear IR array detectors. Calibration of these spectra from pixel numbers into wavenumbers was achieved by curve-fitting one of the pixel spectra and comparing the positions of the bleach bands (in pixels) with the ground state FTIR bands (in cm⁻¹) taking into account a spectrograph dispersion of *ca.* 12 nm/pixel. This procedure was complicated somewhat by the presence of “dead pixels” in the detector array, most notably pixel number 39. This resulted in some erroneous signals near the centre of the spectra collected which were disregarded when data was analysed.

Curve-fitting was performed using commercially available software (OriginPro 7e, OriginLab Inc.). Individual band parameters for the transient and parent bands in the ps-TRIR spectra were obtained from multi-curve fitting of the ps-TRIR spectra presuming their Lorentzian band shape in non-polar solvents, with the facility to employ Gaussian band shapes in case of line broadening in polar solvents. For ps-TRIR spectra in the metal carbonyl region the Lorentzian parameters of the parent bands (band positions, widths and the ratio between the parent bands) were obtained by fitting the ground state FTIR spectrum and kept constant during the fitting procedure. The parameters of vibrationally cool bands were determined by curve-fitting of one of the spectra at late time delays, typically 100 ps, and again were fixed as constants during the fitting procedure.

In many $\nu(\text{CN})$ TRIR spectra presented in this work, the parent bands are heavily overlapped with the transient bands and this complicates the calibration of the ps-TRIR spectra. In extreme cases a ground state IR spectrum was recorded with ps-TRIR apparatus by plotting the \log_{10} of the ratio between reference only signals for the sample and pure solvent to allow a precise calibration and fitting of time-resolved

spectra. The obtained ground state IR spectrum was again fitted with the sum of Lorentzian bands and the band parameters were kept constant during the fit of ps-TRIR spectra.

As a result of heavy ground and excited state band overlap in the ps and ns-TRIR spectra in this Thesis it was often not feasible to obtain kinetic information from the multi-curve fitting of the ps-TRIR spectra due to the large number of overlapping bands and associated uncertainty in the band parameters. In this case the kinetic information was obtained by recording intensity of the signal in a single point, at the maximum of the band of interest or in the point where this band is least likely to be influenced by overlap with surrounding bands. When this was the case the Figure captions mention this explicitly.

Conformational Calculations using SPARTAN

Conformational analysis was conducted using the commercially available software package SPARTAN (Wavefunction Inc.) by constructing the supramolecular system and performing geometric optimisation through semi-empirical energy minimisation using the PM3 algorithm. Following this the Conformational Analysis function was performed which in combination with manual verification gave approximate internuclear distances between metal centres. These are meant to be used as a “rule of thumb” and molecular dynamics or full DFT calculations with a supercomputer would be preferable to obtain more precise and meaningful data.

6.2. References

- ¹ T. L. Easun, Ph.D. Thesis, University of Sheffield, submitted.
- ² K. Levenberg, *Quart. Appl. Math.*, 1944, **2**, 164; D. Marquardt, *SIAM J. Appl. Math.*, 1963, **11**, 431.
- ³ J. V. Caspar and T. J. Meyer, *J. Am. Chem. Soc.* 1983, **105**, 5583.
- ⁴ P. Glyn, M. W. George, P. M. Hodges and J. J. Turner, *J. Chem. Soc. Chem. Commun.*, 1989, 1655.
- ⁵ M. Towrie, D. C. Grills, J. Dyer, J. A. Weinstein, P. Matousek, R. Barton, P. D. Bailey, N. Subramaniam, W. M. Kwok, C. S. Ma, D. Phillips, A. W. Parker and M. W. George, *App. Spec.*, 2003, **57**, 367.
- ⁶ M. Towrie, A. Gabrielsson, P. Matousek, A. M. B. Rodriguez and A. Vlček, *App. Spec.*, 2005, **59**, 467.
- ⁷ X.-Z. Sun, S. M. Nikiforov, J. Yang, C. S. Colley and M. W. George, *App. Spec.*, 2002, **56**, 31.
- ⁸ M. Krejčík, M. Danek, and F. Hartl, *J. Electroanal. Chem.*, 1991, **317**, 179.
- ⁹ F. P. A. Johnson, M. W. George, F. Hartl, and J. J. Turner, *Organomet.*, 1996, **15**, 3374.
- ¹⁰ J. Dyer, Ph.D. Thesis, University of Nottingham, 2003.